2008-01-01

A Macro-Bend Fiber Based Wavelength Demodulation System for Optical Fiber Sensing Applications

Ginu Rajan
Technological University Dublin

A Macro-Bend Fiber Based Wavelength Demodulation System for Optical Fiber Sensing Applications

A Thesis presented for the Degree of
Doctor of Philosophy

by

GINU RAJAN, *MSc.*

Supervisors: Dr. Gerald Farrell and Dr. Yuliya Semenova

School of Electronic and Communications Engineering

Faculty of Engineering

Dublin Institute of Technology

November 2008

Dedicated to the poor and illiterate children of the world, who have the thrust to learn, to enlighten their lives with knowledge and wisdom

Abstract

This thesis considers the design and development of a wide range all-fiber interrogation system with a rapid measurement capability for extracting reliable measurand information from fiber Bragg grating sensors. Existing passive and active interrogation systems have certain limitations and do not satisfy all requirements. In this thesis a wavelength demodulation system is proposed, based on a macro-bend fiber filter employed in a ratiometric detection scheme. A theoretical model and analysis of an edge filter based ratiometric wavelength measurement (RWM) system is presented. A fiber edge filter is realized by carefully selecting an appropriate bend radius and number of bend turns of a standard single-mode fiber with an applied absorption layer. The calibration and characterization of the system are carried out experimentally and the effect of the signal-to-noise ratio (SNR) of the source is studied. It is shown that the SNR limits the measurable wavelength range of the system. A complete noise model for an edge filter based ratiometric system is developed and the noise analysis shows that increasing the slope of the edge filter is not necessarily a guaranteed approach to increasing the resolution of the system. The effect of polarization on the system is also investigated. The origins of the polarization dependency of the components, the macro-bend fiber filter and the 3 dB coupler, are identified and the effect of polarization dependent loss (PDL) on the RWM system with concatenated PDL components is investigated. To eliminate the polarization dependency, a novel twisted macro-bend fiber edge filter based system is proposed and demonstrated. As the bend loss in single-mode fiber is a function of temperature, an investigation to estimate the temperature induced instabilities in the system is carried out. The macro-bend fiber based interrogation system is used to extract information from an array of FBGs with different peak wavelengths using a best fit slope. A performance evaluation of the interrogation system is carried out and static strain, dynamic strain and temperature are measured. The investigation of the temperature dependence of the bend loss edge filter also led to the development of a new all-fiber temperature sensor, which is described, demonstrating a linear relation between the bend loss of a single-mode fiber and temperature in a sensing application for the first time.

DECLARATION

I certify that this thesis which I now submit for examination for the award of **Doctor of Philosophy**, is entirely my own work and has not been taken from the work of others, save and to the extent that such work has been cited and acknowledged within the text of my work.

This thesis was prepared according to the regulations for postgraduate study by research of the Dublin Institute of Technology and has not been submitted in whole or in part for another award in any Institute.

The work reported on in this thesis conforms to the principles and requirements of the Institute's guidelines for ethics in research.

The Institute has permission to keep, lend or copy this thesis in whole or in part, on condition that any such use of the material of the thesis be duly acknowledged.

Ginu Rajan

26^{th} November 2008

Acknowledgements

It was the best of times, it was the worst of times, it was the age of wisdom, it was the age of foolishness, it was the epoch of belief, it was the epoch of incredulity, it was the season of Light, it was the season of Darkness, it was the spring of hope, it was the winter of despair ...

The above opening passage from 'A Tale of Two Cities' by Charles Dickens would aptly sum-up the high and low points of past few years! And now, I am indeed delighted to acknowledge people who mattered the most during this phase.

First and foremost, I would like to thank my supervisor Dr. Gerald Farrell for giving me an opportunity to work with him. Without his constant support and able guidance, this thesis would not have been complete. I am also grateful to him for creating good lab facilities and a very congenial work atmosphere that helped me to carry out the research work smoothly and independently. With his enthusiasm, inspiration, and great efforts to explain things clearly and simply, made my thesis work more effective.

I sincerely thank Dr. Yuliya Semenova, my co-supervisor for her valuable suggestions and advice on many occasions. Her positive attitude and encouraging support gave me the confidence on approaching many problems.

I am grateful to Dr. Qian Wang for his guidance and suggestions during the initial years of my research. I wish to express my sincere thanks to Dr. Marek Rebow for all the encouragement and enthusiastic advices. I must thank Mr. Thomas Freir for all his help during the thesis work.

I am deeply indebted to my fellow colleagues for providing a stimulating environment in the office and lab. Many thanks to Agus Hatta, Pengfei Wang, Sunish Mathews, Dean Callaghan and Vimal Alex for being quite considerate and accommodating.

It was the inspiration given by Dr. Rajan. K. John helped to reach this level. My sincere thanks to Rajan Sir and Susan miss for their flattering support and encouragement.

I wish to thank Shynu and Suni, for bearing with me for 1 year during the stay with them and also having some good discussions out of my research topics. Many thanks to my friends in Ireland, Soumya, Jolly, Maby and Salmon, especially for the occasional dinner parties, which made my life more enjoyable in Ireland.

Friends and cousins back home, Pradheesh, Blesson, Jebouy, Vigeesh, Sabitha, Anupama, Pradeep, Jomon, Chitra, Srividya, Radhika, Jessy, Shahina, Mustafa and Biman were quite affectionate and concerned. It is with great pleasure, I acknowledge their wholehearted support and appreciation.

Special thanks to my fiancee Ramya for being patience and understanding for past 5 years. Despite my prolonged isolation and sometimes negligence, she supported me the most during my thesis work.

Many thanks to my elder brother Jeny and younger sister Jeena for all their prayers, encouragement and support during the thesis work. I wish to thank my entire extended family, my uncles and aunties and my sister in law for all their support.

Finally I would like to thank my mother for everything. Without her prayers, sacrifice and never ending support, I wouldn't be writing these lines of my thesis.

Ginu Rajan

List of Publications

Patent

- Rajan. G, Semenova. Y, Farrell. G, "*Temperature sensor using a single-mode bend fiber filter*," Patent pending, UK Patent Appl. No.GB0803583.4.

International Refereed Journals

- Rajan. G, Semenova. Y, P. Wang, Farrell. G, "*Temperature induced instabilities in macro-bend fiber based wavelength measurement systems*," IEEE J. Lightwave Technol., Accepted for publication.
- Rajan. G, Semenova. Y, Farrell. G, "*Analysis and performance evaluation of an all-fiber interrogation system for a Bragg grating array*," J. Opt. A: Pure Appl. Opt., Accepted for publication.
- Rajan. G, Semenova. Y, Freir. T, Wang. P, Farrell. G, "*Modeling and analysis of the effect of noise on an edge filter based ratiometric wavelength system*," IEEE J. Lightwave Technol., 26, 3434-3442, 2008.
- Rajan. G, Semenova. Y, Farrell. G, "*All-fibre temperature sensor based on macro-bend singlemode fibre loop*," Electron. Lett., 44, 1123-1124, 2008.
- Rajan. G, Semenova. Y, Farrell. G, Wang. Q, Wang. P, "*A low polarization sensitivity all-fiber wavelength measurement system*," IEEE Photon. Technol. Lett., 20, 1464-1466, 2008.
- Rajan. G, Wang. Q, Semenova. Y, Farrell. G, Wang. P, "*Effect of polarization dependent loss on the performance accuracy of a ratiometric wavelength measurement system*," IET Optoelectron., 2, 63-68, 2008.
- Rajan. G, Semenova. Y, Wang. Q, Farrell. G, Wang. P, "*A method to measure the reference strain of FBG interrogation system involving actuators*," Microwave and Optical Technology Letters, 40, 2658-2661, 2007.
- Rajan. G, Wang. Q, Farrell. G, Semenova. Y, Wang. P, "*Effect of SNR of input signal on the accuracy of a ratiometric wavelength measurement system*," Microwave and Optical Technology Letters, 49, 1022-1024, 2007.

- Wang. Q, Rajan. G, Wang. P, Farrell. G, "*Macrobending fiber loss filter, ratiometric wavelength measurement and application*," Meas. Sci. and Technol., 18, 3082-3088, 2007
- Wang. Q, Rajan. G, Wang. P, Farrell. G, "*Resolution investigation of ratiometric wavelength measurement system*," Appl. Opt., 46, 6362-6367, 2007.
- Wang. Q, Rajan .G, Wang .P, Farrell. G, "*Polarization dependence of bend loss for a standard singlemode fiber*," Optics Express, 15, 4909-4920, 2007.
- Wang. Q, Farrell. G, Freir. T, Rajan. G, Wang. P, "*Low cost wavelength measurement based on macrobending singlemode fiber*," Opt. Lett., 31, 1785-1787, 2006.

Conference Proceedings

- Rajan. G, Semenova. Y, Farrell. G, "*Evaluation of the performance of a novel low-cost macro-bend fiber based temperature sensor*," SPIE Defense, Security and Sensing, Florida, April 2009, Accepted.
- Rajan. G, Semenova. Y, Farrell. G, "*Applications of macrobend loss in singlemode fibers: FBG interrogator and temperature sensor*," Photonics 2008, NewDelhi, December 2008.
- Rajan. G, Semenova. Y, Farrell. G, "*An all-fiber interrogation system for a fiber Bragg grating array*," IOP Photon 08, Edinburgh, August 2008.
- Rajan. G, Semenova. Y, Farrell. G, Wang. Q, Pengfei. W, "*Investigation of the influence of 3 dB coupler on ratiometric wavelength measurements*," SPIE Photonics Europe, Strasbourg, April 2008.
- Rajan. G, Semenova.Y, Wang. Q, Farrell. G, Pengfei. W, "*Fiber bend loss ratiometric wavelength demodulation system for an FBG strain sensor*," Photonics 2006, Hyderabad, December 2006.
- Wang. Q, Rajan. G, Wang. P and Farrell. G, "*Resolution of ratiometric system for wavelength measurement*," SPIE Europe: Optics and Optoelectronics, Prague, March 2007.

Acronyms

FBG	Fiber Bragg Grating
WDM	Wavelength Division Multiplexing
LPG	Long Period Grating
MMI	Multi-mode Interference
SMF	Single-mode Fiber
RWM	Ratiometric Wavelength Measurement
SNR	Signal-to-Noise Ratio
SSE	Source Spontaneous Emission
WGM	Whispering Gallery Mode
DWDM	Dense Wavelength Division Multiplexing
ECL	External Cavity Laser
PXI	PCI Extensions for Instrumentation
ADC	Analog to Digital Converter
PDL	Polarization Dependent Loss
PI	Polarization Insensitive
TEC	Thermal Expansion Coefficient
TOC	Thermo-optic Coefficient
V	Normalized Frequency
GF	Gauge Factor
CGF	Corrected Gauge Factor
BBS	Broadband Source
PCF	Photonic Crystal Fiber

Contents

List of Figures

List of Tables

Chapter 1

Introduction

A concise review of wavelength encoded fiber sensors such as fiber Bragg gratings and the different wavelength demodulation schemes used in fiber optic sensing is presented in this chapter. It is also intended to give a general overview of bend loss in optical fibers and its applications. This chapter also provides a specific account of the concepts and literature surveys that form the basis for the work presented in later chapters. The first section briefly discusses wavelength encoded fiber sensors and the necessity of a precise wavelength demodulation system for fiber Bragg grating sensors. The operating principle of the most common wavelength encoded optical fiber sensor, the fiber Bragg grating sensor, and the general requirements of an ideal interrogation system are also discussed. A quantitative review of different wavelength demodulation systems in optical fiber sensing involving components such as passive and active filters is presented in Section 1.2. The main research work proposed and presented in this thesis is the investigation of the suitability of employing bent single-mode fiber filter as an interrogation system for FBG sensors and there by achieving an all-fiber system. As a platform to the studies presented in later chapters, in Section 1.3 of this chapter a general overview of bend loss in single-mode optical fibers, the different theoretical approaches to determining bend loss in single-mode fibers and the application of bend loss in different areas are presented. In Section 1.4, the thesis synopsis is presented.

1.1 Wavelength encoded optical fiber sensors

Optical fiber sensors may be defined as a means through which a physical, chemical, biological or other measurand interacts with light guided in an optical fiber or guided to an interaction region by an optical fiber to produce an optical signal related to the parameter of interest. The advantages of fiber-optic sensing are well known and have been widely presented [1–3]. The inherent advantages of fiber optic sensors include their small size, passive nature, resistance to electromagnetic interference etc. A fiber optic sensor can be based on intensity modulation, phase modulation or spectral modulation of the light passing through the sensor. Fiber sensors based on intensity modulation and phase modulation principle have some problems that need to be solved in practical applications. The fluctuations of optical source power, loss in couplers and absorption effects which will significantly influence measurement performance of intensity based fiber sensors [4]. Measurement accuracy of phase-based fiber sensors is often compromised due to the existence of temperature drifts and vibration. Among the spectrally modulated fiber sensors the most promising developments are those based on grating technology, the fiber Bragg grating (FBG) [5, 6]. FBG sensors have attracted widespread attention and have been the subject of continuous and rapid development since FBGs were used for the first time for sensing purposes in 1989. In a fiber Bragg grating the measurand information is encoded in the reflected or transmitted wavelength from the grating. To extract the measurand information from the FBG sensor a wavelength demodulation system is required. Conventional spectrometers and monochromators are not an effective solution owing to their bulk-optical design, lack of ruggedness, low measurement speed and in some cases limited resolution. The limitations of the conventional systems led to research and development in the area of novel interrogators for optical fiber sensing, especially for FBGs. Two decades have passed since the use of FBGs began. Various ideas have been proposed and various demodulation techniques

have been developed for various measurands and applications. A review of the those developments are summarized in the later sections of this chapter.

1.1.1 Fiber Bragg grating sensors

An elementary fiber Bragg grating comprises of a short section of single-mode fiber in which the core refractive index is modulated periodically using an intense optical interference pattern [7, 8], typically at UV wavelengths. A schematic of an FBG is shown in Fig. 1.1. The periodic index modulated structure enables the light to be coupled from the forward propagating core mode into a backward propagating core mode generating a reflection response. The light reflected by periodic variations of the refractive index of the Bragg grating having a central wavelength λ_G is given by,

$$\lambda_G = 2n_{eff}\Lambda, \tag{1.1}$$

where n_{eff} is the effective refractive index of the core and Λ is the periodicity of the refractive index modulation.

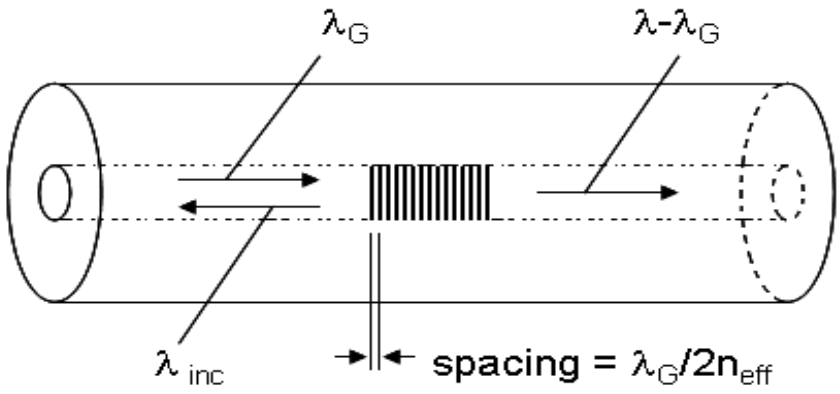

Figure 1.1: A fiber Bragg grating.

The basic principle of operation of any FBG based sensor system is to monitor the shift in the reflected wavelength with changes in the measurands like strain

or temperature. The principles of FBG sensing and its strain and temperature sensitivity are explained in Chapter 6 and in Appendix A.

Compared with other fiber-optic sensors, FBG sensors have a number of distinguishing advantages:

- The FBG sensor devices are simple, intrinsic sensing elements;
- FBGs can be directly written into the fiber without changing the fiber diameter, making them compatible with a wide range of situations where small diameter probes are essential;
- The signal obtained from an FBG sensor is encoded directly in the wavelength domain and this facilitates wavelength division multiplexing (WDM) of multiple sensors;

Most of the research on fiber Bragg grating sensors has focused on the use of these devices to provide quasi-distributed point sensing of strain or temperature [9]. FBGs have been also used as point sensors to measure pressure [10, 11], acoustic emissions levels [12–14], and to monitor the curing process of composites [15, 16].

1.1.2 General requirements of a wavelength measurement system for FBG sensors

The measurement of an unknown optical wavelength is common in many systems, either for test purposes or as an integral part of the operation of the system. Interrogators or demodulators in fiber grating sensor systems are the measurand-reading units that extract measurand information from the light signals coming from the sensor head. The measurand is encoded spectrally and hence the demodulators are usually meant to measure the Bragg wavelength shifts and convert the results to measurand data. In the laboratory, for experimental purposes one can use an optical spectrum analyzer, however it is not well suitable for real time

applications of optical sensing because of their high cost and low scanning speed. In the case of an FBG to resolve a temperature change of 1 ^0C or a strain change of 10 $\mu\varepsilon$ requires a wavelength resolution of about 10 pm at 1310 nm [17]. Thus, precision measurement of the FBG wavelength shift induced by the measurand is critical in achieving good sensor performance. The general requirements for an ideal interrogation method are as follows:

1. High resolution and accuracy with large measurement range: Typically a wavelength - shift detection resolution ranging from sub pico meters (<10 pm) is required for most applications. A wide wavelength range (tens of nanometers) is required when interrogating multiple FBGs with different Bragg wavelengths.

2. Compatiblity with multiplexing: An interrogation scheme should be able to cope with multiplexing topologies such as WDM.

3. High measurement speed: The measurement speed capabilities of the interrogation system should be good enough to measure dynamic strain and also to measure data from multiple FBGs if multiplexing is employed.

4. Cost effective: The cost of an interrogation system should be competitive with those of other optical sensors or conventional electrical sensors.

Conventional spectrometers have a typical resolution of 0.1 nm, hence they are normally only used for evaluation of the optical properties of FBGs during fabrication rather than for a precise wavelength-shift detection. Research on high resolution interrogation methods has been very active topic in recent years. A number of interrogation techniques have been reported for high resolution wavelength-shift detection. To achieve a low cost and commercially valuable FBG interrogation system, the system should be made of cheap raw materials such as unmodified single-mode fibers. One example for such an interrogation

system is an all-fiber system. However the optical fiber components have their own characteristic properties that may affect its performance. Hence, when such components are used in the interrogation system, it is necessary to study the characteristic properties such as polarization dependence of the components involved in the system and also the influence of any external parameters like temperature on the system. Another important factor that affects any measurement system is the noise associated with the system, which can limit the resolution of the system. Therefore, the system's dependence on any parameters that affect the resolution and accuracy needs to be minimized to achieve high performance in the interrogation system.

1.2 An overview of different demodulation techniques

Optical wavelength detection in sensing can be basically categorized into two types; passive detection schemes and active detection schemes [1, 18]. In passive schemes there are no power driven components involved. Examples in such cases are those based on linear wavelength dependent devices. In active detection schemes the measurement depends on externally powered devices and examples of this scheme include those based on tunable filters and interferometric scanning methods. A detailed review of different wavelength demodulation schemes is presented in the following sections.

1.2.1 Passive detection schemes

A passive detection scheme refers to those that do not use any electrical, mechanical or optical active devices in the optical portion of the system. Most of the passive devices are linearly wavelength dependent devices such as bulk edge filters [19, 20], biconical fiber filters [21], wavelength division couplers [22], gratings [24–26, 28], multimode interference couplers [29, 31] etc. Other passive devices

are those which perform by detecting the optical power of ASE sources [32] and CCD spectrometers [16].

Linear wavelength dependent devices

The simplest way to measure the wavelength change of light is to use a wavelength dependent optical filter with a linear response. This method is based on the usage of an edge filter, which has a narrow linear response range with a steep slope or a broad band filter, which has a wide range with less steep slope. In both cases, the wavelength-change interrogator is based on intensity measurement, i.e., the information relative to wavelength change is obtained by the intensity monitoring of the light at the detector as shown in Fig. 1.2(a). For the intensity based demodulators, the use of intensity referencing is necessary because the light intensity might be changed. This could occur not only due to a wavelength change but also due to a power fluctuation of the light source, a disturbance in the light-guiding path or the dependency of light source intensity on the wavelength. Generally, because of these factors, most of the edge filter based systems are used in a ratiometric scheme which renders the measurement system independent of input power fluctuations. Fig. 1.2(b) shows the schematic of a ratiometric wavelength measurement system based on an edge filter. The input light splits into two paths with one passing through the wavelength dependent filter and other used as the reference arm. The wavelength of the input signal can be determined using the ratio of the electrical outputs of the two photo detectors, assuming a suitable calibration has taken place. For the edge filter involved in a ratiometric system, the two important parameters are its discrimination range (wavelength attenuation range) and baseline loss (transmission loss at the starting wavelength). A ideal edge filter will have a very low baseline loss and a high discrimination range. In Fig. 1.2(c) the concept of discrimination range and baseline loss is shown. In the figure three spectral responses (A, B and C) with different discrimination ranges and baseline losses are shown. However the

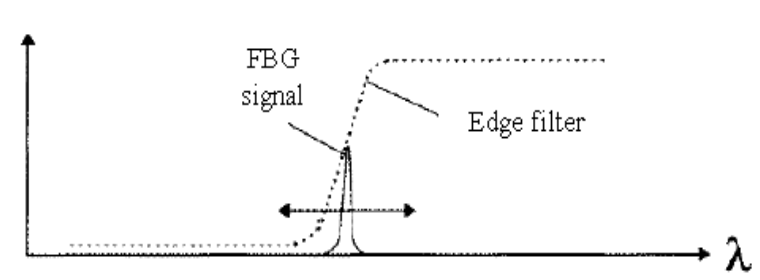

(a)

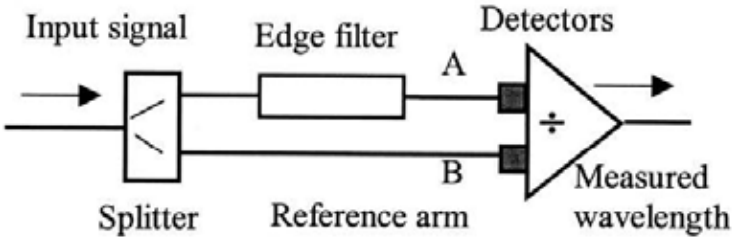

(b)

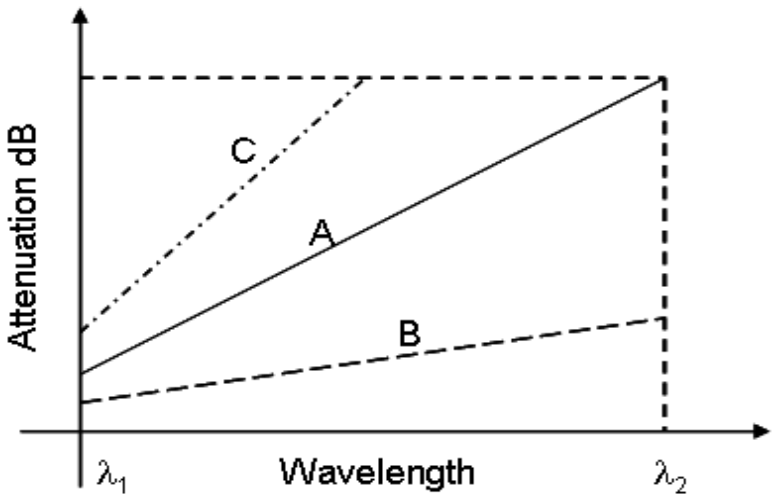

(c)

Figure 1.2: (a)Transmission response of an edge filter and the peak spectrum showing the FBG signal (b) Schematic of a ratiometric wavelength measurement system (c) Spectral responses of edge filters with different discrimination range and baseline loss.

selection of a proper response requires an optimization of the system which is explained in Chapter 2 of this thesis.

The first experiment based on a ratiometric scheme was reported in 1992 and used a bulk edge filter, a commercial infrared high-pass filter (RG830), which has a linearly wavelength dependent edge of 815 nm - 838 nm [19, 20]. Two configurations were used in this method, one with a single filter and other with filters of opposite polarities. The first configuration had a wavelength range of 23 nm while the second one had only 2.8 nm, but had higher sensitivity. Later on the use of a biconical fiber filter was proposed as an edge filter [21]. This filter is basically a section of single mode depressed-cladding fiber, which consists of a contracting tapered region of decreasing fiber diameter followed by an expanding taper of increasing fiber diameter. The wavelength response of the filter is oscillatory with a large modulation depth propagating only a certain wavelengths through the fiber while heavily attenuating others. The reported filter was designed with an oscillation period of 45 nm and an extinction ratio of 8 dB. Over the range 1520 nm - 1530 nm the filter shows a near linear response with a slope of 0.5 dB/nm.

Another type of passive wavelength filter is one based on a wavelength division multiplexing coupler which was first proposed by Mille *et. al.* and demonstrated by Davis and Kersey [22]. In this scheme the WDM coupler has a linear and opposite change in coupling ratios between the input and two output ports. The schematic of the WDM fiber coupler scheme is shown in Fig. 1.3. Compared to bulk edge filters the wavelength shift in this case results in no power loss but rather a change in the relative powers out of the coupler outputs. A highly over coupled coupler was also used to increase the steepness of the slope and hence the sensitivity. The use of a coupler based on a dichroic mirror sandwiched between two graded-index lenses has also been proposed for a similar purpose as well as to reduce polarization dependency [23].

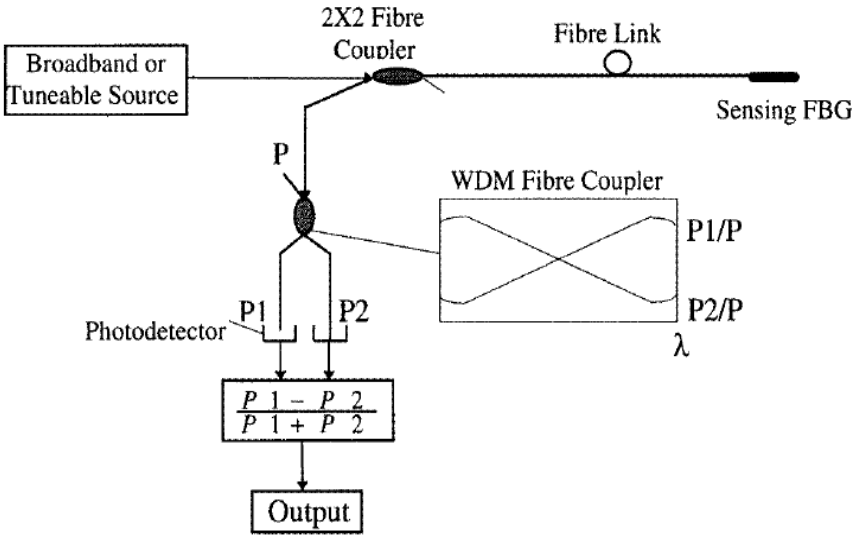

Figure 1.3: Schematic of a WDM fiber coupler scheme [21].

A substantially cheaper and simpler interrogation method is to use a grating to interrogate an FBG sensor or array of sensors. The first report of this method was based on a matched grating based on active methods, which is explained in later sections. The passive filters in this category are chirped gratings and long period gratings. Two identical chirped gratings with a quasi-square reflection spectrum are used as a sensor head and an interrogating filter [24]. Later fiber edge filters with an arbitrary spectral response based on tilted chirped grating structures were proposed [25, 26]. A long period grating (LPG) utilizes the spectral rejection profile to convert wavelength into intensity encoded information [27, 28]. LPGs are periodic structures that couple the guided fundamental mode in a single-mode fiber into forward propagating cladding modes. This coupling is wavelength dependent and hence, the grating acts as a loss element at certain frequencies. Commonly LPGs have a typical period between 300 μm - 600 μm.

The latest addition to the linear edge filter family are those based on multimode interference (MMI). Two types of edge filters based on MMI have been

reported, the first one was based on two-mode interference in an asymmetrically excited waveguide that is coupled to a Y-branch [29]. This device has a wavelength range of 30 nm. The other is an all-fiber edge filter, in which a multimode fiber section is sandwiched between input and output single mode fibers, utilizing multimode interference in the MMF section [30, 31]. Using this configuration a wavelength range of 50 nm is reported.

Power detection

In some fiber sensor applications, a simple detection of reflected or transmitted power is sufficient for the measurand interrogation. Instead of using a linearly wavelength independent optical filter, one can use a light source that has intensity linearly dependent on wavelength. An example is the amplified spontaneous emission (ASE) profile of an erbium doped fiber amplifier [32]. However, in this case reference power monitoring is necessary to avoid errors arising from the effects such as an optical source power fluctuation or a disturbance in a guiding path.

CCD spectrometer

One of the wavelength- change interrogators suitable for multipoint fiber grating sensors is parallel detection using a detector array such as a CCD [16]. Light of different wavelengths is directed to a fixed diffractive element such as finely ruled diffraction gratings and then focused on to a CCD. For a light incident to the diffraction grating, the diffraction angle is dependent on the wavelength of the light. Therefore, light with different wavelengths illuminates different areas of pixels. The change in the light wavelength results in the shift of the light at the detector array of the CCD, which is detected electronically. This system can be used as a wavelength change interrogator for multiple FBG sensors.

1.2.2 Active detection schemes

Active detection schemes usually involve tracking, scanning, or modulation mechanisms to monitor the wavelength change. In general although the active detection schemes require more complex systems compared to passive detection schemes, the active schemes show better resolution (1 pm) [33–41]. Based on the operating principles, active schemes can be classified into two categories; tunable filer and interferometric scanning.

Tunable filter

A tunable filter can be used to measure the wavelength shift of an FBG. As shown in the Fig. 1.4. when the spectrum of the filter matches that of the FBG, maximum output occurs and by measuring this maximum and the corresponding wavelength change of the tunable filter, the wavelength shift of the FBG can be obtained. The measurement resolution is mainly determined by the signal-to-noise ratio of the return FBG signal and both the line widths of the tunable filter

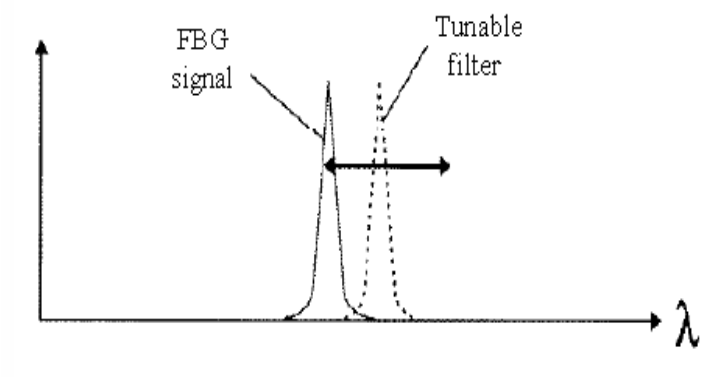

Figure 1.4: Principle of a tunable filter method.

and the FBG. Normally, such an approach has a relatively high resolution plus a large working range. One disadvantage of this method is the time taken for the filter tuning to settle on the FBG peak. The common wavelength interrogators based on the principle of tunable filters are an FBG based tunable filter [33],

Fabry-Perot (FP) tunable filter [34] and tunable acousto- optic filters [35–37].

In the first case the wavelength shift of the sensing FBG can be detected with a tunable FBG-based filter which is formed by wrapping a receiving FBG, with the same properties as the sensing FBG, onto a cylindrical piezoelectric transducer (PZT) or other fiber stretchers. When a voltage is applied to the PZT, the receiving FBG is stretched by the PZT and hence the Bragg wavelength of the receiving FBG is tuned due to the applied strain [33]. The measurement range and accuracy of this method are mainly constrained by the characteristics of the PZT used.

Tunable F-P filters have become important for spectral noise rejection for fiber optic amplifiers used in optical fiber telecommunications. One of the distinguishing features of a tunable F-P filter is that the operational range is large (typically tens of nanometers). A modulation system using a high-finesse fiber F-P filter tuned by a piezoelectric element has been reported [34] and a resolution of 1 pm over a working range of more than 40 nm has been demonstrated for a single FBG sensor. This scheme has also been used for WDM of multiple FBG's on a section of fiber by scanning the F-P filter with a triangular spectral waveform. The resolution of this scheme is mainly limited by the finesse of the F-P cavity.

Compared with the two schemes mentioned above, an acousto-optic tunable filter has a much wider wavelength tuning range (up to a few micrometers) [35]. Therefore, this device could be potentially very attractive in the context of both demodulation and multiplexing of a large number of FBG sensors if a light source or a source array with a similar bandwidth were available. A block diagram of an interrogation scheme with such a device is shown in Fig. 1.5 . The wavelength of the light transmitted by the acousto-optic filter is a function of the RF frequency which is generated by a RF signal generator. To lock the mean optical wavelength of the filter to the instantaneous wavelength of the sensing FBG, a feedback signal is generated by dithering the applied RF frequency about a nominal value

and detecting the amplitude modulation of the received optical carrier. When the mean wavelength of the filter coincides with the FBG wavelength, the amplitude modulation is zero [36]. The amplitude modulation is produced by using a voltage-controlled oscillator with a low frequency square wave input plus a DC bias signal to tune the mean frequency. This system has been applied to temperature measurement and an initial temperature sensitivity of -0.95 kHz ${}^0C^{-1}$ has been achieved. Due to the wide bandwidth of the filter used (typically a few nanometers), the measurement resolution is limited. High resolution detection of <1 pm has also been reported [37] using an acousto-optic tunable filter with a much smaller bandwidth of 0.2 nm and a measurement range of 120 nm.

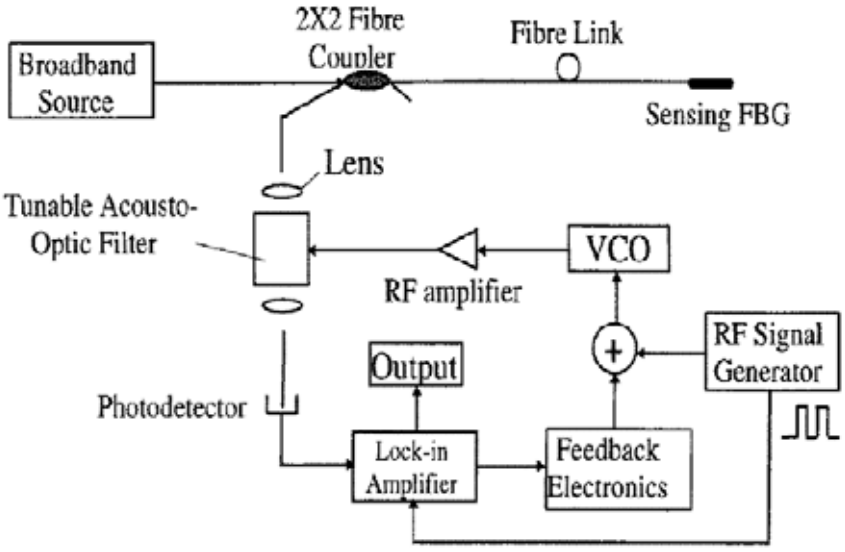

Figure 1.5: Schematic of the tunable acousto-optic filter [35].

Interferometric Scanning

The FBG wavelength shift induced by strain and/or temperature can be detected with a scanned interferometer (SI), which has been demonstrated for high-resolution dynamic and quasi-static strain measurements, known as the interferometric scanning method [38]. The principle of interferometric scanning method

is shown in Fig. 1.6.

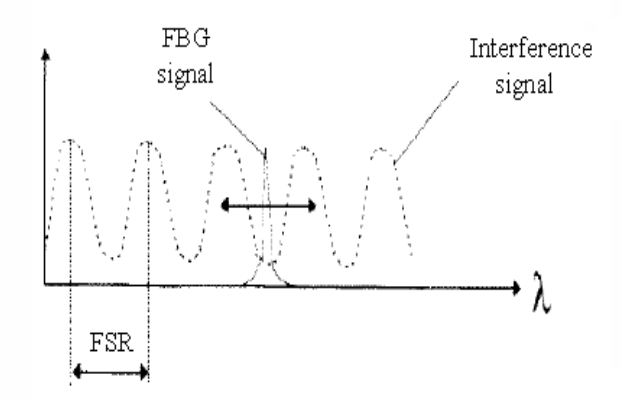

Figure 1.6: Principle of interferometric scanning method.

The normalized interference signal from a scanned interferometer (SI), can be expressed as

$$\frac{I}{I_0} = 1 + Bcos[\Delta\Phi_B + \phi(t)], \tag{1.2}$$

Where I_0 is the intensity of the incident light and B the visibility of the interference signal. $\phi(t)$ is the thermally induced phase drift in the SI. The SI acts as a wavelength scanner for FBGs when the optical path of the SI is modulated. The strain or temperature induced change in the reflected wavelength from a FBG produces a change in the optical phase $\Delta\Phi_B$:

$$\Delta\Phi_B = -\frac{2\pi\Delta Ł_{SI}}{\lambda_B^2}\Delta_B = -\frac{2\pi\Delta Ł_{SI}}{\lambda_B}\xi_g\Delta_Y, \tag{1.3}$$

where Δ_Y is the variation in strain or temperature applied to the FBG and $\Delta Ł_{SI}$ is the optical path difference (OPD) of SI. ξ_g is the normalized FBG sensitivity for strain or temperature, given by $\xi_g = (1/\lambda_B)/(\delta Y)$. Hence, the phase sensitivity in response to strain or temperature $\Delta\Phi_B/\Delta_Y$ is directly proportional to the OPD in the SI. By measuring $\Delta\Phi_B$ with the pseudo- heterodyne processing scheme, the strain or temperature change can be determined.

An interrogation system using the interferometric scanning method is shown in

Fig. 1.7 in which an unbalanced fiber Mach-Zehnder interferometer is used as the wavelength scanner for dynamic strain measurement [39]. Furthermore, a single frequency FBG fiber laser sensor [40] with a similar interrogating arrangement has also been demonstrated [41]. A strain sensitivity of $5.6 \times 10^{-5}\, n\varepsilon\, Hz^{-1/2}$ at 7 kHz was obtained with a 2.5 cm long laser cavity and a readout interferometer with an OPD of 100 m. The interferometric scanning scheme has achieved the highest resolution among the current detection methods, but the phase measurements make the system complex.

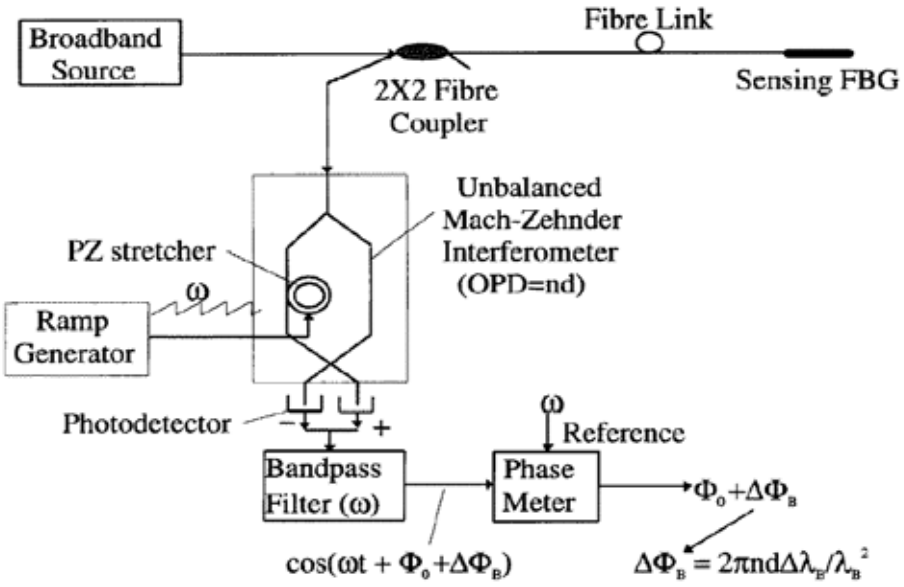

Figure 1.7: Schematic of the interferometric scanning scheme [38].

1.2.3 Advantages and disadvantages of active and passive systems

Active and passive schemes are common as interrogating systems in FBG sensing. Both systems have their own advantages and disadvantages. No single wavelength demodulation system can accommodate the wide wavelength range and resolution required in different applications. Passive systems are more common

given the cost effectiveness and also ease of use compared to active systems, but to achieve the highest resolution, active systems such as interferometric methods are preferable. However interferometric methods requires complex signal processing methods to retrieve phase information which in turn yields the wavelength information. Furthermore active systems are very slow compared to passive systems. Some of the real time applications require very high measurement speed, especially when used in different multiplexing topologies. Most of the passive systems are based on intensity based wavelength decoding and scanning speed does not limit their operation. The speed of the detector electronics is the only limit on their measurement speed and this can be improved by using high speed detectors. Thus, where very high resolution and single point measurement is needed, active systems are more suitable, whilst for multi point measurements with high speed, passive wavelength demodulators are preferable. A comparison of common passive interrogation systems and their strain resolution, dynamic range and wavelength range is presented in Table 1.1. From the table it can been seen that most of the passive systems, wavelength range is limited and not all the parameters have been determined. This points out the requirement of further research and development of passive demodulation schemes for FBG sensors.

1.3 Bend loss in single mode fibers

Since the advent of optical waveguides the phenomenon of bend-induced losses have been recognized [42, 43]. In general bend losses fall into two broad categories; micro bend loss and macro bend loss. Losses in optical fibers that are basically due to periodic axial micro deformations or minute distortions in the fiber is termed as micro bend loss and have been used as the transduction mechanism in intensity modulated optical fiber sensors. Macro-bend loss is referred to as the radiative loss that occurs when the bend radius is relatively small. Generally, macro-bend losses strongly increase as the bend radius decreases and also for longer

Edge filters	Static Strain $\mu\varepsilon$	Dynamic Strain $\mu\varepsilon/\sqrt{Hz}$	Dynamic range	Wavelength range nm
Bulk optical filter S. M. Mille et al.	-	3.6	28 dB	23
Wavelength division coupler M. A Davis et al.	3	0.5	-	40
Biconical Filter A. Ribeiro et al.	3.5	1.5	-	20
Long period gratings R. W. Fallon et al.	0.5	-	8100 $\mu\varepsilon$	20
Chirped tilted Bragg Gratings Y. Liu et al.	-	-	-	20
MMI Based structures B. Mason et al.	-	-	34 dB	30

Table 1.1: A comparison of different passive interrogation systems.

wavelengths. Although, it could be oscillatory due to the interference of light reflected at the cladding-coating boundary and or at the outer coating surface with the propagation mode [44, 45]. Bend loss in optical fiber attracts a lot of attention in fiber and cable manufacturing, as minimizing the bend loss improves telecommunication networks, while in the sensing area it attracts attention as a transduction mechanism to measure different parameters. Over the last two decades researchers have developed various experimental or theoretical methods for calculating bend loss in optical fibers [44–52] and applying the techniques to a variety of requirements in sensing and elsewhere [53–58].

Power losses in the core of a single-mode fiber, due to a uniform bend, result mainly through two mechanisms [45, 53]. When the fiber is bent energy can be dissociated from the wave front at a point where the angular phase velocity of the light in the bend region exceeds the allowed velocity of light in the medium which is called the pure bend loss. The second type of power loss is attributed to

a mismatch in the mode profiles between straight and bent waveguide segments and is termed as transition loss. Both mechanisms may occur simultaneously for a particular fiber geometry.

1.3.1 Pure bend loss

The schematic representation of a bent single mode fiber core profile shown in Fig. 1.8(a) explains pure bend loss. In the straight region of the fiber before the bend, the transverse mode of power, P_o, is confined to the core so that it propagates along the fiber axis. While in the bend region of radius r_b and angle Φ the confining path is circular and hence modal wave front will propagate with a velocity linearly dependent on the radial distance from the center of curvature of the bend. A guided mode when propagating around a bend must maintain the same angular phase velocity at all points over the plane that is transverse to the propagation direction. That is at a certain radial position outside the bend known as critical radius r_c (radiation caustic), the mode tangential velocity is equal to the speed of the light in the medium. At radii beyond this, the velocity exceeds that of light and hence as shown in Fig. 1.8 the power in the shaded tail P_c propagates along a tangential path and thus radiates away. The resultant reduced guided power is given by

$$P(r_b, \Phi) = P_o - P_c \tag{1.4}$$

Loss of power in the fiber core through this mechanism is known as pure bend loss. For a single mode fiber of length L, the pure bend loss can be calculated using the equation,

$$L_s = 10log_{10}[exp(2\alpha L)] = 8.8686\alpha L, \tag{1.5}$$

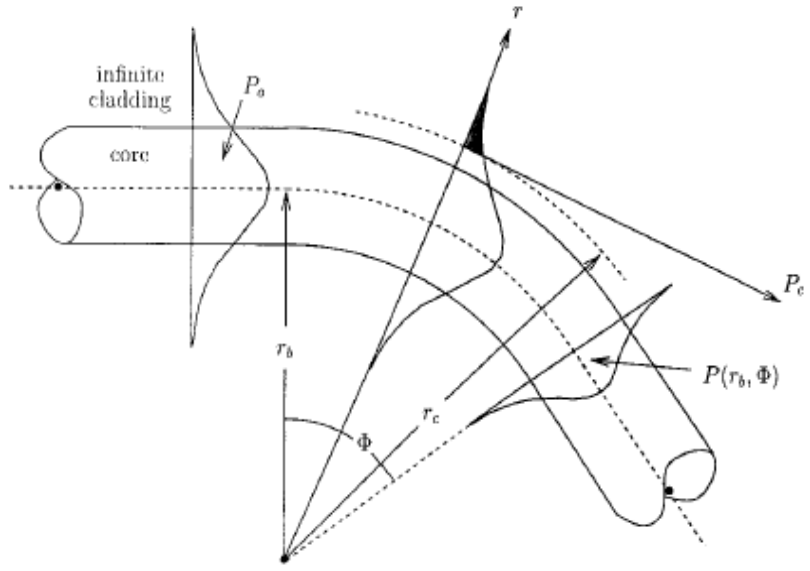

(a)

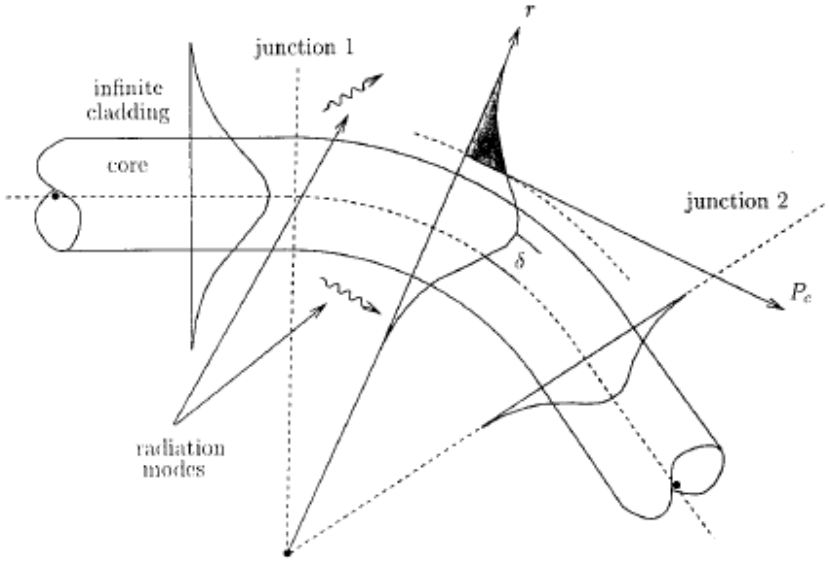

(b)

Figure 1.8: (a) Pure bend loss mechanism (b) Transition loss mechanism [53].

where α is the bend loss coefficient which is determined by the fiber structure, bending radius and wavelength of the light. Most theoretical investigations on fiber bend losses are focused on the calculation of this bend loss coefficient [44–52].

1.3.2 Transition loss

Transition loss arises due to the changes in the mode field characteristics when the fiber is bent. The mode profiles in the straight and the bent fiber segments are not identical and this leads to an incomplete transformation of a guided mode in the straight section into a superposition of guided modes in the bent section. As shown in Fig. 1.8(b) in the bend the central maximum of the mode profile is shifted radially outward by a distance δ in comparison with the straight fiber segment mode profile. At junction 1 between the straight and the bent fiber segments, a portion of the incident power excites the guided mode in the bent segment and the remaining power is coupled to the radiation modes in the cladding region. This power coupling process between the guided and the radiation modes also occurs at junction 2. The total transition loss resulting from the presence of the bend takes into account the losses that occur at both junctions. The mode shifting also has the effect of enhancing the pure bend loss by increasing the power in the shaded tail region.

1.3.3 Calculation of bend loss in single-mode fibers

Conventional theories assume the simplified model of a fiber with an infinitely extending cladding and consequently predict a monotonic increase of the losses with wavelength or curvature. However, it has been shown experimentally that the finite dimensions of the cladding and the presence of coating can significantly affect the loss behavior [48–51]. Oscillations of the losses versus both the wavelength and the bending radius have been observed and have explained this behavior by the coupling of the fundamental mode with the so-called whispering gallery mode (WGM) [54]. Researchers have presented several analytical expressions for mod-

eling the fiber bend loss. There are mainly two types: one treats the fiber to be a 3-layer structure (taking the cladding to be infinite) [47] and the other treats the fiber to be 5-layer structure (considering the interface between the cladding and the coating) [48, 49]. As for these analytical expressions, the transition loss between the straight fiber and the bending fiber is neglected.

A practical fiber will have one or two coating layers over the cladding to offer mechanical protection. The existence of the coating layers will produce whispering gallery modes in the bent fiber due to the reflection of the radiated field at the interface between the cladding and the coating layer. The 5-layer structure considers only one coating layer and later another model is proposed considering two buffer coatings [50]. This was the first reported model of a practical bent fiber. The bent geometry is shown in Fig. 1.9. However, this method only considers the reflection of the outer most interface, i.e., between the outer coating layer and air.

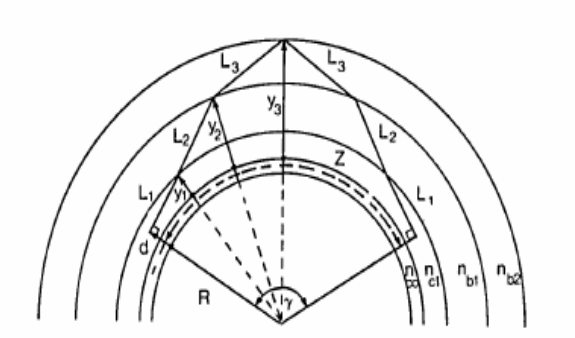

Figure 1.9: Geometry of the WG mode interference model for a two layer buffered fiber [48].

In the approach proposed by Wang *et. al.* [51] the bend loss of a standard single mode fiber is presented by considering multiple buffer coatings. It is also shown that the most of the radiated field is absorbed in the inner coating layer and the so-called elasto-optical correction factor is not required for the standard single mode fiber (SMF28). Most of the models use the elasto-optical correction factor or a so-called effective bending radius to make the calculated bend losses

agree with the experimental results due to the refractive index change caused by the bending stress. The simulation and experimental results from [51] show a comparison of all the models and is shown in Fig. 1.10. Throughout this thesis the model proposed Wang *et. al.* is followed as it is applicable to standard single fiber SMF28, which is also used in this research.

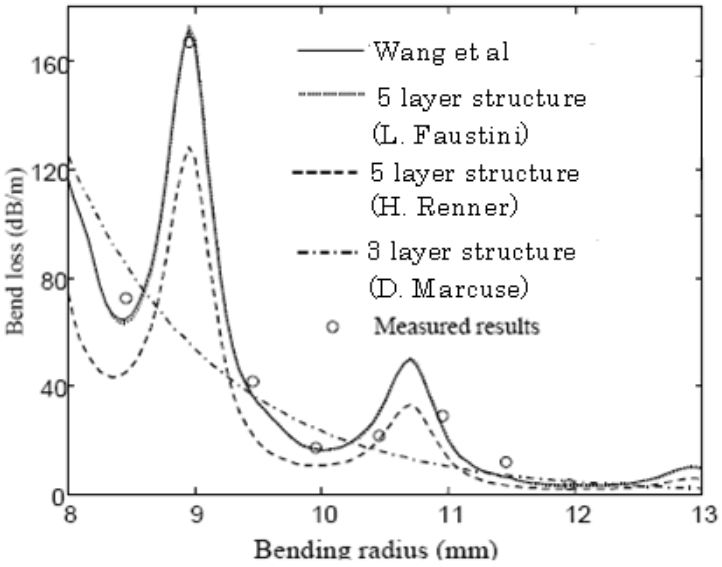

Figure 1.10: Calculated bend loss using different models and its comparison with the measured bend loss [51].

1.3.4 Applications of bend loss in optical fibers

For most of the applications which use optical fibers, such as in communications, the phenomena of bend loss is a disadvantage because of its adverse effect on the power budget. However, it has also been exploited in a range of practical devices [55–58]. It has been used as a transduction mechanism in fiber optic sensors such as water level sensors and displacement sensors. It has been used as a means to monitor the optical power level in fibers without breaking the transmission path. The dependence of loss on wavelength is especially important with developments in wavelength division multiplexed systems in both communications and in sen-

sors that use multiple wavelength techniques [59]. The bend loss properties of the fiber have also formed the basis in many fiber optic components. The whispering galley mode of a bent fiber is also being made used for high temperature sensing applications [60]. Thus, even though the bend loss in a general sense is a drawback of optical fibers, it does form the basis of a number of promising applications.

1.4 Objective of the Thesis

This thesis presents an application of bend loss in single-mode optical fiber for wavelength measurement in an FBG sensing system. In this thesis a macro-bend fiber filter utilized in a ratiometric scheme is proposed for wavelength measurements. From a system point of view, parameters such as the signal-to-noise ratio (SNR) of the source and noise in the receivers strongly influence the performance of the proposed system. The first objective of this thesis is to develop and verify a general model for an edge filter based ratiometric wavelength measurement system that takes account of such noise effects.

For any fiber based system polarization and temperature dependence are two main parameters that affect the system performance. A second important objective of this thesis is to analyze the impact of the polarization and temperature dependence of the edge filter and other components in a ratiometric system on wavelength measurements.

A key objective of the thesis is to investigate the use the proposed wavelength demodulation system to interrogate multiple FBG sensors, taking into account the influence of different phenomena such as source SNR, receiver noise, polarization and temperature, that affect the performance of the system. This objective involved carrying out an analysis of the system considering all these phenomena in order to develop a low cost FBG interrogation system with a competitive resolution and accuracy with a target of a wide wavelength range of 100 nm (from

1500 - 1600 nm) coupled to a resolution of 10 pm.

Finally an ancillary objective of this thesis is refinement of another application of the bend loss: a temperature sensor based on a high bend sensitive single-mode fiber, by obtaining a direct linear relation between bend loss in a single mode fiber and temperature for the first time.

1.5 Thesis synopsis

The subject of this thesis is to investigate the suitability of the phenomena of bend loss in a single-mode optical fiber to measure unknown wavelength with high precision and resolution over a wide wavelength range, for use specifically as a demodulation technique for wavelength encoded fiber sensors such as FBGs. In the first chapter an overview of different wavelength demodulation systems for fiber Bragg grating sensors is provided. This is followed by an introduction to bend loss and the different models used to predict bend loss in single-mode fibers, which provides an insight to the possibility of using bend loss phenomena in single-mode fibers as the basis of a method to measure the wavelength of an optical signal.

In Chapter 2 a theoretical analysis of transmission and ratio response of an edge filter based ratiometric system is initially presented. The wavelength measurement system involving the source, the edge filter and the photodiodes is modeled and the simulated transmission response and ratio response of the edge filter and system is presented in the first portion of this chapter. The use of a macro-bend single-mode fiber as an edge filter is also introduced in this chapter. The design and surface processing methods needed to utilize the macro-bend fiber as an edge filter and to use it as a wavelength measurement device is explained in Section 2 of this chapter. In the last section of the chapter experimental investigations to verify the theoretical findings are presented.

Chapter 3 presents the fundamentals of optoelectronic receivers and the dif-

ferent noise mechanisms of the receivers. Theoretical modeling, analysis and experimental investigation of the effect of noise on an edge filter based ratiometric are presented in this chapter. A basic noise model for a ratiometric system considering both optical and electrical noise is introduced. Theoretical and experimental investigations on the resolution of the system in the presence of noise is also presented in this chapter.

Chapter 4 is dedicated to the studies of the polarization properties of the components of the system and its effects on the performance of the system. The polarization dependent loss (PDL) of the components of a ratiometric system and the corresponding ratio fluctuation of the system is modeled, from which the accuracy of the measured wavelength can be estimated and is verified experimentally. Eliminating the polarization dependent loss is essential when macro-bending single mode fiber is utilized as an edge filter to ensure high accuracy. A new bending configuration to eliminate the PDL of a fiber edge filter is proposed in this chapter by twisting the fiber by 90^0 between two bending sections with equal length. The PDL of a 3 dB coupler and its influence on ratiometric wavelength measurement system is also investigated in this chapter.

Chapter 5 presents the temperature dependence studies of an all-fiber wavelength measurement system. The effect of temperature on bend loss filters using the standard single-mode fiber and a special fiber with high bend loss, and its effect on wavelength measurements are studied. Fiber filters without a buffer and with an absorption coating give a linear drift in ratio with temperature, which can be accounted by proper temperature calibration while other fiber filters may require active temperature controllers to maintain the temperature of the system to provide high accuracy. The studies of the temperature dependency of fiber edge filters also leads to the development of a new all-fiber temperature sensor based on a macro-bend fiber loop, which is presented in the last section of this chapter.

Chapter 6 presents the application of the developed macro-bend fiber edge filter based wavelength measurement technique as an interrogation method for fiber Bragg grating sensors. Analysis of the whole system and optimization of the slope of the filter considering all the parameters for an FBG array with peak wavelengths between 1525 nm - 1575 nm has been carried out. Performance evaluation of the system has been carried out and temperature, static strain and dynamic strain measurement is measured with the developed system. A method to measure reference strain in FBG strain sensor involving actuators is also presented in this chapter.

Finally the overall conclusions arising from the research and future research plans are presented in Chapter 7.

Chapter 2

Transmission and ratio response of a macro-bend fiber based wavelength measurement system

2.1 Introduction

A passive measurement technique based on ratiometric wavelength measurement (RWM) scheme employs an edge filter and utilizes the transition region of its transmission response. Earlier investigations on the ratiometric scheme have mainly focused on different types of edge filters. However, the effect of various parameters such as the signal-to-noise ratio (SNR) of the source were not investigated in detail. In principle a ratiometric scheme should allow for measurement of the wavelength of an input signal without a dependency on the parameters of the input signal such as signal power or signal-to-noise ratio. Initial investigations on the transmission response show that the the SNR has a significant impact on the measurable wavelength range of the system [61]. Defining the transmission response, specifically the wavelength range and slope of the edge filter response is the first step in the design of edge filter based ratiometric wavelength measurement system. In any system that uses a tunable laser or a similar source, source spontaneous emission (SSE) produces noise and the SNR deteriorates, impacting the performance of the system. For example a strongly reduced SSE is recommended for many applications involving dense wavelength division multiplexing

(DWDM) [62]. In this chapter extensive investigations on the factors determining the slope and wavelength range of an edge filter based ratiometric system is presented. To begin with, in Section 2.2 a theoretical modeling and analysis of the transmission and the ratio response of a general edge filter based ratiometric system is presented. The wavelength dependency of the 3 dB coupler which is an essential component in any ratiometric system is presented. A study on the influence of SNR on the transmission response of the edge filter and ratio response of the system is also presented in this section.

The exploitation of a macro-bending fiber as an edge filter is introduced in Section 2.3. For a macro-bending single-mode fiber, earlier investigations were focussed on how to predict and lower the bend loss, which is regarded as an adverse effect in the context of light transmission. However in contrast with this, the bend loss phenomenon in single-mode fiber can be utilized to measure unknown wavelengths. Compared with the existing passive and active wavelength measurement techniques macro-bend fiber has a simple configuration with no mechanical movement involved and offers a potential for high speed measurement [63, 64]. The design and surface processing methods that allow a macro-bend fiber to act as an edge filter and to be used as a wavelength measurement device are explained in this section. Experimental investigations to verify the theoretical findings are presented in Section 2.4. The summary of the investigations and findings are presented in Section 2.5.

2.2 Theoretical modeling and analysis of an edge filter based ratiometric system

As explained in Section 1.2.1, an edge filter provides a steep linear response with wavelength, and can be used in a ratiometric scheme to measure wavelength. Intuitively it could be argued that it is important that the slope of the response is as large as possible to achieve higher resolution if the system is not affected by

any other parameters. The schematic configuration of a ratiometric wavelength-measurement system employing an edge filter was shown in Fig. 1.2(b). The input signal is split into two equal signals. One passes through a reference arm (arm B) and the other passes through the edge filter (arm A). Two identical photodiodes are placed at the ends of both arms. The system effectively operates as a discriminator, where the ratio of the power levels reaching the photo detectors is wavelength dependent. The wavelength of the input signal can then be determined, assuming a suitable system calibration has taken place.

2.2.1 Ratio response of the system considering source SNR

In practice a narrow-band input signal with a center wavelength λ_0 could originate from a tunable laser source or a reflection from a fiber Bragg grating. Such an input signal can be approximated as a Gaussian function with a spectral width $\Delta\lambda$ and center wavelength λ_0 [65, 66]. An input signal from any source generally has a limited SNR, which means that there is measurable power even far from the center wavelength of the spectrum. For example in Fig. 2.1, the typical spectral distributions of the output intensity from a tunable laser at different central wavelengths, measured by an optical spectral analyzer in a wavelength range from 1500 nm - 1600 nm are shown. From these measured spectral distributions it can be seen that, for this tunable laser the source spontaneous emission ratio is >40 dB and it has different values for different output center wavelengths. Taking account of the SNR, the output spectral response of the source can be described as [67, 68] (the power at the peak wavelength is assumed as 0 dBm),

$$10\log_{10}[I_{\lambda_0}(\lambda)] = \begin{bmatrix} 10\log_{10}(exp[-4\ln 2\frac{(\lambda-\lambda_0)^2}{\Delta\lambda_0{}^2}]), & |\lambda-\lambda_0| \leq \Omega, \\ -S + Rand.Rs, & |\lambda-\lambda_0| > \Omega \end{bmatrix}, \tag{2.1}$$

where S is the SNR of the source. To describe the random fluctuations in the noise floor of the optical source, the term *Rand.Rs* is used, where *Rand* is

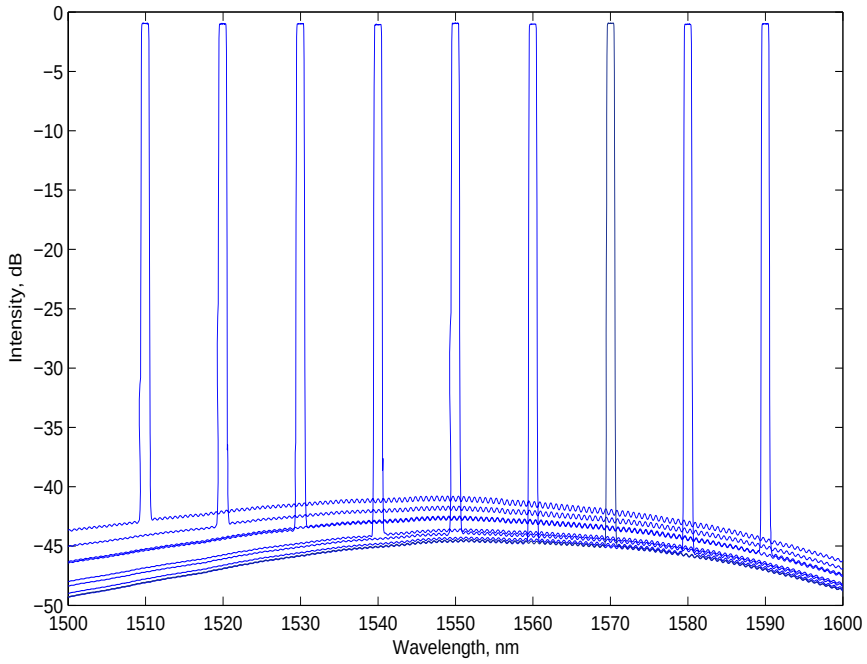

Figure 2.1: Intensity distribution of a typical tunable laser source in the wavelength region 1500 nm to 1600 nm.

a random number (between +0.5 and -0.5) and Rs is a parameter in dB which dictates the peak fluctuation in the SNR and is dependent on the nature of the source. Ω is a parameter which is determined by the noise level and can be determined for a source with a given SNR from the relation:

$$10log_{10}\Big[\exp(-4ln2\frac{\Omega^2}{\Delta\lambda_0^2})\Big] = -S \tag{2.2}$$

It is assumed that the transmission response of the edge filter is $T_f(\lambda)$. A simple description of the transmission response $T_f(\lambda)$ of an edge filter in a wavelength range (λ_1, λ_2) is a linear function, i.e.,

$$T_f(\lambda) = T_f(\lambda_1) + \frac{T_f(\lambda_2) - T_f(\lambda_1)}{(\lambda_2 - \lambda_1)}(\lambda - \lambda_1) \tag{2.3}$$

It is known that photodiodes integrate optical power over a wavelength range in converting optical power to a current. Therefore, the basic equation for ratio of

the system, which is the ratio of the outputs of the photodiodes at a wavelength λ_0 can be expressed as:

$$R(\lambda_0) = -10log_{10}\Big[\frac{\int I_{\lambda_0} T_f(\lambda) d\lambda}{\int I_{\lambda_0} d\lambda}\Big] \tag{2.4}$$

From this equation it can be seen that for an ideal source, i.e., where the SNR is infinite, the integral power measured by the photodiode is the same as the peak power for the central wavelength and hence the ratio $R(\lambda_0)$ of the system is identical to the transmission response $T_f(\lambda)$ of the edge filter.

2.2.2 Wavelength dependency of the 3 dB coupler

Ideally, the coupler used in ratiometric wavelength measurements should be wavelength flattened, i.e. the splitting ratio should have negligible wavelength dependence over the operating range. But a typical commercially available wavelength flattened fused optical fiber 3 dB coupler are not ideal and hence would not satisfy the above condition [69].

Fig. 2.2 shows the measured output power variation of a wavelength flattened 3 dB coupler when wavelength varies from 1500 nm to 1600 nm. From the figure it is clear that the wavelength dependency of the 3 dB coupler has to be considered in the design of a wavelength measurement system.

Considering the coupler as a wavelength dependent device and having a linear response, for each of the arms of the coupler in a wavelength range (λ_1, λ_2), their responses S_1 and S_2 can be expressed as a linear fit to the above measured response as,

$$S_1(\lambda) = S_1(\lambda_1) + \frac{S_1(\lambda_2) - S_1(\lambda_1)}{(\lambda_2 - \lambda_1)}(\lambda - \lambda_1) \tag{2.5}$$

$$S_2(\lambda) = S_2(\lambda_1) + \frac{S_2(\lambda_2) - S_2(\lambda_1)}{(\lambda_2 - \lambda_1)}(\lambda - \lambda_1). \tag{2.6}$$

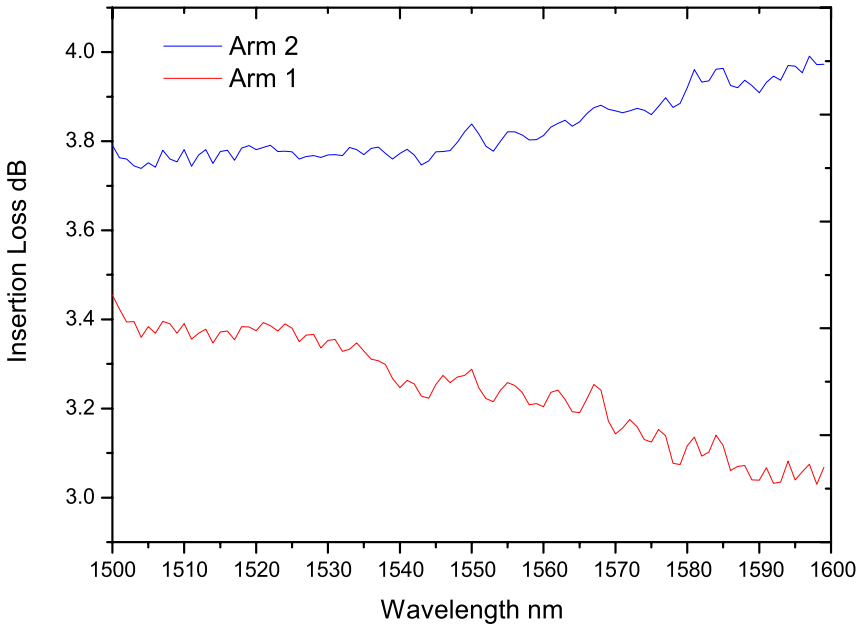

Figure 2.2: Response of a 3 dB coupler versus wavelength (T=20 ^{0}C).

When a wavelength dependent 3 dB coupler is connected to an edge filter of transmission response $T_f(\lambda)$, the ratio response of the system expressed in Equation (2.4) has to be modified as given below [70],

$$R(\lambda_0) = -10log_{10}\Big[\frac{\int S_1(\lambda)T_f(\lambda)I_{\lambda_0}(\lambda)d\lambda}{\int S_2(\lambda)I_{\lambda_0}(\lambda)d\lambda}\Big] \tag{2.7}$$

2.2.3 Influence of SNR on the transmission and response of the system

With the linear filter transmission response defined in Equation (2.3) and the ratio response as in Equation (2.4) and (2.7), the performance of the ratiometric wavelength-measurement system is modeled. It is assumed that the input signal has an SNR of 50 dB in a wavelength range from 1500 to 1600 nm with a maximum noise floor fluctuation (Rs) of 1 dB. Six edge filters are considered with discrimination range varying from 10 dB to 60 dB with an increment of 10 dB for a wavelength range of 1500 nm - 1600 nm. It is also assumed that for all edge

filters $T_f(\lambda_1) = 0$, i.e. the baseline loss is zero. Two cases are considered in the modeling; one assuming the 3 dB coupler is an ideal wavelength flattened coupler and the second one assuming the 3 dB coupler is wavelength dependent.

In the second case, for the simulation of the ratio response, it is assumed that the 3 dB coupler has a linear response as given by the Equations (2.5) and (2.6). In general depending on the wavelength dependence depth, the coupling ratio of the arms of the coupler vary from the ideal 50:50. To be consistent with the experimental results in the simulation a linear fit of the measured response of the arms of the 3 dB coupler used in the experiment as shown in Fig. 2.2 is taken, whose coupling ratio varies from 51 % to 54 % for arm 1 and from 49 % to 44 % for arm 2 when the wavelength changes from 1500 nm - 1600 nm. Arm 2 is assumed to be connected to the edge filter. Fig. 2.3(a) presents the numerical results of the transmission response of the edge filter and ratio response of the system with an ideal 3 dB coupler. In Fig. 2.3(b) the comparison of the ratio of the system with a wavelength dependent and wavelength independent 3 dB coupler is presented.

From these results one can see that, with the increase in slope of the transmission response of the edge filter, the calculated ratio R starts to diverge from the transmission response of the edge filter in the higher wavelength regions. This happens because at higher wavelengths the transmission power from the edge filter is increasingly affected by the total noise power, which results from the limited SNR of the source. This indicates that the straight forward design approach, which assumes higher resolution for systems with higher filter slope for the entire wavelength could be wrong because of the non-linearities at higher wavelengths. Thus, there exists a maximum permissible slope for the transmission response of the edge filter beyond which significant measurement error will occur because of the finite SNR of the signal source. It is also clear from Fig. 2.3(a) that the response of the 3 dB coupler is added to the original response of the edge filter

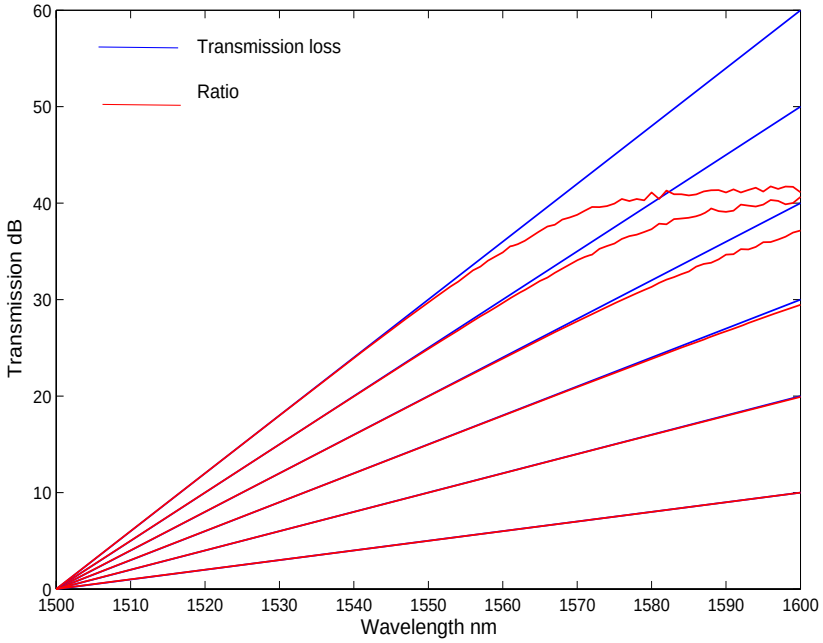

(a)

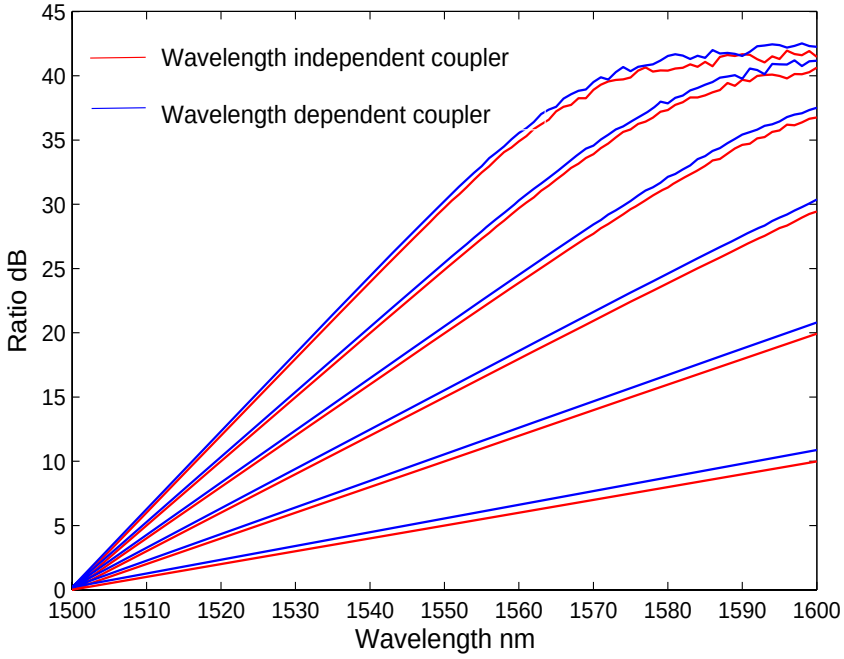

(b)

Figure 2.3: Comparison of responses at an SNR of 50 dB (a) Transmission response of the edge filter and ratio of the system with wavelength independent coupler (b) ratio response of the system with wavelength dependent and wavelength independent couplers.

and hence, in the design of any ratiometric wavelength measurement system the response of the coupler must be accounted for.

Fig. 2.3(a) and 2.3(b) gives the ratio response of the the system with edge filters of different slope at a fixed SNR of 50 dB. Practically for wavelength measurement practice there is always a possibility that the input signal's SNR may change from that used in the initial calibration. This can happen, for example, when the system is switched to a different source. In such cases the measured wavelength will have an error. In order to estimate the accuracy of the wavelength measurements the variation in the ratio response with change in SNR needs to be calculated. To do this the edge filter's discrimination range is fixed to 25 dB and the system is modeled for different SNR values in a wavelength range 1500 nm - 1600 nm. The modeled results are shown in Fig. 2.4, and it can be seen that a decrease in SNR of the source produces higher non-linearities in the discrimination characteristic.

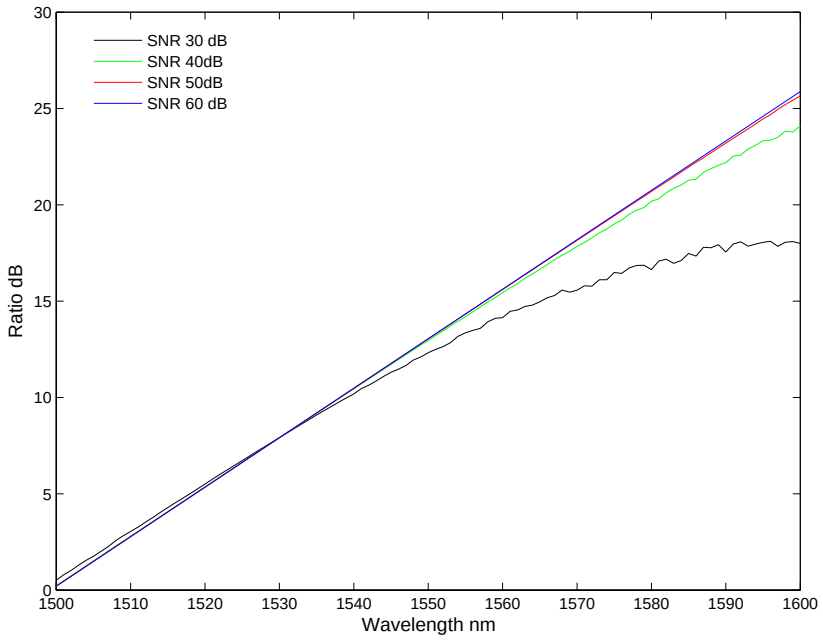

Figure 2.4: Ratio of an edge filter with slope 0.25 dB/nm at different SNR's of the source.

In Fig. 2.5 a numerical example of the influence of SNR on the output ratio

for a fixed wavelength is shown. Assume that the wavelength of the input signal is 1520 nm and the slope of the edge filter is 0.25 dB/nm. When the SNR of the source decreases from 50 dB to 45 dB the calculated ratio variation is 0.0042 dB, which could lead to a wavelength error of 0.017 nm. Thus, from the modeling results it is seen that the SNR has a significant influence on the accuracy of wavelength measurements of the system [71].

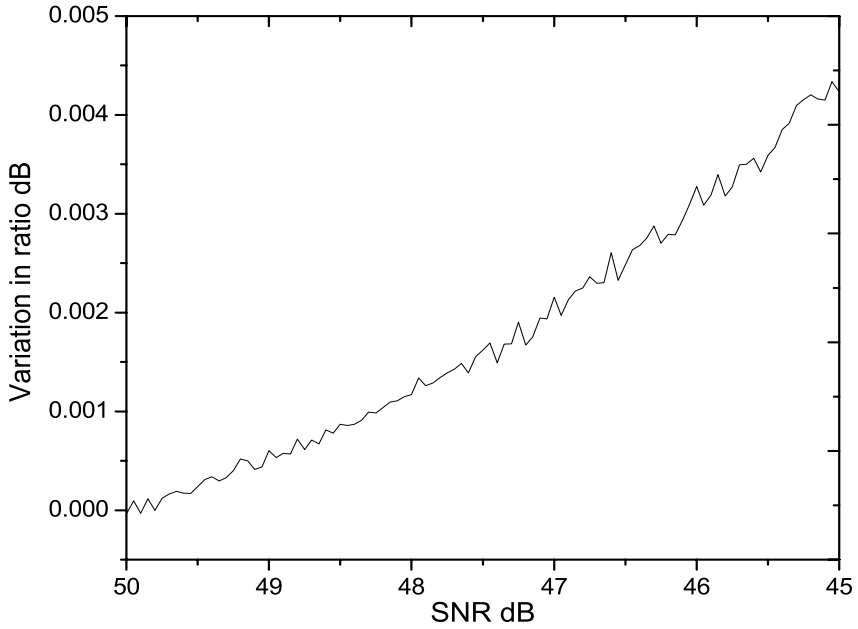

Figure 2.5: Variation in the ratio of the system when SNR changes from 50 dB to 45 dB.

To find the maximum ratio response slope for a given wavelength range and for a given SNR, for which the response remains linear and therefore, to obtain the highest accuracy the following technique is used. One method is to find the difference between the transmission response and ratio response for a given SNR and the maximum wavelength range can be estimated based on the differences between the two responses when it exceeds the permissible limits. But in the case of a system which uses wavelength dependent couplers, the ratio response has an overall shift from the transmission response so that difference between the

transmission response and ratio response cannot be effectively used to find the maximum transmission response. However, the difference between an ideal ratio response (infinite SNR, 100 dB is used in the simulation) and the ratio response at a real source SNR can give the variation in ratio response due to the non-linearity induced by SNR. Thus, the difference can be calculated from the equation;

$$\Delta R = R_{ideal}(\lambda_2) - R_{real}(\lambda_2), \tag{2.8}$$

where R_{ideal} is the ratio with infinite SNR and R_{real} is the ratio with the real SNR of the source. Figures 2.6(a) and 2.6(b) show the calculated ΔR against the ratio $R_{ideal}(\lambda_2)$ for two source signals with SNRs of 50 dB and 70 dB, respectively. The considered wavelength ranges in Figs. 2.6(a) and 2.6(b) are 1500 nm - 1600 nm and 1500 nm -1550 nm respectively.

It is assumed that the maximum permissible difference is to be less than 0.01 dB (comparable with the precision of the power detectors). From these calculation results it can be seen that for the signal with a SNR of 50 dB and measurement range of 1500 nm - 1600 nm, the ratio value at 1600 nm should be no larger than 16 dB (i.e., slope of 0.13 dB/nm). When the required measurable wavelength range is 1500 nm - 1550 nm, the ratio at 1550 nm should be no larger than 19 dB (i.e., slope of 0.34 dB/nm). When the SNR of the input signal is higher at $\sim$ 70 dB, the ratio at 1600 nm should be no larger than 35 dB (i.e., slope of 0.35 dB/nm) and the ratio at 1550 nm should be no larger than 38 dB (i.e., slope of 0.76 dB/nm). Thus, in the context of the limited precision of the power detectors, one can see that the SNR of the signal source has a significant impact on the transmission spectrum of edge filters and the ratio response of the system, and as a consequence, it affects the measurement systems resolution and accuracy. The experimental verification of the simulation results are presented in later sections of this chapter.

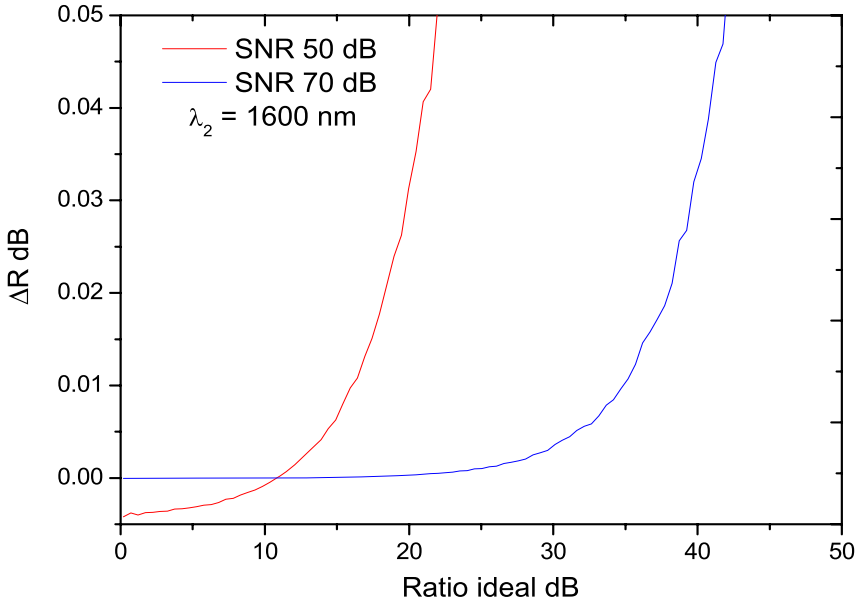

(a)

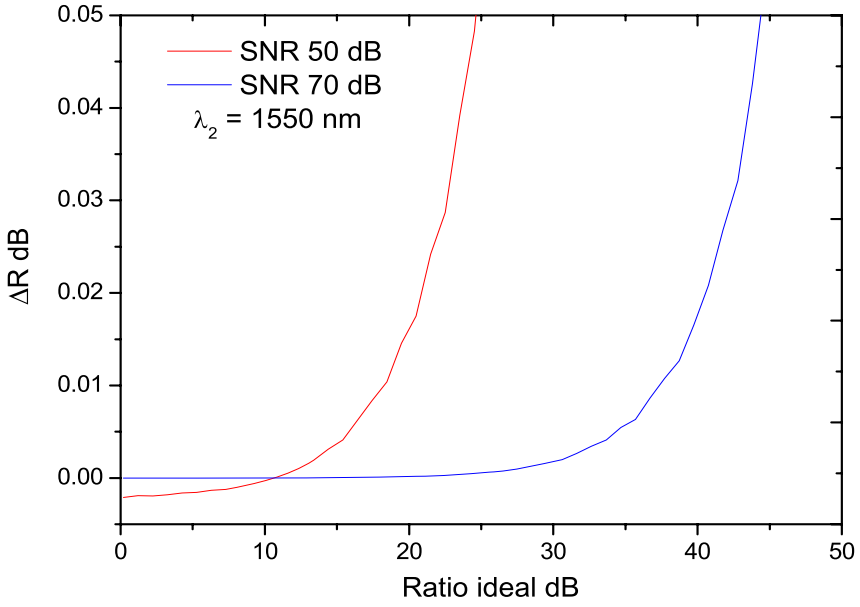

(b)

Figure 2.6: Differences between the ideal ratio response and real ratio of the system (a) λ_2 =1600 nm (b) λ_2 =1550 nm.

2.3 Macro-bend single-mode fiber as an edge filter

As mentioned in Section 1.3, for a macro-bending single-mode fiber, most previous investigations were focussed on how to predict and lower the bend loss. Some investigations were carried out in employing the bent fibers as optical sensing elements [55–58]. The wavelength dependency of a bending fiber is well known, but its practical application as a wavelength measurement device was not explored effectively. One method based on extracting the light from the bends of a single-mode fiber has been reported for use as a wavelength de-multiplexer [59]. But this approach requires unclad fiber with a very small bend radius which results in a high probability of failure of the fiber and hence is not reliable. Recent studies of the macro-bend loss of a practical single mode fiber, such as SMF28, opened the possibility of use as an edge filter [51]. The main parameters of the SMF28 fiber are shown in Table 2.1 [51, 72].

To use a macro-bend fiber as an edge filter for wavelength measurements, the optimal design of the bend radius and surface processing methods are required to achieve a linear transmission response with wavelength. It is known that for an optical waveguide with an infinite cladding the bend loss will increase as the bend radius decreases. However, a practical fiber contains one or two coating layers outside the cladding to offer mechanical protection. Because of the reflection of the radiated field at the interface between the cladding layer and the coating layer, so-called whispering gallery modes are created and the fiber shows significantly different bend loss characteristics as compared to the simple case of an infinite cladding. The sections below explain the methods and techniques involved in utilizing a macro-bend single mode fiber as an edge filter for wavelength measurements.

	Refractive index	Diameter, μm
Core	1.4504	8.3
Cladding	1.4447	125
Primary coating	1.4786	190
Secondary coating	1.5294	250

Table 2.1: Parameters of standard single-mode fiber SMF28 [72].

2.3.1 Transmission response of a macro-bend fiber filter

For a practical fiber such as SMF28, due to the finite cladding and coating which produces whispering gallery modes, bend loss does not increase monotonically with bend radius. Thus, by selecting the correct bend parameters, eg. the bend radius and bending length, one can achieve an acceptable discrimination range over the wavelength of interest. It is also important to have a very low baseline attenuation. Intuitively the slope of the transmission response is expected to be as large as possible to ensure high resolution for and ideal the measurement system. However, a real system has limitations such as noise and the resolution is limited as explained in the following chapters.

The theoretical and experimental investigations, which model the bend loss in SMF28 standard single-mode fiber, considering two coating layers, show that the bend loss is in the measurable range (40 dB) of photo detectors for bend radii in the range of 9.5 mm - 11 mm. But to use the macro-bend loss fiber as a edge filter it is also important to have a linear response and an acceptable discrimination range. Fig. 2.7 shows the bend loss in SMF28 fiber at 1500 nm and 1600 nm. From this response one can determine the baseline attenuation and the discrimination range of the filter. By changing the bending length, by increasing or decreasing the number of bend turns, at a fixed bend radius baseline attenuation and discrimination range can be varied.

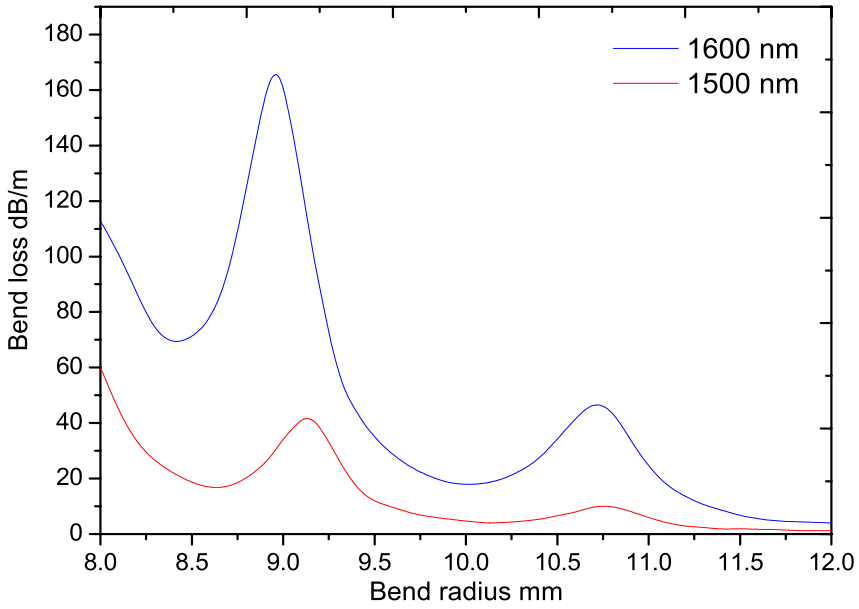

Figure 2.7: Bend loss of a SMF28 fiber at different bend radii from Ref 51.

Based on the investigations in [51] the base line attenuation (bend loss at 1500 nm) and the discrimination range for a range of bend radii starting from 8 mm to 12 mm, for different bending lengths, starting from 2 bend turns to 20 bend turns is obtained. Fig. 2.8(a) and Fig. 2.8(b) show the predicted baseline loss and discrimination range for all the filters. From these figures it is clear that for filters with bend radii less that 9.5 mm the baseline loss is very high while the discrimination range is also very large, and both values are not practical for a real system. But for bend radii around 10 mm - 10.5 mm the base line loss is relatively low. Determining the optimal value of the bending radius and bending length will involve a compromise between a higher discrimination range and a lower baseline loss. From the figure it is clear that for a filter with bend radius of 10 mm and with 10 turns the base line loss is around 4 dB and the discrimination range is approximately 9 dB. For a filter with a radius of 10.5 mm and the same number of turns the baseline loss is around 5 dB and the discrimination range is 17 dB. This comparison shows that the filter with a radius of 10.5 mm is more suitable

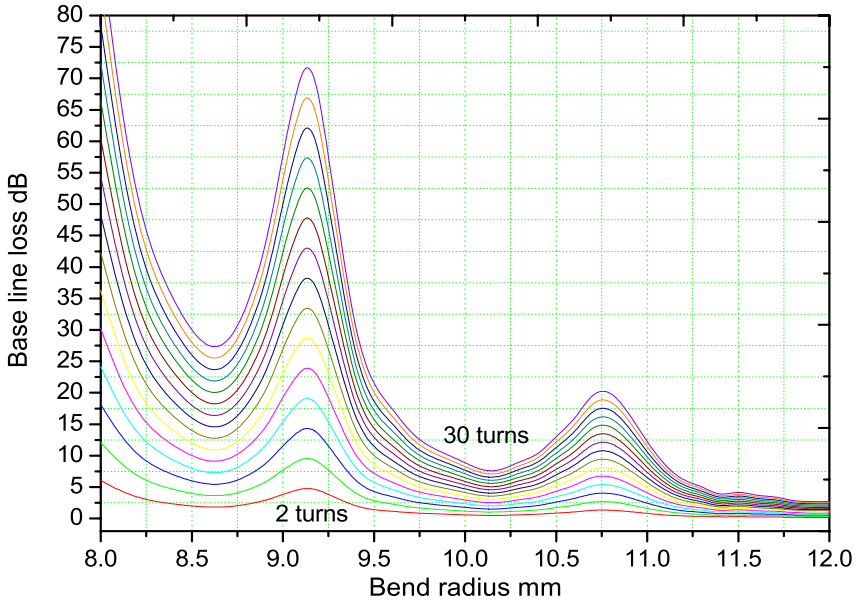

(a)

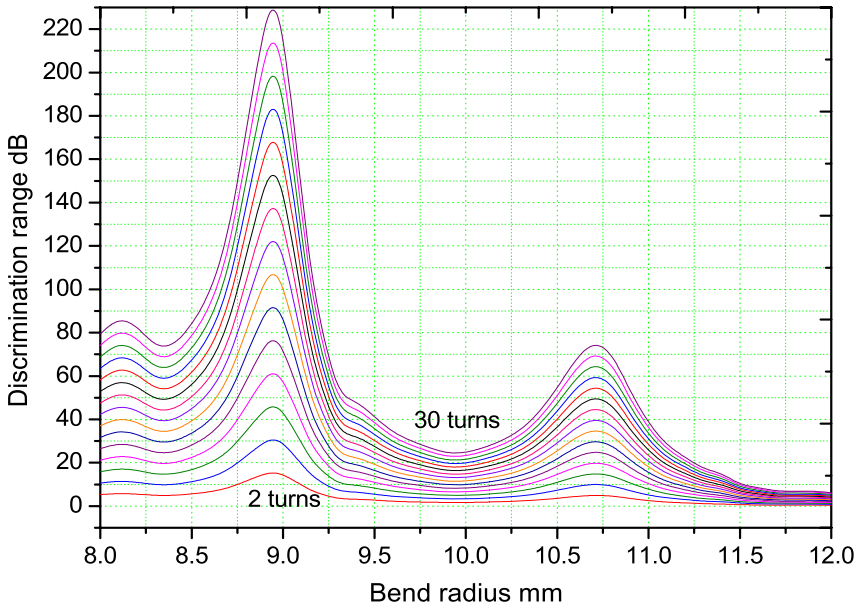

(b)

Figure 2.8: Estimated (a) baseline loss and (b) discrimination range for filters with different number of bend turns and bend radii.(T= 20 ^{0}C)

for an edge filter. The difference between two consecutive bend radii considered here was 0.5 mm as it is practically difficult to obtain a physical increment less than that for a large number of turns due to the mechanical tolerance in the size of the mandrels used to wrap the fiber filter.

To investigate the transmission spectrum over a wavelength range 1500 nm-1600 nm, the fiber is wrapped over a mandrel as shown in Fig. 2.9 with different bend radii and with a different number of bend turns. The bend loss is then measured using a tunable laser (Nettest OSICS ECL) and an optical spectrum analyzer (Agilent 86140B). The power stability of the laser source was ±0.01 dB for 0 dBm output power. The wavelength resolution and accuracy of the laser was 10 pm and ±10 pm respectively at a constant temperature after a 1 hour warm-up period. The bend radius is varied from 10 mm to 11.5 mm for a fiber bend turn length of 10. The measured transmission responses are shown in Fig. 2.10. From the figure, it can be seen that the measured bend loss increases as the wavelength increases, but with some random variations rather than a monotonic increase. This will affect the repeatability of the wavelength measurements. In the case of a bend fiber, when the radiated field escapes from

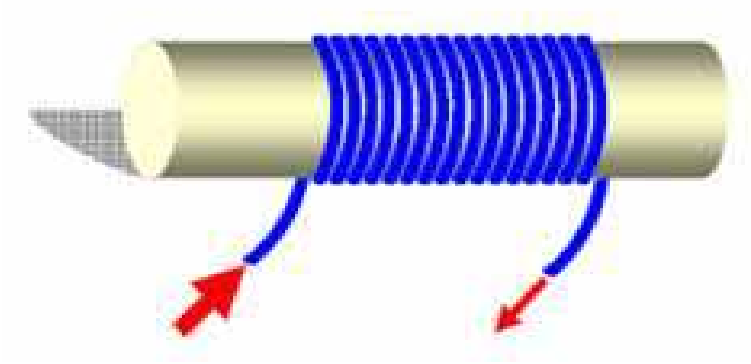

Figure 2.9: Macro-bending single-mode fiber wrapped over a mandrel.

the cladding layer, some of the radiated field is reflected and forms whispering-gallery modes, while the rest penetrates into the coating layers. Most of the penetrated radiated field is absorbed or scattered in the coating layers, but a

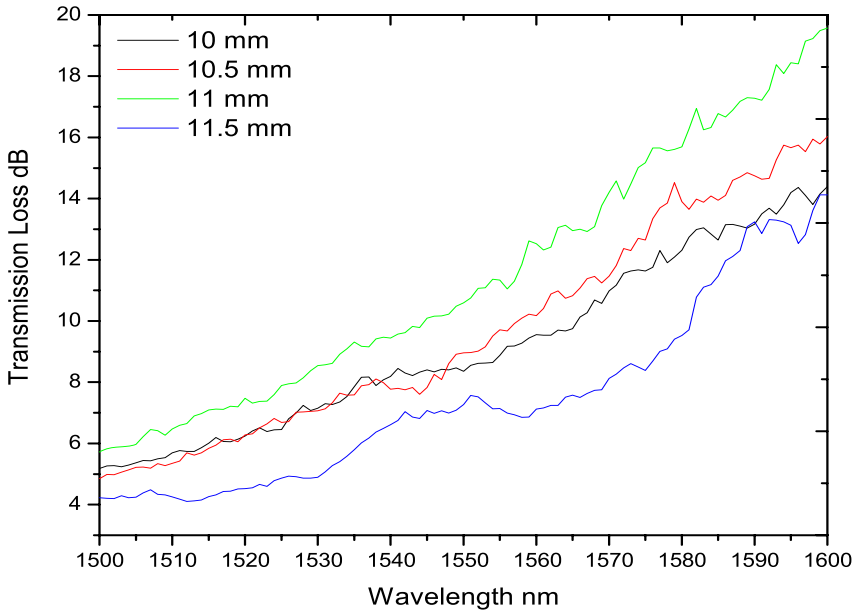

Figure 2.10: Measured transmission loss of bent SMF28 fiber for different bend radii and with 10 bend turns.

small amount of the radiated field reaches the fiber surface. Because of the strong reflection at the interface between the outer coating layer and the air, the reflected field affects the transmission in the bending fiber. The effect of WGMs makes it difficult to accurately predict the bend loss in a macro-bending fiber for a range of wavelengths, although the formulation presented in [51] can model the bend loss for SMF28 with satisfactory agreement with the experimental results.

To remove such random variations and to make the bending fiber suitable as an edge filter one has to eliminate the back reflections at the coating-air interface. One simple method to remove the reflections at the air boundary is to apply an absorption layer which absorbs light in the wavelength range of 1500 nm - 1600 nm. The simplest example of such a coating is a black pigment ink (Indian ink) or a carbon paste. Indian ink is generally considered as a good optical absorber [73]. The schematic of a bending section of a macro-bend fiber with an absorption layer is shown in Fig. 2.11. The transmission response of the filter after applying the absorption layer is shown in Fig. 2.12(a) and Fig. 2.12(b) for filters with

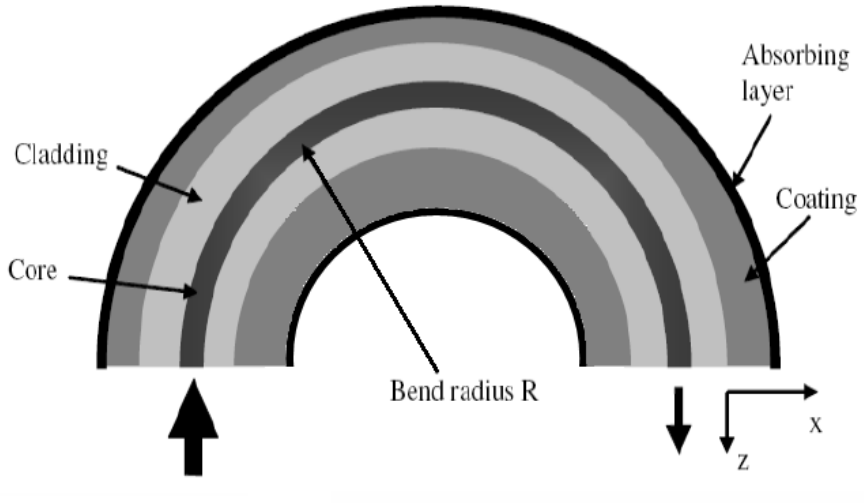

Figure 2.11: Bending section of a fiber with radius R and with absorption layer applied to the outer coating.

bend radii from 10 mm to 11.5 mm, with 10 and 15 bend turns. It can be seen the transmission responses are much smoother and quasi linear in comparison to those in Fig. 2.10. This allows a macro-bend fiber to be used as an edge filter.

From these investigations (Fig. 2.8 and Fig. 2.13) it is clear that the macro-bend fiber filter with bend radius close to 10.5 mm is the optimal bend radius as it gives low baseline loss and high discrimination range compared to other radii. To investigate the slope of the the filter with 10.5 mm radius, transmission responses are obtained for a variety of bend turns and are shown in Fig. 2.13. Discrimination ranges of 7.5 dB, 15 dB, 22 dB, 28 dB and 36 dB with baseline losses of 4.5 dB, 6 dB, 8 dB, 10.1 dB and 11.2 dB respectively can be obtained when the number of bend turns is changed from 5 to 25 respectively with a 5 bend turns interval. It can be seen from the figure that a greater number of bend turns leads to a steeper response but also an increase in the baseline loss. The ultimate discrimination range for the ratio response of the system depends on the signal-to-noise ratio of the source as presented in Section 2.2 and the experimental verification is presented in the next section.

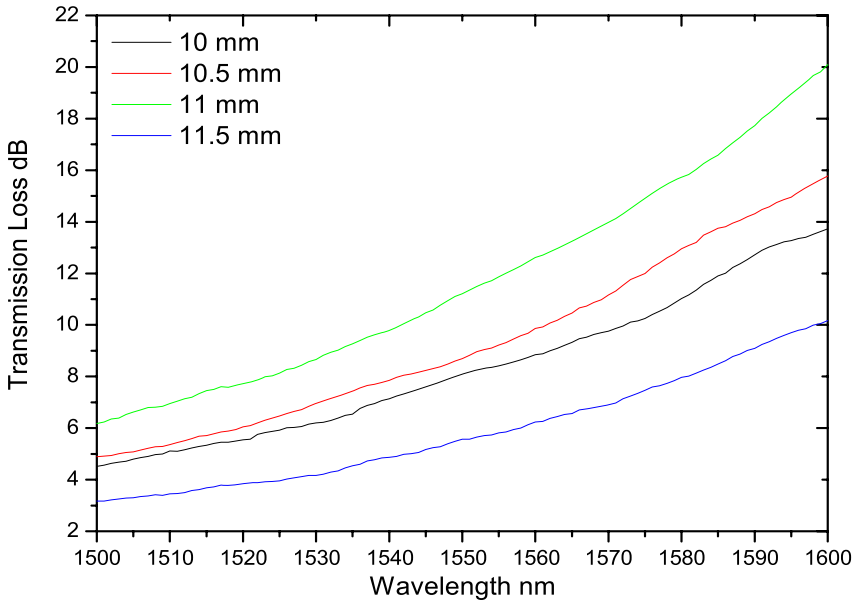

(a)

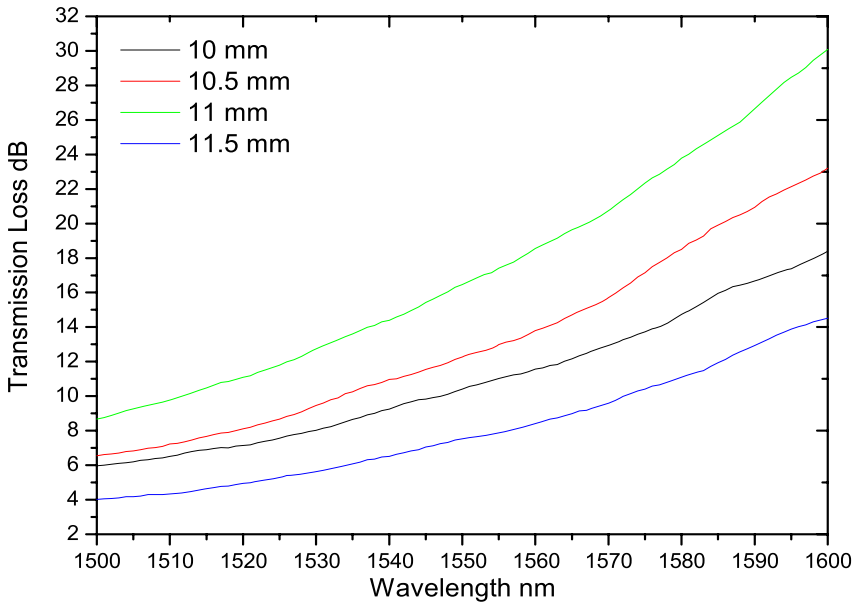

(b)

Figure 2.12: Measured transmission loss of the macro-bend fiber filters for different bend radii (a) 10 turns (b) 15 turns.

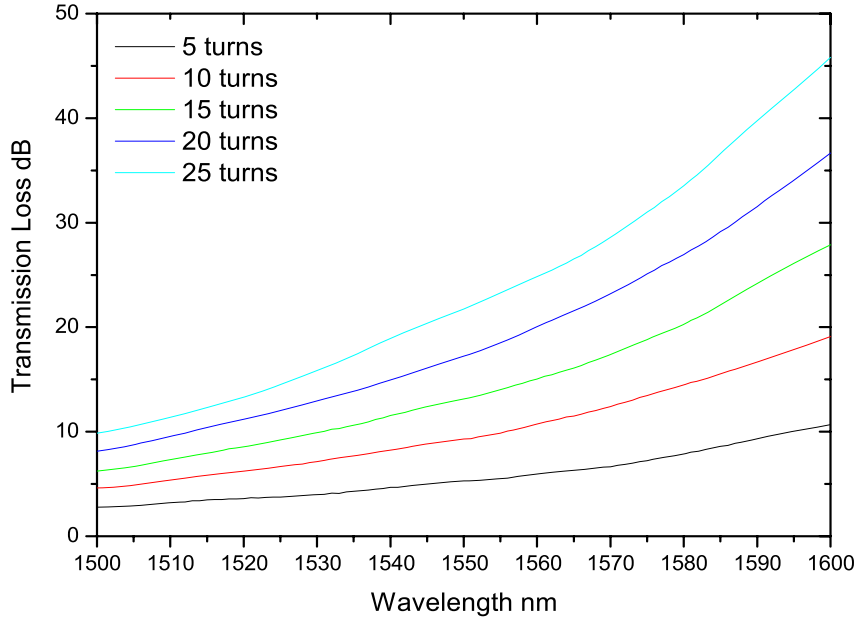

Figure 2.13: Measured transmission loss for the filters with bend radius 10.5 mm and with different number of bend turns with an absorption layer applied to the outer coating.

2.4 Wavelength measurement system based on a macro-bend fiber edge filter

Using the developed macro-bend fiber edge filter a ratiometric wavelength measurement system is built as shown in Fig. 2.14. A commercially available wavelength flattened fused 3 dB coupler is used to split the signal into two equal parts. The single mode fiber used was the SMF28 from Corning, whose parameters are as shown in Table 2.1. To use the system for wavelength measurements, initially a calibration spectrum has to be obtained for the reference. Data acquisition and control programmes were developed using a National Instruments LabView 8.0 platform [74, 75]. The section below explains the calibration of the whole system and the experimental investigation carried out to study the impact of the SNR of the source on the measurable wavelength range.

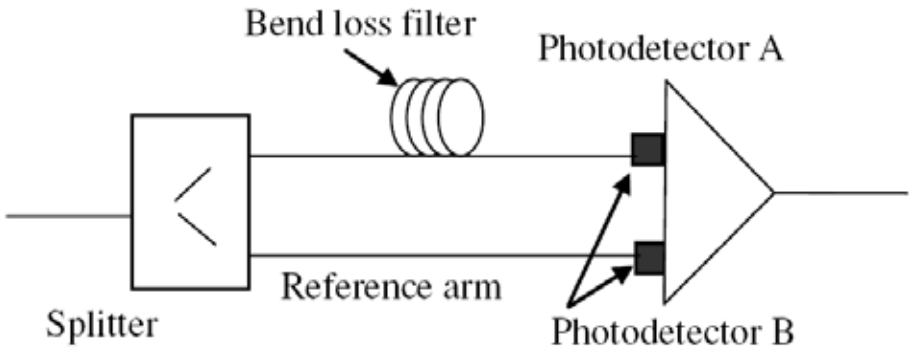

Figure 2.14: Schematic structure of a bend loss filter based ratiometric wavelength measurement system.

2.4.1 Calibration of the system and experimental investigation of the impact of SNR of the source

The fiber was wrapped on the mandrel with a bend radius 10.5 mm and the number of bend turns is changed to obtain different slopes. For the calibration of the system a tunable laser with a wavelength range of 1500 nm - 1600 nm is used ((Nettest OSICS ECL). A very low noise dual channel optical power meter (PXIT 306) integrated into a PXI platform (PXIR 800A) and is controlled with the developed LabVIEW based programs (See Appendix B) is used to measure the power outputs from the filter arm and the reference arm. The power meter employs two InGaAs photo detectors with a wavelength range from 900 nm to 1700 nm. The specified measurable minimum power of the power meter is -70 dBm and the maximum is +10 dBm. To create a series of edge filters the fiber was wrapped on to a mandrel with different bending lengths corresponding to 10, 15, 20 and 25 turns with a bend radius of 10.5 mm. A prototype of the built system is shown in Fig. 2.15. The ratio of the system is obtained with a wavelength interval of 1 nm in the wavelength range 1500 nm - 1600 nm for the system with all the filters. The measurements were taken at a room temperature of 20 degC. The measured ratio response and and its comparison with the modeled response

Figure 2.15: A prototype of the filter section of the wavelength measurement system.

is shown in Fig. 2.16. It should be noted that the real transmission responses of the edge filters are not strictly linear as per the ones used in the modeling. To compare the measured ratio response to the modeled ratio response, the original transmission loss measured by the optical spectrum analyzer is used in the model rather than the linear response which is initially used.

The experimental and simulation results show that, because of the limited SNR of the source, with an increase in the slope of the transmission response of the edge filter the output ratio of the system diverges from the actual transmission response of the edge filter at the longer wavelengths. Thus, the system becomes less accurate for wavelength measurement in this range (greater than 1580 nm). Therefore, the slope of the transmission response of the edge filters is limited. From the figure one can see that for the edge filter with a 10.5 mm bend radius and 15 turns a wavelength range around 80 - 90 nm can be achieved with an average slope of 0.22 dB/nm. Higher slopes can be achieved by increasing the

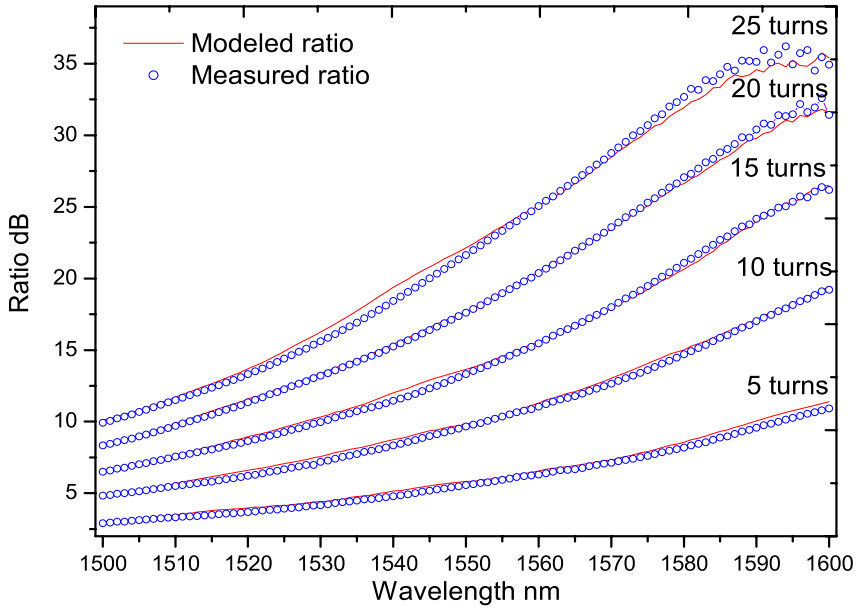

Figure 2.16: Comparison of the measured and simulated ratio responses of the system with different filters.

number of turns, but the wavelength measurement range will be reduced. Thus, the SNR of the source needs to be considered when designing the system to optimize the required slope and wavelength range of the system.

The 3 dB coupler used is a commercial coupler with the response shown in Fig. 2.2. It should be noted that both the measured ratio response and the modeled ratio responses includes the response of the 3 dB coupler. To demonstrate the effect of the wavelength dependency of the 3 dB coupler, the measured ratio response is compared with the simulated response considering both the wavelength dependent case and wavelength independent case. From Fig. 2.17 one can see that the ratio response is closer to the simulated response with the wavelength dependent 3 dB coupler. Thus, it is obvious that in the design of any ratiometric wavelength measurement system the wavelength dependency of the 3 dB coupler should be considered.

The above results show that the calibration ratio response is highly dependent on the SNR of the source and any change in the SNR of the source changes the

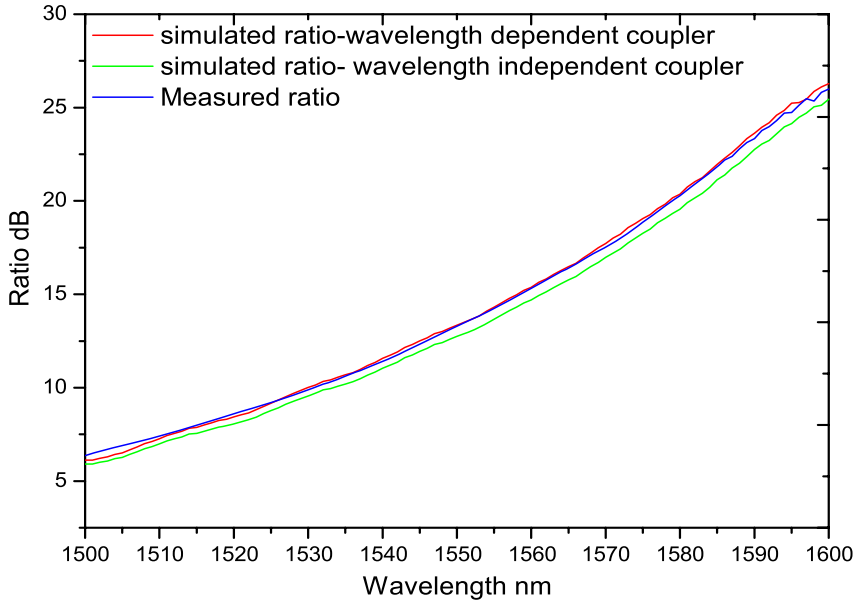

Figure 2.17: Ratio response showing the influence of a 3 dB coupler.

ratio response. When there is a change in the input source, or the use of an input signal other than the one used for calibration, the SNR may change and this results in inaccuracy in the measured wavelength. Hence, it is important to estimate the allowed change in source SNR within the required limits of accuracy. To study the effect of SNR on the accuracy of the system fiber edge filters with slopes of 0.15 dB/nm (10 turns) and 0.22 dB/nm(15 turns) are used. To change the SNR of the input signal, a tunable laser was used which can provide a different SNR for different output power levels for the same peak wavelength. Alternatively, by using a wavelength insensitive variable optical attenuator, the output power of the tunable laser can be changed while retaining the same SNR. Fig. 2.18 shows the spectrum of the tunable laser with a peak wavelength 1520 nm for three cases: (1) output power for the peak wavelength is 0 dBm and the SNR is about 47 dB; (2) output power for the peak wavelength is -5 dBm and the corresponding SNR is about 42 dB; (3) output power for the peak wavelength is -5 dBm obtained using the attenuator and in this case the SNR remains as 47

dB.

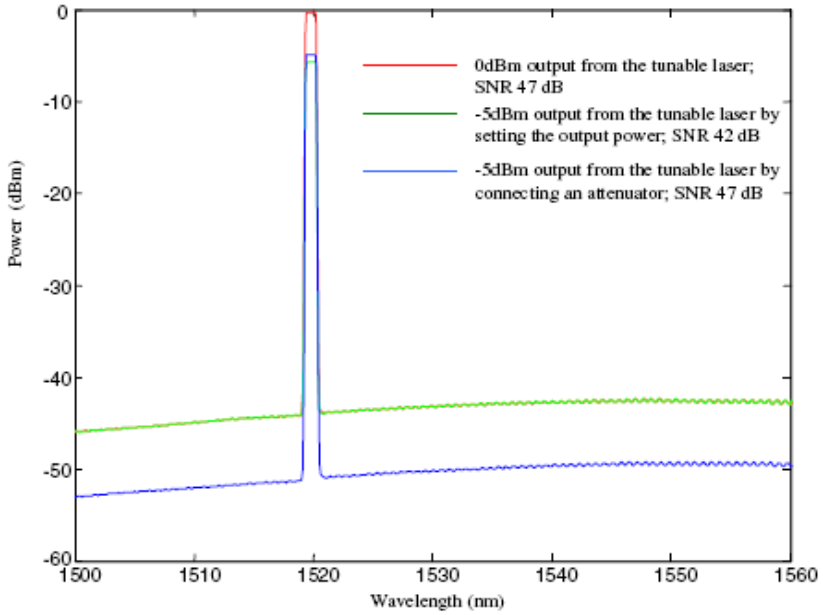

Figure 2.18: The spectrum of the tunable laser for 3 different cases.

To illustrate the influence of the SNR on the system's accuracy, the first case, i.e., a laser source with 0 dBm output power and SNR of 47 dB, is chosen to obtain the calibration ratio response. The input power of the laser source is changed to -5 dBm, which changes the SNR to 42 dB. The ratio response is again obtained at this SNR for a wavelength range of 1500 nm - 1600 nm. The variation in ratio response due to the change in SNR from 47 dB to 42 dB is shown in Fig. 2.19(a) for a system with a filter of 15 bend turns. A comparison with the simulated results is also presented, which shows that both the measured and the simulated data are in reasonably good agreement which clearly demonstrates the effect of the SNR of the source on the system.

From Fig. 2.19(a) it can be seen that the ratio variation different for different wavelengths. Setting a maximum limit of 0.025 dB (to obtain an accuracy better than ± 0.1 nm) for the present system, a filter with 15 turns, can measure wavelength within this accuracy for a wavelength range of 1500 nm - 1540 nm

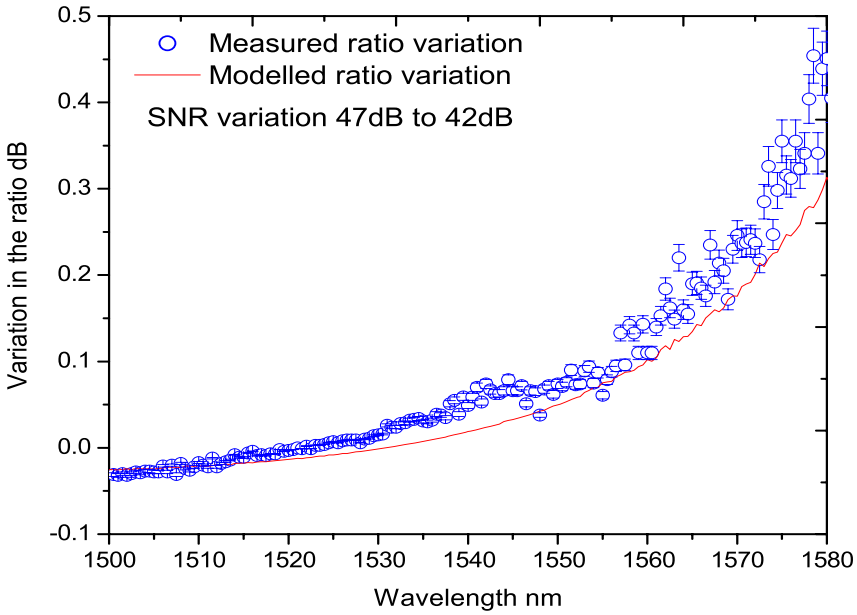

(a)

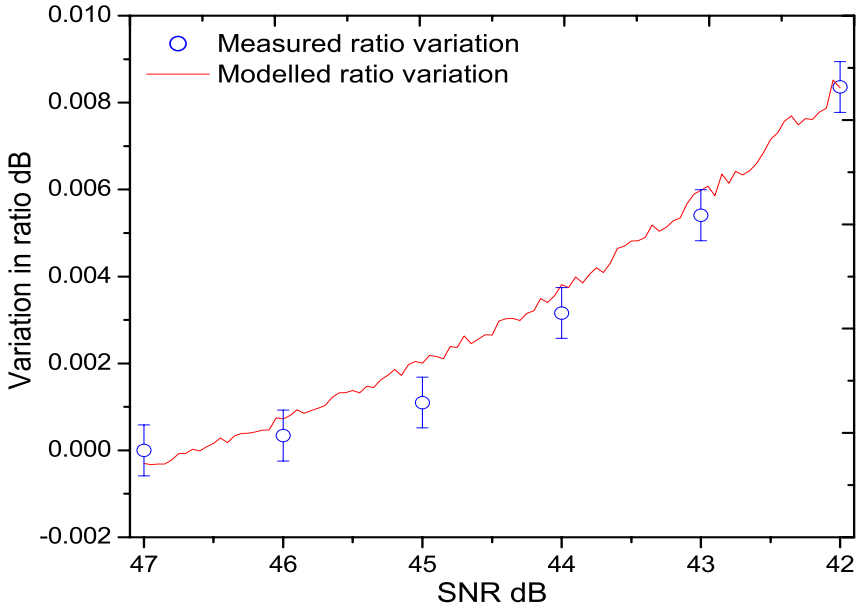

(b)

Figure 2.19: (a) Ratio variation for a step change in SNR from 47 dB to 42 dB for a wavelength range 1500 nm - 1600 nm (b) Ratio variation at 1520 nm when SNR changes from 47 dB to 42 dB.

when SNR changes for 5 dB from 47 dB to 42 dB. To have a more clear picture on its impact on wavelength measurements, a wavelength 1520 nm is chosen as an example to demonstrate the wavelength error, where the ratio variation is considerably less compared to other wavelengths for an SNR variation of 5 dB from 47 dB to 42 dB. The measured and simulated ratio variation for all SNRs within the range of 47 dB to 42 dB is shown in Fig. 2.19(b). From the figure it is clear that at a wavelength 1520 nm, a 5 dB SNR variation could give a ratio change of 0.008 dB. The wavelength error due to this change in ratio depends on the local slope of the ratio response as the ratio response is not linear and the slope is different for different wavelength.

To estimate the wavelength inaccuracy the wavelength variation is measured at 1520 nm for a step change of SNR from 47 dB to 42 dB. The measured wavelength variation is shown in Fig. 2.20(a). It can be seen that the wavelength error reaches 0.055 nm due to the change in the SNR. But this error also includes the error due to the power variation which changes the shot noise of the system, which is explained in detail in the next chapter. By using averaging techniques, the noise effect from the receiver can be minimized. Hence, an averaging of 256 is used to isolate the receiver noise from the effect of SNR, but reduces the measurement speed of the power meter to 50 measurements/sec. To confirm the wavelength error, the wavelength variation of the system with a filter with 15 turns is also obtained by following the same procedure as described earlier and is shown in Fig. 2.20(b). Thus, from the experimental results it is evident that the dynamic range of the ratio spectrum and hence the measurable wavelength range is limited by the SNR of the source. It is also demonstrated that and a change in SNR of the source induces inaccuracies in the wavelength measurements and the level of inaccuracy is different for different wavelengths as the ratio error is different for different wavelength shown in Fig. 2.19.

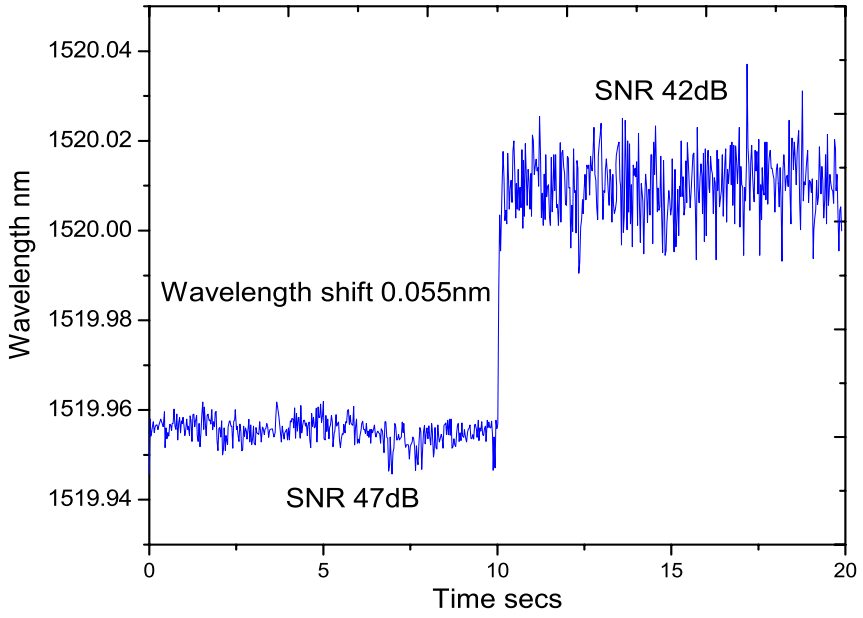

(a)

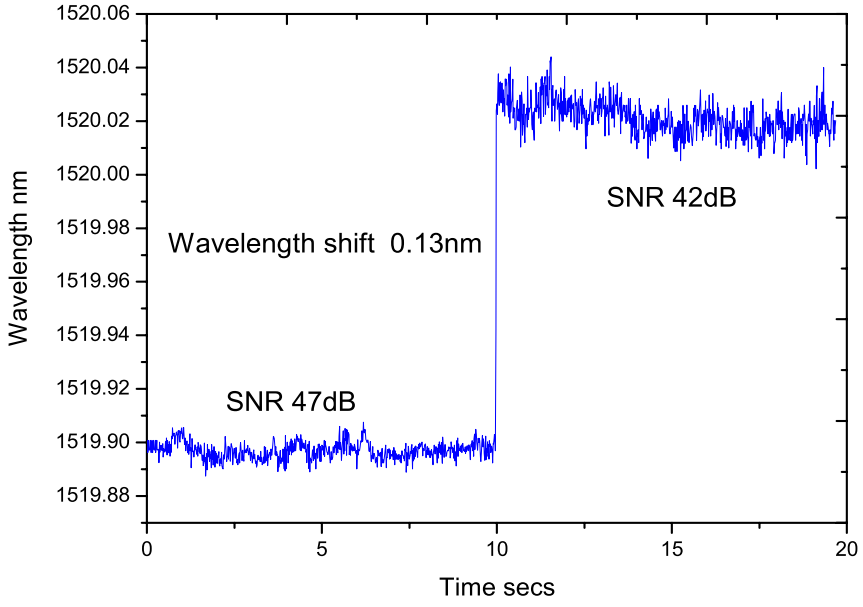

(b)

Figure 2.20: Measured wavelength shift at 1520 nm when SNR changes from 47 dB to 42 dB (a) filter with 10 turns (b) filter with 15 turns.

2.5 Summary

The modeling and analysis of the transmission response of a general edge filter and the ratio response of an edge filter based ratiometric system was discussed in this chapter. It is shown that the limited signal-to-noise ratio of the source has an impact on the system. The limited SNR determines the slope of the edge filter and also the measurable wavelength range. The wavelength error induced by a change in SNR of the source, which changes the calibration response, is also modeled. It has been shown that a different SNR for the input signal corresponds to a different effective discrimination characteristic and hence any change in the SNR from the one used for calibration will induce an error. The wavelength dependency of the 3 dB coupler is also considered in the modeling of the system. It is also shown that commercially available wavelength flattened 3 dB couplers exhibit a small wavelength dependency and affects the ratiometric system. From the simulation and experimental results, it is shown that it is important to consider the wavelength dependency of the coupler while designing the system.

In this chapter a macro-bend fiber filter is introduced as an edge filter. It is shown that the bend loss phenomena in standard single-mode fiber, SMF28, can be used for wavelength measurements when employed in a ratiometric scheme. A macro-bend fiber filter is optimized to obtain a very low baseline attenuation and high discrimination range for a wavelength range of 1500 nm - 1600 nm. The bend radius and the number of bend turns determine the baseline attenuation and the discrimination range. Because of the whispering gallery modes which are inherent in the bend single-mode fiber, the change in bend loss of the fiber with wavelength is not monotonic. To obtain a strict linear response, an absorption layer is applied to the bend fiber, which effectively eliminates the reflections at the buffer coating-air interface. Thus, an optimized macro-bend fiber edge filter is realized for wavelength measurements. A fiber filter with a bend radius of 10.5 mm and 15 bend turns can give a discrimination characteristic with a low baseline

loss and is useful for wavelength measurements in the range 1500 nm - 1580 nm.

A ratiometric wavelength measurement system is built using the developed macro-bend fiber filter. Investigations are carried out to prove the effect of the SNR of the source on the system. The experimental results verified the modeled results, and it was shown that the slope and wavelength range of the system is determined by the SNR of the source. The system was tested at different source SNRs to estimate the inaccuracy induced by a change in SNR of the source. The importance of maintaining the source SNR at the same level as that of the calibration to achieve the highest wavelength accuracy is verified from the simulation and experimental results.

The key conclusions from this chapters are;

- For any edge filter based ratiometric wavelength measurement system, source SNR is an important factor that needs to be considered in the modeling of the system as the limited SNR of the optical source affects the system by limiting the slope of the filter and also the measurable wavelength range.

- A macro-bend fiber filter was demonstrated as an effective and viable way of implementing an edge filter for a ratiometric wavelength measurement system.

- To suit different measurement experiments the slope of the system can be varied by changing the bend radius and number of bend turns, however there is a trade-off between the baseline loss and the discrimination range. For example, a filter with a bend radius of 10.5 mm and 15 bend turns can give a low baseline loss and a useful discrimination characteristic which can cover a wavelength range of 1500 nm - 1580 nm.

Chapter 3

Overall noise analysis on an edge filter based ratiometric wavelength measurement system

3.1 Introduction

Precision, accuracy and resolution are extremely important for wavelength measurement applications, for example, involved in fiber Bragg grating based optical fiber sensing systems. While in the second chapter it is shown that source noise limits the wavelength range and adds inaccuracy to the measured wavelength due to the change induced to the calibration spectrum when there is a change in the source SNR. In any realistic measurement system the actual noise in the receivers is also important. The ratiometric nature of the system does not protect against the effect of optical-to-electrical conversion at the receivers [76–78] as the noise sources are uncorrelated. Thus, because of the uncorrelated random nature of the receiver noise [79–81], the effect of noise sources will not be eliminated, but will affect the system's performance adversely.

For wavelength measurement applications of a macro-bend fiber based ratiometric system, resolution and accuracy are very important and hence, it is necessary to consider the noise of the detection circuit as well as optical source noise while modeling the ratio response of the system. This chapter presents the modeling and analysis of all the noise effects on a ratiometric system. Fun-

damental noise mechanisms in an optical receiver are explained in Section 3.2. The main noise contributions to the ratiometric system has been identified, and a noise model for a ratiometric system is presented in Section 3.3. Based on the presented noise model, the ratio response of the system is modeled and ratio fluctuations due to the receiver noise and the SNR of the source are calculated and presented in Section 3.3. In Section 3.4 the impact of noise on the resolution of the system is analyzed theoretically and the achievable resolution for a filter with a fixed slope is predicted. An experimental verification of the noise model has been carried out and presented in Section 3.5. The experimental result agree with the theoretical model proposed, proving that the noise in the system determines the maximum permissible slope of the filter to achieve the best resolution for a widest wavelength measurement range. Utilizing higher slope possibility will be appropriate only for ideal systems. In a real system a lower slope will frequently give a better resolution, depending on the total noise associated within the system. This chapter gives an insight to the noise associated limitations in determining the slope of the system and shows how the resolution and wavelength range is limited due to noise associated within the system.

3.2 Optical front ends in receivers and their fundamental noise mechanisms

An optical receiver's front-end utilizes a photodiode to convert an optical signal to a photo current, which is then converted to a voltage [81, 82]. Electronic signal processing stages then process the recovered voltage to extract the desired information. The various front-end designs can be grouped into four basic configurations: (1) Resistor termination with a low impedance voltage amplifier (2) High-impedance amplifier (3) Trans-impedance amplifier (4) Noise matched or resonant amplifier [81]. Among these the most simple and commonly used pre-amplifier is the trans-impedance amplifier [82, 83]. In this analysis only the

trans-impedance amplifier is considered. This front-end architecture is the most popular and provides a good compromise between the low noise characteristics of the high-impedance front-end and the wide band nature of the low impedance voltage amplifier front-end. A basic circuit diagram of a trans-impedance front-end is shown in Fig. 3.1. The amplifier is called as trans-impedance amplifier because it utilizes shunt feedback around an inverting amplifier. A feedback resistor determines the trans-impedance and thus, the sensitivity of the amplifier. Larger feedback resistors increase the sensitivity of the amplifier, but simultaneously reduce the amplifiers bandwidth, however and advantage of trans-impedance amplifier is that by changing the gain of the amplifier the trade off between noise and bandwidth can be controlled.

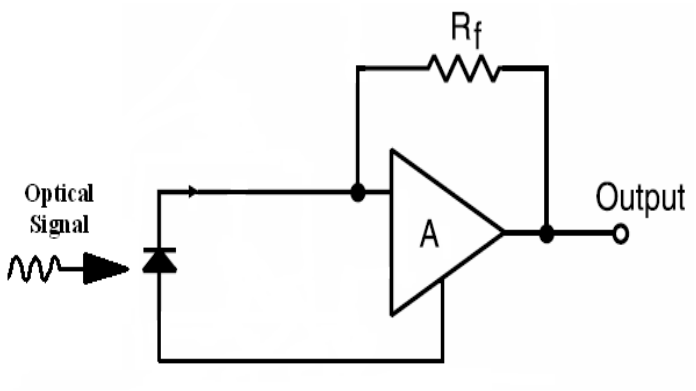

Figure 3.1: A trans-impedance amplifier front-end.

3.2.1 Properties of noise in an optical receiver

Noise in the broadest sense can be defined as any unwanted disturbance that destructively interferes with a desired signal and is random in nature. It consists of frequency components that are random in both amplitude and phase. Although the long term rms value can be measured, the exact amplitude at any instant of time cannot be predicted. For a receiver the noise process in the photodiode (shot noise) has a statistical nature that can be represented by a Poisson distribution.

Noise processes in the amplifier and trans-impedance resistor can be represented by a Gaussian distribution. However, the Poisson distribution does not lend itself to convenient analytical manipulation, and the use of exact Poisson photo detection statistics in addition to the Gaussian noise from the receiver electronics will usually require numerical mathematical evaluation techniques [84, 85]. In the cases where the mean photo carrier density is high exceeding about one hundred generated photons per observation-time, the photo detection statistics can be well approximated by a Gaussian distribution [86, 87]. Thus, in general noise in an optical receiver is approximated as a Gaussian distribution of instantaneous amplitudes with time as shown in Fig. 3.2.

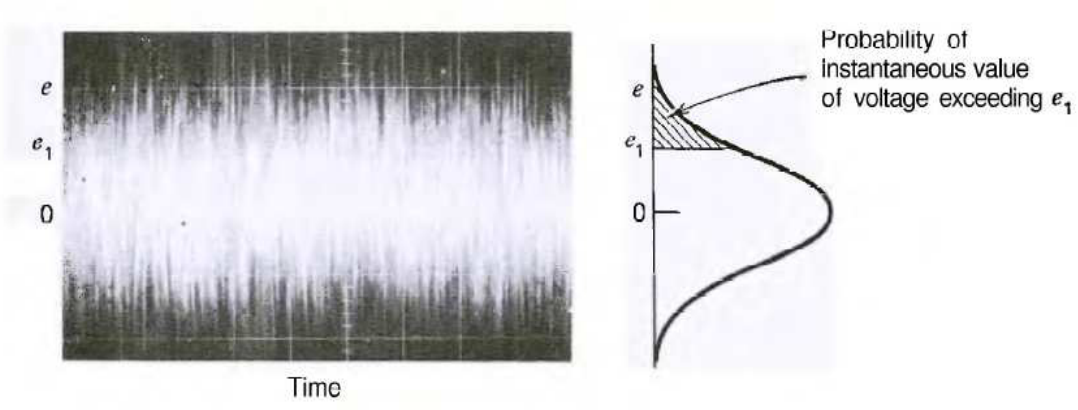

Figure 3.2: Noise waveform and Gaussian distribution of amplitudes [80].

Mathematically the Gaussian probability density function can be expressed as [88],

$$f(x) = \frac{1}{\sigma\sqrt{2\pi}} \exp -\Big[\frac{(x-\mu)^2}{2\sigma^2}\Big], \tag{3.1}$$

where μ is the mean or average value and σ is the rms value of the variable x. As a good engineering approximation, common electrical noise lies within $\pm 3\sigma$ of the mean μ. In other words, the peak-to-peak value of the noise is less than six times the rms value for 99.7 % of the time. If one considers a value such as e_1, the probability of exceeding that level at any instant in time is shown as the

cross sectioned area in Fig. 3.2.

As noise is a random process it cannot be described as an explicit function of time. Regardless of the number of times one observes the noise, there is no way to determine exactly what value a noise process will have at any instant in the future. Noise in the time domain must therefore be characterized in probabilistic terms such as mean and variance. Another widely used characteristic is the root mean square (rms) value. For an observed noise process the rms value is defined as,

$$n_{rms} = \sqrt{\frac{1}{T}\int_0^T n^2(t)dt}. \tag{3.2}$$

When noise voltages are produced independently and there is no relationship between the instantaneous value of the voltages then they are uncorrelated. Examples of this include the thermal and shot noise in the same receiver or shot noise sources in two different receivers. In the case where two noise voltages arises from a common phenomenon as well some independently generated noise, then one can say that those noise voltages are partially correlated. Whenever two noise sources are added the instantaneous sum is the sum of the individual instantaneous values [80]. Thus, the sum of two partially correlated waves can be expressed as,

$$E^2 = E_1^2 + E_2^2 + 2CE_1E_2. \tag{3.3}$$

The term C is called the correlation coefficient and can have any value between +1 or -1, including 0. When C=0, the voltages are uncorrelated and the expression will be,

$$E^2 = E_1^2 + E_2^2. \tag{3.4}$$

In the case of optical receivers the different sources of noise are fully uncorrelated and therefore to add the noise voltages in a receiver Equation (3.4) must be used.

3.2.2 Noise mechanisms in an optical receiver

An understanding of the origin of noise is required for a receiver performance to be accurately characterized. The amount of noise present in a receiver will be the primary factor that determines the receiver sensitivity [89]. Fig. 3.3 shows a simple but adequate noise model of a trans-impedance optical receiver, where I_{th}, I_{sh}, I_{amp} and e_{amp} are the thermal noise, shot noise, amplifier current noise and amplifier voltage noise respectively. C_f and C_d are the feedback and photodiode capacitance respectively. In addition, in optical sensing applications, it is very likely that every receiver has an analog-to-digital converter (ADC) associated with it. So the receiver system will also contain the quantization noise from the ADC. For simplicity the main noise mechanisms considered in this analysis are (a) shot noise of the photodiode (b) thermal noise and (c) quantization noise . In this experiment a low noise pre-amplifier is used which has a very low I_{amp} (in the order of fA) and e_{amp} (15 nv/$\sqrt{Hz}$, f=1kHz, shunt resistance=100 Ω) [90]. As a result in the model presented in Section 3.3, the effect of amplifier noise is neglected.

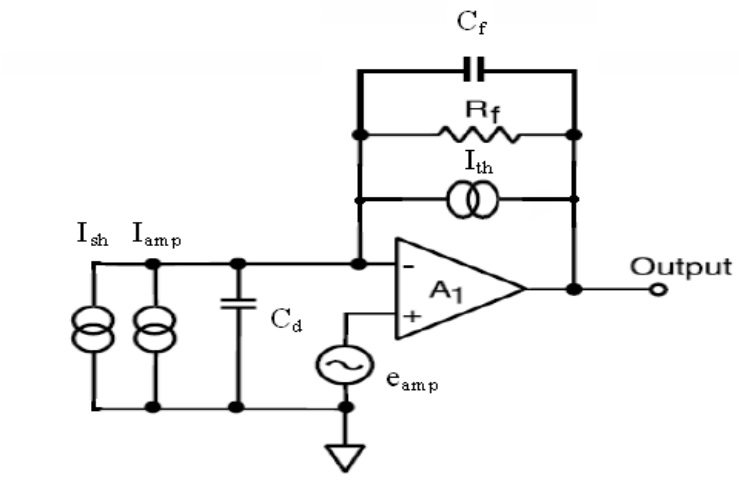

Figure 3.3: Noise equivalent circuit of a trans-impedance amplifier.

Shotnoise: In a photodiode the conversion of photons to charge carriers is

a random process and the noise generated in this process is called shot noise. It was first studied by Schottky in 1918 and has been thoroughly investigated since then [91]. Because shot noise is associated with current flow, it is naturally modeled as a current-noise source in parallel with the photodiode whose mean square value is given as,

$$I_{sh}^2 = 2eI_{ph}B, \tag{3.5}$$

where I_{ph} represents the average photon generated current flowing through the photodiode and B is the post-conversion electrical bandwidth of the system and e is the elementary charge. When a photodiode is used together with a trans-impedance pre-amplifier, the shot noise produced in the photodiode gets amplified together with the original signal. If A_{sig} is the amplification factor of the pre-amplifier, the rms shot noise voltage will be,

$$e_{sh} = \sqrt{2eI_{ph}B}A_{sig}. \tag{3.6}$$

Thermal noise: Thermal noise is a result of thermally induced random fluctuations in the charge carriers in an electrical resistance element. Carriers are in random motion in all resistances at a temperature higher than absolute zero. The amount of motion is a direct function of the absolute temperature of the resistance. Nyquist showed that the open circuit rms voltage produced by a resistance R is given by [92],

$$e_{th} = \sqrt{4kTBR}, \tag{3.7}$$

where k is the Boltzmann's constant, T is the absolute temperature in Kelvin and B is the electrical system bandwidth. In the case of a trans-impedance amplifier front end the main source of thermal noise is the feed back resistor R_f.

Quantization noise: Quantization noise is a noise error introduced by

quantization in the analog-to-digital converter while converting an analog signal to a digital signal. An analog signal is continuous with ideally infinite accuracy, while the digital signal's accuracy depends on the quantization resolution or number of bits used to represent samples in the analog to digital converter. Thus, while converting the continuous level into discrete levels, the actual analog value is approximated to a digital value and the error during this conversion is called quantization error [93]. If the peak-to-peak range of the original signal had been quantized into equal intervals of magnitude S each, the rms quantization error would be proportional to S.

3.3 Theoretical investigation of the system considering noise effects

In the previous chapter a ratiometric system was analyzed in the context of the limited signal-to-noise ratio of the input signal and it was shown that for a given measurable wavelength range, the slope of the edge filter is effectively limited due to the noise level of the input signal. In order to have a full understanding of the impact of the receiver noise as well as the SNR of the source on the system performance it is necessary to consider both factors in the modeling of a ratiometric system. In the next subsection initially a noise model of a ratiometric system is presented and based on this model, which considers the total noise of the system, the ratio response of the system is analyzed.

3.3.1 A complete noise model of a ratiometric system

As a starting point to determine the effects of noise on a ratiometric system a basic noise source representation of the system is considered and is presented in Fig. 3.4. Since the different noise mechanisms are statistically independent the total mean square electrical noise that contributes to each arm of the system can be expressed as the sum of the individual mean square noises. Thus, the total

rms noise voltage can be expressed as,

$$e_o = (e_{sh}^2 + e_{th}^2 + e_{adc}^2)^{1/2}. \tag{3.8}$$

The noise bandwidth of the amplifier was measured as 3.75 kHz. The amplification factor of the pre-amplifier used was 10^5 V/A. The e_{adc} considered in the simulation was 122 μV_{rms}, the random noise of the ADC used in the experiment.

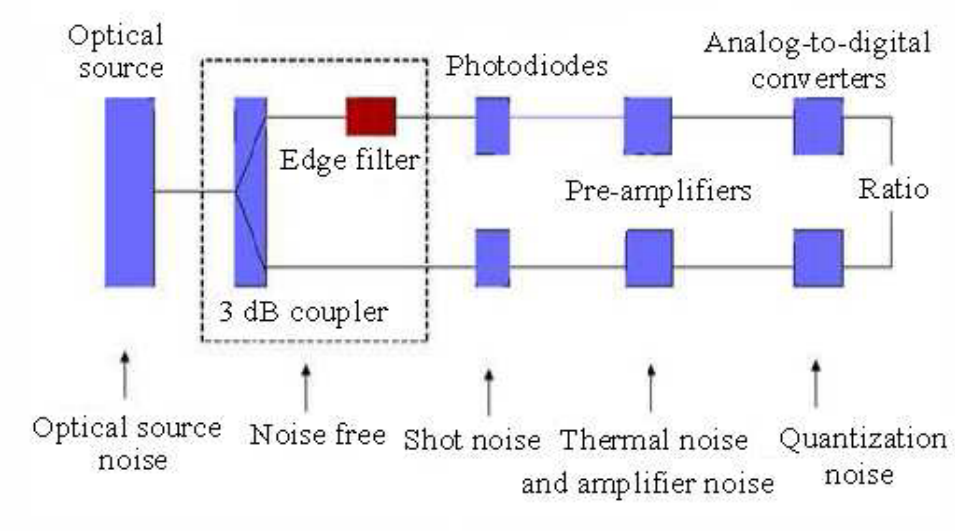

Figure 3.4: Noise model of an edge filter based ratiometric system.

Assuming the transmission response of the edge filter is a linear function of wavelength, the shot noise generated in the photodiode connected to the edge filters of different slope is calculated. The total noise in the receiver connected to the edge filter vary with the wavelength as the power reaching the photodiode changes with wavelength which results a variation of shot noise generated in the photodiode. The baseline losses of the edge filters at the starting wavelength is estimated from the transmission responses of the edge filters used in the experiment. The rms values of other types of noise are considered constant assuming a constant temperature. The system input power is assumed as -10 dBm and the insertion loss at the 3 dB coupler is assumed to be of 3.5 dB. Three edge filters

are considered in the modeling with slopes 0.16 dB/nm, 0.22 dB/nm and 0.31 dB/nm. These slopes are selected to match those used in the experiment where three macro-bend fiber edge filters are used which give a discrimination range of 16 dB, 22 dB and 31 dB respectively for a wavelength range from 1500 nm to 1600 nm. The calculated total rms noise voltage from all sources for a wavelength range from 1500 nm to 1600 nm for the receivers connected to both the reference arm and edge filter arm is shown are Fig. 3.5. Thus from Fig. 3.5, it is clear that at higher wavelengths, due to the low optical power level shot noise is very low and the dominant noise contribution at these wavelengths is therefore the quantization noise of the analog-to-digital converter.

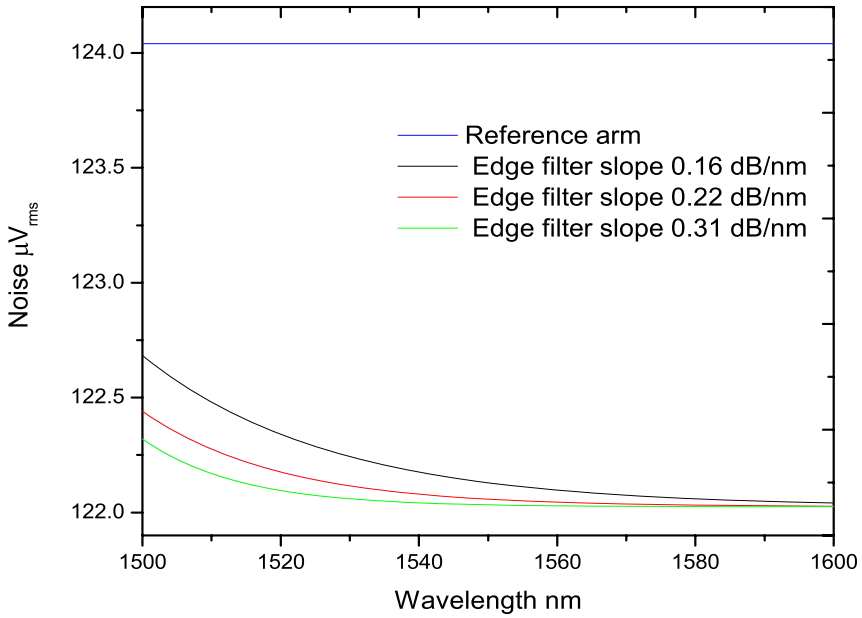

Figure 3.5: Calculated total noise of the receivers connected to reference arm and edge filter arms of different slope.

3.3.2 Modeling the ratio response of the system considering noise

To take account of the noise of the receivers connected to the reference arms and edge filter arm, together with the signal-to-noise ratio of the input signal, the

ratio of the system for a wavelength λ_0 can be expressed as,

$$R(\lambda_0) = -10log_{10}\Big[\frac{\int I_{\lambda_0} T_f(\lambda) d\lambda + Grand_{e\lambda_0}}{\int I_{\lambda_0} d\lambda + Grand_r}\Big], \tag{3.9}$$

where T_f is the transmission response of the edge filter which in the simplest case is a linear function within a wavelength range (λ_1, λ_2). Gaussian statistics are used to model the electrical noise. $Grand_e$ and $Grand_r$ are Gaussian random numbers used to represent the receiver's noise with a mean value 0 and standard deviation equal to the rms noise of the receivers connected to the edge filter and reference arms respectively and are uncorrelated to each other. As the shot noise of the receiver connected to edge filter is a function of wavelength it makes $Grand_e$ also wavelength dependent. The output spectral response of the source which has a limited SNR is represented as $I_{\lambda 0}$ as given in Equation (2.1).

The ratio response of the system considering the limited SNR of the source and noise of the detection circuit is modeled. To understand the separate effect of optical noise and receiver noise on the ratio fluctuation, the ratio fluctuation is calculated for the system with different edge filters in the presence of receiver noise only by keeping the source SNR infinite (effectively 100 dB). Secondly, to calculate the ratio fluctuation that arises due to the noise of the input signal only, the receivers are assumed to be noise free. The calculated ratio fluctuations in both cases are shown in Fig. 3.6(a) and Fig. 3.6(b) respectively. For a system with an infinite source SNR, the ratio fluctuation is due to the receiver noise and is very low at lower wavelengths as shown in Fig. 3.6(a). For an ideal receiver with zero noise the ratio fluctuation is due to the source's noise only and changes as the SNR of the source changes as shown in Fig. 3.6(b).

In practice all optical sources have a limited signal-to-noise ratio and the net ratio fluctuation of the system is determined by the combined effect of optical noise and the receiver noise. Considering the limited SNR and receiver noise the net ratio fluctuation is calculated using Equation (3.9). Three edge filters

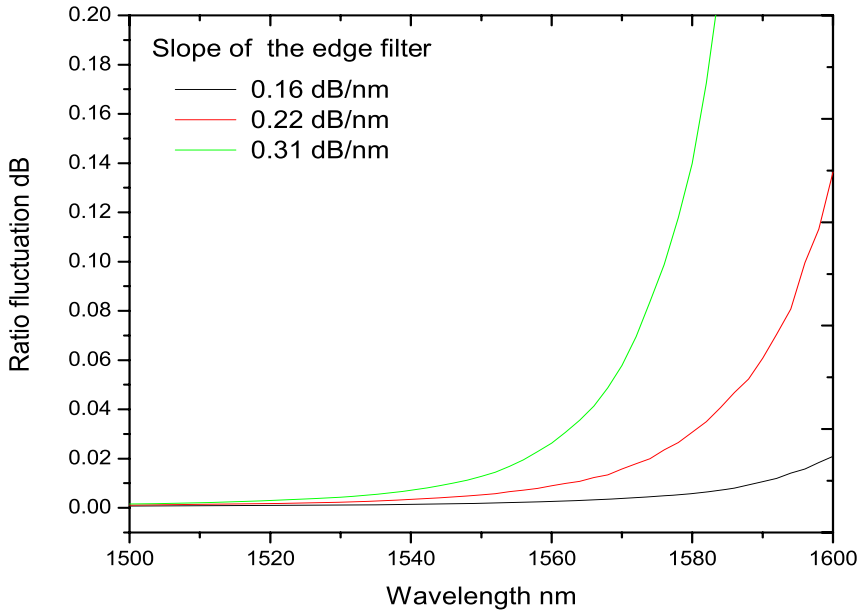

(a)

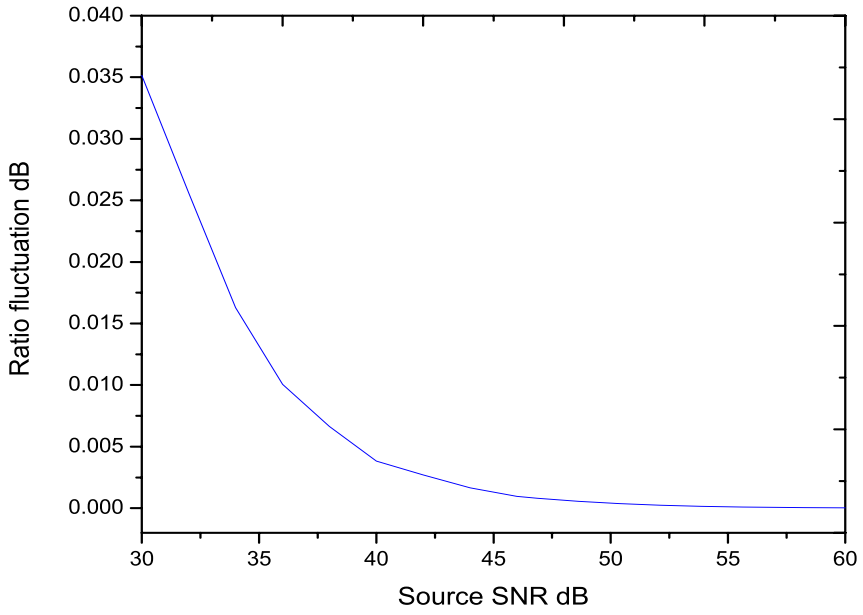

(b)

Figure 3.6: (a) Calculated ratio fluctuation of the system arises from the receiver noise (b) Calculated ratio fluctuation arises from the source noise.

with slopes of 0.16 dB/nm, 0.22dB/nm and 0.31 dB/nm are considered in the simulation. Fig. 3.7 shows the total ratio fluctuation of the system with different edge filters and with input signals of different SNR. Three cases are considered in the simulation, input signals with an SNR of 30 dB, 40 dB and 50 dB. From the figure it is clear that the ratio fluctuation is higher at longer wavelengths due to the effect of receiver noise. The level of noise fluctuation increases irrespective of wavelength when the SNR of the input signal changes.

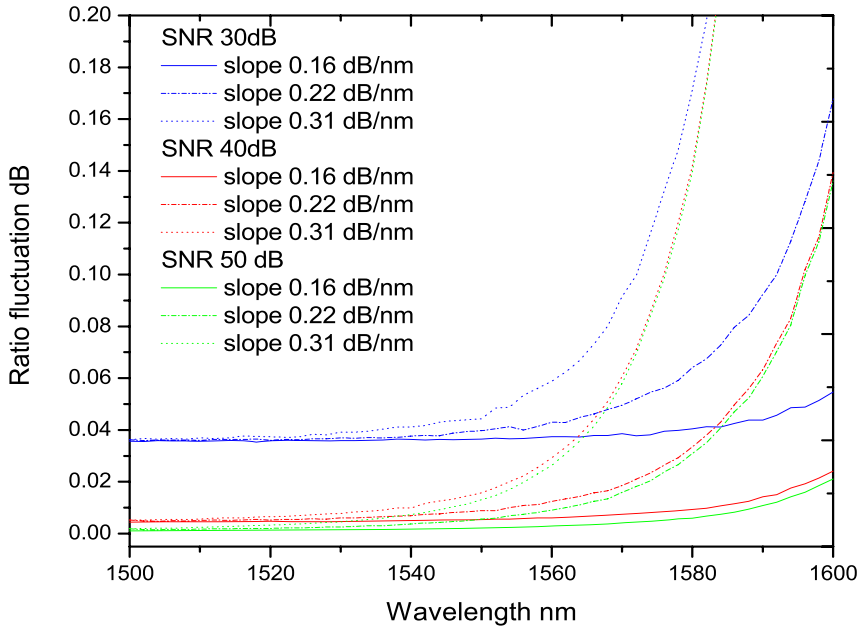

Figure 3.7: Calculated ratio fluctuation of the system for different optical SNR and for edge filters with different slopes.

Apart from the increase in the fluctuation in the ratio, the limited SNR of the input signal limits the wavelength measurement range. From the simulation results it is clear that the measurement range with a required resolution (determined by the noise) is determined jointly by the receiver noise and the source noise of the input signal. It should also be noted that a change in the SNR of the source also affects the accuracy of wavelength measurements as explained in Section 2.4 of Chapter 2.

3.4 Impact of noise on the resolution of the system

From the Fig. 3.7 it can be seen that the ratio fluctuation increases as the wavelength increases, which limits the wavelength resolution of the system in addition to the wavelength range. In any measurement system perturbed by noise, the resolvable step change should be higher than the peak-to-peak fluctuation of the parameter being measured. In the case of a ratiometric wavelength measurement system the minimum detectable ratio variation corresponding to a wavelength shift is assumed to be equal to the peak-to-peak ratio fluctuation and can be expressed as,

$$\Delta R(\lambda_0)_{min} = [R(\lambda_0)]_{p-p} \tag{3.10}$$

For a system of known slope m_r the wavelength resolution can be determined from the ratio fluctuation, which is given as,

$$Resolution = \frac{[R(\lambda_0)]_{p-p}}{m_r} \tag{3.11}$$

Assuming a linear slope, the wavelength resolution is estimated for systems consisting of edge filters of slope 0.16 dB/nm, 0.22 dB/nm and 0.31 dB/nm. Fig. 3.8(a), Fig. 3.8(b) and Fig. 3.8(c) show contour plots of the resolution of the system at different wavelengths (different receiver noise levels) and at different optical source SNRs. It is clear that a 10 pm resolution is possible for all systems below 1520 nm if the SNR of the source is above 50 dB. When the source SNR reduces, for a system with an edge filter having a higher slope a better resolution at lower wavelengths is achieved. For systems with slope 0.16 dB/nm, 0.22 dB/nm and 0.31 dB/nm a 10 pm resolution can be achieved for a range of 36 nm, 22 nm, 16 nm respectively starting from 1500 nm in the presence of receiver noise and an input signal SNR of 50 dB. Thus, the slope used within a system in the presence of receiver noise and optical noise depends on the required resolution

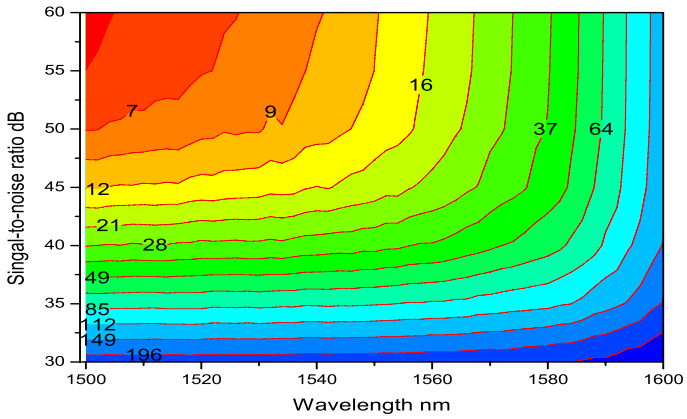

(a)

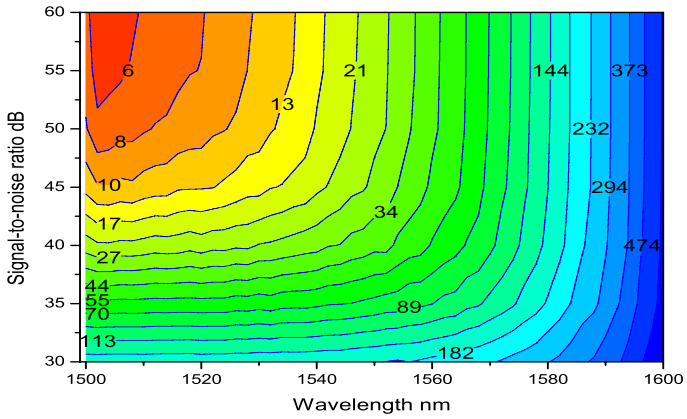

(b)

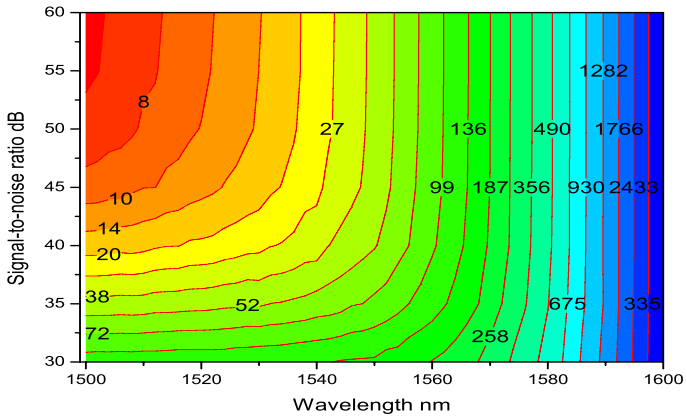

(c)

Figure 3.8: Contour plots of achievable resolution in pico meters for system contains edge filters of slope (a) 0.16 dB/nm (b) 0.22 dB/nm (c) 0.31 dB/nm.

and wavelength range. High resolution in a very narrow wavelength range can be obtained with an edge filter of higher slope, while for a wide wavelength range a reasonable resolution can be obtained with an edge filter of lower slope.

The direct effect of noise on resolution is clearly shown in Fig. 3.9. A ratio variation equivalent to a 10 pm wavelength shift is applied to the systems with different edge filters and source SNR of 40 dB at 1550 nm. From the figures it is clear that a system with an edge filter of slope 0.16 dB/nm can resolve 10 pm wavelength shift reliably than filters of higher slope at 1550 nm. The usual method to minimize the noise is averaging which can be applied here also to minimize noise effects and to improve the effective resolution of the system, but when the system is used for dynamic measurements averaging limits the speed of the measurements. Here the results are presented based on raw data without any post processing to give a real picture of the impact of noise on any ratiometric wavelength measurement system's performance.

3.5 Experimental investigation of noise effects

To verify the theoretical modeling of the system when considering noise effects, a ratiometric wavelength measurement system based on a macro-bending fiber edge filter was built and a series of experimental investigations were carried out. The slope of the macro-bend fiber edge filter can be varied by changing the number of bend turns or bend radius. The schematic of the experimental arrangement is shown in Fig. 3.10. In the experiment a bend radius of 10.5 mm and bend turns of 10, 15 and 20 were used. The tunable laser source used was the same as that specified in Section 2.4.1. At the receiver end two InGaAs photodiodes (G9801) with a measurable range of 900 nm to 1700 nm together with a dual channel low noise trans-impedance pre-amplifier with an amplification factor of 10^5 V/A are used. The analog-to-digital converter used was a NI6143 data acquisition card which gives simultaneous sampling at high sampling rates (max. 250 kHz).

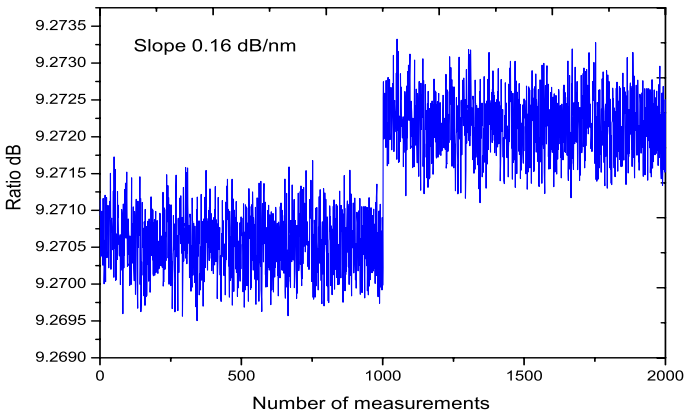

(a)

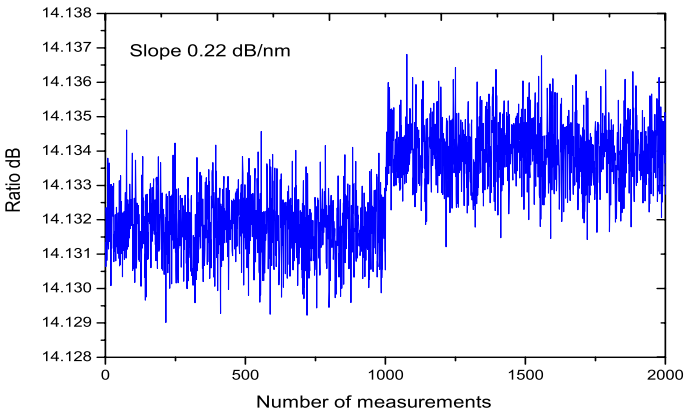

(b)

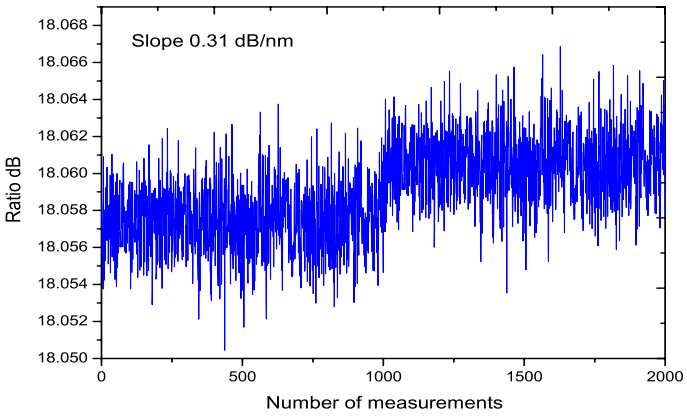

(c)

Figure 3.9: Calculated ratio variation for 10 pm wavelength step at 1550 nm for the system with edge filters of slope (a) 0.16 dB/nm (b) 0.22 dB/nm (c) 0.31 dB/nm.

The cables used were shielded and a noise rejecting connector block was used to connect the amplifier output to the data acquisition card.

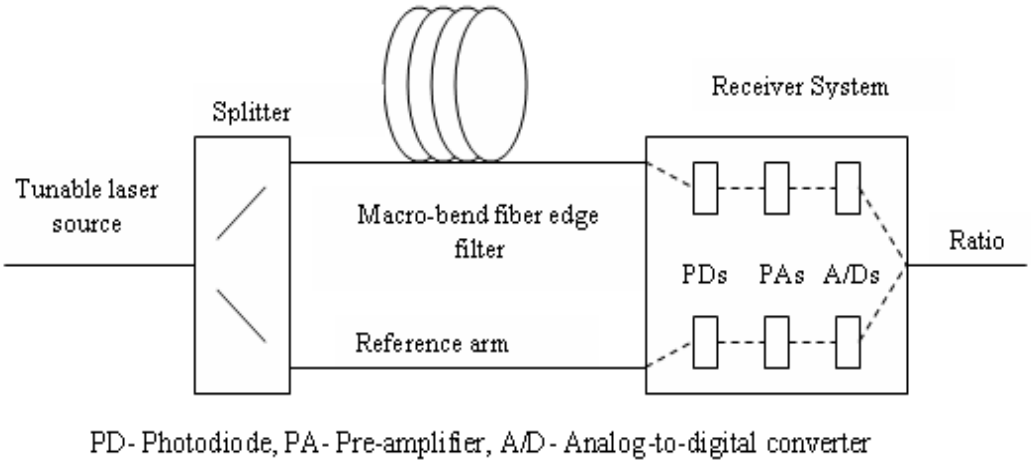

Figure 3.10: Schematic of the experimental arrangement of a ratiometric wavelength system employed with a macro-bend fiber edge filter for noise studies.

The transmission response of the edge filters for a wavelength range 1500 nm - 1600 nm was measured using an optical spectrum analyzer to calculate the discrimination range and average slope of the edge filters. The measured transmission response of the edge filters is shown in Fig. 3.11. The discrimination ranges of the edge filters are 16 dB, 22 dB and 31 dB respectively for the wavelength range of 100 nm from 1500 nm to 1600 nm, which gives an average slope of 0.16 dB/nm, 0.22 dB/nm and 0.31 dB/nm respectively. The input signal power was set to -10 dBm. The baseline loss (bend loss at 1500 nm) for the edge filters were 4.5 dB, 7 dB and 8.3 dB respectively. The wavelength flattened coupler used to split the input signal contributes an insertion loss of 3.5 dB including the excess loss. It should be noted that the transmission loss of each different edge filter together with the coupler's insertion loss was used to calculate the shot noise generated in the receivers due to this power and then the total noise which is presented in Fig. 3.5. To validate the model presented above, the ratio

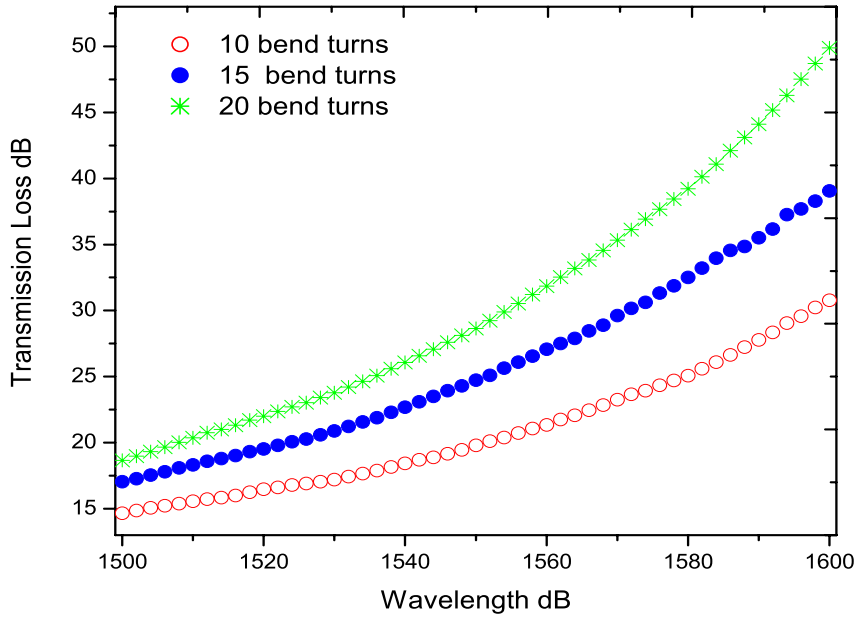

Figure 3.11: Measured transmission response of the edge filters using an optical spectrum analyzer.

fluctuation of the system for a wavelength range of 1500 nm - 1600 nm with a 10 nm interval was measured with all the three edge filters and is shown in Fig. 3.12. A comparison with theoretical values is also presented. The small discrepancy between the measured and the modeled values at higher wavelengths is mostly due the small change in the responsivity of the photodiodes when wavelength changes from 1500 nm - 1600 nm. Due to the difficulty in extracting responsivity values for all the discrete wavelengths from the manufacturers data for the photodiodes used in the system, in the model the responsivity of the photodiodes is assumed constant. However, in practice the responsivity of a photodiode is slightly lower at higher wavelengths, as a result the photocurrent produced at higher wavelengths will be lower. This means that the signal voltage in the receiver is reduced at higher wavelengths due to a decrease in the responsivity. Due to the constant level of thermal noise the relative magnitude of the wanted signal and the noise is reduced at higher wavelengths due to the small decrease in the responsivity, resulting in an increase in the measured ratio fluctuation.

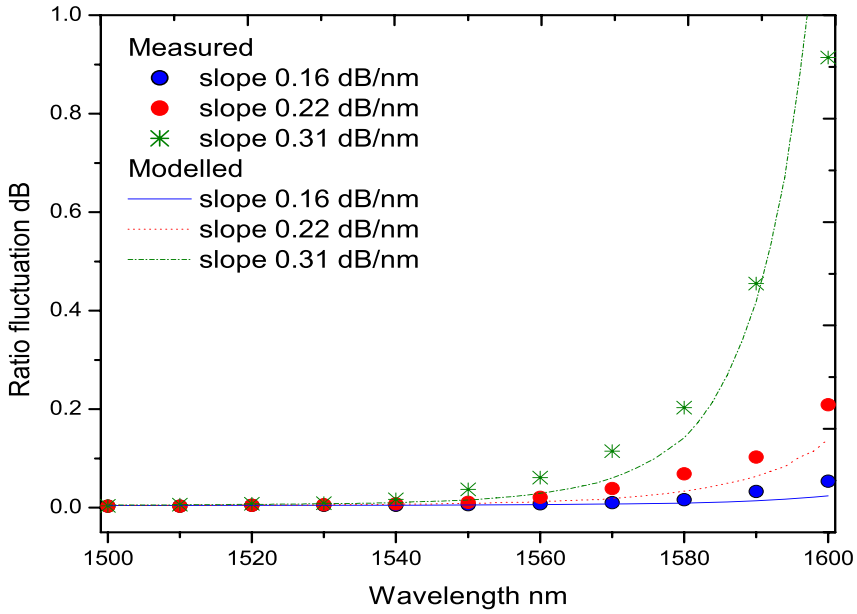

Figure 3.12: Measured ratio fluctuation of the system and its comparison with the calculated ratio fluctuation.

Overall the measured and modeled results agree and verify the noise model and the consequences of noise on a ratiometric wavelength measurement system. In Fig. 3.13 the corresponding ratio response of the system with different edge filters and a comparison with the simulated response is presented. The measured ratio response and the simulated ratio response obtained considering the SNR of the source and noise of the detection circuit are in close agreement.

3.5.1 Experimental verification of impact on noise on the resolution of the system

From the modeling result it can be seen that, to improve the resolution, increasing the slope of the edge filter is not a guaranteed approach as it will not necessarily serve this purpose, rather it may degrade the resolution as well as the wavelength range of the system. To prove this experimentally the resolution of the system is measured with different edge filters and also at different wavelengths.

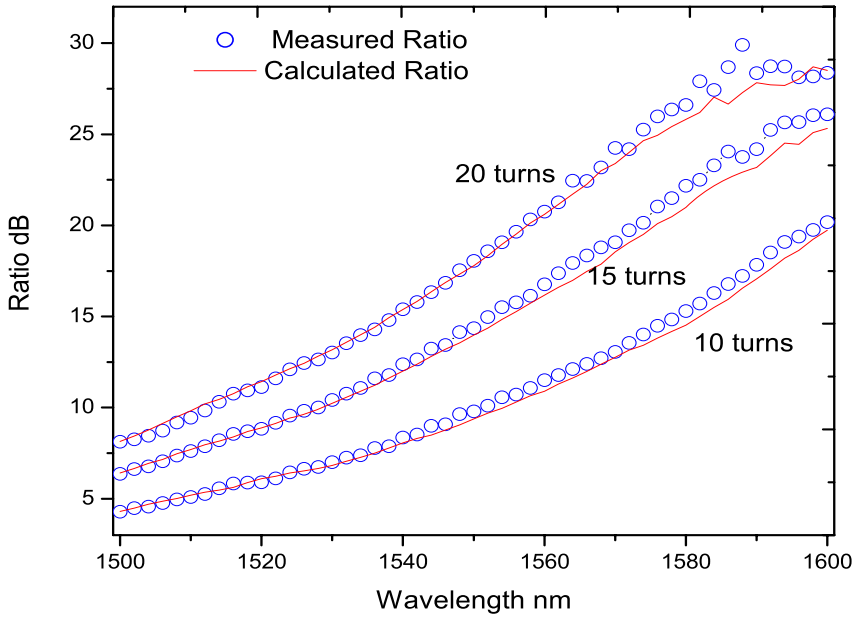

Figure 3.13: Measured ratio response of the system with different edge filters and its comparison with simulated ratio response.

It has to be noted that the transmission response of the edge filter is not strictly linear as considered in the modeling. So in practice to estimate the resolution one has to calculate the local slope in the vicinity of a spot wavelength to avoid any wavelength error due to the non-linear nature in reality of the ratio response. The local slopes of the response at 10 nm intervals are calculated for all the edge filters and are shown in Fig. 3.14(a). As a result of the difference in slope for different wavelengths, the wavelength resolution of the system will also be different. The estimated resolution of the system which is limited by the noise in the system is shown in Fig. 3.14(b). This figure validates the theoretical prediction that the resolution is a function of both wavelength and ratio response slope.

As a further confirmation of the results the ratio variation was measured for a wavelength step of 20 pm for the system with all the three edge filters at 1550 nm and the results are shown in Fig. 3.15. From the figure it is seen that a wavelength change can be resolved more readily for the system with an edge

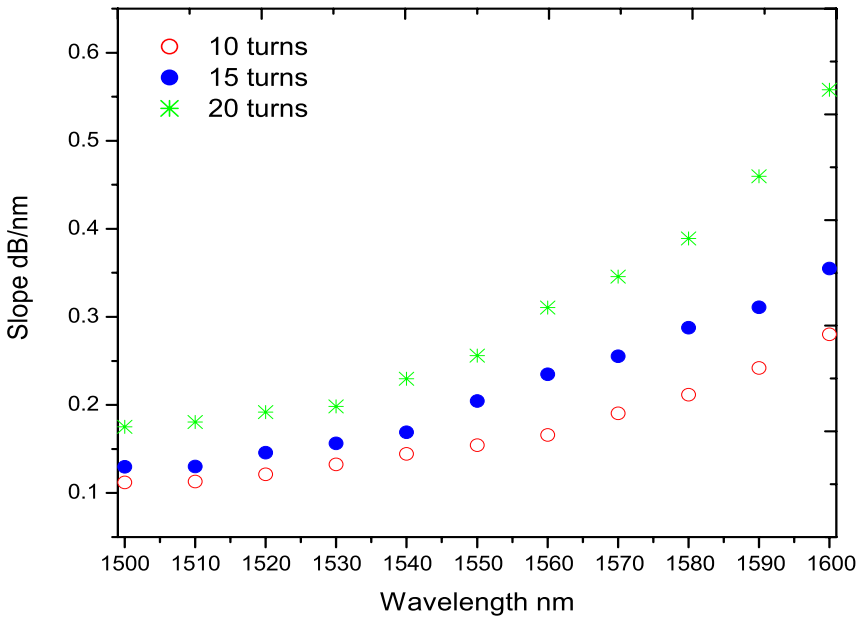

(a)

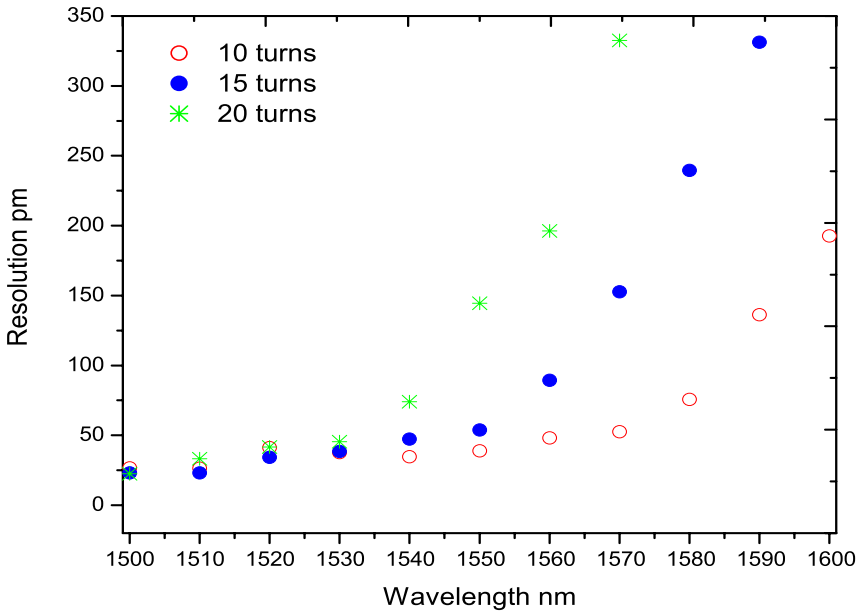

(b)

Figure 3.14: (a) Measured local slope of the system at different wavelengths (b) Estimated wavelength resolution considering noise and the local slope of the system.

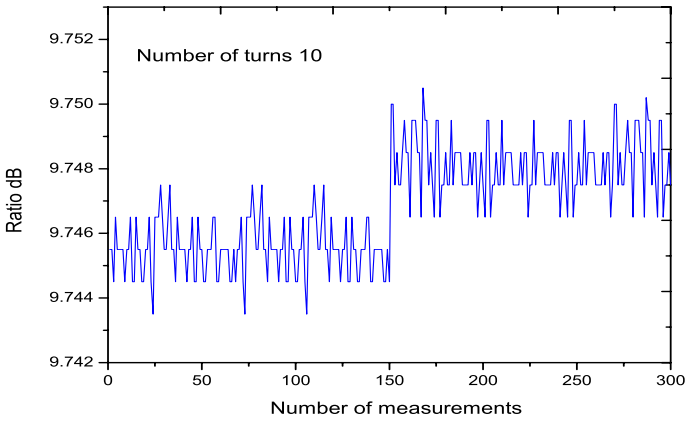

(a)

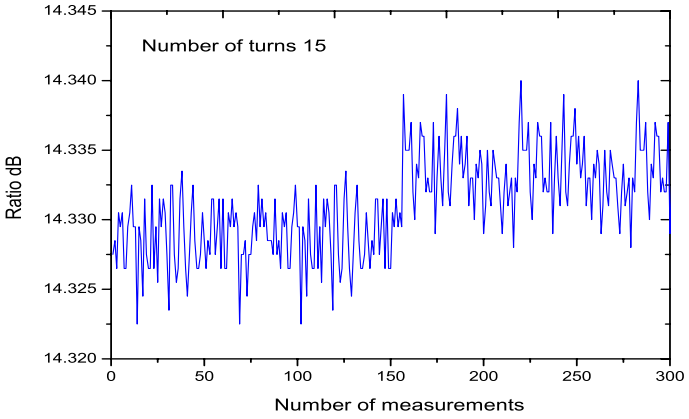

(b)

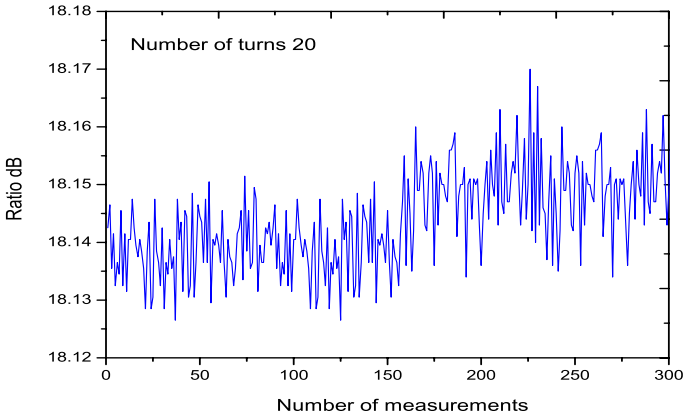

(c)

Figure 3.15: Measured ratio variation for 20 pm wavelength step at 1550 nm for the system with edge filters (a) 10 turns (b) 15 turns (c) 20 turns.

filter of 10 turns than by systems that use edge filters with a large numbers of turns (and thus higher slopes). This confirms the assertion above from the model that increasing the slope of itself will not improve the resolution. Also it is not possible to achieve the same resolution throughout the wavelength range and for a system with a given edge filter a higher resolution will be always be achieved in the lower wavelength regions.

It is been established from the modeling and experimental results that in the design of an edge filter based ratiometric system noise is an important parameter which determines the achievable resolution for a given wavelength range. Furthermore, an increase in the slope of the edge filter will not improve the resolution as it is bounded by the limited optical SNR and receiver noise. An optimization of the slope of the edge filter is required to minimize the noise effects and obtain the best resolution together with a wider wavelength range.

3.6 Summary

In this chapter an overview of the noise mechanisms in an optical receiver is provided and a noise model for a ratiometric wavelength measurement system is presented. Theoretical modeling of the noise effects on an edge filter based wavelength measurement system has been carried out and verified experimentally. The ratio response of the system is modeled considering the SNR of the source and the noise from the optical-to-electrical conversion circuit. From the investigation it was proven that detector circuit noise and the SNR of the input signal determines the resolution of the system for a given wavelength range. It has been demonstrated theoretically and experimentally that increasing the slope of the edge filter is not a guaranteed approach to increasing the resolution of the system. An optimization of the slope of the system considering the total noise of the system is required to achieve the best possible resolution for a wider wavelength range.

The conclusions from this chapter are summarized as follows;

- A noise model for an edge filter based ratiometric wavelength measurement system is proposed.

- A complete model of the system is necessary to determine the overall performance of any edge filter based ratiometric system. The proposed noise model of a ratiometric system and the studies based on this model show that the widely held presumption about using a higher ratio slope for higher resolution is incorrect.

- It was shown that increasing the slope of the edge filter is not a guaranteed approach to increasing the resolution of the system. An optimization of the slope of the system considering the total noise of the system is required to achieve the best possible resolution for a wider wavelength range.

Chapter 4

Polarization dependent loss of the system and its consequences

4.1 Introduction

Virtually all optically transparent materials interact with light and affect to some degree its polarization state [94, 95]. In general, optically transparent materials exhibit a spatial polarization distribution. As an optical signal passes through a material, due to spatial polarization interaction the signal suffers selective power reduction or optical power loss, in specific directions. This power loss due to local polarization influences is wavelength dependent. This is known as polarization dependent loss (PDL) and is usually measured in decibels.

Most of the components used with optical fibers, such as optical couplers, optical circulators, optical connectors, wavelength division multiplexers, etc. exhibit polarization dependency and have a finite PDL [96, 97]. The polarization dependence of optical components has many sources. Some of the most common effects are: dichroism, fiber bending, angled optical interfaces and oblique reflection. When these components are used in optical networks containing single mode fiber, which does not maintain the transmitted polarization state, the output power will change when the input polarization state changes. The evolution of polarization along a conventional fiber is random in nature and, in consequence, is totally unpredictable [98, 99]. Thus, PDL can lead to a degradation of the performance quality of any optical measurement system and the systems require

components with low PDL [100].

Prior to the introduction of systems demanding very high accuracy(±10 pm) the role of PDL in a ratiometric measurement system was not considered important. If a system contains more than one polarization sensitive component connected by standard single mode fibers, its global polarization dependent loss may fluctuate and hence the measured ratio also fluctuates [101, 102]. The fluctuation in the ratio will have an impact on the performance accuracy of the system. The fluctuation arises because the state of polarization of the input light to the system may vary randomly, for example as a result of the stress variations in the transmission fibers or due to a change of light source etc. A system calibrated at a particular input polarization state gives errors as the attenuation ratio will be different because of the polarization dependency of the elements. Some work has been reported on the wavelength dependency of PDL of bulk optical devices and optical transmission systems [103, 104]. However, the polarization dependency of the entire ratiometric system and its consequences in the wavelength accuracy have been not studied to date.

To have a highly accurate wavelength measurement system it is important to estimate the error originating from the polarization sensitivity of the components and reduce the effect of polarization sensitivity on the system's performance. In this chapter the origin of the polarization dependency of the components used in the ratiometric system is firstly studied, along with the effect on the wavelength measurements. Subsequently, to reduce the polarization dependency of the system a new configuration is proposed. The first section discusses the origin of polarization sensitivity of the 3 dB coupler and the bend fiber filter. A theoretical model to estimate the range of PDL and ratio fluctuation is presented in Section 4.3. Based on the model, an estimation of the ratio and wavelength fluctuation caused by the PDL is determined and experimentally verified in Section 4.4. From the investigations on the influence of PDL on a ratiometric system, it

is realized that it is very important to minimize the PDL of the system. Section 4.5 describes a configuration which minimizes the PDL of the fiber bend loss filter and in Section 4.6 a low polarization sensitive wavelength measurement system is presented.

4.2 Polarization sensitivity of a macro-bend fiber and a 3 dB coupler

The operational characteristics of many fiber optic systems depend on the polarization of the light guided by the optical fiber and optical fiber components. Hence, polarization dependence management and elimination is necessary to avoid errors originating from the polarization sensitivity of optical fiber components. To achieve this initially the origin of the polarization sensitivity, which leads to PDL has to be studied. The PDL of an optical component is commonly defined as the difference between the maximum and the minimum insertion losses for all the possible states of polarization. If T_{min} and T_{max} are the minimum and maximum transmission coefficients of an optical element, then PDL can be expressed as,

$$PDL_{dB} = 10log_{10}\Big[\frac{T_{max}}{T_{min}}\Big] \tag{4.1}$$

In a fiber bend loss filter based ratiometric wavelength measurement system the components that exhibit PDL are the macro-bend fiber filter and the 3 dB coupler. The origin of polarization sensitivity of these devices are explained in the following sections.

4.2.1 PDL of a 3 dB coupler

It is very well known that a 3 dB coupler is a polarization sensitive device. The common fabrication technique for a coupler is the fused-fiber method which involves twisting, melting, and pulling two single-mode fibers so they are fused

together over a uniform length section. During fabrication the deviation of the coupler geometry from circular symmetry to the elliptical shape in the fused tapered region changes the coupling characteristics of polarization states and leads to birefringence, which makes the coupler polarization sensitive and eventually a device exhibiting PDL [105]. The polarization sensitivity of a 3 dB coupler mainly depends on the geometrical structure parameters and degree of fusion [106–109].

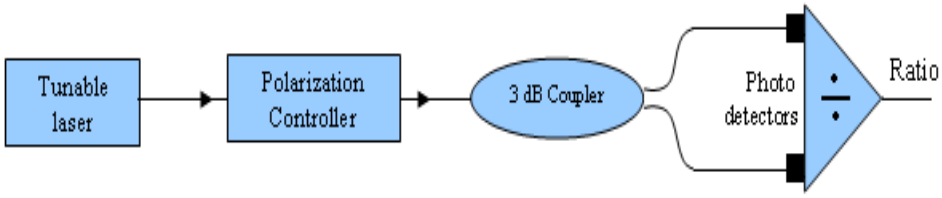

Figure 4.1: Experimental arrangement to measure PDL of a 3 dB coupler.

The PDL of any device is commonly characterized at a specific wavelength. But because of the wavelength dependency of PDL and especially in wavelength measurements, the PDL of the components has to be considered for the whole range of wavelengths from 1500 - 1600 nm. Typical commercially available 2x2 fused couplers have a PDL of 0.1 - 0.15 dB at the central wavelength, but the value does vary with wavelength. To experimentally verify this an experimental arrangement as shown in Fig. 4.1 is used. A manual fiber polarization controller is used to change the polarization state of the input signal from a tunable laser source. The polarization controller allows for the complete control of the output polarization state and the output power varies with the change in polarization states for a particular wavelength. It is assumed that the fiber polarization controller covers all the possible polarization states at a fixed wavelength. The measured PDL of the arms of a 3 dB coupler for a wavelength range of 1500 nm - 1600 nm is shown in Fig. 4.2. Each arm of the coupler exhibits a different PDL and the power variation will be different for different arms for a change in input polarization state. The error bar in the measured values shows the uncertainty

in the measurement due to the noise of the receivers. The photodiodes used to measure the power and the connection fibers also exhibit PDL and the measured PDL consists of the PDL of the connection fibers, polarization controllers and the photodiodes. The components taken together contribute a PDL value of approximately 0.03 dB.

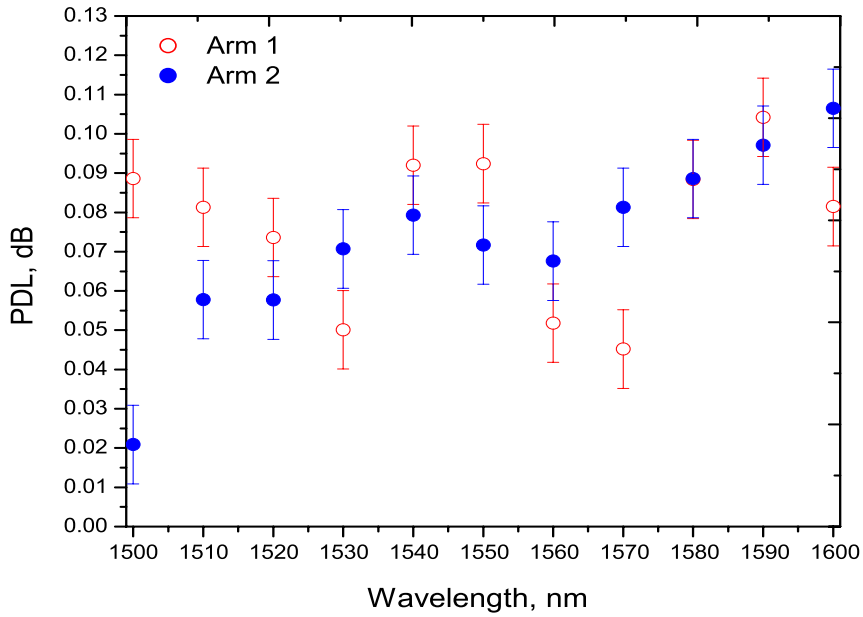

Figure 4.2: Measured PDL of the arms of a 3 dB coupler.

4.2.2 Polarization sensitivity of macro-bend single-mode fiber filter

There are a couple of reasons which underpin the polarization sensitivity of a bent fiber. The state of polarization of light propagating along a single-mode fiber can be influenced by perturbations, such as bending and twisting. In a macro-bend fiber filter it can originate from the anisotropic nature of the refractive index caused by the bending stress [110, 111]. Single-mode fibers with nominal circular symmetry about the fiber axis are in fact bimodal and they can propagate two nearly degenerate modes with orthogonal polarizations, the TE and TM modes. The bend induced mechanical stress can induce birefringence by

changing the modes of polarization. In the case of a standard single-mode fiber SMF28, the stress induced refractive index variation is very small. As a result, the bend induced birefringence will have only a small impact on the polarization modes propagating through the fiber. A practical single-mode fiber consists of a core, a cladding and a polymer coating layer which offers mechanical protection. The difference in the refractive index between the polymer coating layer and the cladding layer is much higher as compared to that between the cladding and core. The reflectance of the radiated field occurring at the interface between the coating layer and cladding layer is believed to be different for different polarization states. This can lead to polarization dependence of the bend loss, which originates because of the coupling between the reflected radiated field and the guided fundamental mode. Thus, the main contributor to the polarization sensitivity of a bend single-mode fiber is the polymer coating.

The theoretical model presented in [112] shows that the TE and TM modes propagating along the fiber suffer from different values of bend losses. Similar to the bend loss behaviour of a single-mode fiber (Fig. 2.7) the absolute PDL does not increase monotonically with the bend radius. The normalized polarization dependence has a quasi-periodical characteristic with bending radius and this quasi-periodical behaviour is very close to that of the bend loss vs. bending radius of a standard single mode fiber. Since the bend loss varies with wavelength, the PDL also changes with wavelength. The normalized PDL for 10 turns of SMF28 for different bend radii is shown in Fig. 4.3 [112].

To study the PDL of the fiber filter in use, the PDL for a fiber filter of 15 bend turns and bend radius of 10.5 mm is measured for a wavelength range of 1500 nm -1600 nm with an interval of 10 nm and is shown in Fig. 4.4. The polarization state is changed using a fiber polarization controller as explained in Section 4.2.1. As the fiber bend loss is temperature dependent (explained in the next chapter), the temperature in the vicinity of the fiber filter is monitored so that the error in

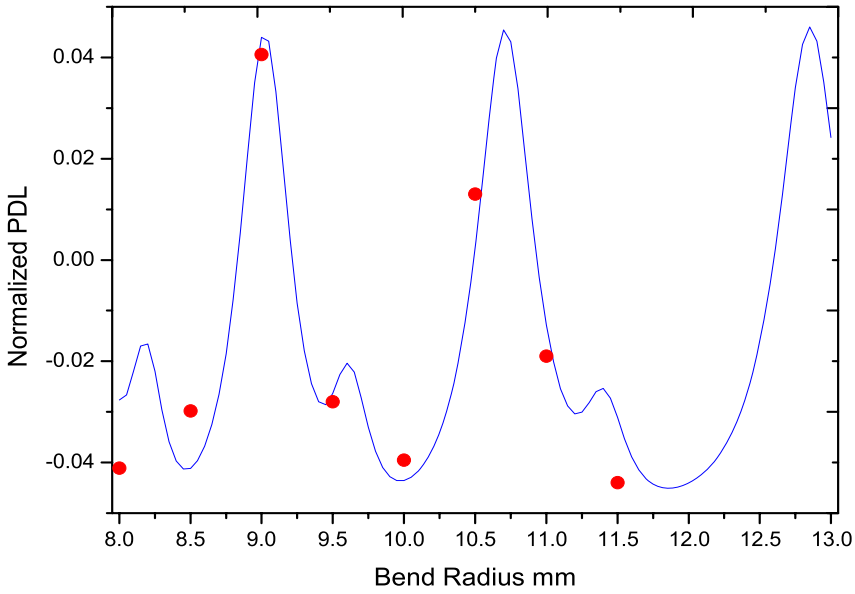

Figure 4.3: Normalized PDL of 10 turns of SMF28, simulated and measured [112].

PDL measurements due to the ambient temperature variation can be determined. Based on the known variation in bend loss with temperature of the fiber type in use (From chapter 5), an error bar is included in the PDL measurements which is approximately ±0.018 dB. The error bar includes the errors contributed by the temperature fluctuation and the noise of the system.

4.3 Theoretical model to estimate the total range of PDL and its associated ratio fluctuation

As mentioned above, since a macro-bend fiber filter ratiometric system contains two PDL components, the total PDL of the system is not simply the sum of the contributions of each PDL element. If the polarization sensitive axis of the 3 dB coupler and the fiber filter are not aligned with each other, the resulting PDL depends on the relative orientation of the PDL axes at each connection. Thus, in the case of a macro-bend fiber filter based ratiometric wavelength measurement system the total attenuation ratio fluctuation of the system depends on the PDL

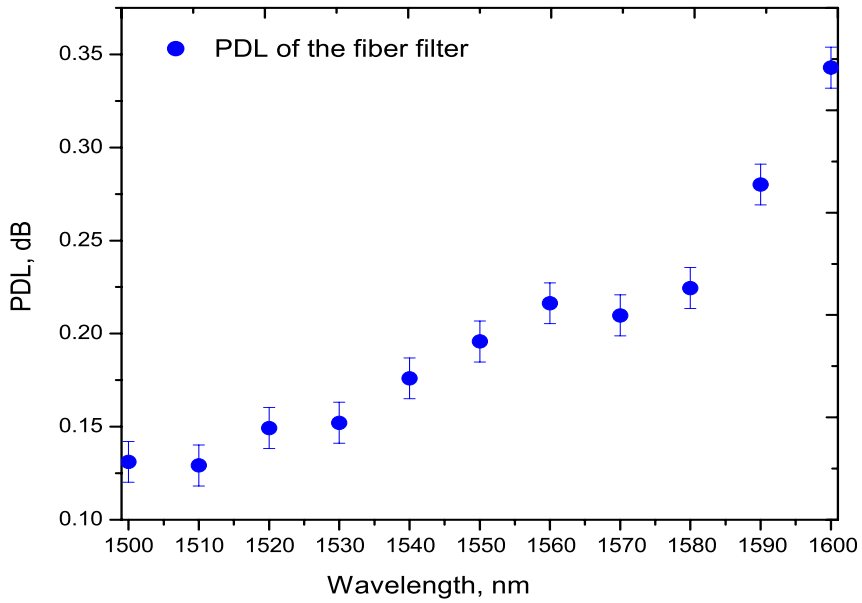

Figure 4.4: Measured PDL of the macro-bend fiber filter.

of both the filter arm and the reference arm. The general expression for PDL of any optical component is given in Equation (4.1). But the more convenient way is to express the PDL as a 3 dimensional vector $\vec{\Gamma}$ of length Γ as [101],

$$\Gamma = \frac{T_{max} - T_{min}}{T_{max} + T_{min}}. \tag{4.2}$$

If Γ_{3dB} and Γ_{bend} are the PDL of the 3 dB coupler and the fiber filter, the net PDL of filter arm can be expressed as [102],

$$\vec{\Gamma}_{3dBbend} = \frac{\sqrt{1-\Gamma_{bend}^2}}{1+\vec{\Gamma}_{3dB}\vec{\Gamma}_{bend}}\vec{\Gamma}_{3dB} + \frac{1+\vec{\Gamma}_{3dB}\vec{\Gamma}_{bend}(1-\sqrt{1-\Gamma_{bend}^2})/\Gamma_{bend}^2}{1+\vec{\Gamma}_{3dB}\vec{\Gamma}_{bend}}\vec{\Gamma}_{bend}. \tag{4.3}$$

To calculate the the maximum and minimum PDL values one has to calculate the norm of $\vec{\Gamma}_{3dBbend}$. The norm of $\vec{\Gamma}_{3dBbend}$ is a function of different orientations between $\vec{\Gamma}_{3dB}$ and $\vec{\Gamma}_{bend}$ and the magnitude of $\vec{\Gamma}_{3dBbend}$ can be calculated from,

$$\sqrt{\vec{\Gamma}_{3dBbend}\vec{\Gamma}_{3dBbend}} = \sqrt{\frac{\Gamma_{3dB}^2 + \Gamma_{bend}^2 - \Gamma_{3dB}^2\Gamma_{bend}^2 - 1 + (1 + \vec{\Gamma}_{3dB}\vec{\Gamma}_{bend})^2}{(1 + \vec{\Gamma}_{3dB}\vec{\Gamma}_{bend})^2}}. \quad (4.4)$$

The maximum value of the PDL will occur when $\vec{\Gamma}_{3dB}$ and $\vec{\Gamma}_{bend}$ are parallel, i.e., $\vec{\Gamma}_{3dB}\vec{\Gamma}_{bend} = \Gamma_{3dB}\Gamma_{bend}$, and minimum occurs when they are antiparallel, i.e., $\vec{\Gamma}_{3dB}\vec{\Gamma}_{bend} = -\Gamma_{3dB}\Gamma_{bend}$. The maximum and minimum global PDL of the fiber filter arm Γ_{Gmax} and Γ_{Gmin} can thus be expressed as,

$$\Gamma_{Gmax} = \frac{\Gamma_{3dB} + \Gamma_{bend}}{1 + \Gamma_{3dB}\Gamma_{bend}} \quad (4.5)$$

$$\Gamma_{Gmin} = \frac{|\Gamma_{3dB} - \Gamma_{bend}|}{1 - \Gamma_{3dB}\Gamma_{bend}} \quad (4.6)$$

Using these equations the range of PDL of the fiber filter arm can be predicted and together with the PDL of the reference arm of the system the ratio error of the system can be estimated. The maximum variation in the ratio from the calibrated value occurs when one arm gives the maximum attenuation and the other gives the minimum attenuation for a given state of polarization. From the expression for the ratio of the system as given in Section 2.2 of Chapter 2, where the photodiodes give the integral power over the wavelength range and by knowing the maximum and minimum power at the output arms of the system when the polarization state changes, the maximum possible polarization dependent change in ratio of the system for any wavelength can be expressed as,

$$\Delta R_{max} = 10log_{10}\Big[\frac{\int P_{1max}(\lambda)I_{\lambda_0}(\lambda)d\lambda}{\int P_{2min}(\lambda)I_{\lambda_0}(\lambda)d\lambda}\Big] - 10log_{10}\Big[\frac{\int P_{1min}(\lambda)I_{\lambda_0}(\lambda)d\lambda}{\int P_{2max}(\lambda)I_{\lambda_0}(\lambda)d\lambda}\Big], \quad (4.7)$$

where P_{1max} and P_{1min} are the maximum and minimum output power of the filter arm when the polarization state changes and P_{2max} and P_{2min} are that of

the reference arm. I_{λ_0} is the narrow band input signal with a central wavelength λ_0 which in this case is from a tunable laser source. By knowing the variation in ratio the corresponding wavelength variation can be calculated.

4.4 Estimation of ratio and wavelength fluctuation and its experimental verification

An all-fiber ratiometric wavelength measurement system based on macro-bend fiber filter was built to investigate the ratio and wavelength fluctuation due to PDL. A commercially available fused wavelength flattened 3 dB coupler was used as the splitter whose response is shown in Fig. 2.2. Arm 1 of the filter is used as the reference arm and arm 2 is connected to the fiber edge filter. The fiber edge filter used has a bend radius of 10.5 mm and 15 turns. This configuration of the fiber edge filter gives a very good discrimination range and measurable wavelength range from 1500 nm up to 1580 nm without SNR effects as described in Chapter 2. The average slope of the edge filter used was 0.22 dB/nm. The input power level of the signal supplied to the system was 0 dBm, while there is an insertion loss due to splicing and a 3.3 dB loss (including the excess loss) from the coupler. When the wavelength exceeds 1580 nm the bend fiber arm's output power drops below -30 dBm resulting in a poor signal-to-noise ratio, which affects the ratio response's linearity. So the measurable wavelength range is effectively limited from 1500 nm - 1580 nm. Since the PDL is highly dependent on the bend radius as shown in Fig. 4.3, it is very important to maintain a constant radius throughout the measurements. The fiber was wrapped on a mandrel with a fixed radius to maintain the radius of the fiber filter. The measured PDL of the 3 dB coupler and the fiber filter were presented in Fig. 4.2 and Fig. 4.4 respectively.

The ratio spectrum of the system is also measured at different polarization states to allow an estimation of the maximum wavelength error from the calibrated value. The shift in the ratio spectral response of the system at different

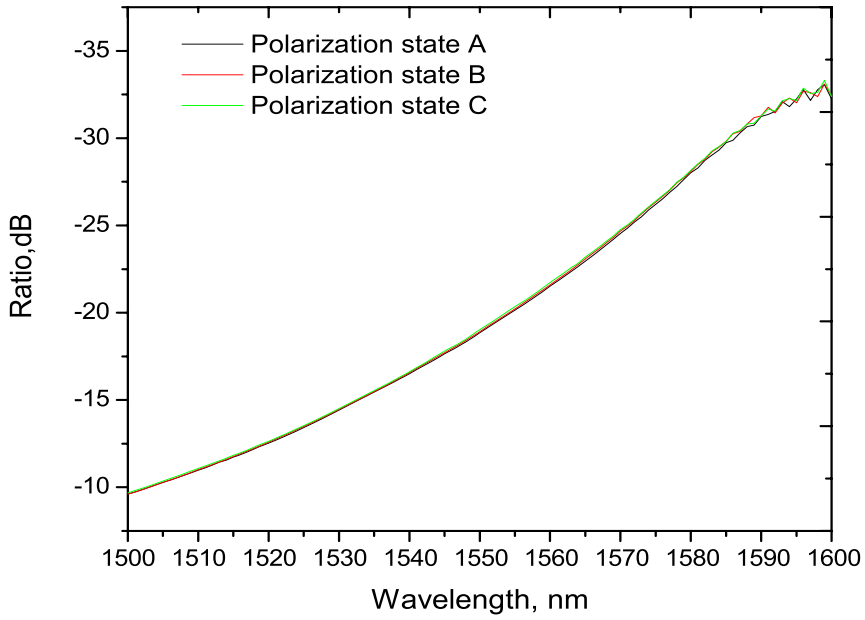

(a)

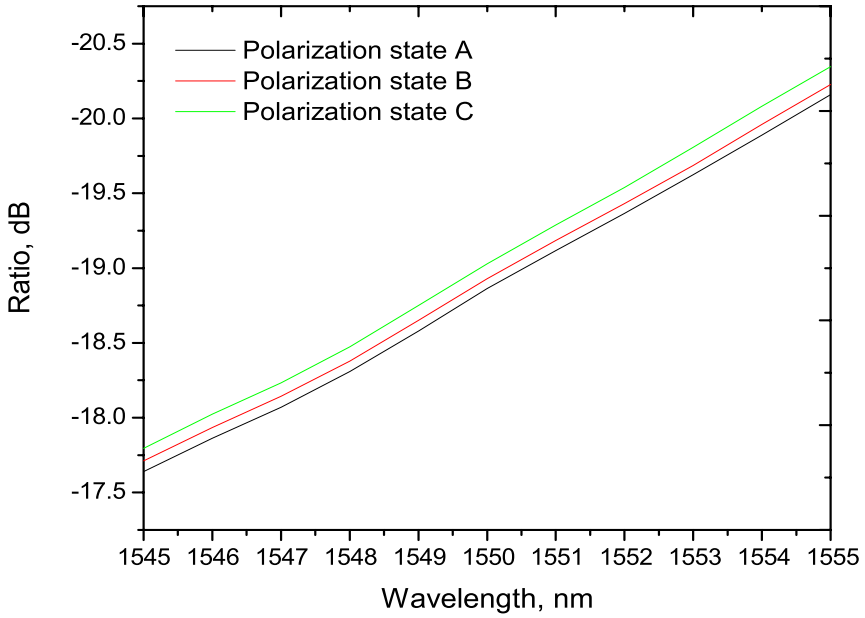

(b)

Figure 4.5: (a) Overall ratio response of the system at different polarization states (b) Expanded ratio response showing ratio variation at different states of polarization for a narrower wavelength range.

polarization states gives rise to the variations in the measured wavelength. Fig. 4.5(a) shows the overall response from 1500 nm - 1600 nm, which is obtained by tuning the laser from 1500 nm to 1600 nm with a 1 nm interval, while Fig. 4.5(b) focuses on the response over a narrower wavelength range, 1545 nm - 1555 nm, to better illustrate the variation in ratio that occurs when the polarization state changes. The ratio response for polarization state A is used as the calibrated response, while the response curves for the two other states B and C show the variation in ratio response from the calibrated response as the polarization state changes. For the measured ratio spectrum the slope is not strictly linear and hence one has to find the local slope to determine the wavelength error as explained in Section 3.5 of Chapter 3.

4.4.1 Estimation of maximum ratio and wavelength fluctuation due to PDL

The estimation of the maximum variation in the measured wavelength is important in order to determine the system's worst case performance. The maximum and minimum values of the fluctuation of PDL of the filter arm due to the 3 dB coupler and the fiber filter are calculated using Equations (4.5) and (4.6). The PDL of the fiber filter arm is measured (which constitutes one arm of the 3 dB coupler) and the fiber filter, whose PDL are shown in Fig. 4.2 and Fig. 4.4 respectively. A comparison of the estimated maximum and minimum of the PDL of the filter arm with the measured PDL of the filter arm is shown in Fig. 4.6.

The measured PDL lies within the estimated range. For the system the combination of both of the arms gives the total ratio variation. The PDL of the reference arm and filter arm obtained from the experiment provide the maximum and minimum power levels of each arm. Based on that a numerical simulation has been carried out to find the maximum ratio variation and estimated using Equation (4.7). The estimated variation in the ratio and the wavelength of the system are shown in Fig. 4.7(a) and Fig. 4.7(b). To estimate the wavelength

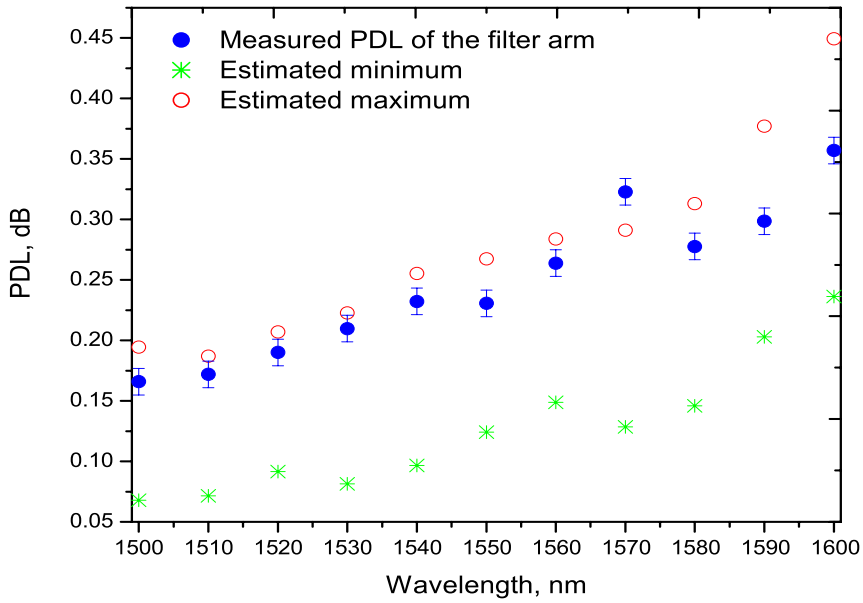

Figure 4.6: Estimated maximum and minimum PDL of the fiber filter arm and its comparison with the measured PDL.

error the local slope of the ratio spectrum shown in Fig. 4.5(a) is calculated with a 5 nm window at 10 nm intervals from 1500 nm - 1580 nm. The wavelength error, which is a consequence of the ratio variation, depends in practice on the slope of the system which is lower at shorter wavelengths and higher at longer wavelengths. This results in greater error at shorter wavelengths than at longer wavelengths. It is estimated that the maximum wavelength change at 1500 nm is 1.9 nm from the original value, which is the highest for the entire wavelength range. Any measured error in wavelength should be within this range. The PDL of the different components involved in the ratiometric system and the estimated

Components contributing to PDL	PDL	Estimated maximum ratio /wavelength error
3 dB coupler (arm 1 and arm2)	arm1 - 0.09 dB arm2 - 0.07 dB	ratio - 0.30 dB wavelength - 1.40 nm
bend fiber filter	0.19 dB	

Table 4.1: PDL of the components and the estimated maximum error in ratio and wavelength at 1550 nm.

variation in the ratio and wavelength at 1550 nm are summarized in Table 4.1. Thus, one can see that for a system with a filter of 15 bend turns and with a conventional wavelength flattened 3 dB coupler the maximum wavelength error that can occur at 1550 nm is 1.40 nm.

4.4.2 Experimental verification of the ratio and wavelength fluctuation because of PDL

Using the experimental system as shown in Fig. 4.8, the variation in the ratio and wavelength of the system due to PDL is measured for the wavelength range 1500 nm - 1580 nm. Its comparison with the estimated maximum variation is shown in Fig. 4.9(a) and Fig. 4.9(b). The error bars represent the possible variation in the measured ratio and the wavelength error due to the temperature variations monitored during the course of the experiment.

It is seen that the ratio variation increase as the wavelength increases. As predicted in the above section the wavelength error changes with wavelength due to the difference in slope of the ratio spectrum, which being lower at shorter wavelengths results in a greater error at shorter wavelengths. In practice when the measurement system is been used for live measurements at any spot wavelength, the system estimates the slope of the ratio response in the vicinity of the spot wavelength. Therefore, small irregularities in the calibrated ratio response can result in errors.

The discrepancy between the estimated and the measured wavelength variation at 1540 nm originates as a result of these small irregularities in the calibrated response. At 1550 nm the measured wavelength error was 1.41±0.09 nm. The measured ratio and wavelength variation of the system are well within the estimated limits. The fundamental fact about the fluctuation in attenuation due to PDL which leads to the variation in the ratio and wavelength is experimentally confirmed with the above results. Without predicting the wavelength error due to PDL of the components used in the system, characterizing a system to a

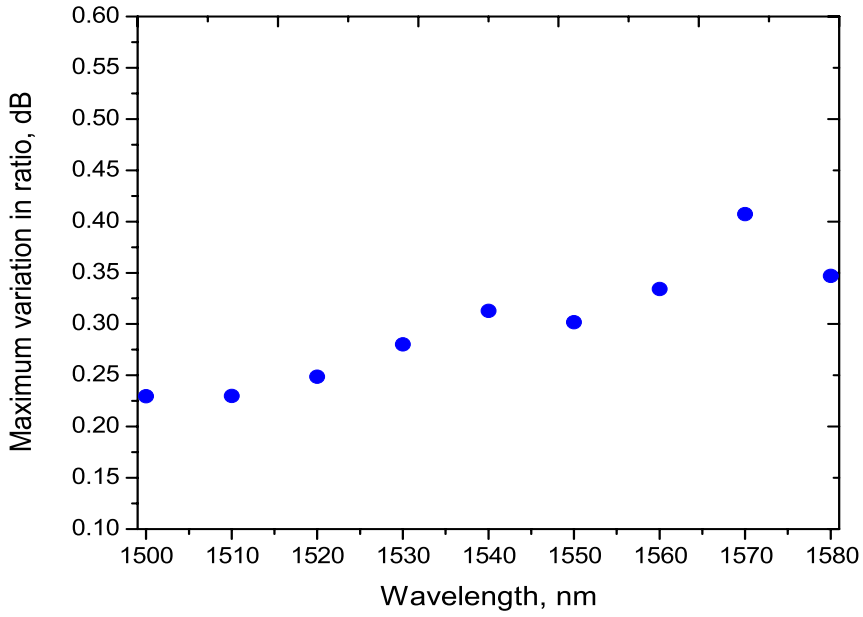

(a)

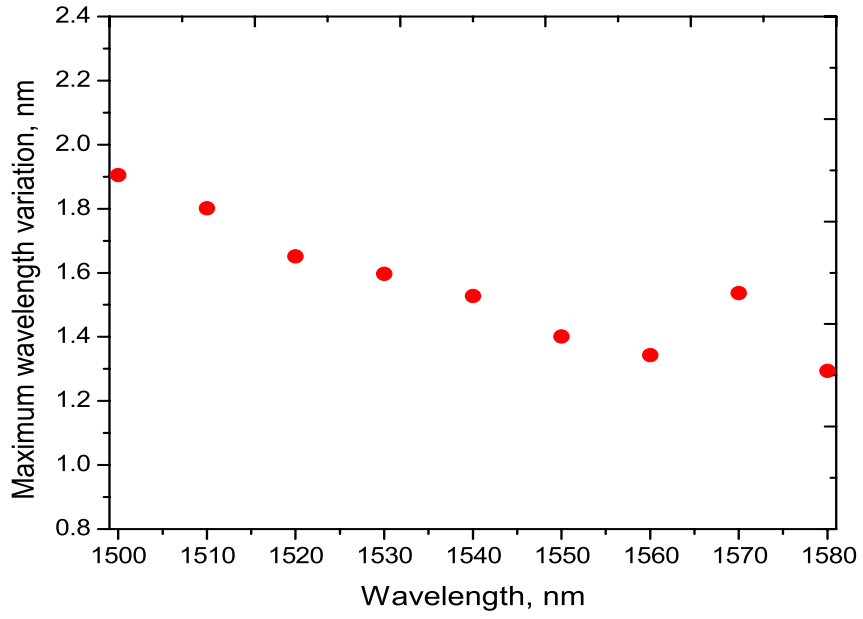

(b)

Figure 4.7: (a) Estimated maximum variation in the ratio of the system (b) Estimated maximum variation in the wavelength of the system.

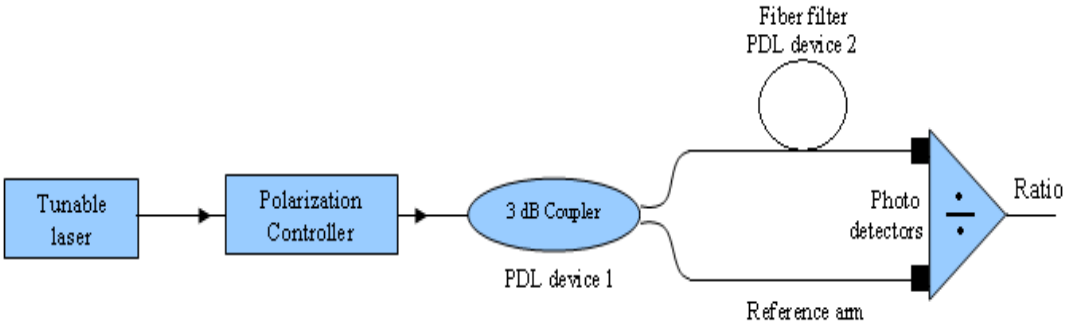

Figure 4.8: Experimental arrangement to find the ratio and wavelength error caused by PDL.

wavelength resolution or accuracy better than 0.01 nm is meaningless. Thus, for determining the accuracy and resolution of the system the PDL of the system and its effects on the system performance have to be determined [113].

4.5 A method to minimize the polarization dependency of a macro-bend fiber filter

From the investigations in the above section it is clear that the PDL of the components of the system has a significant impact on the accuracy of the system. So it is important to minimize the polarization sensitivity of the components. It was shown in Section 4.2, that the polarization dependence of the macro-bend fiber filter is highly sensitive to the bend radius [112]. A filter with minimal PDL can be obtained by choosing the correct bending radius corresponding to the minimal PDL. However, this requires strict fabrication tolerance for the bending radius. Furthermore, it is known that the discrimination range can be increased by increasing the bending length, but increasing the bend length increases PDL. This means that in designing a fiber bend loss edge filter there is an undesirable trade off between the discrimination range and the PDL.

Since the PDL of the bend fiber originates from the difference in bend loss for TE and TM modes one method to compensate the bend loss of the modes is

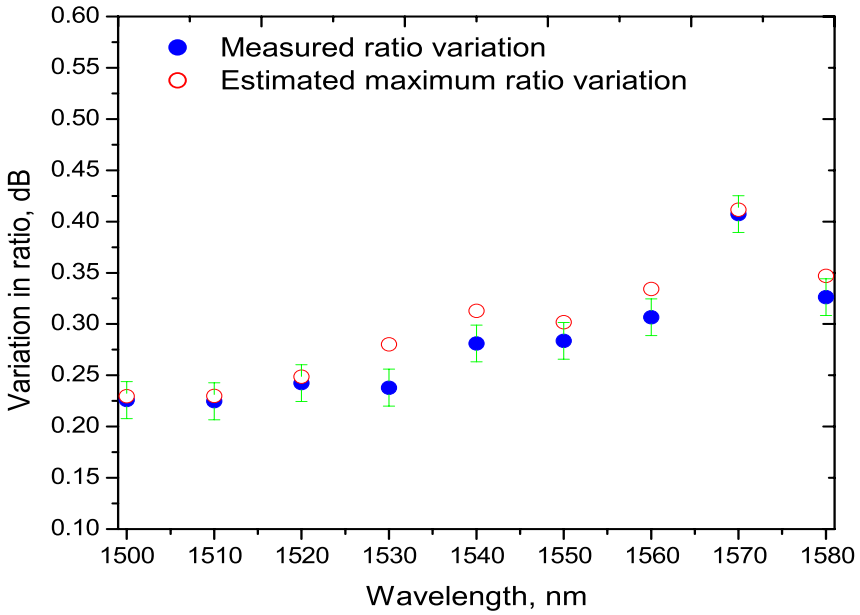

(a)

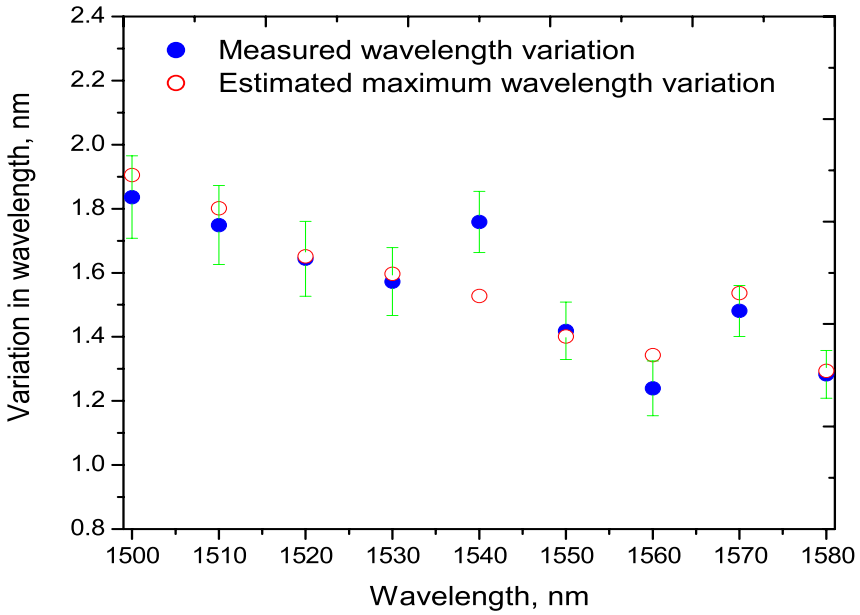

(b)

Figure 4.9: Comparison of measured error with the estimated maximum error because of PDL (a) ratio error (b) wavelength error.

to split the fiber filter into two bending sections with equal length and introduce a 90^0 twist in the middle of the filter between the two sections. This changes the polarization state for the second bending section, i.e., the TE (TM) mode is turned to be the TM (TE) mode for the second bending section. The net effect is that the individual losses for the input TE and TM modes are equalized over the total length of the fiber so that the PDL can be minimized for the whole bending section. The schematic of the filters with and without a twist is shown are Fig. 4.10(a) and Fig. 4.10(b) respectively.

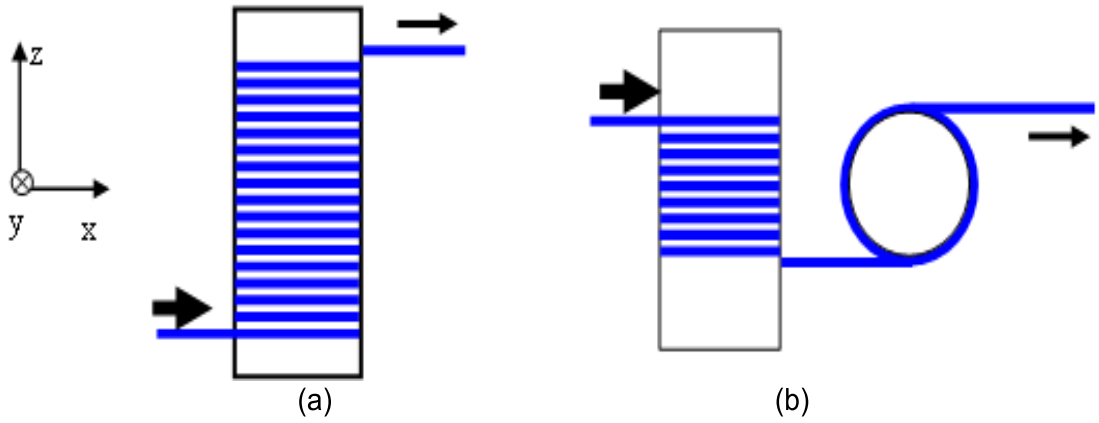

Figure 4.10: Bending configurations of the macro-bend fiber filter (a) conventional bending (b) configuration with a 90^0 twist between the bending sections.

Three configurations of the fiber filter were tested. A conventional fiber filter without a twist and filters with 90^0 and 180^0 twists in the middle of the fiber were tested. For the second and third configurations, the fiber was wrapped with equal bend length (7.5 turns each) on two separate mandrels and the second mandrel is rotated by 90^0 and 180^0 respectively to create a 90^0 and 180^0 twist in the middle between the two sections. The length of the fiber between the two sections was approximately 2.5 cm. The spectral responses of the filters with all the three configurations are shown in Fig. 4.11(a). From the figure it is clear that the twist in the middle of the fiber has no significant influence on the bend loss response of the filter. However, the PDL shows a significant difference. The measured PDL

for all the three configurations for a wavelength range 1500 nm - 1600 nm at an interval of 10 nm is shown in Fig. 4.11(b).

For the 180^0 twist, the TE (TM) and TM (TE) modes return to their original state after the first bending section and such a filter shows the same PDL as the filter without twist. But for the filter with a 90^0 twist, after the first bending section the TE (TM) mode is turned to TM (TE) and the individual losses for the input TE and TM modes are equalized resulting in a low PDL. The polarization controller, the connection fibers and the photodiodes used to measure the power also exhibit PDL. So the PDL of the system without the fiber edge filter is also measured and presented as the inherent PDL of the system. It is also known that the inherent PDL of the filter increases as the number of turns increases, which is necessary to get a steeper response. To see how the 90^0 twist eliminates the PDL at higher bend lengths, the PDL of the filter is measured for different bend lengths and is shown in Fig. 4.12. For comparison the PDL of fiber filters without a twist is also presented for the same number of turns.

PDL is not eliminated completely in the fiber filter due to physical inaccuracies such as small variations in the bend length of the two sections of the filter and variations in the twist angle of 90^0 leading to residual PDL. The remaining PDL of the twisted configuration shown in Fig. 4.11(b) and Fig. 4.12 arises from these factors. It should be noted that a twist in the fiber induces circular birefringence and can make the fiber polarization dependent [114]. However, such stress induced birefringence is very low in SMF28 fiber [51] and this can be confirmed by the results from Fig. 4.11(b), where the PDL of the filter with 180^0 twist and a filter without a twist are closely matched which means that the twist induced birefringence is negligible and its contribution to the PDL of the fiber filter is very small. Overall from the figures it is clear that the PDL of the fiber filter decreases considerably with a 90^0 twist at higher bend lengths which in turn allows the filter to utilize a larger number of turns to obtain the required

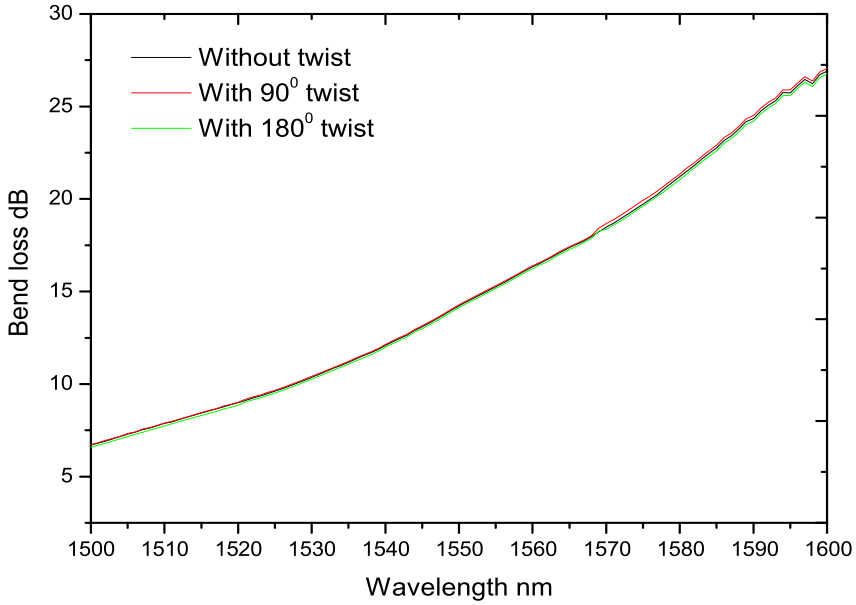

(a)

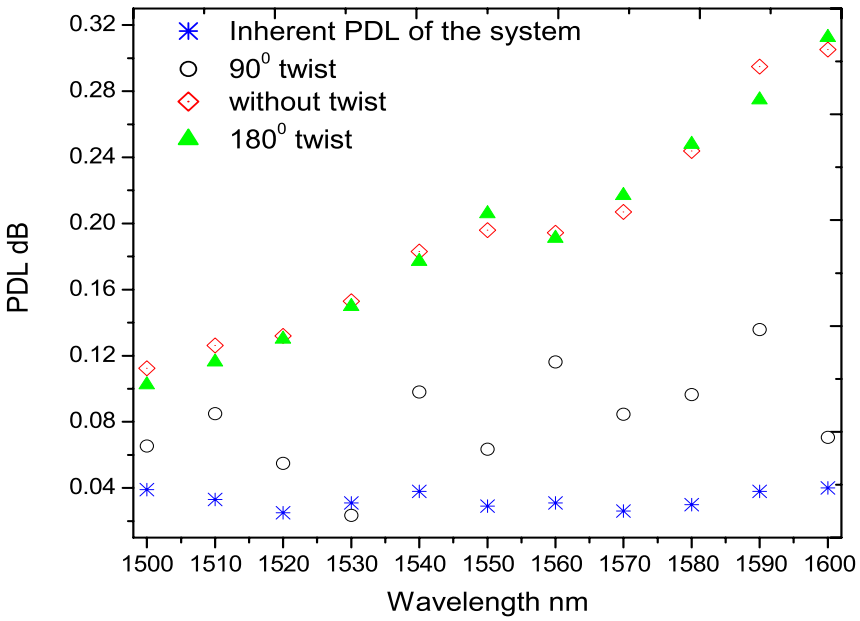

(b)

Figure 4.11: (a) Bend loss response of the filter with the three configurations (b) PDL of the three configurations.

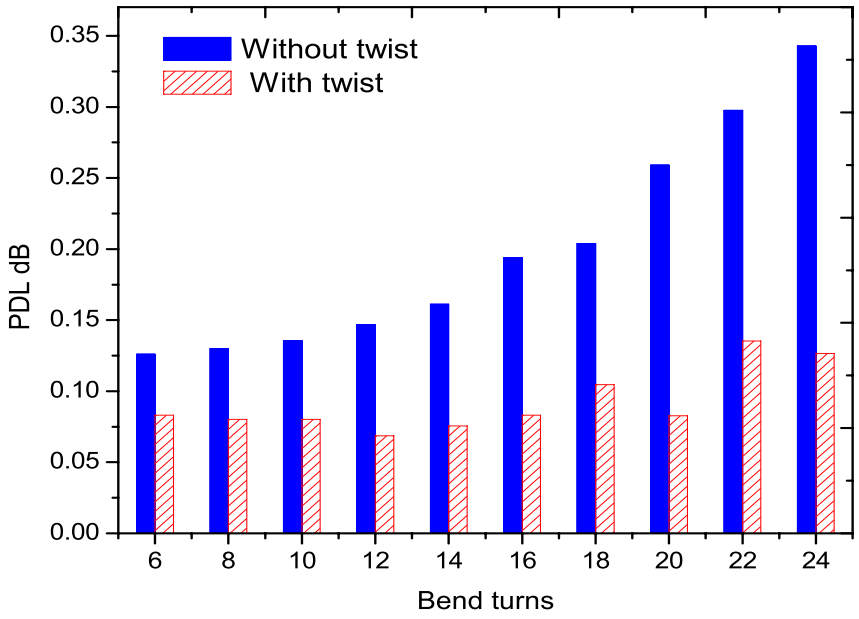

Figure 4.12: Measured PDL of the fiber filters with 90^0 twist and its comparison with the PDL of the filters without twist.

steepness and thus increase the measurement resolution of the system without reaching an unacceptable level of PDL [115].

4.6 A low polarization dependent wavelength measurement system

Minimizing the polarization dependency of the fiber filter alone will not minimize the polarization dependency of the whole system. As the system contains another PDL component, the 3 dB coupler, it is important to minimize the PDL of the coupler also. The PDL of a conventional wavelength flattened 3 dB coupler employed in a ratiometric system was shown in Fig. 4.2. The PDL of the fiber filter can be eliminated by introducing a 90^0 twist in the middle of the bending section as explained in the earlier section. But the PDL of the 3 dB coupler still will affect the system performance. One way to minimize the total polarization dependency of the system is using of polarization insensitive (PI) 3 dB couplers (couplers with very low PDL, in the range of 0.01 - 0.02 dB) [116, 117]. For

comparison the measured PDL of an ordinary 3dB coupler and a PI 3 dB coupler is shown in Fig. 4.13. The measured PDL also includes the inherent PDL of the system. Thus, the combination of a PI coupler and a twisted macro-bend fiber filter can effectively reduce the total polarization dependency of the wavelength system.

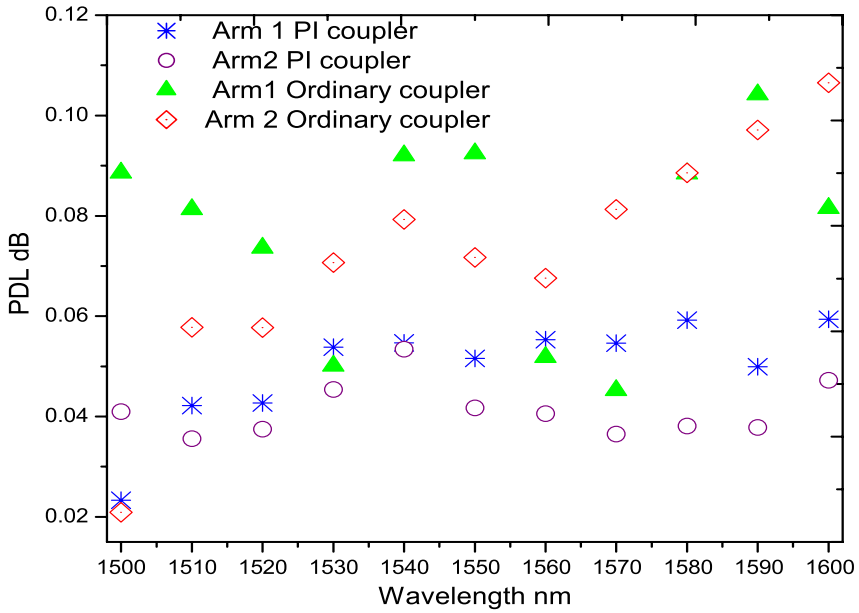

Figure 4.13: Measured PDL of the arms of a PI and an ordinary 3 dB coupler.

In a low polarization sensitive wavelength measurement system a fiber edge filter with a 90^0 twist is used together with a PI 3 dB coupler. The system is calibrated for a fixed polarization state. The input polarization states are changed using a fiber polarization controller as explained in the earlier sections. The ratio and wavelength errors are calculated which is the deviation from the calibrated response. The measured ratio and wavelength error are shown in Fig. 4.14(a) and Fig. 4.14(b) respectively. A comparison of the ratio and wavelength error of conventional system is also presented in the figures. The measured wavelength errors are based on the local slope of the calibrated ratio response. The conventional system gives a wavelength error of 1.401 nm at 1550 nm, while the low

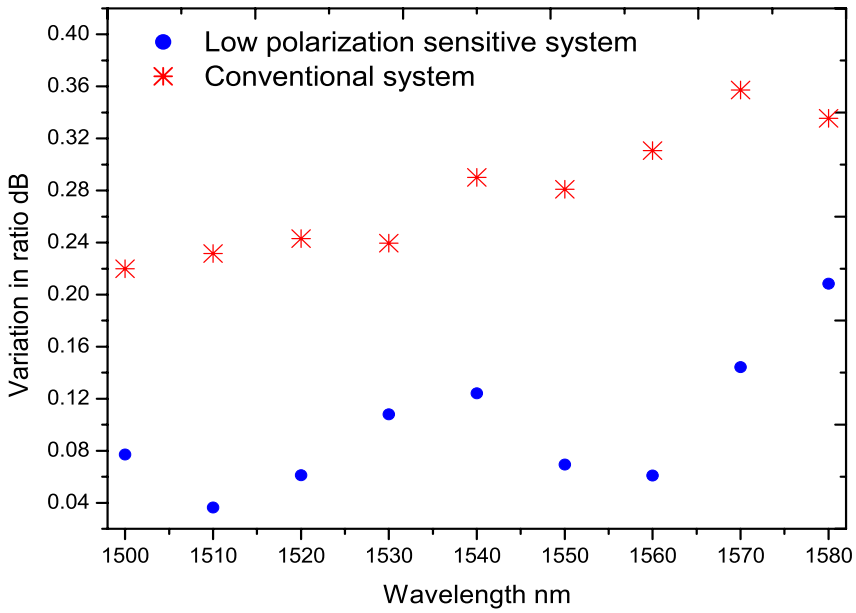

(a)

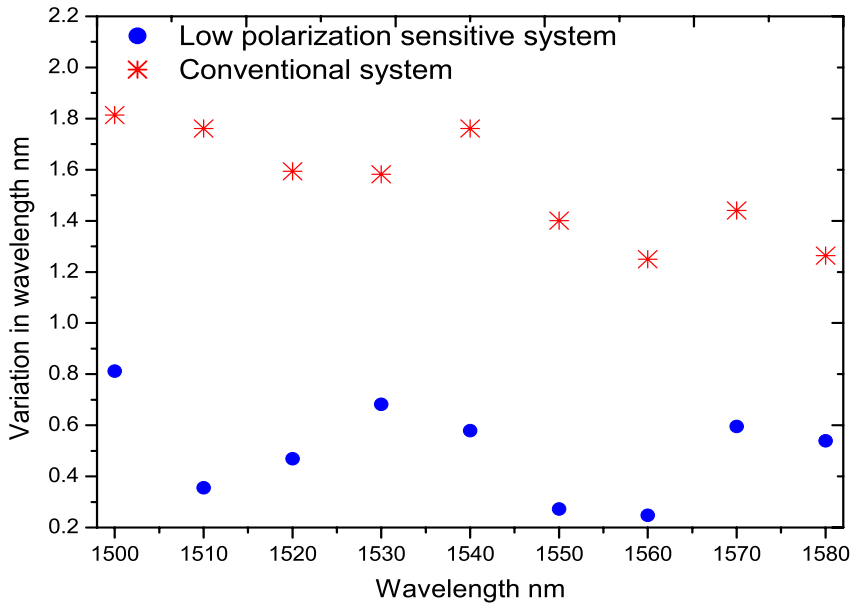

(b)

Figure 4.14: Comparison of errors in a low polarization system vs conventional system (a) ratio (b) wavelength.

PDL system reduces the wavelength error to 0.272 nm. From the figure it is clear that for the conventional system PDL is a significant problem and induces a large wavelength error, but for the system with a twisted fiber filter and PI coupler the wavelength error is effectively reduced which makes the system more accurate. Thus, for wavelength measurements based on macro-bend fiber filters the polarization dependency can be significantly reduced by the configuration proposed above and can deliver measurements with a high wavelength accuracy irrespective of the input state of polarization

4.7 Summary

In this chapter the origin of polarization sensitivity of 3 dB coupler and the macro-bend fiber filter were discussed. Since the macro-bend fiber based wavelength measurement system consists of more than one PDL component, the net PDL fluctuates, which eventually leads to wavelength error. A theoretical model to estimate the maximum ratio error is presented. The PDL of the individual components are measured and the maximum and minimum limits of the PDL of the filter arm are calculated from that. Experimental measurements of the PDL of the filter arm were compared to the estimated limits and it lies well within the limits. Also the total ratio variation of the system which comes from the PDL of the filter arm and the reference arm, was measured and compared with the estimated maximum limit. From this investigations it is concluded that PDL is an important factor determining the accuracy of a macro-bend fiber filter based ratiometric system.

To minimize the PDL of the system, a new configuration is proposed and experimentally proved, where the macro-bend fiber filter is split into two sections with a 90^0 twist in the middle between the two sections. In the twisted configuration the number of turns of the filter can be increased to obtain a steeper response to increase the resolution of the system without a consequent increase in

the PDL. The wavelength and ratio error for the low polarization dependent system is compared with that of a conventional fiber filter based system and found to be significantly reduced. Thus, this system can be used in cases where high accuracy is required, irrespective of the input polarization state.

The main conclusions from the studies conducted in this chapter are;

- Since a ratiometric system contains concatenated PDL elements, the net effect of the PDL is different from the effect caused by individual PDL components and because of this an estimation of the range of the wavelength error is necessary to determine the accuracy of the system. From the investigations it is also concluded that PDL is an important factor determining the accuracy of a macro-bend fiber filter based ratiometric system and needs to be minimized to improve the performance of the system.

- Since the PDL of a macro-bend fiber filter originates from the difference in the propagation of TE and TM modes, an effective solution to reduce the PDL is to introduce a 90^0 twist in the middle between the two sections of the bend fiber. This will compensate for the individual polarization induced bend loss for each section and thereby reduce the PDL of the fiber filter.

- When this configuration is used together with a polarization insensitive 3 dB coupler, the inaccuracy due to the change in input polarization can be minimized to a great extent. Furthermore a 90^0 twist does not impact on the bend loss spectral response of the filter.

Chapter 5

Temperature induced instabilities in macro-bend fiber based wavelength measurement systems

5.1 Introduction

The characteristic properties of the constituent components of any wavelength measurement system can degrade its performance. In the proposed RWM system, it has been shown in previous chapters, that the noise in the system and the polarization dependency of the components limits the resolution and accuracy of the system. Another significant contributor that can degrade the performance of the system is temperature drift. It has been proved previously that the temperature has a significant influence in the bend loss of macro-bend fibers [118–120] and therefore, on the ratio of the system and the measured wavelength. Due to its sensitivity to temperature change, bend loss phenomena have also been used in temperature sensing [121]. Commonly a ratiometric system is calibrated and the ratio response is obtained at a fixed temperature and hence a change in temperature can alter the ratio response. Overall it is important to study the nature of ratio variation with temperature at different wavelengths in order to evaluate its impact on the measurement system.

In macro-bend fiber edge filters, an absorption layer is applied to the buffer coating to absorb the WG modes, which are inherent in bent single-mode fibers

as explained in Chapter 2. Macro-bend fiber edge filters can be fabricated from a standard low bend loss single-mode fiber (SMF28) [63]. However, bend sensitive fibers can also be utilized as edge filters having advantages such as shorter bend length, which reduces the problem of stress related failure [122]. In this chapter a bend sensitive fiber (1060XP) is also introduced as an alternative to SMF28 in the context of temperature effects. A detailed investigation of the temperature dependence of a ratiometric system based on either a SMF28 fiber filter or a 1060XP fiber filter and its effect on wavelength measurements are presented in this chapter. In Section 5.2 the origin of the temperature dependence of macro-bend fiber filters are presented. An experimental setup to measure the temperature induced ratio and wavelength variation is described in Section 5.3. Results, discussion and a comparison of temperature induced wavelength variation in both fiber types are presented in Section 5.4.

Temperature sensors based on optical fibers have generated wide interest due to their all-fiber nature. Different kinds of fiber optic sensors are used in temperature measurements based on different technologies [123–127]. Disposable sensors are necessary in many applications such as in harsh environments or to measure the internal temperature of composites or other cured materials during manufacturing where the sensor is expected to be destroyed after a period of time or is unrecoverable [128–130]. However, none of these sensors are disposable in nature due its higher cost. In this chapter, based on the study of temperature dependence of a bend sensitive fiber (1060XP) based edge filter, a new temperature sensor with a simple configuration and high resolution is proposed. In Section 5.5, the principle of operation of this new temperature sensor and an experimental demonstration is presented.

5.2 Origin of temperature dependence of macro-bend fiber filters

When a single-mode fiber forms a macro-bend WGMs may be created, which propagates in the cladding or buffer. These WGMs can interfere with the guided core mode to produce interference induced oscillations in the bend loss spectral response [118]. The dominant source of WGMs occurs at the buffer-air interface and also at the cladding-buffer interface. The formation of such whispering gallery modes effectively creates an interferometer within the fiber, with the core and buffer/cladding as the two arms. To utilize a macro-bend fiber as an edge filter, an absorption layer is applied to the buffer coating to eliminate these WG modes, which makes the bend loss spectral response smoother and ideally achieves a linear response versus wavelength [51]. The temperature sensitivity of such a fiber filter arises mainly from the characteristic properties of the buffer coating such as the thermo-optic coefficient (TOC) and thermal expansion coefficient (TEC). The TOC and TEC of the buffer coating, such as acrylates, are much higher than those of fused silica of the core and the cladding of the fiber.

Macro-bend fiber edge filters can be based on low bend loss fiber such as SMF28 fiber or high bend loss fiber such as 1060XP. A cross section view of both fiber filters are shown in Fig. 5.1. The most common single-mode fiber, SMF28 fiber, has two buffer coating layers [51, 112]. Due to the coating layers, even with the absorption layer a low level of reflection from the cladding-primary coating boundary will still exist and interfere with the core mode. As a result of this when there is a change in temperature which changes the refractive index and thickness of the buffer coating, the path length variation of the WG modes and phase difference between the WG mode and the core mode leads to constructive and destructive interference between the WG mode and the core mode. This leads to oscillatory variations in the spectral response of the bend loss. A macro-bend fiber filter without a buffer coating together with an absorption layer can eliminate

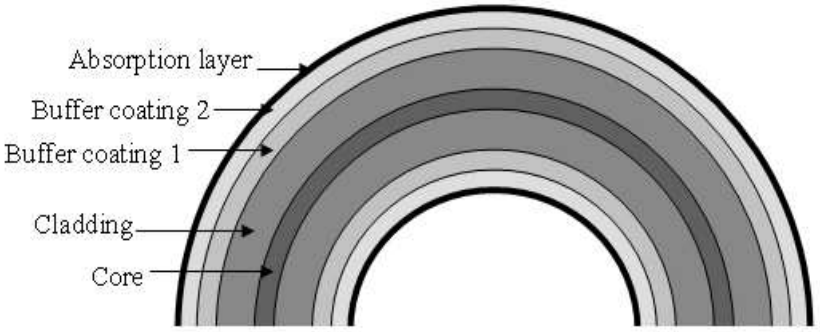

(a)

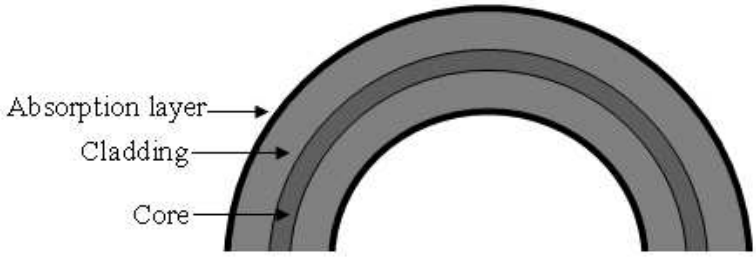

(b)

Figure 5.1: Cross section view of the bend fiber in the two cases (a) with buffer and absorption layer (SMF28) (b) without buffer and with absorption layer (1060XP).

the temperature induced periodic variations in the bend loss. A fiber filter based on SMF28 fiber requires multiple bend turns with small bend radii to achieve a better slope and high wavelength resolution. The removal of the buffer coating over a meter or more of fiber is beyond practical limits as the fiber breaks if it is wrapped for more than one turn at small bend radii without a buffer. However, a fiber such as 1060XP is highly sensitive to bend effects due its low normalized frequency (V). The V parameter for 1060XP fiber is 1.5035 while for SMF28 fiber it is 2.1611. Since the normalized frequency of the 1060XP is smaller, power will be less confined in the core and will be more susceptible to bending loss and will be higher when compared to SMF28. Therefore, an edge filter based on bend sensitive fibers such as 1060XP requires only one bend turn and hence the buffer can be stripped easily and an absorption layer applied to directly to the cladding.

This configuration eliminates the different TOCs and TECs of the buffer, cladding and the core. Together with an absorption layer for the cladding which absorbs the radiated modes, prevents any possibility of a re-coupling with the core mode and hence the reflections caused at the interfaces will be completely eliminated. Since the cladding and core are made of silica material and have a positive thermo-optic coefficient, the thermally induced effective change in refractive index of the core and cladding is linear in nature, resulting in a linear variation of bend loss with temperature. Since the temperature dependent loss is proportional to the bend loss in the fiber filter, 1060XP fiber shows higher temperature induced loss, when compared to its SMF28 counterpart, both with a single turn. The parameters of both fiber types are shown in Table 5.1. The removal of the buffer coating and the application of an appropriate absorption layer also results in a monotonic increase in bend loss with bending radius and wavelength which is approximately equivalent to a core-infinite cladding structure. For a system with this configuration, a temperature corrected calibration is feasible. A temperature corrected calibration means that temperature of the fiber filter is continually measured and therefore, the measurement system can apply correction factors to the calibration in use. This allows the system to be used over a wide range of ambient temperatures.

5.3 Experimental investigation of the temperature dependence of the system

A macro-bend fiber based wavelength measurement system was built utilizing a ratiometric scheme. The following fiber filters were fabricated for the temperature studies:

(a) SMF28 fiber with the buffer retained with an absorption coating and with multiple bend turns;

(b) A single bend turn SMF28 fiber filter without a buffer and with an absorption

	Core	Cladding	Buffer Coating 1	Buffer Coating2
SMF28				
Radius (μm)	4.15	62.5	95	125
Refractive index	1.4504	1.4447	1.4786	1.5294
TEC α (K^-1)	5.5 x 10^-7	5.5 x 10^-7	800 x 10^-7	$<$ 100 x 10^-7
TOC β (K^-1)	1 x 10^-5	1 x 10^-5	-29 x 10^-4	-
Normalized frequency (V)		2.1611		
1060XP				
Radius (μm)	2.65	62.5	NA	NA
Refractive index	1.4631	1.4564	NA	NA
TEC α (K^-1)	5.5 x 10^-7	5.5 x 10^-7	NA	NA
TOC β (K^-1)	1 x 10^-5	1.1 x 10^-5	NA	NA
Normalized frequency (V)		1.5025		

Table 5.1: Comparison of parameters of SMF28 and 1060XP fibers at 1550 nm.

layer;

(c) A single bend turn 1060XP fiber filter without buffer and with an absorption layer;

Fig. 5.2 shows the schematic of the experimental setup used to study the influence of temperature on the wavelength measurements. In the case of the SMF28 fiber filter, the fiber was wrapped around a mandrel with a fixed radius which is attached to the metal plate base. The metal plate base was connected to the Peltier cooler, which was driven by a temperature controller and with

the temperature of the fiber filter accurately monitored. The bend radius of the SMF28 fiber filter was fixed at 10.5 mm. The discrimination range of the system can be varied by changing the number of bend turns. For SMF28 fiber, three filters were tested with 5, 10 and 15 bend turns.

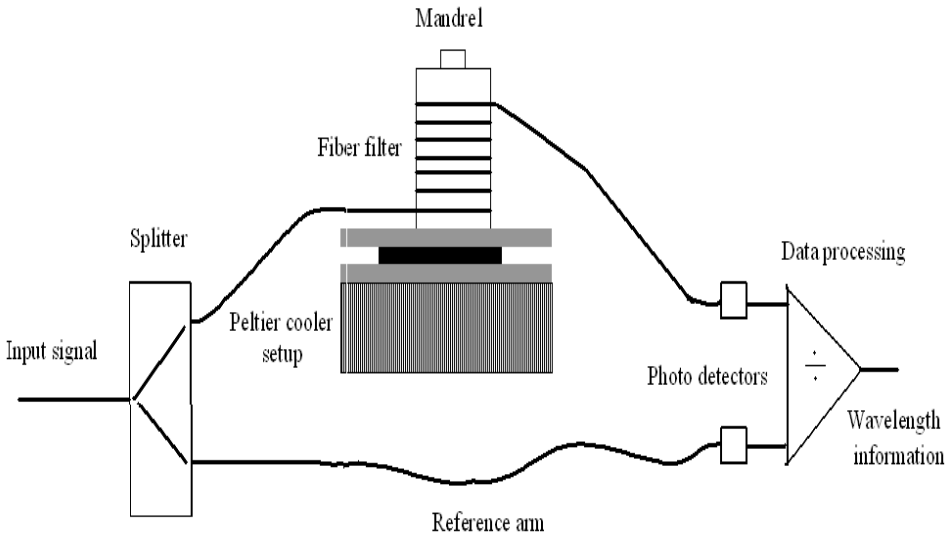

Figure 5.2: Experimental arrangement to study the effect of temperature on wavelength measurement.

For the 1060XP fiber filter, since it requires only one bend turn, the fiber filter is directly fixed to the metal plate, instead of being wrapped around a mandrel. The bend radius of the 1060XP fiber filter was fixed at 11 mm. The calibration ratio responses of both the systems were obtained at 20 ^0C. The variation in ratio from the calibrated response and the corresponding wavelength variation were measured for a temperature range of 0 ^0C to 60 ^0C with an interval of 2 ^0C. As the temperature controller requires time to settle down, and also to allow for a uniform distribution of the temperature within the fiber filter, the individual measurements were taken at 5 minute time intervals. The temperature dependence results for both SMF28 and 1060XP fiber filter systems are discussed in the next section.

5.4 Results and Discussion

5.4.1 SMF28 fiber filter based system

The ratio response measured for the system based on SMF28 fiber with an absorption layer for all the three filters with 5, 10 and 15 bend turns and with bend radius 10.5 mm is shown in Fig. 5.3. The fiber filter with 15 turns provides a useful discrimination slope while also covering a wavelength range 90 nm between 1500 nm to 1600 nm with an average slope of 0.22 dB/nm. Further increases in the number of bend turns affects the linearity of the ratio response at higher wavelengths and reduces the measurable wavelength range due to the limited SNR of the source. Filters with 5 and 10 turns give a 100 nm wavelength range with an average slope of 0.075 dB/nm and 0.14 dB/nm respectively.

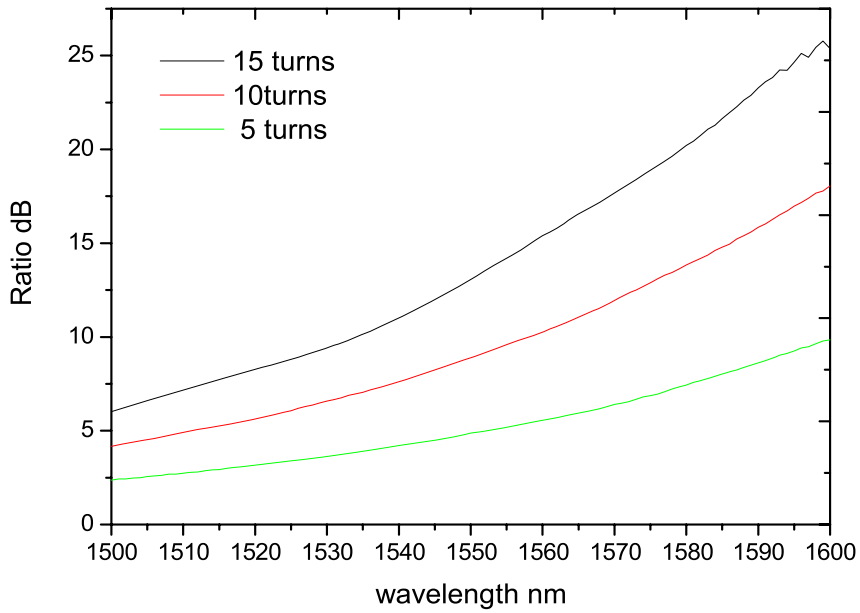

Figure 5.3: Ratio response of the system with SMF28 fiber filter with different number of bend turns.

To investigate the influence of temperature variation on the ratio response the change in ratio of the system was measured from the calibrated response (obtained at 20 ^0C) for all the filters at 1550 nm for the temperature range from

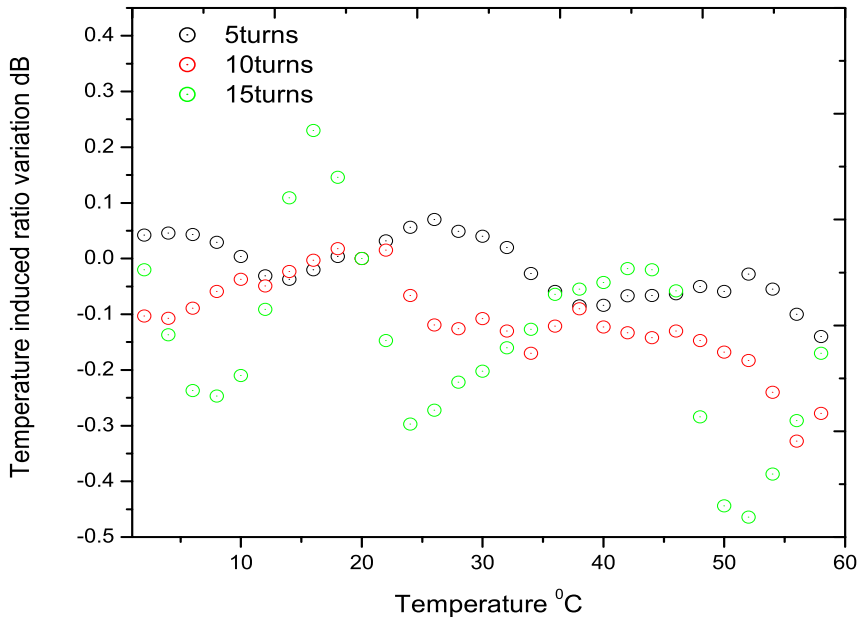

(a)

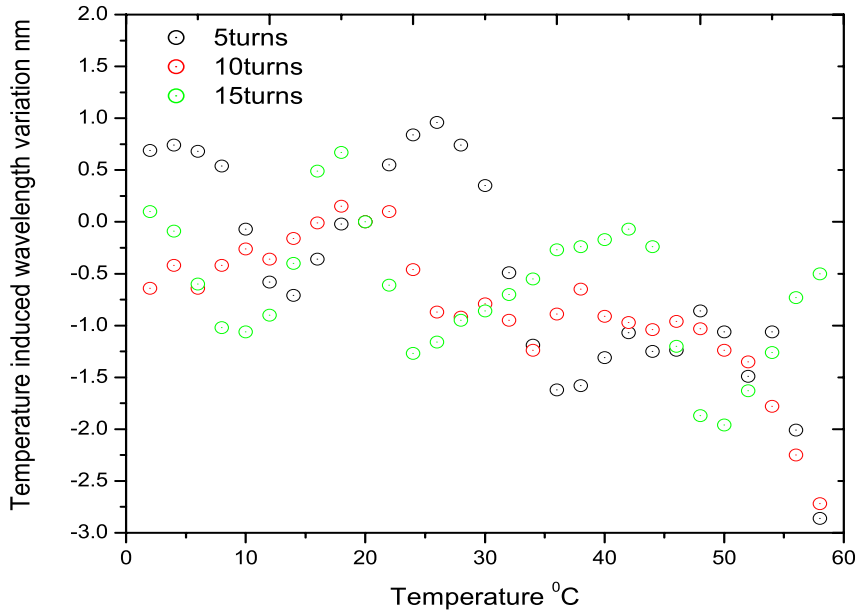

(b)

Figure 5.4: Temperature induced variation at 1550 nm for the SMF28 fiber filter based system with 15 bend turns and 10.5 mm radius (a) variation in ratio (b) variation in wavelength.

0 ^0C to 60 ^0C. The results are presented in Fig. 5.4(a). From the figure it is clear that the absorption layer did not eliminate the WG modes completely and the remaining WG modes produce reflections at the cladding-primary coating boundary. This results in an oscillatory nature for the variation in bend loss and the same for the ratio of the system. The total bend length is high for a larger number of bend turns resulting in stronger WGM effects and hence higher amplitude oscillations in the ratio of system. This variation in ratio from the calibrated response will induce wavelength inaccuracy. The temperature induced wavelength variation measured at 1550 nm is shown in Fig. 5.4(b). From the figure it can be seen that the wavelength variations for the systems with all the three filters are similar. This is due to the difference in the slope of each filter, i.e. for the same ratio variation in the case of a system with a filter of 5 turns there is a large wavelength variation, while for a system with a filter of 15 turns, which has a higher slope, there is a smaller wavelength variation. Thus, even though the temperature induced ratio variation is higher for systems with a larger number of turns, due to the difference in the ratio slope of the system, all systems will produce similar wavelength measurement variations. As a result, a reduction in the number of turns for the filter will not eliminate the temperature induced wavelength error even though it reduces the amplitude of temperature induced ratio oscillations.

It is known that the relative phase of the WG mode and the core mode is also dependent on the wavelength of the light used [121]. To gain an insight into the complexity of the temperature calibration procedure, the temperature induced ratio variation is measured at different wavelengths. The measured ratio variation of the system with a fiber filter with 15 bend turns at wavelengths 1530 nm and 1550 nm is shown in Fig. 5.5. At lower wavelengths since the bend loss is low, the temperature dependent bend loss and ratio will also be smaller. It is clear from the figure that for the same filter the temperature induced oscillations

are different at different wavelengths. Thus, in the case of systems based on the SMF28 fiber filter with a fiber buffer and absorption layer, a correction in the calibrated ratio response to compensate the temperature induced ratio and wavelength variation is too complex to be feasible.

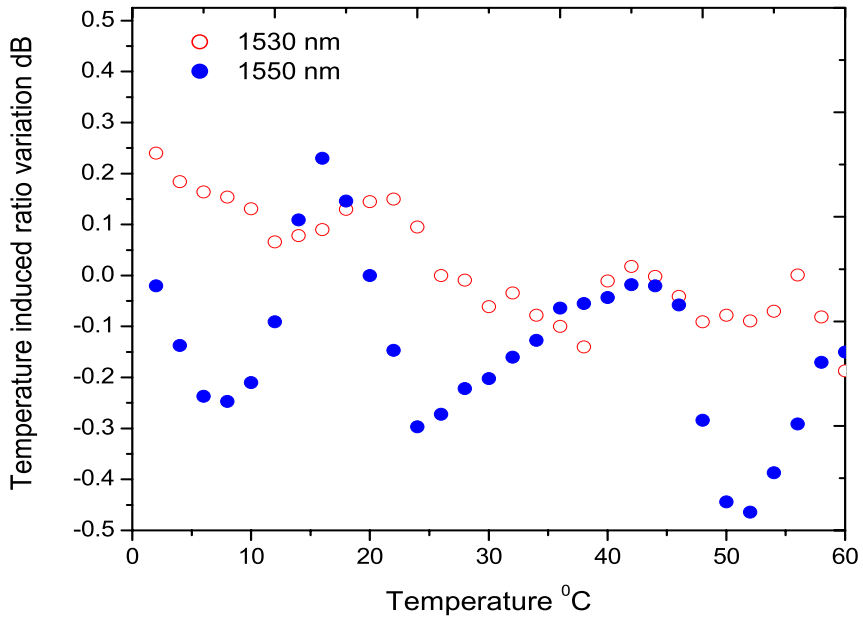

Figure 5.5: Temperature induced ratio variation at different wavelengths.

A correction of the calibration of the ratio of the system to take account of the temperature change is possible only when there is linear change in ratio with temperature for a fixed bend radius and number of turns. To achieve this the filter has to be buffer stripped and coated with an absorption layer. Since the standard SMF28 fiber requires multiple turns to achieve a large discrimination range, winding the fiber without a buffer will very likely lead to fiber breakage. However, to illustrate the temperature dependence of an unbuffered SMF28 fiber filter with an applied absorption coating, the ratio response of a single turn fiber filter is measured and is shown in Fig. 5.6(a) while the ratio variation at 1550 nm when temperature changes from 0 ^0C to 60 ^0C is shown in Fig. 5.6(b). From the figure it is clear that the oscillatory behavior is eliminated by

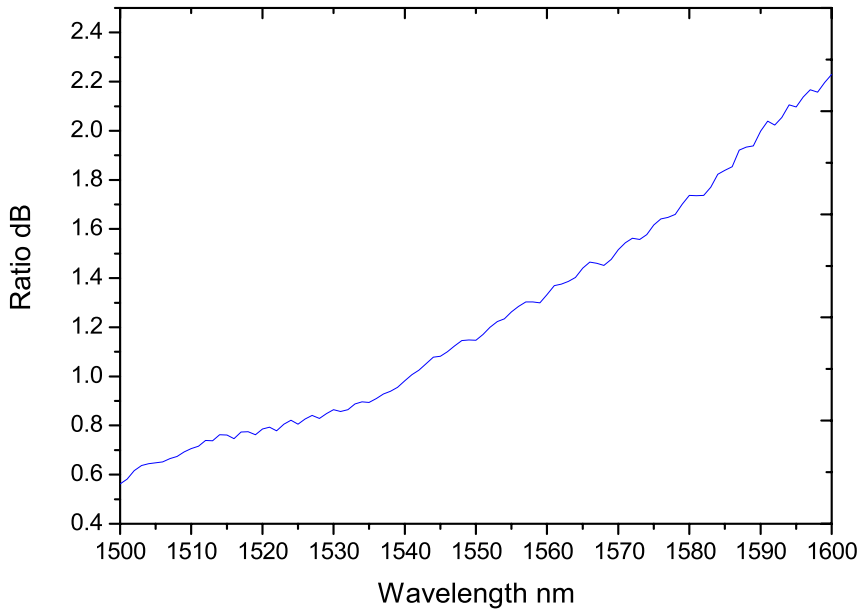

(a)

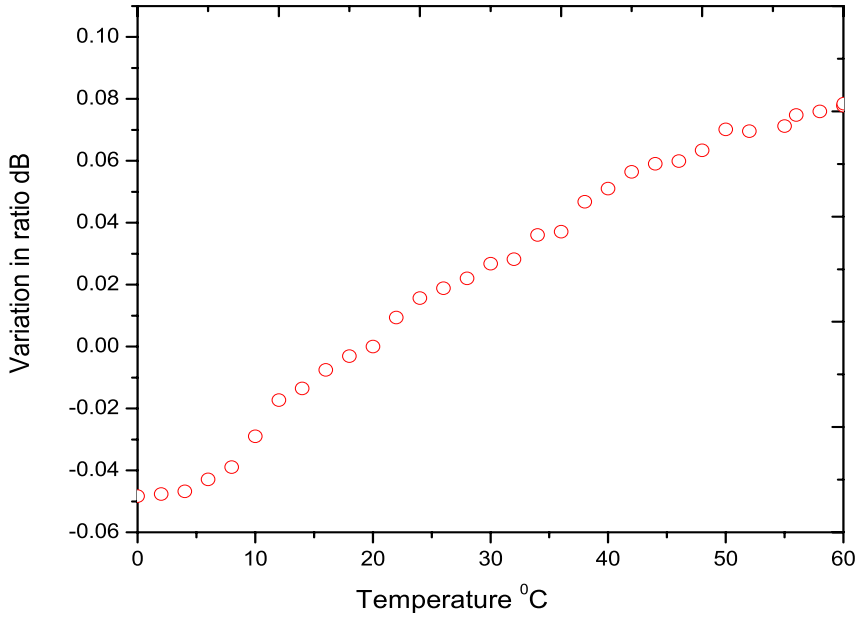

(b)

Figure 5.6: (a) Ratio response of the system with one turn of SMF28 fiber filter without buffer and with absorption layer (b) ratio variation at 1550 nm when temperature varies from 10 ^{0}C to 60 ^{0}C.

removing the buffer, which allows a correction to the calibrated ratio response for a temperature induced variation, but a filter with such a small slope of 0.016 dB/nm is not suitable for wavelength measurements as it would severely limit the measurement resolution .

5.4.2 1060XP fiber filter based system

The use of a high bend loss fiber such as 1060XP eliminates the requirement of multiple bend turns to achieve larger discrimination ranges. For the 1060XP fiber, a bend radius of 11 mm with one bend turn gives a slope approximately equal to 10 turns of SMF28 fiber. Since it requires only one bend turn the removal of the buffer coating is possible in the case of 1060XP fiber. The ratio response of the system at 20 ^0C with a bend radius of 11 mm and one bend turn, with an applied absorption layer to absorb the WG modes, is shown in Fig. 5.7 which covers the wavelength range from 1500 nm to 1600 nm with an average slope of 0.122 dB/nm.

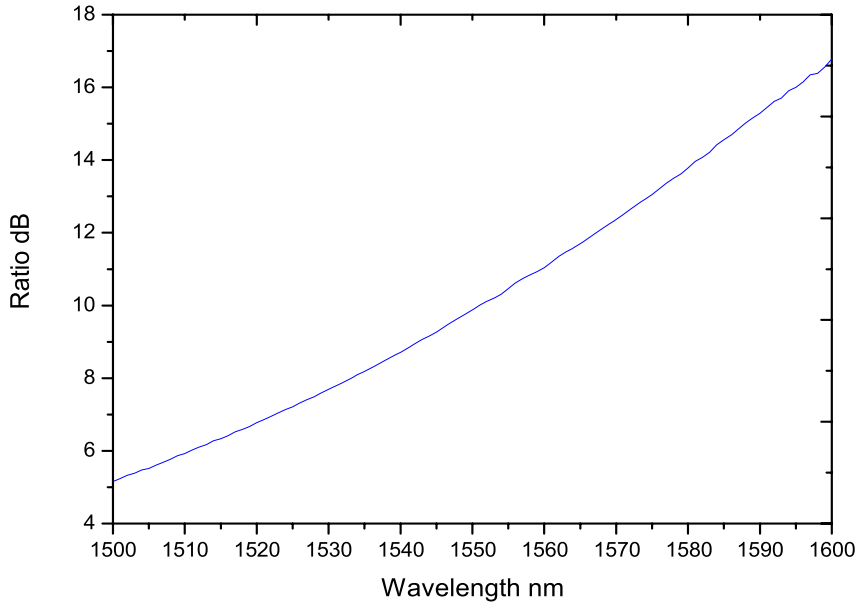

Figure 5.7: Ratio response of the 1060XP fiber filter with radius 11 mm and one bend turn.

From the experiments conducted with the SMF28 fiber filter, it was clear that removing the buffer and applying an absorption layer gives a monotonic variation in the ratio with temperature at a fixed wavelength and bend radius. The temperature induced ratio variation for the 1060XP fiber filter system is shown in Fig. 5.8(a) when the temperature changes from 0 ^0C to 60 ^0C for a range of wavelengths from 1500 nm to 1600 nm at 10 nm intervals. The 1060XP fiber filter without a buffer provides a linear change in the ratio with temperature. The result shows that even though the ratio variation of the system is linear for the 1060XP fiber filter, the filter is highly temperature dependent. The difference between the measured wavelengths and actual wavelengths for 1500 nm, 1530 nm, 1550 nm and 1570 nm due to temperature variation is shown in Fig. 5.8(b). From the figure it is clear that at higher wavelengths the temperature dependent ratio and wavelength error is higher than for lower wavelengths. This results in larger inaccuracies at higher wavelength regions than in lower wavelength regions for a same temperature variation.

Regardless of the high temperature dependency of the 1060XP fiber filter the linear variation in the ratio means it is feasible to apply calibration correction factors to minimize the temperature induced errors. Fig. 5.9 shows the required correction for the calibrated response at different temperatures. The required correction for the ratio response is calculated for different temperatures with an interval of 5 ^0C in the range from 0 ^0C to 60 ^0C. By monitoring the temperature of the filter itself and by applying an appropriate correction to the calibration response precise wavelength measurements could be obtained with a system based on 1060XP fiber filter, even with significant ambient temperature changes.

5.4.3 Comparison of SMF28 fiber filter based system and 1060XP based system

A comparison of the wavelength measurement system based on SMF28 fiber filter with a buffer and an absorption layer and the 1060XP fiber filter without a

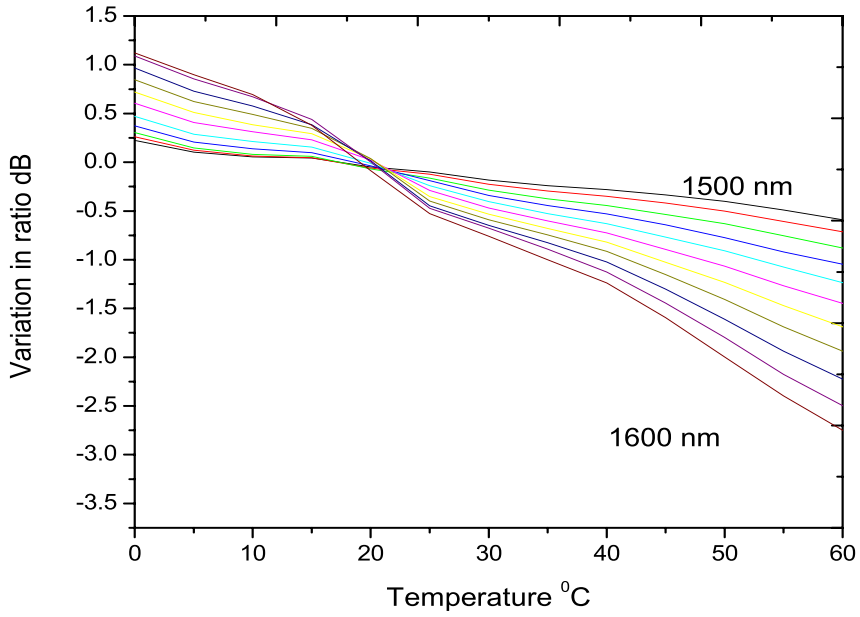

(a)

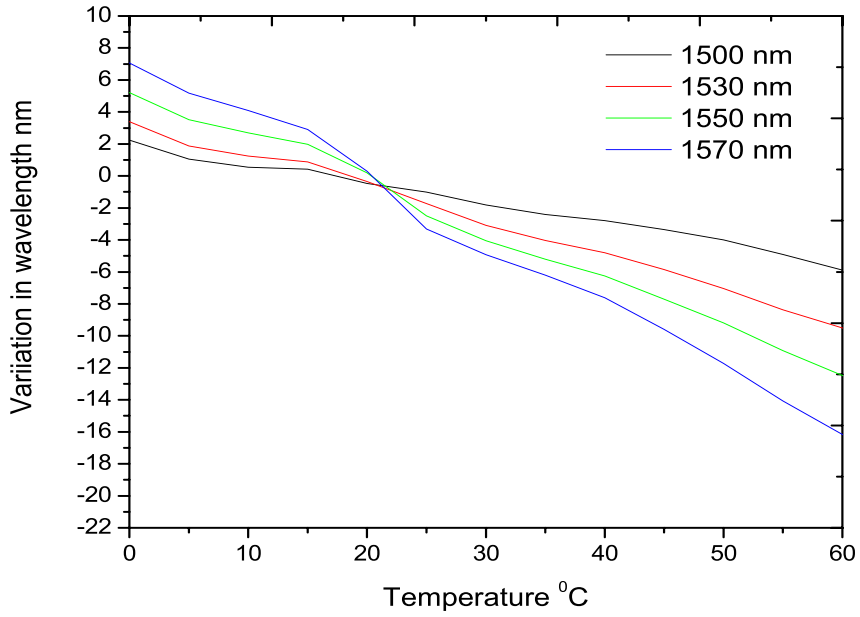

(b)

Figure 5.8: Temperature induced variation of the system based on 1060XP fiber filter (a) variation in ratio (b) variation in different wavelengths.

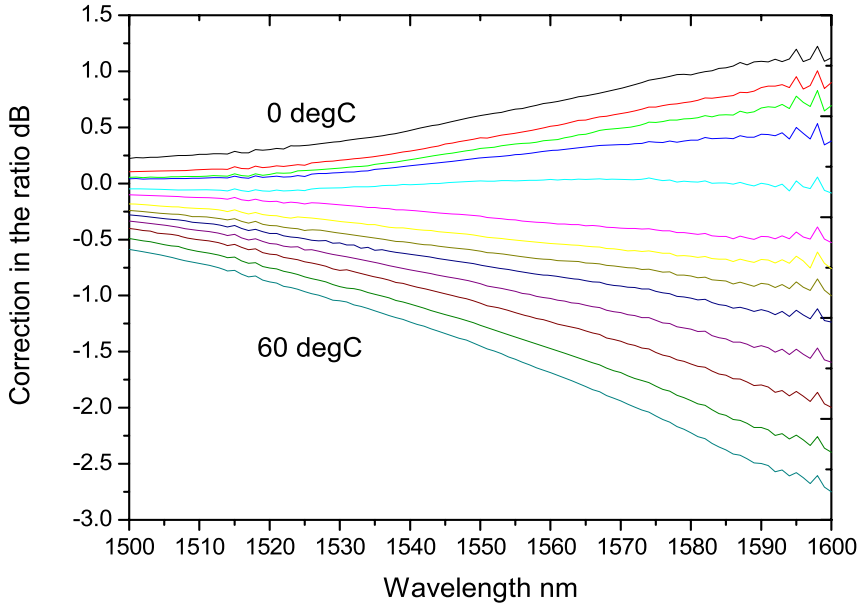

Figure 5.9: Required correction for the ratio response at different temperatures.

buffer and with an absorption layer is shown in Table 5.2 for a wavelength of 1550 nm. From the table it can be seen that the wavelength error is less for system with SMF28 fiber filter. The maximum measured wavelength variation from the wavelength 1550 nm for the system with an SMF28 fiber filter with 15 turns was +0.67 nm at 18 ^0C as the temperature decreases towards 0 ^0C and -1.96 nm at 50 ^0C as the temperature increases towards 60 ^0C. For the system with 1060XP fiber filter the wavelength variation was +5.2 nm when the temperature is 0^0C and -12.4 nm at 60 ^0C. While it is apparent that the SMF28 fiber filter based system is less temperature sensitive, nevertheless the oscillatory nature of the bend loss and ratio of the system makes correction of the calibrated response unfeasible. For the SMF28 based filter the only option is to use active temperature stabilization of the filter temperature. Whereas for a 1060XP based filter temperature compensation requires a sensor and compact electronics only, temperature stabilization will additionally demand a peltier cooler, two heat sinks, a complex feedback control system and, depending on the ambient temperature variation to

be dealt with, will involve significantly higher power consumption by the system. The temperature stabilization approach will thus require more physical space, as well as higher complexity and cost than the temperature compensation approach. The 1060XP fiber filter has a higher temperature dependence than the SMF28 fiber filter, but due to the linear nature of the ratio variation with temperature, the temperature induced error can be compensated by adding correction factors to the calibration ratio response. The wavelength accuracy can be improved by obtaining the correction in the ratio response with smaller temperature intervals or by extrapolating the correction response between the required temperature intervals. Thus, irrespective of temperature dependence of the 1060XP fiber filter, such a filter can be operated over a wide temperature range, if the correction in ratio response is added to the original ratio response and thus precise wavelength measurements can be obtained.

Type of macro bend fiber filter	Radius mm	No. of bend turns	Temp change ^{0}C	Max. ratio change dB	Wavelength change nm	Nature of variation
SMF28 with buffer and absorption layer	10.5	15	0 - 60	0.464 @50^{0}C	1550-1.96 @ 50 ^{0}C	Oscillatory
1060XP withou buffer and with absorption layer	11	1	0- 60	2.05 @60^{0}C	1550 - 12.4 @ 60 ^{0}C	Approx linear

Table 5.2: A comparison of the temperature dependency of the wavelength measurement system with SMF28 fiber filter and 1060XP fiber filter at 1550 nm.

5.5 An all-fiber temperature sensor based on macro-bend fiber loop

The bend loss properties of single-mode fiber have been studied very intensively along with applications such as a fiber filter, based on the bend loss phenomenon, utilized as an edge filter for wavelength measurements as explained in earlier chapters. A significant amount of effort has been made by researchers to use the bend loss properties of single-mode fiber for temperature measurements. One method is based on interferometry [121] where the temperature sensitivity arises from the thermo-optic and thermal expansion sensitivity of the buffer coating leading to interference between the WGMs and the core mode. This method requires the determination of phase information at different wavelengths to extract the temperature information. High temperature sensing using whispering gallery mode resonance in bend fibers is also reported [60], which involves measuring the resonance wavelength peak shift with temperature. Both approaches lack a direct linear relation between bend loss and temperature and the need for phase measurements makes the system complex. In another approach an intrinsic type optical fiber temperature sensor is proposed using a multi-mode fiber by winding the fiber for a number of turns [131]. The sensing mechanism used for temperature measurements is based on mode modulation. However, such a temperature sensor has drawbacks, such as the usage of multi-mode fibers, which carries a large number of propagation modes and the need for a significant number of bend turns which requires more space and also potentially adds a spatial gradient of temperature between the bend fibers. In this section a simple method is presented to measure temperature which uses a bend sensitive bare single-mode fiber loop with an absorption layer utilized in a ratiometric power measurement scheme. The removal of the buffer coating eliminates the effect of the two different thermo-optic coefficients of the buffer and the cladding and the use of an appropriate absorption layer results in a monotonic increase in bend loss with

bending radius as explained in earlier sections. Given the simplicity of fabrication of the sensor head and the use of a single-mode fiber, it can be used as a disposable sensor where the sensor is expected to be destroyed after a period of time or is unrecoverable.

5.5.1 Principle of operation

The temperature sensitive sensor head consists of a buffer stripped high bend loss single-mode fiber arranged in a loop with an absorption layer applied to the cladding as shown in Fig. 5.10. The absorption layer is chosen to absorb light at the wavelength of operation, absorbing the WG modes inherent in a bent single-mode fiber and reducing the reflections back from the air-cladding boundary. By eliminating the WG modes the bend loss variation with temperature at a fixed wavelength and loop bend radius depends only on the thermo-optic coefficients of the cladding and core. Since the cladding and core are made of silica material and have a positive thermo-optic coefficient, the thermally induced effective change in refractive index of the core and cladding is linear in nature, resulting in a linear variation of the bend loss with temperature. Furthermore, there is a monotonic increase in bend loss with bend radius and wavelength and thus the temperature sensitivity of the sensor can be varied by changing the bend radius or the operating wavelength.

The temperature information is extracted using a simple ratiometric power measurement system as it measures a ratio which is independent of source power variations resulting in a more stable and accurate system. The input signal from the source splits into two equal power signals, one goes to the fiber sensor and the other one is the reference signal as shown in Fig. 5.11. Two photodiodes and associated electronic processing are used to measure the power at the outputs of the corresponding arms. By measuring the power ratio of the two signals, which is a function of temperature, temperature can be measured, assuming the system

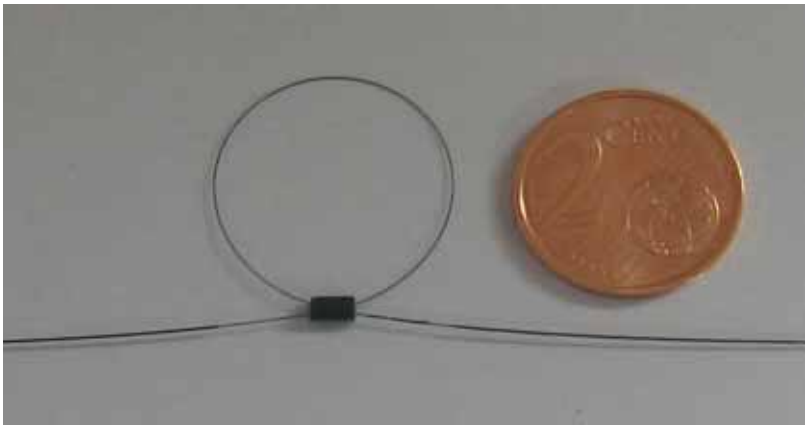

Figure 5.10: A macro-bend temperature sensor head.

is properly calibrated.

5.5.2 Experimental demonstration of the temperature sensor

The fiber used in the experiment was a 1060XP single-mode fiber which has a high bend loss in the wavelength region of 1550 nm and gives a good bend loss response with wavelength as we explained in Section 5.4.2. From the middle section of a length of the fiber, the buffer coating is stripped and an absorption layer is applied. The bend radius used was 12.5 mm with one bend turn and gives a bend loss of 7 dB at 0 ^0C at 1550 nm. The bend radius of 12.5 mm is selected to improve the long term reliability for the sensor, by avoiding the stress induced damage that could caused by smaller bend radius. The sensor is utilized in a ratiometric power measurement scheme as shown in Fig. 5.11. The input wavelength to the system was 1550 nm. The fiber loop was fixed to a metal plate whose temperature is controlled using a Peltier cooler driven by a temperature controller. Using an accurate independent temperature monitor for the purpose of calibration, the ratio response was measured at 1 ^0C intervals for a temperature range of 0 ^0C to +75 ^0C. The range employed was limited by the capabilities of the Peltier cooler used. The ratio response measured as a function of temperature

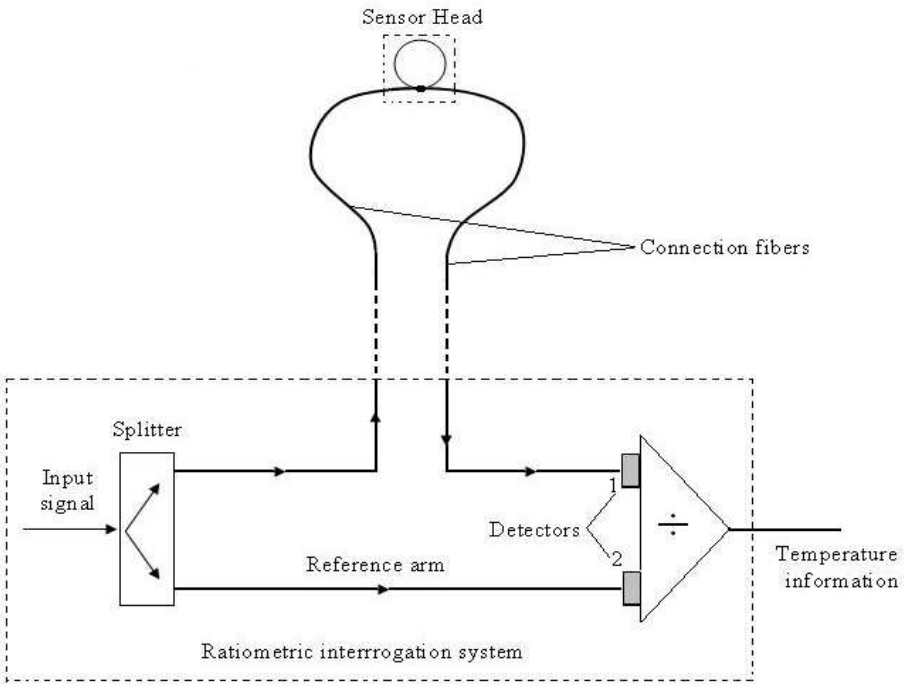

Figure 5.11: Schematic of a macro-bend fiber temperature sensor system.

is shown in Fig. 5.12(a). From the figure it is clear that the average slope of the system is 0.012 dB/^{0}C. To measure the temperature resolution of the system, a step change of 1 ^0C from 30 ^0C to 25 ^0C is applied to the fiber sensor over a time period of 60 seconds. The measured ratio variation is shown in Fig. 5.12(b), which proves that the system is capable of resolving temperature changes less than 1 ^0C. Fiber temperature sensors such as a fiber Bragg grating (FBG) typically provide a 10 pm wavelength shift for a 1 ^0C temperature change, requiring an interrogation system with high resolution to resolve small temperature changes. To illustrate this for an FBG interrogation system based on an edge filter, if a filter slope of 0.5 dB/nm is assumed (Most edge filters slopes are circa 0.5 dB/nm) then the ratio variation is approximately 0.005 dB/^{0}C. By comparison a ratio variation of 0.012 dB/^{0}C for the sensor proposed here confirms the competitive temperature sensitivity of this sensor.

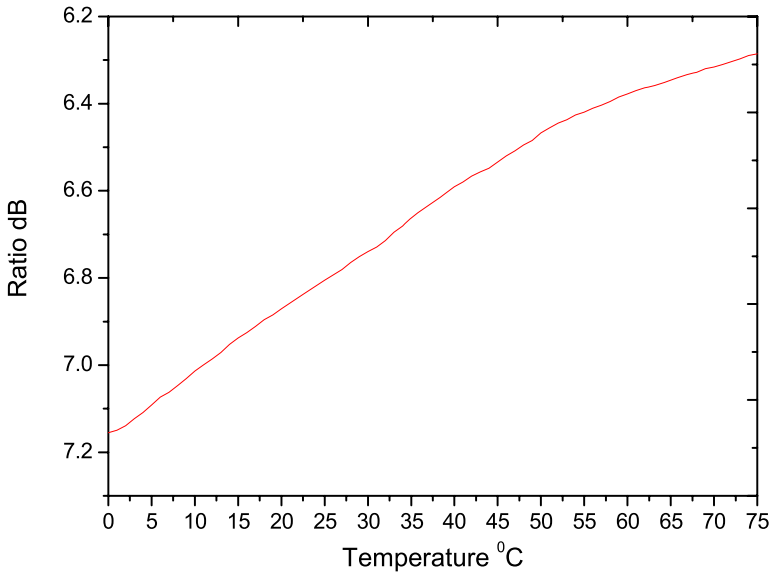

(a)

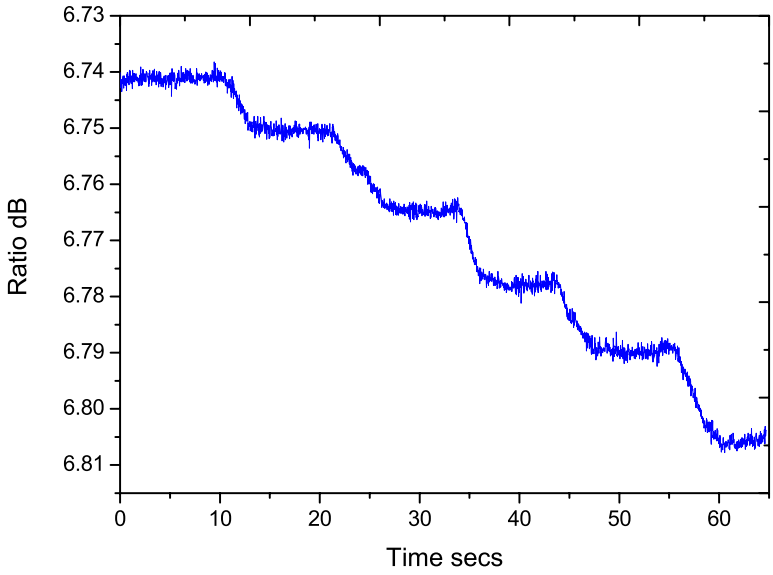

(b)

Figure 5.12: (a) Ratio response of the system as a function of temperature (b) Variation in ratio for a step change of temperature of 1 ^{0}C from 30 ^{0}C to 25 ^{0}C.

5.5.3 Advantages and applications of the temperature sensor

As the sensor head is a silica fiber, then together with a high temperature capable absorption layer, it has a potential to be used for wide range and high temperature applications. Given the simplicity of fabrication of the sensor head and the use of single-mode fiber, it can be used as a disposable sensor for use in harsh environments or to measure the internal temperature of materials used as composites, where the sensor is expected to be destroyed after a period of time or is unrecoverable. Compared to existing fiber optic sensors, this is one of the biggest advantage of this macro-bend single-mode fiber temperature sensor. For temperature measurements during the processing of composite material components such as wind turbine blades, the present practice is to use thermocouples at the outer edges of the composite preform to obtain the data of the temperature profile. However the the actual temperature away from the edges is not measured [132]. This can be overcome by using the proposed disposable fiber temperature sensor. It is also important to note that even though the sensor is disposable, if required it can continue to operate while embedded in the material giving the material smart characteristics. Another promising application of the sensor is in the medical field. Disposable optical fiber sensors are useful for clinical environment where sterilization is an important challenge [133]. Even the most efficient sterilizing methods cannot assure 100 % perfection. So the proposed macro-bend fiber sensor could be utilized in such applications.

5.6 Summary

The effect of temperature on a wavelength measurement system based on macro-bend fiber filter is presented in this chapter. From the results it is shown that for a fiber filter, without a buffer, and with an absorption layer, the oscillatory be-

havior of the ratio variation with temperature, which results from the interference between the WG modes and the core mode can be eliminated. For an SMF28 fiber filter, which has a dual coating layer, the ratio and wavelength variation is oscillatory in nature and different for different wavelengths and this makes the temperature corrected calibration approach too complex to be feasible. For a bend sensitive 1060XP fiber filter without a buffer and with an absorption layer the system produces a linear ratio variation. While the SMF28 fiber filter based system is less sensitive to temperature than the 1060XP fiber filter based system, the linear nature of the temperature dependence of 1060XP fiber filter means that it is feasible to correct for changes in ambient temperature by monitoring the filter temperature and correcting the calibration response. Thus, a 1060XP filter based system can be operated over a wide ambient temperature range for precise wavelength measurement. For a system based on an SMF28 fiber filter active temperature stabilization of the filter will be required to achieve the same result.

Based on the studies of the temperature dependency of 1060XP fiber filter an all-fiber temperature sensor based on macro-bend single mode fiber using a ratiometric power measurement scheme is proposed and demonstrated. A linear variation in bend loss with temperature is obtained by using a buffer stripped single-mode fiber with an absorption layer applied. The sensor has a high temperature resolution and can reliably resolve temperature variations less than 1 ^{0}C. The proposed sensor can be used as a disposable sensor in a range of application areas.

The main conclusions from this chapter are;

- From the investigations of the temperature dependence of the system it is concluded that for a system based on a SMF28 fiber filter, due to the oscillatory variation in ratio response with temperature, temperature corrected calibration approach is too complex to be feasible.

- For a 1060XP fiber filter without a buffer and with an absorption layer the system produces a linear ratio variation. While the SMF28 fiber filter based system is less sensitive to temperature than the 1060XP fiber filter based system, the linear nature of the temperature dependence of 1060XP fiber filter means that it is feasible to correct for changes in ambient temperature by monitoring the filter temperature and correcting the calibration response.

- A direct linear relationship between the bend loss in a single-mode fiber and temperature can be achieved by using a bend sensitive single-mode fiber without a buffer coating applied but with an absorption layer for eliminating the WG modes.

Chapter 6

An all-fiber Bragg grating interrogation system for strain and temperature measurements

6.1 Introduction

Fiber Bragg grating sensors have generated much interest in the area of strain and temperature sensing and are being used in many applications such as in structural monitoring and in smart structures [7–9, 134–138]. The critical aspect related to the practical use of FBG sensors is the necessity to perform accurate measurement of the small wavelength shift associated with the thermal and strain state changes. To facilitate the broad use of this class of sensors compact, rugged, wide range and low cost wavelength demodulation systems are required. In addition, the advancement in the development of phase mask techniques [139, 140] has reduced the cost of grating fabrication, and the interrogation units, rather than the sensors, will account for a large proportion of the cost of a complete sensing system. Many demodulation techniques have been developed to interrogate FBGs and a summary of different techniques was presented in the Chapter 1. Interrogation system based on a macro-bending single-mode fiber edge filter offers the advantages of an all-fiber approach with low fabrication cost together with large dynamic range and wide wavelength measurement range. Due to the wide wavelength range of the demodulation system it can interrogate multiple

FBGs when used together with a fast optical tunable filter.

Investigations of the properties of the macro-bend fiber filter presented in previous chapters showed that macro-bend fiber exhibits polarization dependent loss [112, 113] and temperature dependent loss [118, 141] as well as both these phenomena are functions of wavelength and also depend on the slope of the system which is determined by the bend radius and number of bend turns of the fiber filter. Furthermore, the signal-to-noise ratio of the source and the noise in the receiver also limit the resolution of the system. It has been proved that the noise induced ratio fluctuation is wavelength dependent and hence the resolution of the system itself is wavelength dependent [142]. Overall then the accuracy and resolution of the interrogation system will be different for different wavelengths and will be dependent on the edge filter slope. For a single FBG sensor it is possible to optimize the edge filter slope in the vicinity of the FBG peak wavelength to achieve the best possible resolution and accuracy. However, for an array of FBG sensors with peak wavelengths spread over a wide range it is not possible to adopt a single slope that yields the best resolution and accuracy for all the FBGs. In this chapter an analysis is presented considering all the factors affecting the resolution and accuracy of the system in order to select a fiber filter with a best fit slope which gives the highest possible resolution and accuracy for an array of FBG sensors. A brief description of the basic principles of FBG sensing is presented in Section 6.2. A method to measure the reference strain in an FBG strain sensor interrogation system involving actuators is presented in Section 6.3 of this chapter, which explains the details of different methods to fix a foil strain gauge to an optical fiber and how to use it as a reference in experiments using an FBG sensor. An interrogation system based on macro-bend fiber filter and its analysis and the criteria for selection of a suitable fiber filter for an FBG array is presented in Section 6.4. Performance evaluation of the system has been carried out and is presented in Section 6.5.

6.2 Principles of FBG sensing

As a continuation of the brief description of fiber Bragg grating sensors provided in the introduction chapter, this section provides and overview of the operating and sensing principles of a Bragg grating sensor. As explained in Chapter 1 the operation of an FBG sensor is based on the measurement of the peak wavelength shift induced by an applied strain or a change in temperature [7, 17, 143]. The light reflected by periodic variations of the refractive index of the Bragg grating having a central wavelength λ_G is given by,

$$\lambda_G = 2n_{eff}\Lambda, \tag{6.1}$$

where n_{eff} is the effective refractive index of the core and Λ is the periodicity of the refractive index modulation.

The reflectivity at the Bragg wavelength can be estimated using the equation [144],

$$R = tan^2\Omega, \tag{6.2}$$

where

$$\Omega = \pi n_{eff}(L/\lambda_B)(\Delta n_{eff}/n_{eff})\eta(V) \tag{6.3}$$

The factor $\eta(V) \simeq 1-1/V^2$, $V \geq 2.4$ is the fraction of the integrated fundamental mode intensity contained in the core and V is the normalized frequency of the fiber. It is seen that R is directly proportional to the grating length L and the index perturbation $\Delta n_{eff}/n_{eff}$ which is normally determined by the exposure power and time of the UV radiation used to write the grating on a specified fiber.

The full width at half maximum bandwidth , $\Delta\lambda$, of a grating is approximately given as [7]

$$\Delta\lambda = \lambda_G S\sqrt{(\frac{\Delta n_{eff}}{2n_{eff}})^2 + (\frac{1}{N})^2}, \tag{6.4}$$

where $S \sim 1$ for strong grating (nearly 100 % reflection) and $S \sim 0.5$ for weak gratings and N is the number of grating planes. Because the change in the index is small the main contribution to the line width change is attributed to the change in the modulation depth of the index perturbation.

The sensitivity of the Bragg wavelength to temperature arises from the change in the period associated with the thermal expansion of the fiber, coupled with a change in the refractive index arising from the thermo-optic effect. The strain sensitivity of the Bragg wavelength arises from the change in period of the fiber coupled with a change in the refractive index arising from the strain-optic effect [8]. For the measurement of a temperature change ΔT, the corresponding wavelength shift is given by,

$$\Delta\lambda_T = \lambda_G(\alpha + \xi)\Delta T, \tag{6.5}$$

where α is the coefficient of thermal expansion for the fiber material and ξ is the fiber thermo-optic coefficient.

For the measurement of applied longitudinal strain, the wavelength shift is given by,

$$\Delta\lambda_S = \lambda_G(1 - \rho_\alpha)\Delta\varepsilon, \tag{6.6}$$

where ρ_α is the photo elastic coefficient of the fiber given by the formula,

$$\rho_\alpha = \frac{n^2}{2}[\rho_{12} - \upsilon(\rho_{11} - \rho_{12})], \tag{6.7}$$

where ρ_{11} and ρ_{12} are the components of fiber optic strain tensor and υ is Poisson's ratio. For a silica core fiber the value of (1 -ρ_α) is usually 0.78. Thus by measuring the wavelength shift of the peak reflected signal from the FBG, a change in temperature or strain can be calculated. A detailed expression for the grating strain and temperature sensitivity is given in Appendix A.

6.3 Strain referencing for an FBG sensor system experimentation

Prior to the usage of the FBG interrogation system for different applications, the system needs to be calibrated in the laboratory. Conventionally, a foil strain gauge [145] often serves the purpose of a reference for an FBG strain sensor, where both the FBG and strain gauge are surface mounted to a structure where the strain is applied [146, 147]. By the introduction of actuators like piezo translators and micro screws, strain can be applied directly to the optical fiber which contains the FBG sensor. Conventional methods of surface mounting the foil gauge cannot be used while using it with actuators, instead the gauge has to be fixed directly to the optical fiber. To use a strain gauge as a practical strain sensor, one must measure the extremely small changes in the resistance with high accuracy, which can be achieved with a Wheatstone's bridge circuit together with a voltage excitation source [145]. Different bridge configurations such as full bridge, half bridge and quarter bridge are commonly used. Full bridge and half bridge circuits are more sensitive to strain than a quarter bridge circuit. However, realization of a full bridge and half bridge in the case of optical fiber is very difficult as attaching more than one gauge on to the fiber is not viable. Therefore, a quarter bridge circuit is more suitable for fiber strain measurements and was used in these experiments. Since the variation in the output voltage was very small a strain gauge amplifier (RS 846-171) was used, having a gain of approximately 1000 [148]. A data acquisition card NI PXI 6221 controlled by LabView 8.0 was used to acquire data from the gauge amplifier. The value of the strain can be derived using the following formula [149],

$$\varepsilon = \frac{4V_r}{GF(1-2V_r)}(1 + R_L/R_G), \tag{6.8}$$

where GF is the gauge factor, R_G is the gauge resistance, R_L is the resistance of the wire used and V_r is defined as,

$$V_r = [\frac{V_0}{V_{ex}}]_{strained} - [\frac{V_0}{V_{ex}}]_{unstrained}, \tag{6.9}$$

where V_o is the output voltage of the bridge and V_{ex} is the bridge supply voltage.

The output of the bridge is directly proportional to the excitation voltage applied across the bridge, the strain and the gauge factor. It does not depend on the actual bridge resistance values. A higher value of excitation voltage causes self-heating of the gauge that produces an imbalance in the bridge and increases the error in the measurements. The choice of excitation voltage has to be made such that there is a compromise between the sensitivity and the gauge power dissipation. In this investigation an excitation voltage of 1.65 V is used in conjunction with the overall amplifier gain to achieve the best sensitivity.

6.3.1 Bonding methods

A two-part fibre optic epoxy resin, part number T120-023-C2, was used as an adhesive to bond the strain gauge to the optical fiber. Fig. 6.1 shows different bonding methods to affix the foil strain gauge to the optical fiber. In method (a) the foil strain gauge was affixed directly to the optical fiber using the epoxy. In order to avoid strain caused by the weight of the strain gauge the setup was placed on a supporting surface. One end of the fiber containing the FBG was attached to the supporting surface and the other end was fixed to the micrometer translation stage. For the strain gauge used here the manufacturer's value of GF was two. However, this value can only be used in the case of full strain transfer where the strain gauge is in complete contact with the surface. In the case of the small contact area that arises with a foil gauge and fiber the GF has to be corrected. For a known value of fibre elongation and gauge resistance variation

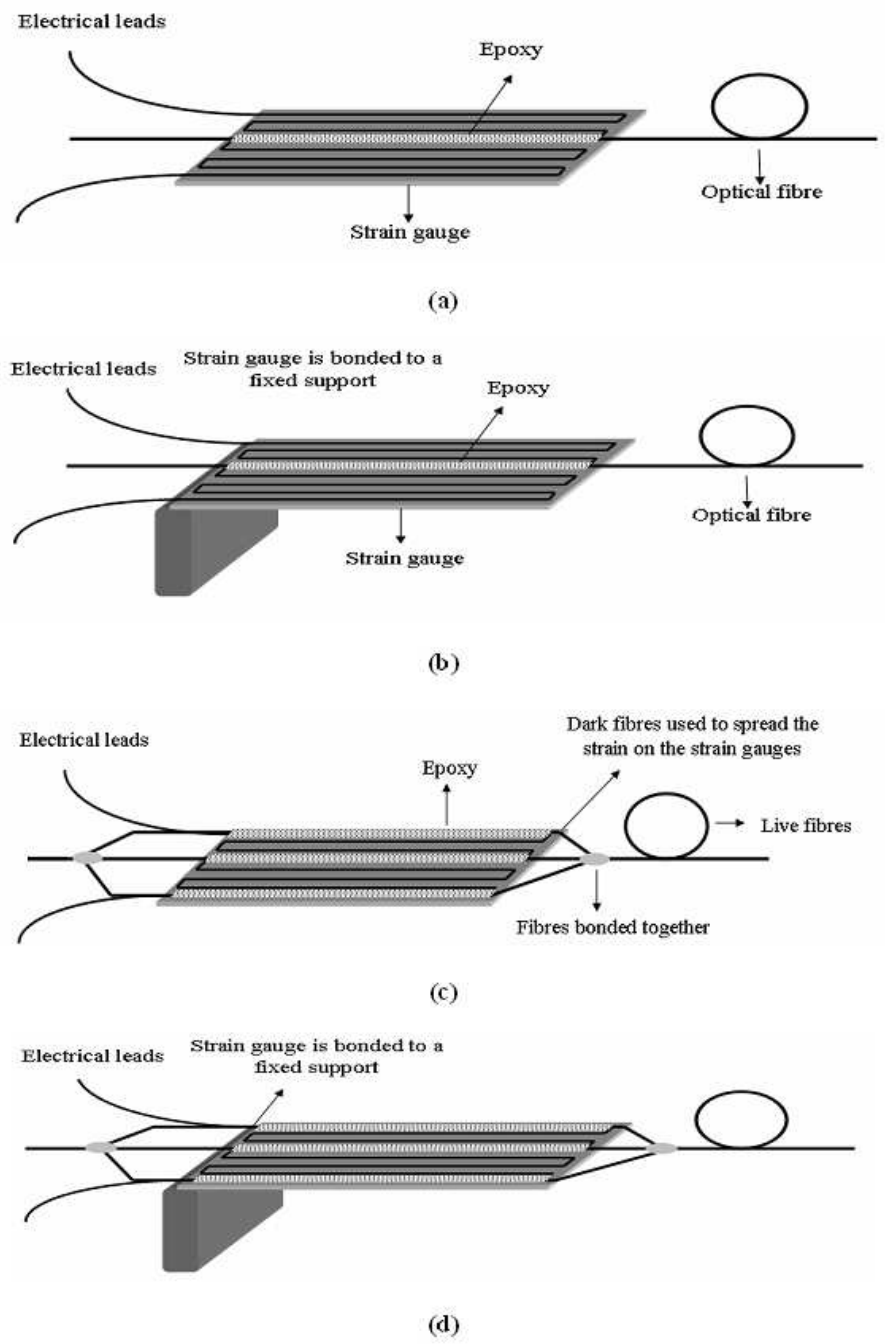

Figure 6.1: Different methods to fix the foil strain gauge to the optical fiber.

the corrected gauge factor (CGF) can be calculated from the equation below.

$$CGF = \frac{\Delta R/R}{\Delta L/L}, \tag{6.10}$$

where ΔR is the variation in the resistance, R is the gauge resistance, L is the length of the optical fiber and ΔL is the fiber elongation. It should be noted that CGF is dependent on the amount and type of the epoxy used. So extreme care has to be taken in fixing the foil strain gauge to the fiber to maintain the CGF value. A large quantity of adhesive may affect the strain transfer from the fiber to the strain gauge. The gauge factor calculated using the above equation was 0.32 which is used to calculate the strain from the measured voltage change. For different bonding methods the CGF is different. In method (b) the lower end of the strain gauge is fixed to the support to ensure proper strain transfer. This may be useful for certain physical configurations. The CGF measured in this method was also 0.32, which shows that the strain transfer is the same as for method (a).

In the above two cases the contact area between the strain gauge and the fiber was very small which may limit the transfer of strain to the strain gauge. In order to increase the contact area and the strain transfer, two dark (no light) fibers are affixed to the gauge and the ends of these fibres are bonded to the live fibre as shown in method (c) in Fig. 6.1. The dark fibres are used to spread the strain across larger areas of the strain gauge. As in method (b) an alternative method was also tested by fixing the lower end of the gauge to a support which is shown as method (d). But contrary to expectations, in the multiple fibre approach the CGF was not measurable because of the poor strain transfer, which is the consequence of the large quantity of adhesive used to fix the dark fibres, which significantly reduces the expansion of the gauge with the applied strain.

6.3.2 Comparison of different configurations

Fig. 6.2(a) and Fig. 6.2(b) show the strain values for an increase and decrease in the fibre elongation for the strain gauge affixed directly (method a) to the fiber and with the lower end of the gauge attached to the support (method b) respectively. Fig. 6.3 shows the comparison between the calculated values of the strain applied to the fiber and the experimental value obtained using different bonding techniques.

It was found that the first two methods [(a) and (b)] are in good agreement with the calculated values. For strain values over 500 $\mu\varepsilon$, the peak error was 3.13 % for method (a) and 10.04 % for method (b). Thus, it can be concluded that the method (a) in Fig. 6.1 is superior. In the multiple fibers approach [method (c) and (d)] the strain transfer was very poor due to the large quantity of adhesive and hence strain was not measurable. Thus, in experiments method (a) is used as a reference for strain measurements using FBG sensors [150]. Other than measuring reference strain of FBG sensors this method of using strain gauges together with optical fibers can be used to measure strain on optical fibers when the fiber is strained using translational devices.

6.4 An FBG interrogation system based on a macro-bend fiber filter

The bend loss wavelength characteristic of a macro bend fiber allows it to be used as an interrogation system for FBG sensors when used in a ratiometric scheme as explained in previous chapters. However, due to the influence of noise in the system, polarization dependency of the components and the temperature dependency of the fiber filter, for an array of FBGs with peak wavelengths spread over a wide range it is not possible to adopt a single slope that yields the best resolution and accuracy for all the FBGs. Thus, for a macro-bend fiber based demodulation system, it is important to have a best fit slope which is most

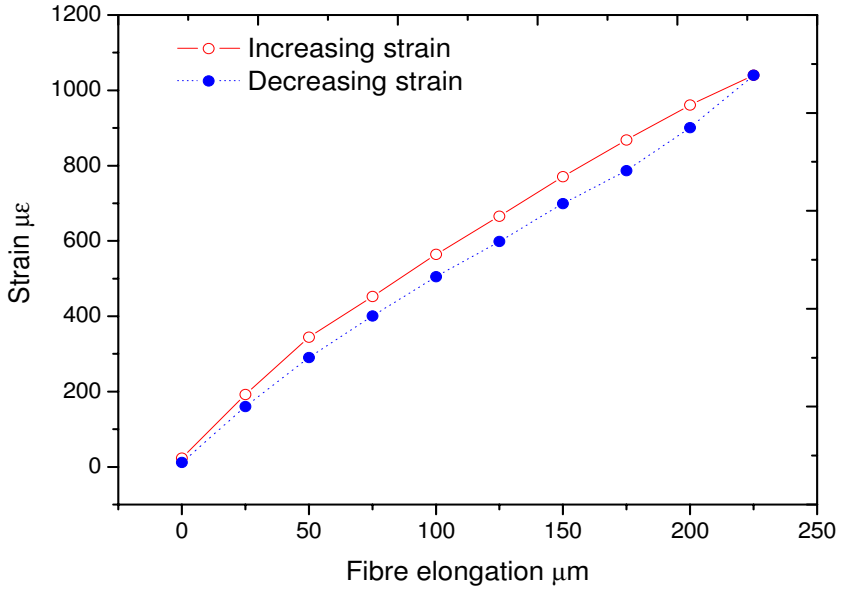

(a)

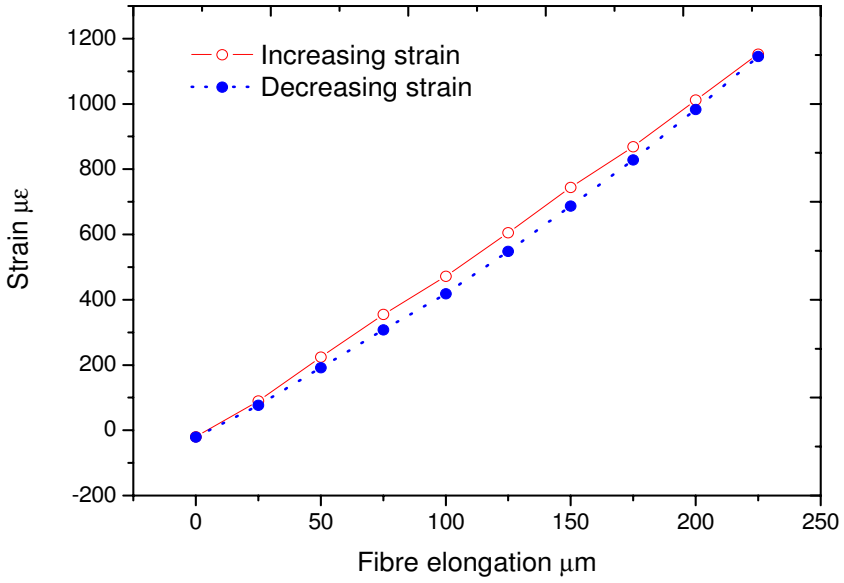

(b)

Figure 6.2: Measured reference strain using strain gauge with increase and decrease in fiber elongation (a) for method a (b) for method b.

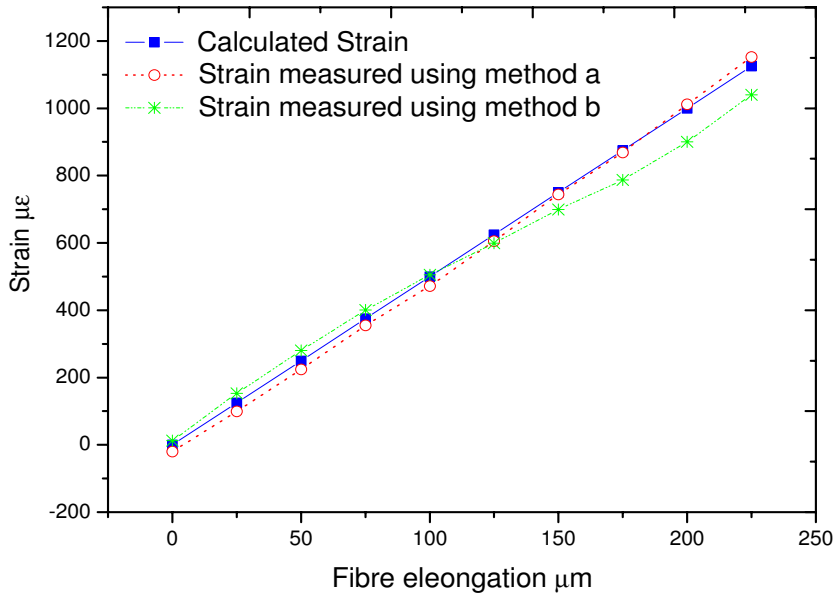

Figure 6.3: Comparison of measured strain using different configurations with the calculated strain.

suitable for a wide wavelength range and which provides the highest achievable resolution and accuracy for all the FBGs in the array. To obtain the best fit slope one has to perform an analysis of a system considering all the above mentioned parameters.

A schematic of the experimental interrogation system used in this investigation for an array of FBG sensors based on macro-bend fiber filter is shown in Fig. 6.4. A super luminescent diode was used as a broadband source (BBS) to drive the interrogation of the Bragg gratings. An optical isolator is used to block any reflected light from reaching the source. An optical circulator is used to direct the reflected signal from the FBGs to the demodulation system. Any edge filter based ratiometric demodulation system can measure only one wavelength at a time. Therefore, an optical tunable wavelength filter is used to extract a single reflected wavelength at a time which is then inputed into the demodulation system whose band pass allows it to measure the wavelength shift induced

by strain or temperature variations. However, the scanning speed of the tunable filter is not considered important in this study as the primary aim of this study is focussed in the selecting a proper fiber filter for interrogating multiple FBGs.

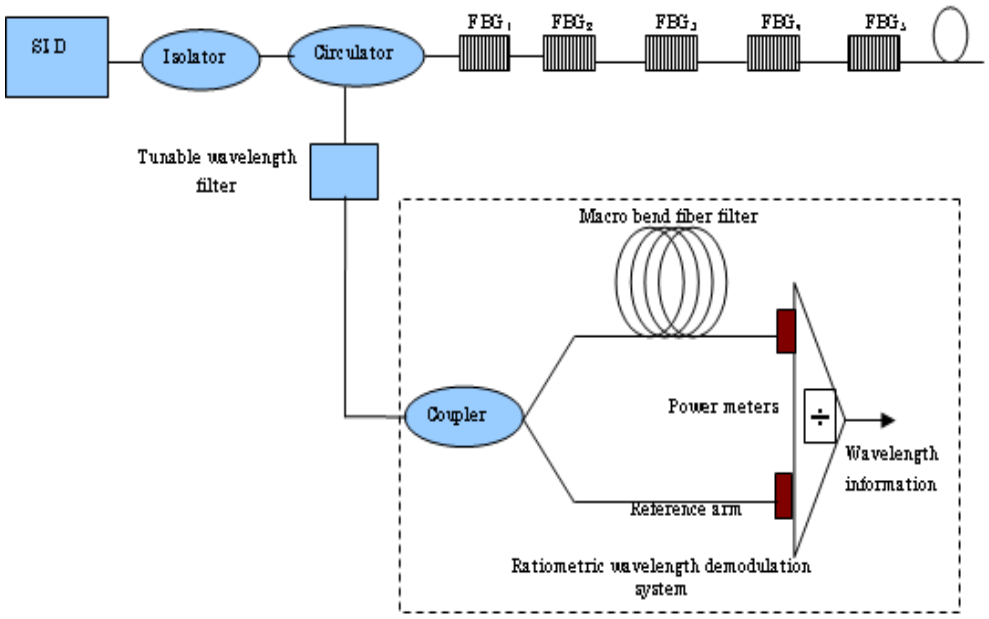

Figure 6.4: Schematic of the interrogations system with multiple FBGs.

Five FBGs with peak reflected wavelengths at 1530.40 nm, 1540.15 nm, 1550.2 nm, 1560.1 nm and 1571.4 nm are used in the experiment. The spectrum of the broadband source used and the reflected spectrum from the undisturbed FBG sensor array are shown in Fig. 6.5(a) and Fig. 6.5(b) respectively. The peak power of the reflected signals depends on the broadband source's intensity distribution, which has a peak intensity at 1560 nm, and the reflectivity's of the FBGs. The reflectivity of the FBGs used in this experiment was approximately 90 %. For optical-electrical conversion, two identical photodiodes (G9 801) are used together with low noise preamplifiers, as the signals reflected from the FBGs are of a very low power and will be further attenuated by the fiber filter. The data acquisition card used to acquire data from the photodiodes was a NI6143 card which can give a very high sampling rate of a maximum of 250 kS/s. The

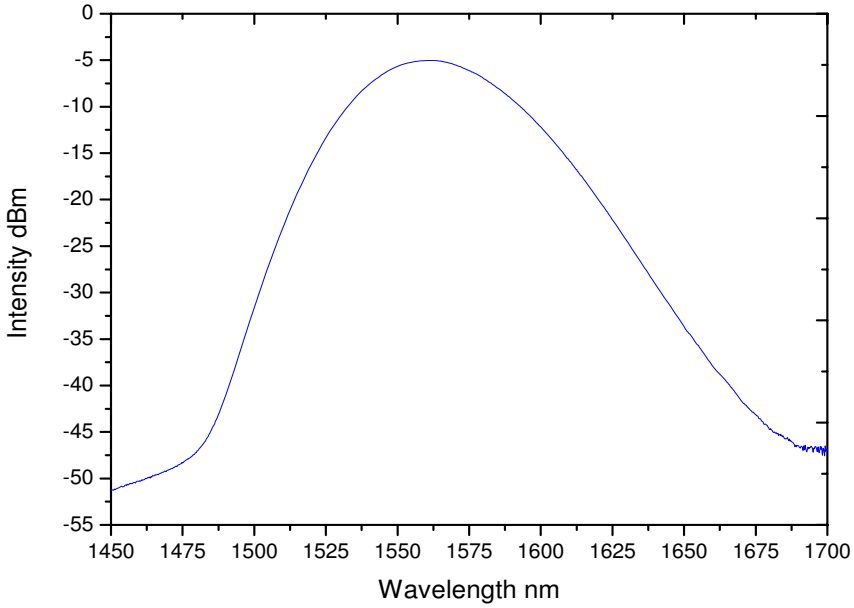

(a)

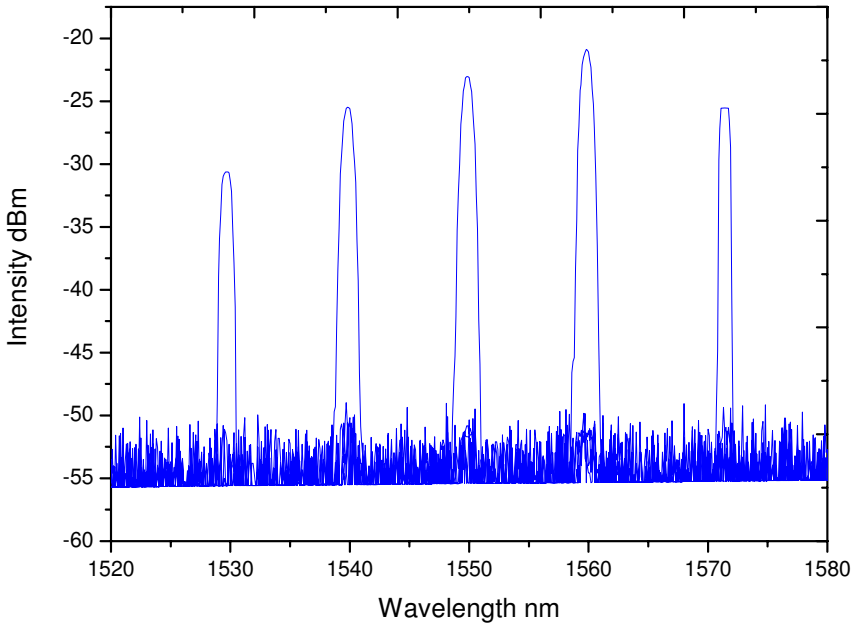

(b)

Figure 6.5: (a) Spectral distribution of the broadband source used (b)Reflected spectra from the FBGs.

bandwidth of the preamplifier used was 2 kHz. The macro-bend fiber demodulation system consists of only passive devices and therefore, it does not affect the measurement speed. Thus, dynamic strain can be measured up to a frequency limit imposed by the speed of the post-detection electronics.

In this study five filters are considered with a bend radius of 10.5 mm and with bend turns 5, 10, 15, 20 and 25 which gives average slopes of 0.07 dB/nm, 0.14 dB/nm, 0.21 dB/nm, 0.28dB/nm and 0.35 dB/nm respectively. The measured ratio response of the system with different filters is shown in Fig. 6.6 which is obtained at a temperature of 20 ^{0}C. The measurable wavelength range is limited by the SNR of the source and the slope of the fiber filter as described in Chapter 2. From Fig. 6.6 it is clear that for a higher number of turns, the slope is higher; also even the filter with 25 turns can offer a measurement range to cover all the reflected wavelengths. However, such a filter cannot guarantee a high resolution and accuracy as it is affected by polarization, temperature and noise. An analysis of the system and selection of a suitable fiber filter considering all these factors is presented in the next section.

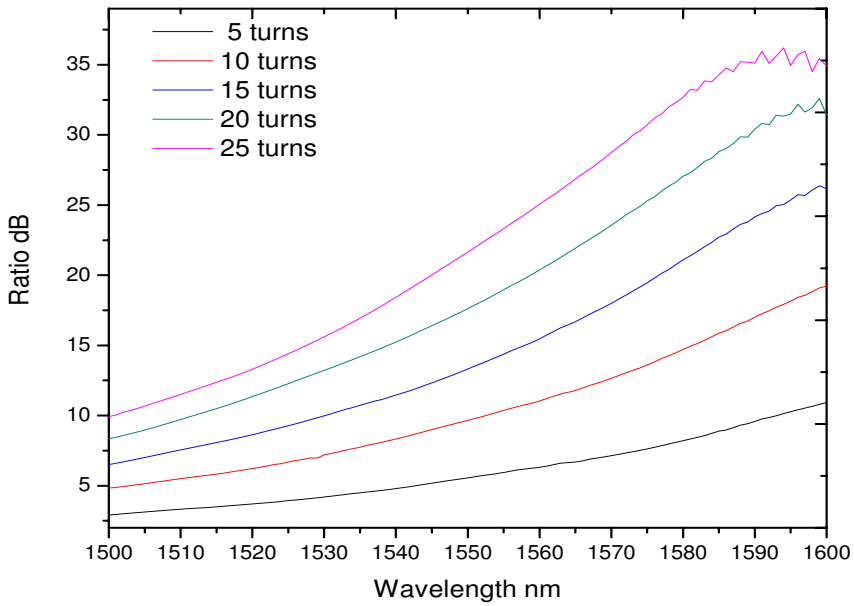

Figure 6.6: Ratio response of the system with different fiber filters.

6.4.1 Analysis of the system

Assuming the BBS has a smooth spectral profile, its spectral response can be modeled as a Gaussian distribution of wavelengths with a spectral full-width at half-maximum of $\Delta\lambda_0$ and a center wavelength of λ_0 and can be expressed as [151, 152],

$$B(\lambda) = I_{peak} exp\Big[-4 \ln 2 \frac{(\lambda - \lambda_0)^2}{{\Delta\lambda_0}^2} \Big], \tag{6.11}$$

where λ is the wavelength in vacuum and I_{peak} is the peak power which can be expressed as,

$$I_{peak} = \frac{P_0}{\Delta\lambda_0} \Big[4ln2/\pi \Big]^{1/2}, \tag{6.12}$$

where P_0 is the total power injected into the system by the BBS.

To simplify the calculation it is assumed that the Bragg grating reflectivity function is a Gaussian function with a center wavelength as the Bragg wavelength λ_b and an FWHM of $\Delta\lambda_b$ and is expressed as,

$$G_{\lambda_b}(\lambda) = R_0 exp\Big[-4 \ln 2 \frac{(\lambda - \lambda_b)^2}{{\Delta\lambda_b}^2} \Big], \tag{6.13}$$

where R_0 is the maximum reflectivity that occurs at the Bragg wavelength.

It has to be noted that in practice the reflected signal from the FBG has a limited SNR. The limited SNR of the signal fed to the demodulation system will affect the linearity of the measured ratio spectrum and hence the wavelength range as explained previously. The spectral width of the BBS is much larger than the spectral width of the FBG. Hence it can be stated that the spectral distribution of the wavelengths reflected from the grating when illuminated by the BBS [151] and with a limited SNR as,

$$I_b(\lambda) = \begin{bmatrix} B_{\lambda_b} G_{\lambda_b}, & |\lambda - \lambda_b| \leq \Omega \\ -S + Rand.Rs, & |\lambda - \lambda_b| > \Omega \end{bmatrix}, \tag{6.14}$$

where $B(\lambda_b)$ is given by equation 6.11 when $\lambda = \lambda_b$. S is the SNR of the reflected signal from the FBG. As described in Chapter 2, to describe the random fluctuations in the noise floor of the reflected signal, the term *Rand.Rs* is used, where *Rand* is a random number (between +0.5 and -0.5) and *Rs* is a parameter which dictates the peak fluctuation in the SNR. Ω is a parameter which is determined by the noise level and can be determined for any reflected signal with a given SNR from the relation,

$$B_{\lambda_b} R_0 \exp\Big[-4ln2 \frac{\Omega^2}{\Delta\lambda_0^2} \Big] = -S. \tag{6.15}$$

Also it has to be noted that the receiver noise has an impact on the ratio of the system and is necessary to consider while modeling the system. Therefore, the total power reaching the photodiodes connected to the filter arm and the reference arm can be represented as follows;

$$I_f(\lambda) = \int I_s(\lambda) S_1(\lambda) T_f(\lambda) d\lambda + Grand_e \tag{6.16}$$

$$I_r(\lambda) = \int I_s(\lambda) S_2(\lambda) d\lambda + Grand_r, \tag{6.17}$$

where $S_1(\lambda)$ and $S_2(\lambda)$ represents the responses of the arms of the 3 dB coupler. Gaussian statistics are used to model the electrical noise as explained in Chapter 3. $Grand_e$ and $Grand_r$ are Gaussian random numbers used to represent the receiver noise with a mean value 0 and standard deviation equal to the rms noise of the receivers connected to the edge filter and the reference arms respectively. The noise in the two receivers employed are uncorrelated to each other. As the shot noise of the receiver connected to the edge filter is a function of optical

power and thus wavelength, so $Grand_e$ varies as the wavelength changes. Since the power distribution of the BBS source also varies with wavelength, $Grand_e$ and $Grand_r$ changes for different peak reflected wavelengths.

Taking into account of the BBS spectral distribution, noise in the receiver and SNR of the reflected Bragg wavelengths, the ratio of the system can be expressed as,

$$R(\lambda_0) = -10log_{10}\Big[\frac{I_{f\lambda_0}}{I_{r\lambda_0}}\Big]. \tag{6.18}$$

Using the above model, the ratio fluctuation in the system is calculated with all the five bend loss filters for all the peak reflected wavelengths from the FBG, caused by the noise in the receivers and limited SNR of the FBG signal. The calculated ratio fluctuation for all the FBG sensors is shown in Fig. 6.7(a). From the figure it can seen that the ratio fluctuation is significantly high, for example at 1550 nm the ratio fluctuation is 0.03 dB for a filter with 10 fiber turns. Due to this high ratio fluctuation the system cannot repeatably resolve small strain or temperature changes and hence averaging should be used to reduce the ratio fluctuation. The ratio fluctuation of the system with an averaging of 256 is shown in Fig. 6.7(b) which is in the acceptable range to resolve small strain and temperature changes. However, as a consequence of averaging, the measurement speed of the system will be reduced and that will affect the dynamic measurement capabilities of the system.

Due to the noise induced fluctuation in the ratio of the system the resolution of the system will be limited and will be a function of wavelength and filter discrimination. The calculated resolution of the system, which is limited by the noise of the receiver and SNR of the reflected Bragg signal, is shown in Fig. 6.8(a), with an averaging over 256 samples. From Fig. 6.8(a) it can be seen that for FBGs with peak wavelengths around 1540.15 nm, 1550.2 nm and 1571.4 nm, a filter with 5 turns gives the best achievable resolution among the 5 filters, while

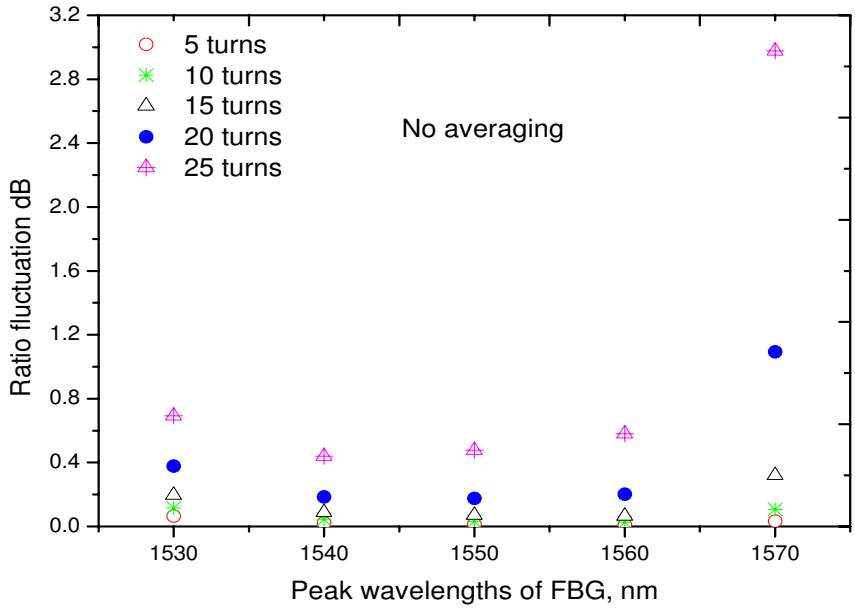

(a)

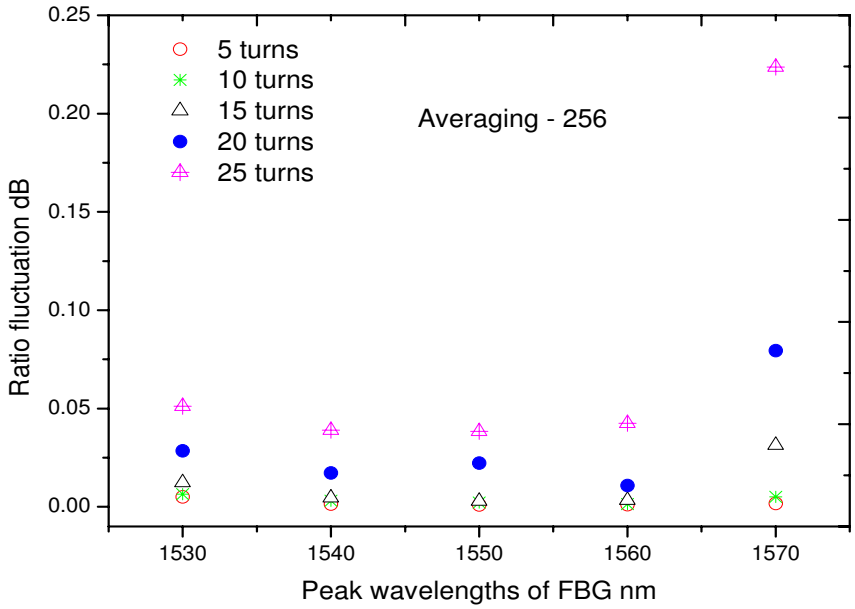

(b)

Figure 6.7: Fluctuation in ratio due to the noise at different FBG peak wavelengths for systems with different slopes.

for 1530.4 nm and 1560.1 nm, a filter with 10 turns gives the highest resolution. Hence, the selection of a suitable filter can be made based on calculations of the deviation of the estimated resolution of each filter from the best individual resolution for each FBG. The calculated percentage deviation in resolution for systems with filters of 5 and 10 turns for all the FBG peak wavelengths from the individual best resolution is shown in Fig. 6.8(b). From the figure it can be seen that for a filter with 5 turns, FBG_2, FBG_3 and FBG_5 can have the highest resolution, while the other two have the largest deviation from the best achievable value. However, for a system with filter with 10 turns FBG_1 and FBG_4 can have much better resolutions.

Ultimately the measurement system is required not to just measure wavelength but also to provide a measure of strain or temperature and for this reason it is necessary to estimate the strain and temperature resolution of the interrogation system. The strain and temperature sensitivity of the FBGs used were 1.2 $pm/\mu\varepsilon$ and 11 pm/^0C respectively. The calculated strain and temperature resolution for all five FBGs obtained with systems using filters with 5 and 10 turns are shown in Table 6.1. The average strain and temperature resolution of the system with 5 turns is 26.7 $\mu\varepsilon$ and 2.9 ^0C respectively while for a system with 10 turns the resolution is 24 $\mu\varepsilon$ and 2.6 ^0C respectively. While these results suggest that the 10 turns filter is best, the effects of polarization and temperature drift for the system and their impact on accuracy also need to be considered before making a final decision of which filter should be used

The accuracy of the macro-bend fiber based interrogation system is determined by the polarization and temperature dependence of the system. The polarization dependency of the macro-bend fiber originates due to the difference in bend loss for the TE mode and TM mode propagating along the fiber due to the different boundary conditions between the cladding and polymer coating layers for the two polarization states which is explained in Chapter 4. However, the

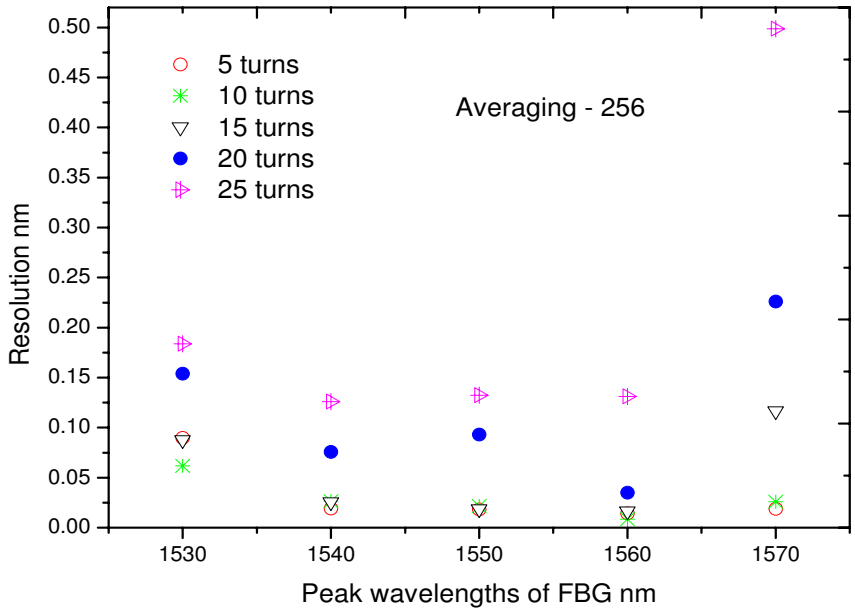

(a)

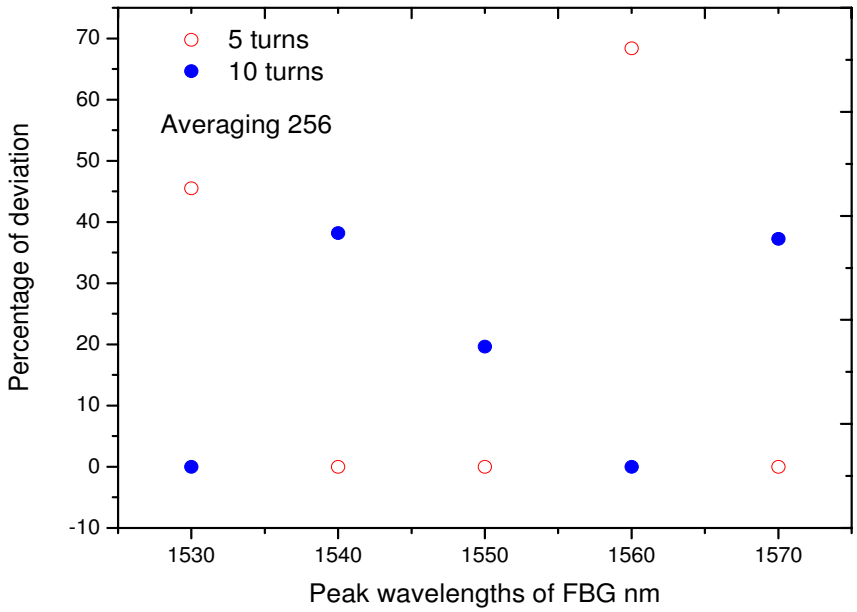

(b)

Figure 6.8: (a) Estimated resolution for FBGs with different peak wavelengths with different system slopes with an averaging of 256 (b) Percentage deviation from the best resolution for different FBGs for system with filters of 5 and 10 turns.

System with different filters	Bragg Wavelengths nm	Strain Resolution $\mu\varepsilon$	Temperature Resolution ^0C
5 turns	1530.40	74.8	8.1
	1540.15	15.9	1.7
	1550.20	15.1	1.6
	1560.10	11.8	1.2
	1571.40	15.6	1.7
10 turns	1530.40	51.4	5.6
	1540.15	22.0	2.4
	1550.20	18.1	1.9
	1560.10	7.0	0.7
	1570.40	21.5	2.3

Table 6.1: Calculated strain and temperature resolution of the system with filters of 5 and 10 fiber turns.

polarization dependency of the fiber filter can be minimized by using a twisted configuration as proposed in Chapter 4 or in [115]. To minimize the PDL of the 3 dB coupler, a polarization insensitive (PI) 3 dB coupler is used together with a twisted fiber filter in the interrogation system. Even with the twisted configuration and with the PI 3 dB coupler, a small finite PDL induced ratio error remains in the system due to the residual PDL of the fiber filter which originates due to the small mismatch between the two bend fiber sections and also due to the small but finite PDL (0.01 - 0.02dB) of the PI 3 dB coupler. This results in wavelength inaccuracies and the measured inaccuracies for the peak reflected wavelengths of the FBGs due to the PDL of the system with filters 5, 10, 15 turns are shown in Fig. 6.9.

Ambient temperature variation is another factor that can create inaccuracies in the measured wavelength of systems based on macro-bend fiber filters. Earlier investigations presented in Chapter 5 on macro-bend fiber edge filters showed that the coating layer has a significant effect on the temperature dependence of the filter. Due to the oscillatory variation in bend loss and hence in the ratio, and the different ratio variations at different wavelengths, a correction in the calibration

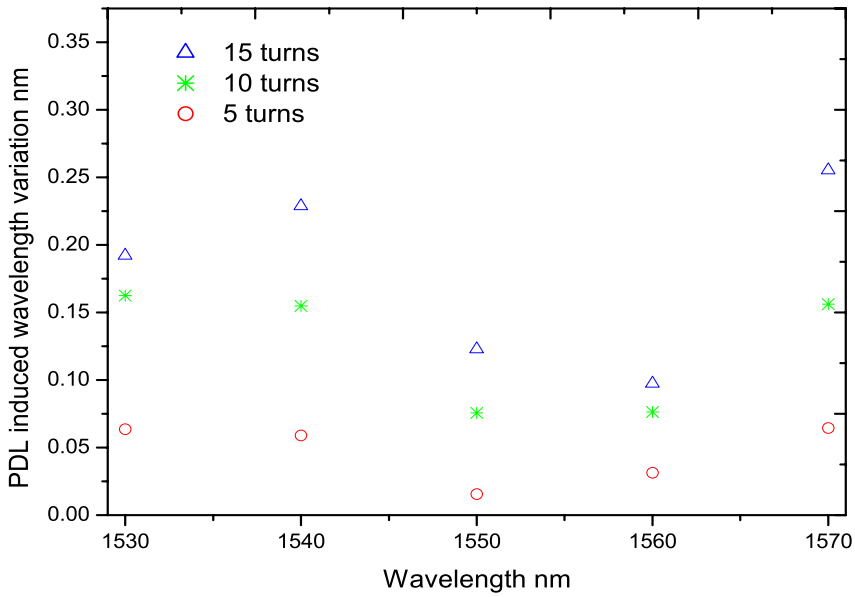

Figure 6.9: Measured inaccuracy at the peak reflected wavelengths of the FBG due the PDL of the system.

response to compensate the temperature variation is very complex for systems based on SMF28 fiber filter. Therefore, for the interrogation system to achieve the highest accuracy, the temperature of the fiber filter has to be maintained as close as possible to the calibration temperature.

The inaccuracies are estimated in strain and temperature measurements due to the PDL of the system and a temperature variation $\pm 1\ ^0C$, from the calibration temperature of 20 ^0C, for fiber filters of 5 and 10 turns. Table 6.2 summarizes the estimated accuracy of strain and temperature measurements for all the five FBGs when used with the demodulation system with filters of 5 and 10 turns. From Table 6.1 and Table 6.2 one can see that the average strain and temperature resolution of a system with 10 turns is slightly higher when compared to 5 turns, but the accuracy is very poor for a system with 10 turns compared to 5 turns. The average strain inaccuracies induced by PDL and temperature dependence for a system with 5 turns are $\pm 38.2\ \mu\varepsilon$ and $\pm 8.9\ \mu\varepsilon$ respectively while for a system with 10 turns the inaccuracies are $\pm 104.2\ \mu\varepsilon$ and $\pm 8.8\ \mu\varepsilon$ respectively. Similarly,

Fiber filter turns	Bragg Wavelengths nm	PDL induced inaccuracy $\mu\varepsilon$	^0C	Temperature induced inaccuracy $\mu\varepsilon$	^0C
	1530.40	±53	±5.8	±5.6	±0.6
	1540.15	±49	±5.3	±6.8	±0.7
5 turns	1550.20	±13	±1.41	±8.2	±0.9
	1560.10	±26.1	±2.8	±20.9	±1.2
	1571.40	±53.7	±5.9	± 13.2	±1.4
	1530.40	±135.4	±14.8	±6.7	±0.7
	1540.15	±129	±14.1	±6.6	±0.7
10 turns	1550.20	±63	±6.9	±9.3	±1
	1560.10	± 63.7	±6.9	±9.2	±1
	1570.40	±130.1	±14.2	±12.4	±1.3

Table 6.2: Estimated accuracy of the system with filters of 5 and 10 turns due to the polarization and temperature dependence of the system.

the average inaccuracy in the measured temperature induced by the polarization and temperature dependence of the system with 5 fiber turns is ±4.2 ^0C and ±0.9 ^0C respectively, while for the system with 10 turns it is ±11.3 ^0C and ±0.9 ^0C respectively. Thus from the analysis it can be concluded that while the average resolution is marginally higher for the 10 turn filter, the accuracy of the system taking into account PDL is substantially better for a filter with 5 turns and for this reason this filter is selected as the one which can give the overall best results for the FBG array. An experimental performance evaluation of the interrogation system with a fiber filter of 5 turns is presented in the next section.

6.5 Performance evaluation of the system

To evaluate the performance of the interrogation system, which is estimated in the last section, static strain, dynamic strain and temperature are measured using the FBG interrogation system. In our experiment, temperature variations are applied to FBG_2, static strain to FBG_3 and dynamic strain to FBG_4 whose reflected wavelengths are 1540.15 nm, 1550.2 nm and 1560.1 nm respectively. The other two FBGs are left undisturbed for the purpose of this experiment. The fiber filter

used in the system has 5 fiber turns. For all the measurements averaging over 256 samples was applied. The temperature of the fiber filter is monitored during the course of the experiment and the recorded variation in the ambient temperature was $\pm 2\ ^0C$ around $20\ ^0C$.

6.5.1 Static and dynamic strain measurements

To apply static strain to FBG_3, one end of the grating is fixed to a translation stage and the other end to a fixed point. Using a micrometer translation stage a strain up to 540 $\mu\varepsilon$ is applied to the FBG using incremental steps of 90 $\mu\varepsilon$. The applied strain is calculated from the ratio of the elongation of the fiber containing the FBG, which is the same as the micrometer translation value and from the length of the fiber between the fixed points. This applied strain is measured with the macro-bend fiber based interrogation system. For strain measurements

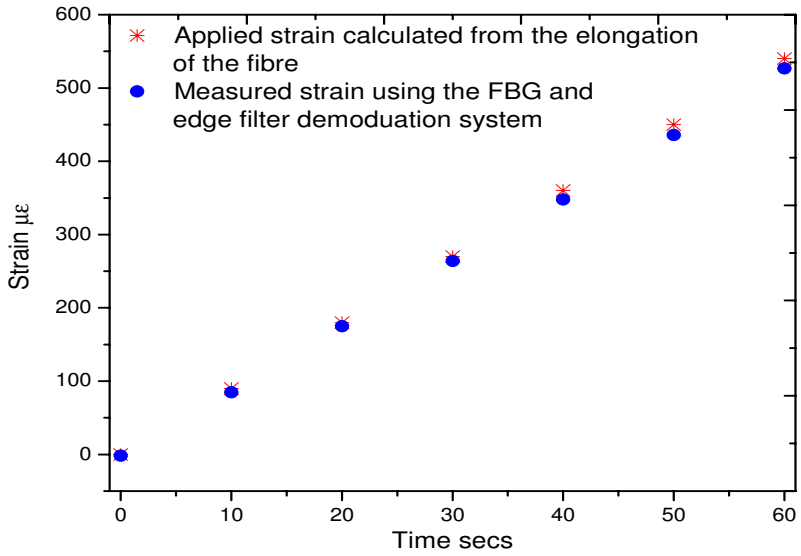

Figure 6.10: A comparison between measured and applied strain.

the temperature of the FBG is kept constant by controlling the temperature of FBG using a temperature controller, which has an accuracy of $\pm 0.1\ ^0C$. This temperature variation can contribute to a strain inaccuracy of $\pm 1\ \mu\varepsilon$. Fig. 6.10

shows the comparison between the measured and applied static strain. Both are in close agreement which shows that the system measures the accurate strain. To examine the resolution of the system a step strain of 10 $\mu\epsilon$ and 20 $\mu\epsilon$ are applied to the FBG. The measured strain variations are shown in Fig. 6.11(a) and Fig. 6.11(b) respectively. From the figure it can be seen that 20 $\mu\epsilon$ is clearly detectable and hence the measured strain resolution agrees with the estimated strain resolution for a system with a filter of 5 fiber turns.

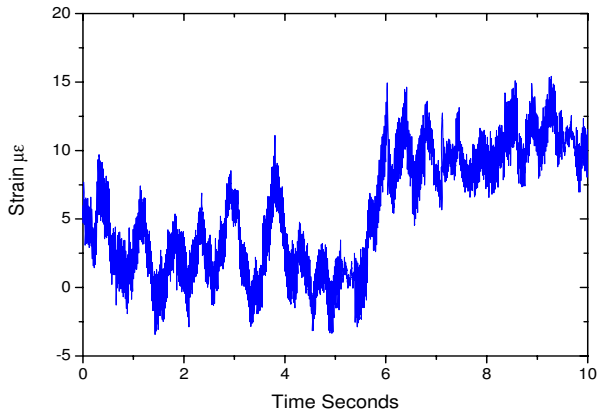

(a)

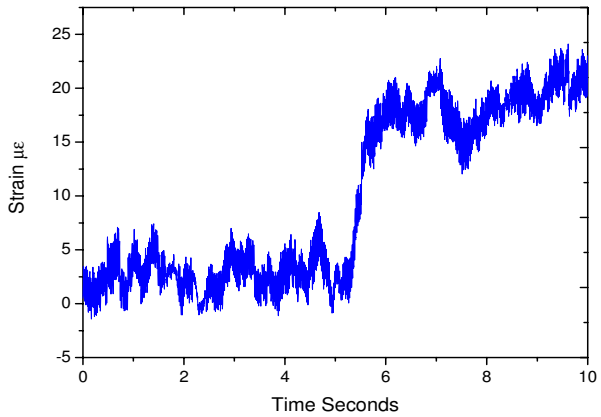

(b)

Figure 6.11: Measured static strain for a step change of (a) 10 $\mu\varepsilon$ (b) 20 $\mu\varepsilon$ (256 averaging applied).

To apply dynamic strain, a piezo actuator (AE0505D18) is used, where one

surface of the piezo actuator is glued to a heavy fixed surface as shown in Fig. 6.12. The purpose of the heavy block was to provide a stable dynamic strain. The other end of the piezo actuator is fixed to a T shaped element to which one end of the fiber containing the FBG is fixed. The other end of the fiber is fixed to a micrometer translation stage, which is used to adjust the static pre-strain. The driver used to supply voltage to the piezo actuator was a MDT694A from Thorlabs. The output current versus frequency characteristic of the driver also needs to be accounted for in the experimental measurements. For the driver used the maximum output current was 60 mA. The maximum sinusoidal frequency that can give the same displacement for a current I_{out} can be calculated from the relation,

$$f = \frac{I_{out}}{2\pi V_{amp} C}, \tag{6.19}$$

where V_{amp} is the voltage applied to the piezo actuator and C is the capacitance of the piezo actuator. The strain amplitude versus frequency characteristic for the driver is shown in Fig. 6.13, for a 0 Hz (or DC) strain value of 25 $\mu\varepsilon$. From the figure it is clear that measured amplitude of the strain deceases considerably as the frequency of strain increases.

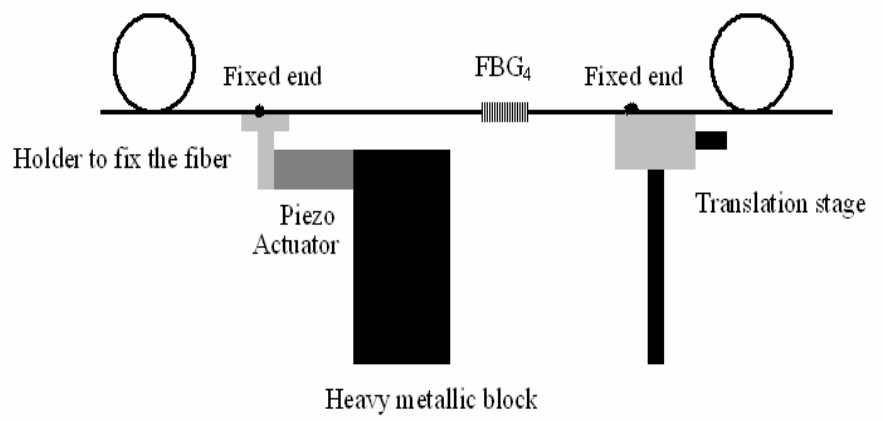

Figure 6.12: Schematic of the setup to apply dynamic strain to the FBG.

Different amplitudes of dynamic strain at a frequency 25 Hz were applied to

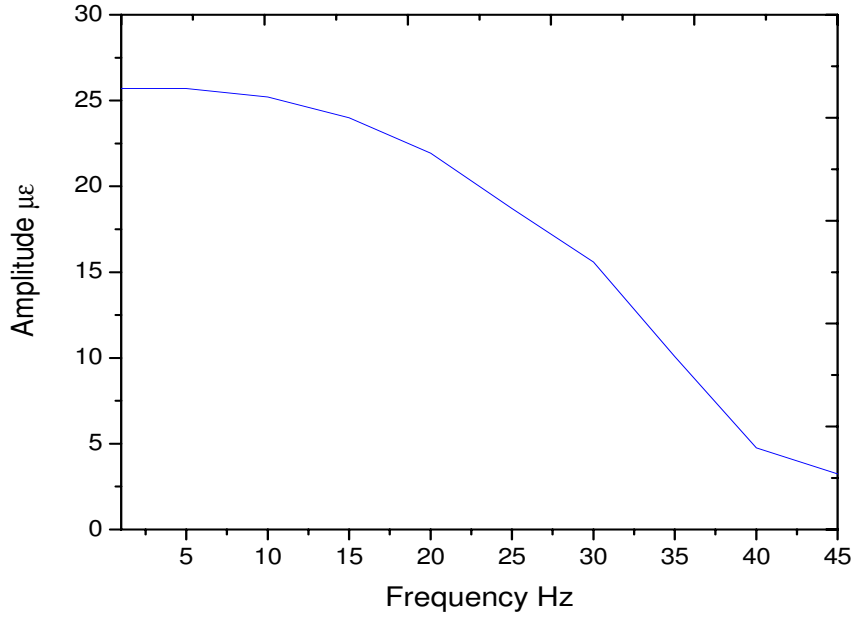

Figure 6.13: Strain amplitude versus frequency characteristics of the piezo driver for a 0 Hz strain of 25 $\mu\epsilon$.

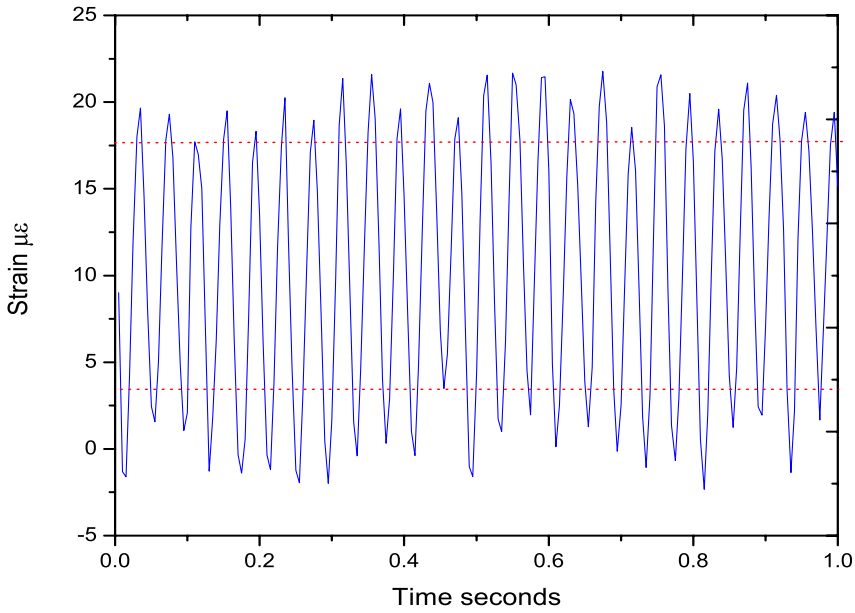

Figure 6.14: Measured dynamic strain for a strain amplitude of 19 $\mu\varepsilon$ and frequency 25 Hz.

FBG_4. Fig. 6.14 shows the measured dynamic strain using the macro-bend fiber based interrogation system with an applied strain amplitude of 19 $\mu\varepsilon$ (equivalent to 25 $\mu\epsilon$ at 0 Hz) with a variation of ± 7 $\mu\varepsilon$. The dynamic strain resolution measured was 5 $\mu\varepsilon/\sqrt{Hz}$. Applying dynamic strain at higher frequencies was not possible due to the limitations of the piezo driver to provide the required current to drive the piezo actuator at higher frequencies. In summary, using a FBG sensor array together with a fiber bend loss filter demodulation system, effective static and dynamic strain measurement is clearly achievable.

6.5.2 Temperature measurements

To demonstrate the ability of the interrogation system to measure the temperature variations, FBG_2 with a peak reflected wavelength of 1540.15 nm was subjected to temperature variations by attaching the sensor to a Peltier cooler which was driven by a temperature controller. To verify the temperature resolution of

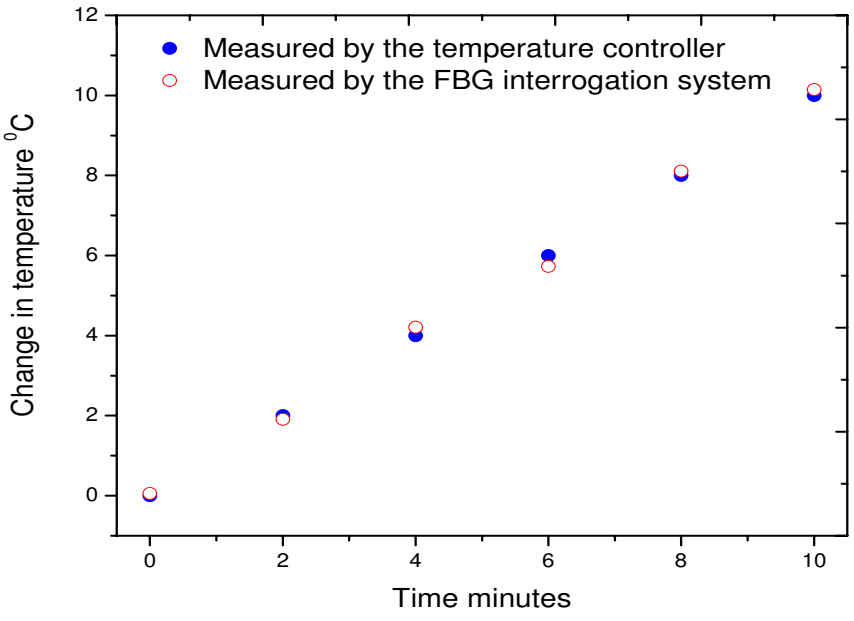

Figure 6.15: A comparison of change in temperature measured using the FBG interrogation system and the temperature controller.

the system, incremental step changes of 2 ^{0}C have been applied from 20 ^{0}C to

30 ^{0}C. As the temperature controller requires time to settle, the measurements were taken at 2 minute time intervals. The measured change in temperature and a comparison with the temperature measured by the temperature controller are shown in Fig. 6.15. The comparison shows that a temperature resolution of 2 ^{0}C can be obtained with the interrogation system which was predicted for a system with an FBG sensor of peak reflected wavelength 1540.15 nm and with a macro-bend fiber filter of 5 turns.

6.6 Summary

In this chapter an analysis and performance evaluation of an all-fiber FBG interrogation system using a macro-bend fiber filter is presented. It is important to have a reference strain measurement for the FBG interrogation system while testing the system. In the present experiment the strain was applied to the fiber containing FBGs using a micro translation stage and piezo actuator. In this case conventional methods of strain gauge references were not suitable and hence another method to use strain gauge as reference strain measurement was demonstrated. Different bonding methods and a modified gauge factor were used to achieve this. The experimental results agreed with the calculations and this method can be used to measure strain in optical fibers using strain gauges for experimental purposes.

Due to the characteristic properties of the macro-bend fiber filter and the total noise associated with the system, a ratio slope for the system to obtain the optimum strain and temperature resolution for all the FBGs in an array is not achievable. The polarization dependent and temperature dependent loss are different for different wavelengths and hence the accuracy of the measurands will be different for different FBGs. Since noise associated with the system determines the resolution of the system, which is a function of wavelength, the resolution of the measurands is different for different FBGs. To demonstrate these effects, a

system was considered with different edge filters, which give different ratio slopes. The maximum achievable resolution and accuracy for FBGs with peak reflected wavelengths at 1530.40 nm, 1540.15 nm, 1550.2 nm, 1560.1 nm and 1571.4 nm were estimated. From the estimation it was found that a system with a filter of 5 turns provides the best fit slope with which the best results for the FBG array can be achieved. Performance evaluation of the system with a macro-bend fiber filter has been carried out and the experimental results agreed well with the estimated values. Temperature, static strain and dynamic strain were applied to three FBGs with peak wavelengths 1540.15 nm, 1550.2 nm and 1560.1 nm respectively. In the demonstration a static strain resolution of 20 $\mu\varepsilon$ and dynamic strain resolution of 5 $\mu\varepsilon/\sqrt{Hz}$ was achieved. Thus, the consequences of the characteristic properties of the system and its effect on the resolution and accuracy of the measurands were successfully demonstrated. The importance of a best fit slope to achieve the best results for an array of FBGs when used together with a macro-bend fiber filter demodulation system was also demonstrated in this study.

The conclusions from this chapter are summarized as following;

- Due to the characteristic properties of the components of the system and the noise associated with the system, which are both a function of wavelength, resolution and accuracy will be different for different wavelengths.

- For a single FBG, it is possible to optimize the system slope to achieve optimal results. But for an array of FBGs, whose peak reflected wavelengths are spread over wide wavelength range, it is not possible adopt a single slope that yields the best resolution and accuracy for all the FBGs.

- For a macro-bend fiber based demodulation system, it is important to utilize a best fit slope which is most suitable for a wide wavelength range and which provides the highest achievable resolution and accuracy for all the FBGs in the array.

- For the developed system under lab conditions, a static strain and dynamic strain resolution of 20 $\mu\varepsilon$ and 5 $\mu\varepsilon/\sqrt{Hz}$ respectively were achieved. The temperature resolution recorded was 2 ^{0}C. The resolution of the system could be improved by reducing the noise level in the system.

Chapter 7

Conclusions and future research

This chapter presents the overall conclusions for the thesis. Irrespective of the order of the material presented in the previous chapters the final conclusions are divided into six sections. The design and fabrication of the macro-bend fiber edge filter, a complete model of an edge filter based ratiometric wavelength measurement system, the characteristic properties of the components involved in the system and their influence on the performance of the system, the design of a low polarization sensitive wavelength measurement system and finally the application of the system as a wide range FBG interrogator are summarized to underpin the conclusions presented in this chapter. The temperature studies of the macro-bend fiber edge filter resulted in a spinoff research and development of a temperature sensor which is also concluded in this chapter.

This chapter also discusses the future research challenges and potential extensions of the work presented in this thesis. FBG interrogation systems and optical fiber sensors have clear research and technological development possibilities in many future applications and in this chapter some specific areas of interest for further research are focussed upon.

1. A macro-bend fiber edge filter for wavelength measurements

In this thesis it was shown that by using an appropriate bend radius and number of bend turns the bend loss phenomenon in single-mode fiber can be used for the fabrication of edge filter for wavelength measurements. However, to

eliminate the whispering gallery modes in bent single-mode fiber and to fabricate a macro-bend fiber edge filter, an absorption layer needs to be applied to the fiber buffer coating. Macro-bend fiber filters were fabricated using standard single-mode fiber, SMF28, and experimental studies and analysis of the transmission response of the filters were carried out. Filters with different slopes were fabricated and the change in baseline loss and discrimination range of the fiber filters with different slopes were studied. The effectiveness of the fabricated filters are demonstrated in a working ratiometric wavelength measurement scheme.

The key conclusions from the studies are;

- A macro-bend fiber filter was demonstrated as an effective and viable way of implementing an edge filter for a ratiometric wavelength measurement system.

- To suit different measurement environments the slope of the system can be varied by changing the bend radius and number of bend turns, however there is a trade-off between the baseline loss and the discrimination range. For example, a filter with a bend radius of 10.5 mm and 15 bend turns can give a low baseline loss and a useful discrimination characteristic which can cover a wavelength range of 1500 nm - 1580 nm.

2. A complete model for edge filter based ratiometric wavelength measurement system

A complete model for an edge filter based ratiometric system is presented in this thesis. A noise model for an edge filter based ratiometric system is proposed in this thesis and the effect of noise on the performance of a ratiometric wavelength measurement system was studied theoretically as well as experimentally. Theoretical modeling of the system considering the limited SNR of the source, the wavelength dependency of the coupler and the noise in the receiver was carried out and verified experimentally. Using this model an edge filter based

wavelength measurement system can be designed with a desired wavelength range and resolution. The impact of the noise on the resolution was also investigated. The wavelength range and resolution of the system with different fiber filters were investigated experimentally and the results were in good agreement with the modeled results.

From these studies it was concluded that;

- The limited SNR of the optical source determines the achievable slope of the system for a desired wavelength range. A change of the SNR of the source so that it differs from that used during calibration also induces wavelength error.

- In the design of any ratiometric system to estimate the exact discrimination ratio response, it is necessary to consider the effect of the 3 dB coupler.

- A complete model of the system is necessary to determine the overall performance of any edge filter based ratiometric system. The proposed noise model of a ratiometric system and the studies based on this model show that the widely held presumption about using a higher ratio slope for higher resolution is incorrect.

- It was shown that increasing the slope of the edge filter is not a guaranteed approach to increasing the resolution of the system. An optimization of the slope of the system considering the total noise of the system is required to achieve the best possible resolution for a wider wavelength range.

3. Characteristic properties of the system and their influence on the system performance The two characteristic properties of the system studied in this thesis were the polarization and temperature dependency. The origin of the polarization dependence of the macro-bend fiber filter and of the 3 dB coupler were discussed in this thesis. Since the system contains concatenated

PDL elements a theoretical model to estimate the maximum ratio and wavelength error was presented. The ratio and wavelength error due to PDL of the fiber filter and of the 3 dB coupler are measured and lie within the estimated limits. The temperature induced instabilities in the system were also investigated. For this investigation two types of fiber edge filters were used, one a standard SMF28 fiber edge filter and another a bend loss sensitive 1060XP fiber based edge filter. The temperature dependence of bend loss of the filters and ratio of the system were studied.

From these studies it was concluded that;

- Since a ratiometric system contains concatenated PDL elements, the net effect of the PDL is different from the effect caused by individual PDL components and because of this an estimation of the range of the wavelength error is necessary to determine the accuracy of the system. From the investigations it is also concluded that PDL is an important factor determining the accuracy of a macro-bend fiber filter based ratiometric system and needs to be minimized to improve the performance of the system.

- From the investigations of the temperature dependence of the system it is concluded that for a system based on a SMF28 fiber filter, due to the oscillatory variation in ratio response with temperature, the temperature corrected calibration approach is too complex to be feasible.

- For a 1060XP fiber filter without a buffer and with an absorption layer the system produces a linear ratio variation. While the SMF28 fiber filter based system is less sensitive to temperature than the 1060XP fiber filter based system, the linear nature of the temperature dependence of 1060XP fiber filter means that it is feasible to correct for changes in ambient temperature by monitoring the filter temperature and correcting the calibration response.

- A 1060XP filter based system can be operated over a wide ambient temperature range for precise wavelength measurements, if calibration correction is provided. For a system based on an SMF28 filter active temperature stabilization of the filter will be required to achieve high accuracy.

4. A low polarization sensitive all-fiber wavelength measurement system

From the studies of the effect of the polarization dependence of the system, it was found that to improve the accuracy of the system, it is essential to reduce the PDL of the macro-bend fiber filter and the 3 dB coupler. The research carried out in that regard resulted in a low polarization sensitive all-fiber wavelength measurement system. In this thesis it has been experimentally demonstrated that for a configuration with a twisted macro-bend fiber filter and a PI 3 dB coupler the wavelength accuracy of the system was greatly improved when compared to the conventional macro-bend fiber based system.

The main conclusion that arises from these studies are:

- Since the PDL of a macro-bend fiber filter originates from the difference in the propagation of TE and TM modes, an effective solution to reduce the PDL is to introduce a 90^0 twist in the middle between the two sections of the bend fiber. This will compensate for the individual polarization induced bend loss for each section and thereby reduce the PDL of the fiber filter.

- When this configuration is used together with a polarization insensitive 3 dB coupler, the inaccuracy due to the change in input polarization can be minimized to a great extent. Furthermore a 90^0 twist does not impact on the bend loss spectral response of the filter.

5. An all-fiber wide range interrogation system for an FBG array

Due to its wide wavelength range and dynamic range, a macro-bend fiber filter based system can be effectively used as an interrogation system for multiple

FBGs. For demonstration five systems were considered with different edge filter slopes and five FBGs with Bragg wavelengths 1530.40 nm, 1540.15 nm, 1550.2 nm, 1560.1 nm and 1571.4 nm. An analysis of the system was carried out and from the studies it was estimated that for the Bragg array, a system with a filter of 5 bend turns can give best results for all the FBG sensors. To verify the estimation, a performance evaluation of the system with a filter of 5 turns were carried out. The experimental results agree with the estimated results and in the demonstration a static strain resolution of 20 $\mu\varepsilon$ and dynamic strain resolution of 5 $\mu\epsilon/\sqrt{H}z$ was achieved. The dynamic strain resolution was limited by the capabilities of piezo driver used in the experiment. The measured temperature resolution of the system was 2 ^{0}C. Thus in this thesis it was shown that a macro-bend fiber based system can be used to interrogate multiple FBGs when used together with a suitable tunable filter.

From the studies it can be concluded that;

- Due to the characteristic properties of the components of the system and the noise associated with the system, which are both a function of wavelength, resolution and accuracy will be different for different wavelengths.

- For a single FBG, it is possible to optimize the system ratio slope to achieve optimal results. But for an array of FBGs, whose peak reflected wavelengths are spread over wide wavelength range, it is not possible adopt a single slope that yields the best resolution and accuracy for all the FBGs.

- For a macro-bend fiber based demodulation system, it is important to utilize a best fit slope which is most suitable for a wide wavelength range and which provides the highest achievable resolution and accuracy for all the FBGs in the array.

- For the developed system under lab conditions, a static strain and dynamic strain resolution of 20 $\mu\varepsilon$ and 5 $\mu\varepsilon/\sqrt{H}z$ respectively were achieved. The

temperature resolution recorded was 2 ^{0}C. The resolution of the system could be improved by reducing the noise level in the system.

6. An macro-bend fiber loop based temperature sensor

In this thesis a temperature sensor based on a macro-bend fiber loop is presented. The development of the sensor was a spinoff outcome from the temperature studies of fiber edge filters. The sensor head consists of a buffer stripped high bend loss fiber loop with an absorption layer and is used in a ratiometric scheme to obtain accurate temperature measurements. The temperature sensor was demonstrated experimentally and a temperature up to 75 ^0C have been measured. Since the sensor head is a silica fiber, then together with a high temperature capable absorption layer, it has a potential to be used for wide range and high temperature applications. The sensor also has a high temperature resolution and can reliably resolve temperature variations less than 1 ^0C.

The key conclusions from the studies are;

- A direct linear relationship between the bend loss in a single-mode fiber and temperature can be achieved by using a bend sensitive single-mode fiber without a buffer coating applied but with an absorption layer for eliminating the WG modes.
- Given the simplicity of fabrication of the sensor head and the use of single-mode fiber, it can be used as a disposable sensor in a range of application areas.

Overall conclusions for the thesis

The key conclusions from the research and this thesis are:

- A macro-bend fiber based ratiometric wavelength measurement system is a viable way to implement the core of an FBG interrogation system;

- The filter response slope is a key parameter in determining the measurable wavelength range and resolution of the system and the slope needs to decided upon by taking into account source noise and receiver noise, as simply maximizing the magnitude of the slope will not guarantee the highest resolution;

- The polarization dependent loss of the fiber filter can be minimized by splitting the filter into equal length sections with a 90^0 fiber twist between sections, with the added benefit that there is no impact on the spectral response of the filter;

- Temperature dependence is a key parameter that degrades the performance of a macro-bend fiber filter, but by correctly utilizing a bend sensitive fiber, such temperature dependent loss can be usefully employed as the basis of a novel disposable temperature sensor.

Future research challenges

A practical working demonstrator of the interrogation system

From the knowledge and experience gained from this research work, the understanding of basic factors which need to be considered in designing an all-fiber edge filter based interrogation system, one would expect a working demonstrator for practical applications. For a practical demonstrator, many engineering problems need to be solved, such as minimizing the noise in the receivers to achieve high resolution for a wide wavelength range, stabilizing the temperature of the system for achieving high accuracy and designing the system for the wavelength range of interest. One immediate future strand of work will concentrate on developing a practical working demonstrator.

Enhancing the range of the temperature sensor and its applications

Another spinoff from the research work presented in this thesis, is the development of a macro-bend temperature sensor. One of the main challenges for the further development of the sensor is to maintain linear operation over an extended temperature range. For room temperature measurement a range of absorption coating materials (e.g., a black pigment coating, an Indian ink) to absorb the WG modes at the operating wavelength can be used. For applications, such as advanced composites, during the curing process the temperature is in the range of 200 - 300 ^0C. While the glass fiber itself can tolerate a high temperature, in order to maintain linear operation over an extended temperature range the absorbing coating must be able to operate over the entire temperature range without degradation. High temperature capable fiber coatings which would absorb radiation in the range 1500 nm - 1600 nm could be used as an absorption coating and more investigations are required in this context. Optimal coating techniques have to be investigated and the effect of coating on the linearity of the response is also needs additional investigation.

The most promising application the macro-bend fiber temperature sensor is the monitoring of the internal temperature during the curing process. The cure reaction in a composite component, such as helicopter rotor blades, aircraft wing structures etc, during manufacturing is an exothermic reaction and hence it is necessary to control and monitor the internal temperature accurately to ensure high strength and quality. For temperature measurements during processing, the current practice is to use thermocouples at the outer edges of the composite preform to obtain data on the temperature profile, however information on the actual temperature(s) away from the edges is not measured. This is an area of concern for large, complex, and thick performs. Thermocouples (metal parts) and other fiber optic sensors (which are expensive) cannot be used for internal temperature measurement as they cannot be left inside the material after the

curing process. A macro-bend fiber sensor is based on an economic single-mode fiber with a simple design offer a good potential as a disposable sensor for insitu cure process monitoring and which can also be used with microwave heating. However further investigations are required to determine the challenges of using this embedded sensor for composite materials.

FBG interrogation system based on photonic crystal fiber loop

In this thesis the edge filter for FBG interrogation used was macro-bend single-mode fiber. However, the emerging new class of optical fibers, photonic crystal fibers (PCF) could also be used as interrogation system for FBGs. The main advantage of using a PCF based system is its temperature insensitivity. As future work, a highly birefringent (Hi-Bi) PCF in a fiber loop mirror could be utilized as an interrogation technique for FBGs. Some initial research work by other authors in this area has shown that an uncoated Hi-Bi PCF is highly temperature independent compared to a coated one. Another advantage of polarization maintaining PCFs in a fiber loop mirror is that, by changing the length of the fiber or by changing the fiber birefringence, the polarity of the slope of the filter can be changed. This allows the use of two fiber loop mirrors in a ratiometric scheme to achieve high wavelength resolution, with high power stability and with very low temperature dependence. Given the superior characteristic properties of the PCF, it is important to explore and develop passive systems based on PCF for different application areas.

Appendix A

Bragg grating strain and temperature sensitivity

Expanding Equation (6.1) in terms of the partial derivatives with respect to the change in length and refractive index of the core due to strain and temperature, the shift in Bragg wavelength can be expressed as [20],

$$\Delta\lambda_G = 2[\Lambda\frac{\partial n_{eff}}{\partial L} + n_{eff}\frac{\partial\Lambda}{\partial L}]\Delta L + 2[\Lambda\frac{\partial n_{eff}}{\partial T} + n_{eff}\frac{\partial\Lambda}{\partial T}]\Delta T \tag{A.1}$$

Here ΔL is the change in physical length of the grating due to strain and ΔT is the change in temperature.

Considering the response of the strain firstly, the path-integrated longitudinal strain is given by $\varepsilon = \Delta L/L$, we can write the strain induced wavelength shift as,

$$\Delta\lambda_G = 2\Lambda[\frac{\partial n_{eff}}{\partial L}\Delta L + 2n_{eff}\frac{\partial\Lambda}{\partial L}]\varepsilon L \tag{A.2}$$

Defining

$$\Delta n_{eff} = \frac{\partial n_{eff}}{\partial L}L \tag{A.3}$$

and since

$$\Delta(\frac{1}{n_{eff}^2}) = -\frac{2\Delta n_{eff}}{n_{eff}^3} \tag{A.4}$$

Therefor Equation (A.2) can be re-written as,

$$\Delta\lambda_G = 2\Lambda[-\frac{n_{eff}^3}{2}\Delta(\frac{1}{n_{eff}^2})] + 2n_{eff}\varepsilon L\frac{\partial\Lambda}{\partial L} \tag{A.5}$$

Strain-optic theory predicts that changes in optical indicatrix tensor $\Delta[\frac{1}{n_{eff}^2}]_i$, resulting from an applied strain to the material are given by,

$$\Delta[\frac{1}{n_{eff}^2}]_i = \beta_{i,j}\varepsilon_j \qquad i,j = 1,2,3 \tag{A.6}$$

where ε_j is the block-reduced strain tensor in the fiber [153] and $\beta_{i,j}$ is the contracted strain-optic tensor of the optical fiber with coefficients p_{ij}, where the subscripts i, j refer to the co-ordinate axis of the fiber as shown in Fig A. 1.

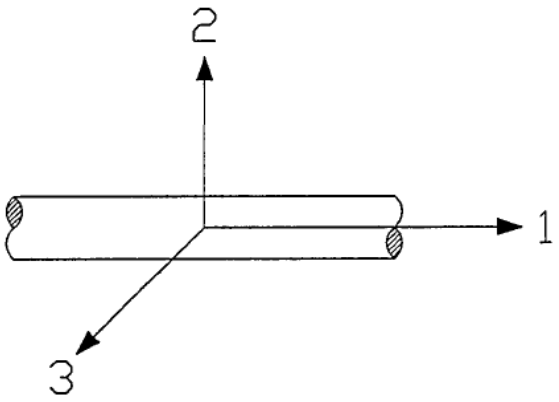

Figure A.1: Coordinate axis of the optical fiber.

For a pure uniaxial longitudinal stress, σ_z, applied to an isotropic, elastic, optical fiber having the l direction oriented in the z-direction, the block-reduced strain tensor of the fiber is given by

$$\varepsilon_j = \begin{pmatrix} \varepsilon_z \\ -\nu_2\varepsilon_z \\ -\nu_3\varepsilon_z \end{pmatrix} \tag{A.7}$$

where ε_j, is the longitudinal strain on the fiber and ν is Poisson's ratio for silica. This assumes a zero shear strain, based on the Butter and Hocker model [154,

155]. The contracted strain-optic tensor is given by,

$$\beta_{i,j} = \begin{pmatrix} p_{11} & p_{12} & p_{13} \\ p_{12} & p_{22} & p_{23} \\ p_{13} & p_{23} & p_{33} \end{pmatrix} \tag{A.8}$$

This is the case for a homogenous, isotropic material such as the core of a low birefringent optical fiber. For this same case the optical indicatrix values for each polarization axis are degenerate, and Equation (A.6) reduces to

$$\Delta[\frac{1}{n_{eff}^2}]_i = [p_{12} - \nu(p_{11} + p_{12})]\varepsilon_z \tag{A.9}$$

where i = 2, 3. Since $\partial\Lambda/\partial L = \Lambda/L$, Equation (A.5) can be written as,

$$\Delta\lambda_G = 2n_{eff}\Lambda\varepsilon_z\{1 - \frac{n_{eff}^2}{2}[p_{12} - \nu(p_{11} + p_{12})]\} \tag{A.10}$$

and the shift in the center wavelength for a grating with a given center wavelength, λ_G, is then given by,

$$\frac{\Delta\lambda_G}{\lambda_G} = (1 - \rho_\alpha)\varepsilon_z \tag{A.11}$$

where we can define an effective strain optic constant, ρ_α, as

$$\rho_\alpha = \frac{n_{eff}^2}{2}[p_{12} - \nu(p_{11} + p_{12})] \tag{A.12}$$

To obtain the response of an FBG to temperature, the change in the center wavelength of a Bragg grating for a given change in temperature can be written as

$$\Delta\lambda_G = 2[\Lambda\frac{\partial n_{eff}}{\partial T} + n_{eff}\frac{\partial\Lambda}{\partial T}]\Delta T \tag{A.13}$$

substituting,

$$\frac{\partial n_{eff}}{\partial T} = \xi n_{eff} \tag{A.14}$$

where ξ is the thermo-optic coefficient and

$$\frac{\partial \Lambda}{\partial T} = \alpha \Lambda \tag{A.15}$$

where α is the coefficient of thermal expansion for silica. Thus Equation (A.13) can be modified as,

$$\Delta \lambda_G = 2 n_{eff} \Lambda \xi \Delta T + 2 n_{eff} \Lambda \alpha \Delta T \tag{A.16}$$

and thus the change in center wavelength of a Bragg grating due to a change in temperature, ΔT, is

$$\frac{\Delta \lambda_G}{\lambda_G} = (\xi + \alpha) \Delta T \tag{A.17}$$

Appendix B

Equipment and Accessories

This appendix covers the details of main instruments and accessories used in the experimental work presented in this thesis. Important specifications and operational characteristics of the tunable laser source, broadband source, optical spectrum analyzer, fiber fusion splicer, power meters, data acquisition and interfacing systems are highlighted in this section.

Nettest OSICS ECL Tunable Laser

The Nettest OSICS tunable laser system consists of the OSICS mainframe and an external cavity laser module. OSICS is an 8 channel modular instrument designed for fiber optic component testing particulary for DWDM. It is a fully integrated system with onboard hardware and software. The OSICS system may be remotely operated via standard RS232 and IEEE-488 interfaces.

OSICS-ECL is a tunable external cavity laser rack module which can be plugged into the main frame. The optical layout of the system is a modified Littman-Metcalf configuration. Double pass reflection on the grating provides maximum dispersion, while the very short cavity, which maximizes mode spacing, yields a spectrally pure and truly single-mode operation. The main specifications of the OSICS ECL tunable laser are listed below [156]:

Wavelength range : 1500 nm - 1620 nm

Output Power range: -5 dBm - +7dBm

Wavelength resolution: 0.0l nm

Wavelength accuracy: 0.01nm

Tuning speed: 10nm/s

Power stability: 0.01dB

Side mode suppression ratio: 45 dB

Relative intensity noise: 145 dB/Hz

Agilent Optical Spectrum Analyzer

In the experiments conducted in this thesis, the spectras are obtained using Agilent 86140B Optical Spectrum analyzer. The analyzer can display input light spectra from 600 nm to 1700 nm which is useful for WDM system and component characterization. The key specifications of the analyzer are given below [157]:

Wavelength range: 600 nm to 1700 nm

Wavelength accuracy: 0.01 nm

FWHM: 0.06 nm

Sensitivity: -90 dB in the wavelength range 1250 nm -1610 nm

Maximum safe power: 30 dBm

Polarization dependence: 0.3 dB in the range 1250 nm -1650 nm

Sumitomo Type 36 Fusion Splicer

For splicing the fibers together, we used Sumitomo Type 36 Fusion Splicer, which is a portable, self contained fully automatic instrument for creating low-loss optical fiber splices [158]. The splicer can handle fiber types such as, singlemode, multimode, dispersion shifted, dispersion compensated, cut off shifted and Er doped fibers. A fiber cladding diameter of 125 microns is preferable for the splicer. A precision CCD camera examines the fiber from the X and Y view and precisely aligns the fibers, before doing the arc splicing. After splicing, high resolution direct core monitoring image processing software incorporated into the

splicer calculates the estimated splice loss. Typical splice loss for single-mode fibers is less than 0.02 dB.

Broadband Source

The broadband source used to interrogate the FBGs is a super luminescent diode SLD-76-HP from Superlum Diodes Ltd [159]. The SLD was driven by a driver PILOT4-AC also from Superlum diodes Ltd. SLD-76-HP is a high power super luminescent diode with a power of 10 mW. The peak wavelength of the SLD was 1560 nm and the total range was from 1480 nm to 1640 nm. The other key specifications of the diode are,

SLD maximum direct current: 600 mA

Package: DBUT

SLD-76-HP was driven by PILOT4-AC driver. The key specifications of the current driver are:

SLD current range: 0-550 mA

Set resolution: 0.1 mA

Stabilized SLD temperature at any value within range of +10 ^{0}C to +40 ^{0}C

Remote control of SLD status and its on/off by external logic

High level of SLD protection against overloading

MDT693A Piezo Controllers

To apply dynamic strain to FBGs, piezo actuators (AE0505D18) controlled by Throlabs MDT693 piezo controllers were used [160]. The controller provide both manual and external control of the piezo drive voltages. A precision 10 turn potentiometer on the front panel can change the drive voltage. The drive voltage can also be be controlled externally by applying an analog voltage from 0 to 10 V to the front panel BNC inputs or remotely controlled by a computer terminal through an RS232 interface. The maximum out current of the controller was limited to 60 mA.

Dual Channel Optical Fiber Power Meters

Two dual channel power meters are used to measure power in the experiments: PXIT 306 dual channel fiber optic power meter, and a custom made power meter with a dual channel amplifier board and two photodiodes. The PXIT 306 is a high performance dual channel power meter compatible with the PXI format. Its two channels were independent and high speed data acquisition is possible when used in the sequence mode. The power meter was able to measure power level up to -70 dBm.

To analyze the noise effect of the system, a custom made optical receiver which contain two InGaAs photodiodes (G9 801) and a two channel trans-impedance amplifier board from Twlux were assembled. The maximum amplification factor of the board was 10^6 V/A and the 3 dB bandwidth was 2 kHz. The photodiodes wavelength range was from 900-1600 nm, with a sensitivity of 0.95 W/A at 1550 nm.

Temperature Controller

A Thermoelectric cooler (Marlow Industries DT12-8) driven by a temperature controller was used for the temperature studies. The Thorlabs ITC 510 Laser Diode Current and TEC Controller provide current and temperature control in one unit. The instruments provide a maximum laser drive current range of $pm1$ A, and a TEC drive current of up to $pm4$A (32W). The ITC 510 Current Controller exhibits exceptionally low current noise and low temperature drift, making this instrument one of the best performing combination controller. The key specifications of the TEC controller of ITC 510 are listed below [161]:

Control range: -4A to -4A

Maximum output power: 32 W

Thermistor: 2kΩ/20 KΩ

NI Data Acquisition cards

The data acquisition cards used in this thesis are NI S series PXI 6143 and M series 6221. PXI 6143 is a high speed data acquisition card with a sampling rate of 250 kS/s, which can acquire simultaneous data through its 8 differential analog input channels. The dedicated ADC per channel make it ideal for simultaneous data acquisition. The card can work with LabVIEW 7.0 or higher, but requires NI DAQmx drivers. The data acquisition cards were configured using NI MAX. The NI PXI 6221 is a M Series card is also a high speed data acquisition card with a sampling rate of 833 kS/s and has 16 analog inputs.

NI LabView Software

LabVIEW (Laboratory Virtual Instrument Engineering Workbench) is a fourth generation graphical programming language from National Instruments, used primarily in data acquisition and instrumentation controls. LabVIEW uses dataflow programming, where the flow of data through the nodes on the block diagram determines the execution order of the VIs and functions. VIs or virtual instruments are LabVIEW programs that imitate physical instruments. The graphical paradigm significantly simplifies programming tools and cuts down on development and debugging time. Each VI has two components, a block diagram and a front panel. Controls and indicators on the front panel allow an operator to input data into or extract data from a running virtual instrument. The main benefit of LabVIEW over other development environments is the extensive support for accessing several types of instrumentation hardware without worrying about the machine level details. The version of LabVIEW used for programming was LabVIEW 8.0.

In the experiment system used for this thesis investigation, all the equipment were automated using the LabVIEW software. Data acquisitions through the NI DAQ cards and the instruments such as, Tunable laser, Optical Spectrum Analyzer, Power meters were controlled via computer using LabVIEW. All these

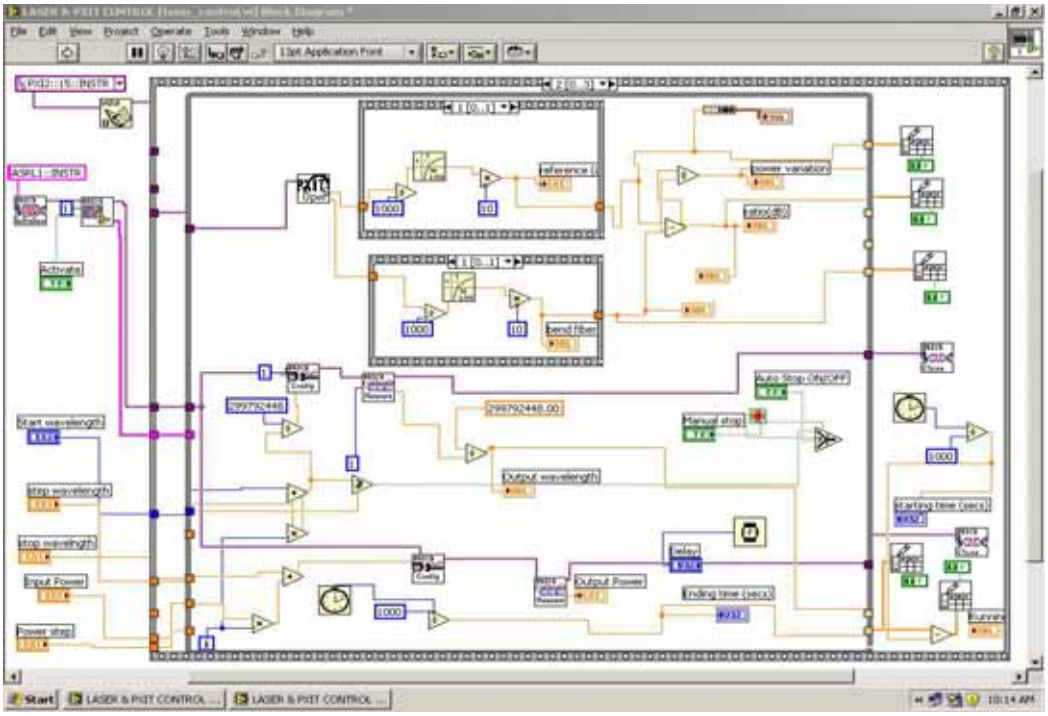

(a)

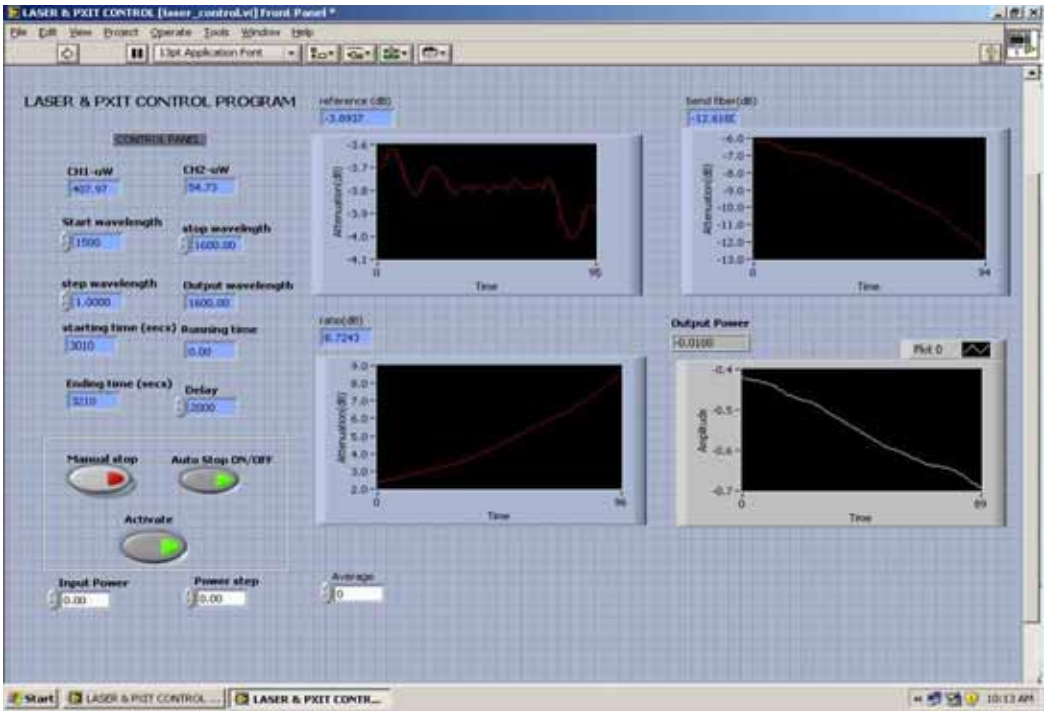

(b)

Figure B.1: Labview program to obtain the ratio response of the system (a) block diagram (b) front panel.

equipments has their own LabVIEW drivers, which allow the instruments to communicate with the computer via RS232/GPIB. The LabVIEW drivers of the spectrum analyzer and tunable contains several VI modules. These VIs have their own functions and reduce the task of programming and control the instrument accurately and remotely. Programs were written to characterize the system, to obtain the strain and temperature from the FBGs, to characterize the fiber filter etc. As an example the front panel and block diagram of a developed VI to characterize the ratiometric system are shown in Fig. B.1(a) and Fig. B.1(b) respectively.

Other Equipment

Other main equipments used in this thesis were Santec OTF-300 optical tunable filter, Thorlabs FPC560 manual polarization controller, PXIT 311 optical attenuator etc. The filter had tunable range of 40 nm from 1530 nm to 1570 nm with a 3 dB bandwidth of 1 nm. The polarization controller utilizes stress induced birefringence to alter the polarization in a single-mode fiber. The loop diameter of the paddle was 2.2". The optical attenuator PXIT 311 gives an attenuation up to 30 dB for a wavelength range of 1240 nm to 1610 nm. The attenuator exhibits a PDL in the range on 0.1 - 0.15 dB.

References

[1] T. S. Yu. Francis and Y. Shizhuo, *Fiber Optic Sensors*, Marcel and Dekker, New York, 2002.

[2] Eric Udd, *Fiber Optic Sensors*, Wiley Interscience, New York, 2002.

[3] K. T. V. Grattan and B. T. Meggit, *Optical Fiber Sensor Technology, Vol. 2, Devices and Applications*, Chapman and Hall, London, 1998.

[4] Y. Zhao, P. Li and Z. Pu, "Shape measurement based on fiber optic technique for complex internal surface", *Measurement*, 30, 289–295, 2001.

[5] W. W. Morey and W. H. Glem, "Fiber Bragg grating sensors", *Proc. SPIE, Fiber Optic and Laser sensors, VII*, 1169, 98, 1989.

[6] W. W. Morey and W. H. Glem, "Formation of Bragg gratings in optical fibers by a transverse holographic method", *Optics Lett.*, 14, 823–825, 1989.

[7] K. O. Hill and G. Meltz, "Fiber Bragg grating technology fundamentals and overview", *J. Lightwave Technol.*, 15, 1263–1276, 1997.

[8] Y. J. Rao, "In-fiber Bragg grating sensors", *Meas. Sci. Technol.*, 8, 355–375, 1997.

[9] Byoungho Lee, "Review of present status of optical fiber sensors", *Optical Fiber Technology*, 9, 57–79, 2003.

[10] L. Liu, H. Zhang, Q. Zhao, Y. Liu and F. Li, "Temperature-independent FBG pressure sensor with high sensitivity", *Optical Fiber Technology*, 13, 78–80, 2007.

[11] Y. S. Hsu, L. Wang, W. F Lie and Y. J. Chiang, "Temperature compensation of optical fiber Bragg grating pressure sensor", *IEEE Photon. Technol. Lett.*, 18, 874–876, 2006.

[12] L. Mohanty, L. M. Koh and S. C. Tjin, "Fiber Bragg grating microphone system", *Appl. Phys. Lett.*, 89, 161109, 2006.

[13] J. R. Lee and H. Tsuda, "A novel fiber Bragg grating acoustic emission sensor head for mechanical tests", *Scripta Materialia*, 53, 1181–1186, 2005.

[14] D. Tosi, M. Olivero and G. Perrone, "Low-cost fiber Bragg grating vibroacoustic sensor for voice and heartbeat detection", *Appl. Opt.*, 47, 5123–5129, 2008.

[15] K. S. C. Kuang, R. Kenny, M. P. Whelan, W. J. Cantwell and P. R. Chalker, "Embeddded fibre Bragg grating sensors in advanced composite materials", *Composites Science and Technology*, 61, 1379–1387, 2001.

[16] V. M. Murukeshan, P. Y. Chan, L. S. Ong and L. K. Seah, "Cure monitoring of smart composites using fiber Bragg grating based embedded sensors", *Sensors and Actuators A*, 79, 153–161, 2000.

[17] A. D Kersey, M. A. Davis, H. J Patrick, M. LeBlanc, K. P Koo, C. G Askins, M. A Putnam and E. J Friebele, "Fiber grating sensors", *IEEE J. Lightwave Technol.*, 15, 1442–1463, 1997.

[18] Y. Zhao and Y. Liao, "Discrimination methods and demodulation techniques for fiber Bragg grating sensors", *Optics and Lasers in Engg.*, 41, 1–18, 2004.

[19] S. M. Mille, K. Liu and R. M. Measures, "A passive wavelength demodulation system for guided wave Bragg grating sensors", *IEEE Photon. Tech. Lett.*, 4, 516–518, 1992.

[20] S. M. Mille, K. Liu and R. M. Measures, "Practical fiber optic Bragg grating strain gauge system", *Appl. Opt.*, 32, 3601–3609, 1993.

[21] A. B. L. Ribeiro, L. A Ferreira, M. Tsvetkov and J. L Santos, "All fiber interrogation technique for fiber Bragg sensors using a biconical fiber filter", *Electron. Lett.*, 32, 382–383, 1996.

[22] M. A. Davis and A. D Kersey, "All-fiber Bragg grating strain sensor demodulation technique using a wavelength division coupler", *Electron. Lett.*, 30, 75–77, 1994.

[23] J. Peupelmann and J. Meissner, "Applications and field tests of a fiber Bragg grating sensor system", *Proc. SPIE*, 3746, 470–473, 1999.

[24] R. W Fallon, L. Zhang, A. Gloang and I. Bennion, "Identical broadband chirped grating interrogation technique for temperature and strain sensing", *Electron. Lett.*, 33, 705–707, 1997.

[25] Y. Liu, L. Zhang and I. Bennion, "Arbitrary spectral response fiber edge filters based on tilted chirped grating structures", *Laser and Electrooptics, CLEO appos 99*, 287, 23–28, 1999.

[26] R. W Fallon, L. Zhang, A. Gloang and I. Bennion, "Fabricating fiber edge filters with arbitrary spectral response based on tilted chirped grating structures", *Meas. Sci Technol.*, 10, L1–L3, 1999.

[27] V. Grubsky and J. Feinberg, "Long-period fiber gratings with variable coupling for real-time sensing applications". *Opt. Lett.*, 25, 203–205, 2000.

[28] R. W Fallon, L. Zhang, L A Everall and J. A. R. Williams, "All fiber optical sensing system: Bragg grating sensor interrogated by a long period grating", *Meas. Sci. Technol.*, 9, 1969–1973, 1998.

[29] B. Mason, S. P DenBaars and L. A. Coldren, "Tunable sampled-grating DBR lasers with integrated wavelength monitors", *IEEE Photon. Tech. Lett.*, 10, 1085–1087, 1998.

[30] Q. Wang and G. Farrell, "Multimode fiber based edge filter for optical measurement and its design", *Microwave and Optical Technology Letters*, 48, 900–902, 2006.

[31] Q. Wang, G. Farrell and W. Yan, "Investigation on single-modemultimode single-mode fiber structure", *IEEE J. Lightwave Technol.*, 26, 512–519, 2008.

[32] S. C Kang, H. Yoon, S. B Lee, S. S Choi and B. Lee, "Real time measurement for static and dynamic strain using a fiber Bragg grating and the ASE profile of an EDFA", *Proc. 13th Int. Conf. Optical fiber sensors (OFS 13)*, SPIE-3746, 530–533, 1999.

[33] D. A. Jackson, A. B. L. Ribeiro, L. Reekie and J. L. Archambault, "Simple multiplexing scheme for a fiber optic grating sensor network", *Opt. Lett.*, 18, 1370–1372, 1993.

[34] A. D. Kersey, T. A. Berkoff and W. W. Morey, "Multiplexed fibre Bragg grating strain-sensor system with a fibre FabryPerot wavelength filter", *Opt. Lett.*, 18, 1370–1372, 1993.

[35] I. C Chang, "Acousto-optic tunable filter", *Opt. Engg.*, 20, 824–829, 1981.

[36] M. G. Xu, H. Geiger, J. L. Archambault, L. Reekie and J. P Dakin, "Novel interrogating system for fiber Bragg grating sensors using an acousto optic tunable filter", *Electron. Lett.*, 29, 1510–1511, 1993.

[37] J. R. Dunphy, G. Ball, F. D'amato, P. Ferraro, S. Inserra, A. Vannucci and M. Varasi, "Instrumentation development in support of fiber grating sensor array", *Proc. SPIE*, 2071, 2–11, 1993.

[38] A. D. Kersey, T. A. Berkoff and W. W. Morey, "High resolution fiber grating sensor with interferometric wavelength shift detection", *Electron. Lett.*, 28, 236–138, 1992.

[39] W. W. Morey A. D. Kersey and T. A. Berkoff, "Fiber optic Bragg grating sensor with drift compensated high resolution interferometric wavelength shift detection", *Opt. Lett.*, 18, 72–74, 1993.

[40] G. A. Ball, W. W. Morey and W. H. Glen, "Standing wave monomode erbium fiber laser", *IEEE Photon. Technol. Lett.*, 15, 267–270, 1993.

[41] A. Koo and A. D. Kersey, "Fiber laser sensor with ultrahigh strain using interferometric interrogation, *Electron. Lett.*, 31, 1180–1182, 1995.

[42] W. A. Gambling, D. N. Payne and H. Matsumura, "Radiation from curved single mode fibers", *Electron. Lett.*, 12, 567–569, 1976.

[43] L. Lewis, D.C. Chang and E.F. Kuester, "Electromagnetic waves and curved structures". *IEE Electromagnetic waves series;2*, 1977.

[44] Y. Murakami and H. Tsuchiya. "Bending loss of coated single mode optical fibers", *IEEE. J. Quantum Electron.*, QE-14, 495–501, 1978.

[45] H. J Haris and P. F Castle, "Bend loss measurements on high numerical aperture single mode fibers as a function of wavelength and bend radius". *J. Lightwave Technol.*, LT-4, 34–40, 1986.

[46] D. Marcuse. "Field deformation and loss caused by curvature of optical fibers", *J. Opt. Soc. Am.*, 66, 311–320, 1976.

[47] D. Marcuse, "Curvature loss formula for optical fibers". *J. Opt. Soc. Am.*, 66, 216–220, 1976.

[48] H. Renner. "Bend losses of coated single mode fibers: A simple approach", *J. Lightwave Technol.*, 10, 544–551, 1992.

[49] L. Faustini and G. Martini, "Bend loss in single mode fibers", *J. Lightwave Technol.*, 15, 671–679, 1992.

[50] R. Morgan, J. S. Barton, P. G. Harper and J. D. C Jones, "Wavelength dependence of bending loss in monomode optical fibers: effect of fiber buffer coating", *Opt. Lett.*, 15, 947–949, 1990.

[51] Q. Wang, G. Farrell and T. Frier, "Theoretical and experimental investigations of macrobend losses for standard single mode fibers", *Optics Express*, 13, 4476–4484, 2005.

[52] S. L. Tsao and W. M. Cheng, "Simplified formula for bending loss for optical fiber sensors", *Fiber and Integrated Optics*, 21, 333–344, 2002.

[53] R. C. Gauthier and R. C. Ross, "Theoretical and experimental considerations for single-mode fiber-optic bend type sensor, *Appl. Opt.*, 36, 6264–6273, 1997.

[54] R. D. Morgan, J. D. C. Jones, J. S. Barton and P. G. Harper, "Determination of monomode fiber buffer properties, *J. Lightwave Technol.*, 12, 1355–1359, 1994.

[55] P. Dinev, "Fiber optic voltage sensor using an optical lever", *IEE Proceedings Optoelectronics*, 144, 253–255, 1997.

[56] A. Todoroki, T. Hotanaka, H. Kobavashi, H. Nakamura and Y. Shimamura, "Strain measurement by curved optical fiber sensor", *Transactions of the Japan Society of Mechanical Engineers*, 62, 3710–3714, 1997.

[57] S. Tomita, H. Tachino and N. Kasahara, "Water sensor with optical fiber", *IEEE J. Lightwave Technol.*, 8, 1829–1832, 1990.

[58] F. Sienkiewicz and A. Shukla, "Asimple fiber-optic sensor for use over a large displacement range", *Optics and Lasers in Engineering*, 28, 293–304, 1997.

[59] A. J. Harris, P. A. Shrubshall and P. F. Castle, "Wavelength demultiplexing using bends in a single-mode optical fiber", *IEEE J. Lightwave Technol.*, 6, 80–86, 1988.

[60] S. Hyun and Y. Shizhuo, "High-temperature sensing using whispering gallety mode resonance in bent optical fibers", *IEEE Photon. Tehnol. Lett.*, 17, 2391–2393, 2005.

[61] Q. Wang, T. Freir and G. Farrell, "Study of transmission response of edge filters employed in wavelength measurements", *Appl. Opt.*, 44, 7789–7792, 2005.

[62] E. Leckel, J. Sang, E. U. Wagemann and E. Muller, "Impact of source spontaneous emission on the measurement of DWDM components", *Optical Fiber Communication Conference*, 2, 31–33, 2000.

[63] Q. Wang, G. Farrell, T. Freir, G. Rajan and P. Wang, "Low cost wavelength measurement based on macrobending singlemode fiber", *Opt. Lett.*, 31, 1785–1787, 2006.

[64] Q. Wang, G. Rajan, P. Wang and G. Farrell, "Macrobending fiber loss filter, ratiometric wavelength measurement and application", *Meas. Sci. Technol.*, 18, 3082–3088, 2007.

[65] F. J. Durate, *Tunable Lasers Hand Book*, Academic Press, 1995.

[66] M. Csele, *Fundamentals of Light Sources and Lasers*. Wiley Interscience, 2004.

[67] M. Bass, E. W. Van Stryland, D. R. William and W. L. Wolfe, *Handbook of Optics*, Vol. 1, 2nd Ed, McGraw-Hill, 1995.

[68] M. G. Xu, H. Geiger and J. P. Dakin, "Modeling and performance analysis of a fiber Bragg grating interrogation system using an acousto-optic tunable filter", *IEEE J. Lightwave Technol.*, 14, 391396, 1996.

[69] T. L. Wu, "Vectorial analysis for polarization effect of wavelength flattened fiber-optic couplers", *Microwave and Optical Technology Letters*, 23, 12–16, 1999.

[70] G. Rajan, Y. Semenova, G. Farrell, Q. Wang and P. Wang, "Investigation of the influence of 3 dB coupler on ratiometric wavelength measurements", *SPIE Proceedings, Optical Sensors*, 7003, 2008.

[71] G. Rajan, Q. Wang, G. Farrell, Y. Semenova and P. Wang, "Effect of SNR of input signal on the accuracy of a ratiometric wavelength measurement system", *Microwave and Optical Technology Letters*, 49, 1022–1024, 2007.

[72] *Corning SMF28 Optical fiber product information, PI1036*, Corning Ltd, 2002.

[73] J. R. Mourant, I. J. Bigio, D. A. Jack, T. M. Johnson and H. D. Miller, "Measuring absorption coefficients in small volumes of highly scattering media: source-detector separations for which path lengths do not depend on scattering properties", *Appl. Opt.*, 36, 5655–5661, 1997.

[74] R. Bishop, *LabView 8*, 2007.

[75] http://www.ni.com/labview/.

[76] R. Pettai, *Noise in Receiving Systems*, Wiley Interscience, 1984.

[77] G. Vasilescu, *Electronics Noise and Interfering Signals*, Springer, 2005.

[78] B. K Jones, "Electrical noise as a reliability indicator in electronic devices and components", *IEE Proceedings- Circuits and Systems*, 149, 13–19, 2002.

[79] P. C. D. Hobbs, *Building Electro-Optical systems, Making it all work*, John Wiley and Sons Inc, 2000.

[80] C. D. Motechenbacher and J. A. Connelly, *Low-Noise Electronic System Design*, John Wiley and Sons, Inc, 1993.

[81] S. B. Alexander, *Optical Communication Receiver Design*, volume IEE Telecommnucation series, Vol 37, SPIE Optical Engineering Press, 1997.

[82] P. Wright, K. B. Ozanyan, S. J. Carey and H. McCann, "Optimization of the signal to noise performance of photodiode receivers in near infrared absorption tomography", *3rd world Congress on Industrial Preocess Tomography, Banff, Cananda*, 2003.

[83] Z. Bielecki, W. Kolosowski, E. Sedek and M. Borejko, "Analysis of signal-to-noise ratio in optical receivers", *TELSIKS, Serbia and Montenegro*, 2003.

[84] S. D. Personick etal, "A detailed comparison of four approaches to the calculation of the sensitivity of optical fiber system receivers", *IEEE Transactions on Communications*, COM 25, 541–548, 1977.

[85] P. Balaban, "Statistaical evalaution of the error rate of the fiber guide repeater using imporatnce sampling", *Bell System Technical Journal*, 55, 745–766, 1976.

[86] W. Davenport and W. Root, *The Gaussian process in an introduction to the theory of random signals and noise - Chap. 8*, NewY ork, 1958.

[87] W. M. Hubbard, "The approximation of a Poisson distribution by a Gaussian distribution", *Proceedings of the IEEE*, 58, 1374–1375, 1970.

[88] J. B. Kennedy and A. M. Neville, *Normal distribution in basic statistical methods for engineers and scientists, Chap. 10*, Harper and Row, NewYork, 1986.

[89] J. J. Morikuni, A. Dharchoudhury, Y. Leblebici and S. M. Kang, Improvements to the standard theory for photoreceiver noise, *J. Lightwave Technol.*, 12, 1174–1184, 1994.

[90] Operation manual, *Low noise J-FET dual operational amplifiers, TL072*.

[91] A. M. Cowley and R. A. Zettler, Shot noise in silicon Schottky barrier diodes, *IEEE Transactions on Electron Devices*, ED-15, 761–769, 1968.

[92] H. Nyquist, Thermal agitation of electric charge in conductors, *Phys. Rev.*, 33, 110–113, 1928.

[93] R. H. Walden, Analog-to-digital converter survey and analysis, *IEEE Journal On Selected Areas In Communications*, 17, 539–550, 1999.

[94] E. Collet, *Polarized Light, Fundamentals and Applications*, Marcel and Dekker, NewYork, 1993.

[95] D. Derickson, *Fiber Optic Test and Measurement*, Prentice Hall, 1998.

[96] A. Mabrouki, M. Gadonna and R. Le. Naour, "Analysis and measurement of polarization sensitivity of single mode fiber passive optical components", *Fiber and Integrated Optics.*, 15, 15–26, 1996.

[97] N. Kashima, *Passive Optical Components for Optical Fiber Transmission*, Artech House, 1995.

[98] I. P. Kaminow, "Polarization in optical fibers", *J. of Quantum Electron.*, QE-17, 15–22, 1981.

[99] R. Roy and G. D. VanWiggeren, "Transmission of linearly polarized light through a single-mode fiber with random fluctuations of birefringence", *Appl. Opt.*, 38, 3888–3892, 1999.

[100] C. Xie and L. F. Mollenauer, "Performance degradation induced by polarization-dependent loss in optical fiber trasmission systems with and without polarization-mode dispersion", *IEEE J. Lightwave Technol.*, 21, 1953–1957, 2003.

[101] N. Gisin, "The statistics of polarization dependent losses", *Optics Communications*, 114, 399–405, 1995.

[102] A. El Amari, N. Gisin, B. Perny, H. Zbinden and W. Zimmer, "Statistical prediction and experimental verification of concatenations of fiber optic components with polarization dependent loss", *IEEE J. Lightwave Technol.*, 16, 332–339, 1998.

[103] R. M. Craig, "Accurate spectral characterization of polarization dependent loss", *IEEE J. Lightwave Technol.*, 21, 432–437, 2003.

[104] N. Gisin, B. Huttner and N. Cyr, "Influcence of polarization dependent loss on birefringent optical fiber networks", *Optical fiber communication conference*, 1, 86–88, 2000.

[105] T. L. Wu and H. C. Chang, "Rigorous analysis of form birefringence of weakly fused fiber-optic couplers", *IEEE J. Lightwave Technol.*, 13, 687–691, 1995.

[106] T. L. Wu, "Rigorous analysis of polarization-dependence loss for equilateral 3x3 fused fiber couplers", *IEEE Photon. Technol. Lett.*, 16, 165–167, 2004.

[107] T. L. Wu, "Vectorial analysis for polarization effect of wavelength flattened fiber-optic couplers", *Microwave and Optical Technology Letters*, 23, 12–16, 1999.

[108] I. J. Wilkinson and C. J. Rowe, "Close - spaced fused fiber wavelength division multiplexers with very low polarization sensitivity", *Electron. Lett.*, 26, 382–384, 1990.

[109] L. B. Jeunhomme, *Single-mode Fiber Optics - Principles and Applications*, Optical Engineering, Vol. 23, 1990.

[110] A. M. Smith, "Birefringence induced by bends and twists in single-mode fiber", *Appl.Opt.*, 19, 2606– 2611, 1980.

[111] H. Renteir, "Bending-induced thermal stress birefringence in single-mode fibers", *Proc. Optical Fiber Communication Conference*, 1, 2004.

[112] Q. Wang, G. Rajan, P. Wang and G. Farrell, "Polarization dependece of bend loss in a standard singlemode fiber", *Optics Express*, 1, 4909–4920, 2007.

[113] G. Rajan, Q. Wang, Y. Semenova, G. Farrell and P. Wang, "Effect of polarization dependent loss on the performance accuracy of a ratiometric wavelength measurement system", *IET Optoelectron.*, 2, 63–68, 2008.

[114] H. Renteir, "Birefringence measurement in twisted single-mode fibers", *Electron. Lett.*, 17, 252–253, 1981.

[115] G. Rajan, Y. Semenova, G. Farrell, Q. Wang and P. Wang, "A low polarization sensitivity all-fiber wavelength measurement system", *IEEE Photon. Technol. Lett.*, 20, 1464–1466.

[116] K. A. Murphy, M. F. Gunther and A. M. Vengsarkar, "Variable-ratio polarization insensitive 3x3 fused biconical tapered couplers", *Electron. Lett.*, 27, 1336–1337, 1991.

[117] I. Kim, R. C. Alferness, U. Koren, T. L. Koch, L. L. Buhl, B. I. Miller, M. G. Young, M. D. Chien, C. H. Joyner and M. Zirngibl, "Compact broadband polarisationinsensitive 3db optical power splitter on inp", *Electron. Lett.*, 30, 953–954, 1994.

[118] R. Morgan, J. S. Barton, P. G. Harper and J. D. C. Jones, "Temperature dependece of bending loss in monomode optical fibers", *Electron. Lett.*, 26, 937–939, 1990.

[119] F. M. Haran, J. S. Barton and J. D. C. Jones, "Bend loss in buffered overmoded optical fibre: LP11 mode and whispering gallery mode interaction", *Electron. Lett.*, 17, 1433–1434, 1994.

[120] U. S Raikumar, A. S. Lalasangi, V. K. Kulkarni and I. I. Pattanashetti, "Temperature dependence of bending loss in singlemode communication fiber: Effect of fiber buffer coating", *Optics Communications*, 273, 402–406, 2007.

[121] F. M. Haran, J. S Barton, S. R. Kidd and J. D. C Jones, "Optical fibre interferometric sensors using buffer guided light", *Meas. Sci. and Technol.*, 5, 526–530, 1994.

[122] P. Wang, G. Farrell, Q. Wang and G. Rajan, "An optimized macrobending-fiber-based edge filter", *IEEE Photon. Technol. Lett.*, 19, 1136–1138, 2007.

[123] N. D. Herrera, M. C. Navarrete, O. Esteban and A. G. Cano, "A fibre-optic temperature sensor based on the deposition of a thermochromic material on an adiabatic taper", *Meas. Sci. and Technol.*, 15, 353–358, 2004.

[124] J. Canning, K. Sommer and M England, "Fibre grating for high temperature sensor applications", *Meas. Sci. and Technol.*, 12, 824–828, 2001.

[125] K. Q. Kieu and M. Mansuripur, "Biconical fiber taper sensors", *IEEE Photon. Technol. Lett.*, 18, 2239–2241, 2006.

[126] M. McSherry and C. Fitzpatrick, "Review of luminescent based fiber optic temperature sensors", *Sensor Review*, 25, 56–62, 2005.

[127] H. Berthou and C. K. Jorgesen, "Optical-fiber temperature sensor based on upconversion-excited fluorescence", *Opt. Lett.*, 15, 1100–1102, 1990.

[128] S. F. Robert, L. S. Kelly and E. P. Mathew, "Harsh-environment fiber optic sensors for structural monitoring applications", *Proc. SPIE*, 5388, 399–409, 2004.

[129] H. N. Li, D. S. Li and G. B. Song, "Recent applications of fiber optic sensors to health monitoring", *Engineering Structures*, 26, 1647–1657, 2004.

[130] D. Degamber and D. F. Fernando, "Fiber optic sensors for noncontact process monitoring in a microwave environment", *Journal of Applied Polymer Science*, 86, 3868–3873, 2003.

[131] M. Remouche, R. Mokdad, M. Lahrashe, A. Chakari and P. Meyrueis, "Intrinsic optical fiber temperature sensor operating by modulation of the local numerical aperture", *Opt. Engg.*, 46, 02440l (1–15), 2007.

[132] G. Tuncol, M. Danisman, A. Kaynar and E. M. Sozer, "Constraints in monitoring resin flow in the resin transfer molding process by using thermocouple sensors", *Composites Part A: Applied Science and Manufacturing*, 38, 1363–1386, 2007.

[133] E. Pinet and C. Hamel, "True challenges of disposable optical fiber sensors for clinical environment", *Proc. SPIE*, 6619, 2007.

[134] R. M. Measures, S. Melle and K. Lie, "Wavelength demodulated Bragg grating fiber optic sensing systems for addressing smart structures critical issues", *Smart Mater. Struct.*, 1, 36–44, 1992.

[135] J. Bang, H. K. Kang, C. S Hong and C. G. Kim, "Optical fiber sensor systems for simultaneous monitoring of strain and fractures in composites", *Smart Mater. Struct.*, 14, N52–N58, 2005.

[136] K. Pran, G. B. Havsgard, G. Sagvolden, O. Farsund and G. Wang, "Wavelength multiplexed fibre Bragg grating system for high-strain health monitoring applications", *Meas. Sci. and Technol.*, 13, 471–476, 2002.

[137] S. C. Tjin, Y. Wang, X. Sun, P. Moyo and J. M. W. Brownjohn, "Application of quasi-distributed fibre Bragg grating sensors in reinforced concrete structures", *Meas. Sci. and Technol.*, 13, 583–589, 2002.

[138] Z. Zhou, T. W. Graver, L. Hsu and J. P. Ou, "Techniques of advanced FBG sensors: fabrication, demodulation, encapsulation and their application in the structural health monitoring of bridges", *Pacific Science Review*, 5, 116–121, 2003.

[139] Y. Qiu, Y. Sheng and C. Beaulieu, "Optimal phase mask for fiber Bragg grating fabrications", *J. Lightwave Technol.*, 17, 2366–2370, 1999.

[140] F. Ouellette, P. A. Krug and R. Pasman, Characterization of long phase masks for writing fiber Bragg gratings, *Optical Fiber Technology*, 2, 281–284, 1996.

[141] G. Rajan, Y. Semenova, P. Wang and G. Farrell, "Temperature induced instabilities in macro-bend fiber based wavelength measurement systems". *IEEE J. Lightwave Technol.*, under review.

[142] G. Rajan, Y. Semenova, T. Freir, P. Wang and G. Farrell, "Modeling and analysis of the effect of noise on an edge filter based ratiometric wavelength measurement system", *J. Lightwave Technol.*, In press.

[143] P. J. Russel, J. Archmabault and L Reekie, "Fibre grating", *Physics World*, 6, 41–46, 1993.

[144] T. Erdogan, "Fiber grating spectra", *IEEE J. Lightwave Technol.*, 15, 1277–1294, 1997.

[145] K. Hoffman, "An introduction to measurements using strain gauges", *Hottinger Baldwin Messtechnik GmbH, Drmstadt*, 1989.

[146] E. Rivera and D. J. Thomson, "Accurate strain measurements with fiber Bragg sensors and wavelength references", *Smart Mater. and Struct.*, 15, 325–330, 2006.

[147] G. Gagliardi, M. Salza, P. Ferraro and P. D. Natale, "Fiber Bragg grating strain sensor interrogation using radio frequency modulation", *Optics Express*, 13, 2377–2384, 2005.

[148] RS componenets data sheet, *1502325957*, 2002.

[149] *The Pressure, Strain and Force Handbook*, Omega Press LLC, 1996.

[150] G. Rajan, Y. Semenova, Q. Wang, G. Farrell and P. Wang, "A method to measure reference strain in FBG strain sensor interrogation system involving actuators", *Microwave and Optical Technology Letters*, 49, 2658–2661, 2007.

[151] A. B. L. Ribeiro, L. A Ferreira, L. Santos and D. A Jackson, "Analysis of the reflective-matched fiber Bragg grating sensing interrogation scheme", *Appl. Opt.*, 36, 934–939, 1997.

[152] P. Niewczas, A. J. Willshire, L. Dziuda and J. R. McDonald, "Performance analysis of the fiber Bragg grating interrogation system based on an arrayed waveguide grating", *IEEE Transactions on Instrumentation and Measurement*, 53, 1192–1196, 2004.

[153] J. F. Nye, *Physical Properties of Crystal*, Oxford U Press, London, 1987.

[154] G.B. Hocker, "Fibre optic acoustic sensors with composite structure: an analysis", *Appl. Opt.*, 17, 3679–3683.

[155] C. D. Butter and G.B. Hocker, "Fibre optic suain guage", *Appl. Opt.*, 17, 2867–2869.

[156] Operation manual, *Nettest, OSICS-ECL tunable laser.*

[157] Operation manual, *Agilent 86140B, Optical Spectrum Analyzer.*

[158] Operation manual, *Sumitomo, type 36 fusion splicer.*

[159] Operation manual, *Superlum Driver Pilot-4AC.*

[160] Operation manual, *Thorlabs MDT694A Piezo Controllers.*

[161] Operation manual, *Thorlabs ITC510 Laser Diode Combi Controller.*

Index